# ELASTOPLASTIC CONSTITUTIVE MODEL FOR SATURATED AND UNSATURATED SOILS CONSIDERING THE DEPOSITED STRUCTURE AND ANISOTROPY

December 2010

Hiroyuki Kyokawa

# ELASTOPLASTIC CONSTITUTIVE MODEL
# FOR SATURATED AND UNSATURATED SOILS
# CONSIDERING THE DEPOSITED STRUCTURE AND ANISOTROPY

A dissertation submitted in partial fulfillment of the requirements for the

Doctoral Degree in Civil Engineering


Submitted by

**Hiroyuki Kyokawa**

Supervised by

Professor **Teruo Nakai**

Department of Civil Engineering

Nagoya Instituted of Technology, Japan


December 2010

# Preface

The Cam clay model (e.g., Schofield and Wroth, 1968) is first model which succeed in describing the consolidation and shear behaviors which had been investigated separately before that time. Since the Cam clay model can only be applied to the prediction of the remolded normally consolidated clay under triaxial compression condition, this model cannot take account of the various features of soils: density and / or confining pressure, naturally deposited soil (structured and bonding), unsaturated soils, time effect (creep deformation and stress relaxation), temperature dependency, ordinary three dimensional stress conditions including the rotation of principal axis, anisotropy and others. Although such complex features are not negligible characteristics in order to predict the actual ground behavior precisely, a unified model considering such features has never been developed. In this study, a constitutive model for the saturated remolded soil, named subloading $t_{ij}$ model (Nakai and Hinokio, 2004), is extended to one considering essential factors which cannot be neglected to predict actual soil behavior, particularly the influence of the bonding, unsaturated condition and an irregular stress path (history).

The explanation of modeling in this study is divided to two parts. The first part is on the modeling of scalar indices features affecting on the mechanical characteristics of soils (Chapter 2 & 3), viz., density, bonding, temperature, strain-rate, partial saturation. The second part is on the modeling of the anisotropy (Chapter 4), viz., the influence of the intermediate principal stress, stress histories, non-coaxiality. Outline of this thesis is summarized as follows.

The back ground and objective of this study is shown with past researches in Chapter 1.

In Chapter 2, the modeling of remolded normally consolidated soil is firstly conducted, and then this model will be extended to one taking account of the influence of density, the bonding effect observed in natural deposited soil, and external factors such as temperature dependency, time effect and partial saturation. In order to modeling of these additional features, the simple one-dimensional elastoplastic model representing the isotropic relation between one-dimensional stress $\sigma$ and void ratio $e$ is firstly developed, and such model is finally extended to the corresponding multi-dimensional model representing the relation stress tensor $\sigma_{ij}$ and strain tensor $\varepsilon_{ij}$. This method based on one dimensional problem is easy to understand the elastoplastic behavior of soils and to be extended to one which can consider several characteristics of soils.

The structured soil shows stiffer behavior than non-structured remolded soil with the same density due to bonding effect. Considering the influence of bonding on the evolution rule of the density state variable $\rho$, which represents the vertical distance between current void ratio and void ratio at *NCL* under same stress level (Nakai and Hinokio, 2004), the natural deposited soil showing the complicated stiffness change with decaying of bonding will be modeled.

The modeling of unsaturated soils will be conducted in Chapter 3. It will be derived from the past experimental evidences that normally consolidated line (*NCL*) of unsaturated soils downward (or upward) in the plane of void ratio $e$ and the effective mean stress $p''$ depending on the increase (or decrease) of degree of

saturation $S_r$, and this feature is closely related to water retention characteristic of soils. Therefore, by introducing the new state variable $\psi$ given as function of degree of saturation $S_r$, the position of *NCL* is shifted. Moreover, the ordinary model of soil water characteristic curve, e.g., van Genuchten model, will be extended to one considering the scanning curve due to wetting / drying history and the influence of density. From the simulations of compression, soaking and shear tests of unsaturated soil, it will be shown that the proposed model can describe the complex behavior of unsaturated soils depending on density, suction and internal moisture.

Soil is a material remembering the past loading history. That is to say, the situation of interparticle contact developing with past loading affects on subsequent mechanical behavior of soil, viz., the induced anisotropy. By using the modified stress tensor $t_{ij}^*$ already considering the induced anisotropy, the new method describing such influence of past stress history on deformation and strength characteristics of soils in the isotropic hardening rule will be proposed. A transformation tensor $a_{ij}^*$ for calculating this modified stress tensor $t_{ij}^*$ is equivalent to the inverse tensor of fabric tensor $F_{ij}$ (e.g., Oda, 1972) representing the orientation of contact normals. Therefore, the physical meaning of the modified stress $t_{ij}^*$ and the transformation tensor $a_{ij}^*$ are clear. Conducting the parametric studies and comparison with observed results of triaxial tests on medium dense Toyoura sand, true triaxial tests and directional shear tests on medium dense Leighton Buzzard sand, the validation of the proposed model will be verified.

Conclusion and future work of this study of this thesis are shown in Chapter 5.

# Acknowledgements

I would like to express my deepest sense of gratitude to Dr. Teruo Nakai, Professor of Nagoya Institute of Technology, for giving worthwhile research theme, his guidance, continuous encouragement and invaluable support throughout this research work. I have been conceived his novel idea for breakthrough of research, and learned a great deal from it. I will be ever grateful to Prof. Nakai for giving me the opportunity to undertake graduate studies under his supervision.

My deepest heartfelt appreciation goes to Dr. Mamoru Kikumoto, Associate Researcher of Nagoya Institute of Technology, for giving lecture of not only Geomechanics, but also continuum mechanics, programming and everything for my research. I have learned a great deal from his tireless devotion, unfailing support and critical suggestions for research. I am also grateful to Dr. Kikumoto for his support in my personal life.

I am deeply grateful to Dr. Feng Zhang, Professor of Nagoya Institute of Technology, for his invaluable suggestions and discussions on the research topic and his concern for my physical condition. I also appreciate to him for giving the important research topic for unsaturated soil and the support in the constructing the experimental apparatus.

I wish to express my indebtedness to Dr. Kenichi Maeda, Associate Professor, for his constructive comments, warm encouragement and interesting topic about overall engineering.

I would like to express my gratitude to the member of my doctoral thesis review committee, Dr. Makoto Obata, Professor of Nagoya Institute of Technology, and Dr. Toshihiro Noda, Professor of Nagoya University, for their valuable suggestions on this research work.

I would like to express my thankful gratitude to Dr. Hossain Md. Shahin, Associate Professor of Nagoya Institute of Technology, for proofreading of this thesis and lecture of numerical analysis.

I wish to express my thanks to Dr. Masaya Hinokio, former Research Associate of our laboratory. I have had the support in the constitutive equations and experimental works of him. I would like to express my sincere thanks to laboratory supervisor, Mr. Tomonori Sato, for his cooperation in solving various computer problems. I would like to express my thankful gratitude to Dr. Marcio Muniz de Farias, Professor of University of Brasilia, Brazil, for his valuable suggestions and comments on the research work.

I would like to emphasize that the present study has been supported by many graduates and students

in the constitutive modeling group of my laboratory. I am grateful to Messrs. Anri Yagyu, Tomoyuki Ikariya, Takahiro Ishihara, Junkei Isero, Yoshito Miyahara, Kazunori Tatematsu, Akimasa Ban, Mana Koike, Hikaru Yamazaki, Tatsuki Ohashi, Kohei Tsukamoto. They cooperated with me in analytical and experimental works.

Sincere thanks to Messrs. Makoto Yamamoto, Hideki Takei, Ryosuke Nagatsu, Msashi Niinomi, Yusuke Tabata, Yasuki Sago, Kenji Noda, Yara da Silva Geraldini, Masashi Nagata, Yasutaka Uetani, Kenji Ishii, Ryosuke Sakai, Morihiro Kato and all of my laboratory members who are friendly to me and have created a good congenial environment for studying in laboratory. Special thanks to Mr. Yoichi Watanabe, PhD students of Kumamoto University, and Mr. Hideto Nonoyama, PhD student of Gifu University, for their valuable discussion on our research and Geomechanics.

I wish to express my acknowledgement to Dr. Akira Asaoka, former Professor of Nagoya University, for his lecture of Geomechanics about constitutive modeling, theory of infinite deformation and others. I also wish to express my indebtedness to Dr. Jun Otani, Professor of Kumamoto University, Kentaro Nakai and Mutsumi Tashiro, Associate Researcher of Nagoya University, Shuji Moriguchi, Associate Researcher of Gifu University, and Kazunori Fujisawa, Associate Researcher of Okayama University, for their kind discussion and advice in my research.

I am grateful to the Japan Society for the Promotion of Science for its financial support with Grants-in-Aid for JSPS Fellows 20-9718.

Finally, and the most importantly, I am deeply grateful to my family for their financial and mental support, encouragement, endless love, faith in me and continuously sustaining me.

Hiroyuki Kyokawa
Nagoya Institute of Technology
December 2009

# ELASTOPLASTIC CONSTITUTIVE MODEL FOR SATURATED AND UNSATURATED SOILS CONSIDERING THE DEPOSITED STRUCTURE AND ANISOTROPY

Table of contents

# Chapter 1 Introduction

## 1.1 Background and Objective

As the initial or boundary problems are solved in a framework of the continuum (solid) mechanics, the governing equations which are generally the momentum conservation law and the mass conservation law are common regardless of a type of material. Then, only the constitutive model describing a stress-strain relation characterizes the mechanical property of each material. The applicability of such numerical analysis, therefore, considerably depends on an accuracy of constitutive model of material. The investigation of mechanical response (stress-strain relation) of each material and its modeling, therefore, have been actively conducted from long ago in various fields of engineering, not to mention also in geotechnical engineering.

Geotechnical engineering and soil mechanics involve various topics: ground subsidence, bearing capacity of foundation, slope stability, ground excavation, earth quake resistance and others. Since most of these topics relate closely with a stress-strain relation of soil, inclusive evaluation of various mechanical phenomenon in actual ground is significant by the numerical analysis using a proper constitutive equation. The improvement of accuracy of such numerical simulation and the extension of the applicability of it depend on whether the constitutive model can adequately describes the various features of soils, which are affected by its property (density, bonding, degree of saturation, temperature) and several loading condition (e.g., cyclic loading, stress history, strain rate and creep).

It is obvious that the mechanical behaviors of soil, which is formed as the aggregation of discrete soil particles, are governed by microscopic slip and rotation between particles, and it can be obtained from calculation of the motion of each particle by using numerical simulations such as the discrete element method. It is, however, laborious to simulate the actual ground behavior by such method because of the limitation of the performance of computer, viz., precise description of various actual particle configurations and huge calculation time for considering an indefinitely large number of discrete particles. So, by referring to the macroscopic stress-strain behavior obtained from the element tests of soil (oedometer test, triaxial test, hollow cylinder test and others), constitutive models for geo-materials in which soil is regarded as continuum should be developed in order to predict the deformation and failure of the ground properly and simply. From such view point, a large number of element tests have ever been conducted and a large number of constitutive models, in which the characteristics of soil as seen in experimental result are considered on the basis of the continuum mechanics, theory of elasticity and plasticity, and other theories, have ever been developed. The Cam clay model (e.g., Schofield and Wroth, 1968), which was developed more than 40 years ago, was an epoch-making constitutive model for geo-materials. This is because this is first model which succeed in describing the consolidation and shear behaviors which had been investigated separately before that time. However, the Cam clay model can only be applied to the prediction of the behavior of the remolded normally consolidated clay under triaxial compression condition. Various features of geo-materials which are not taken into consideration in the Cam clay model and some typical methods against each feature are summarized in

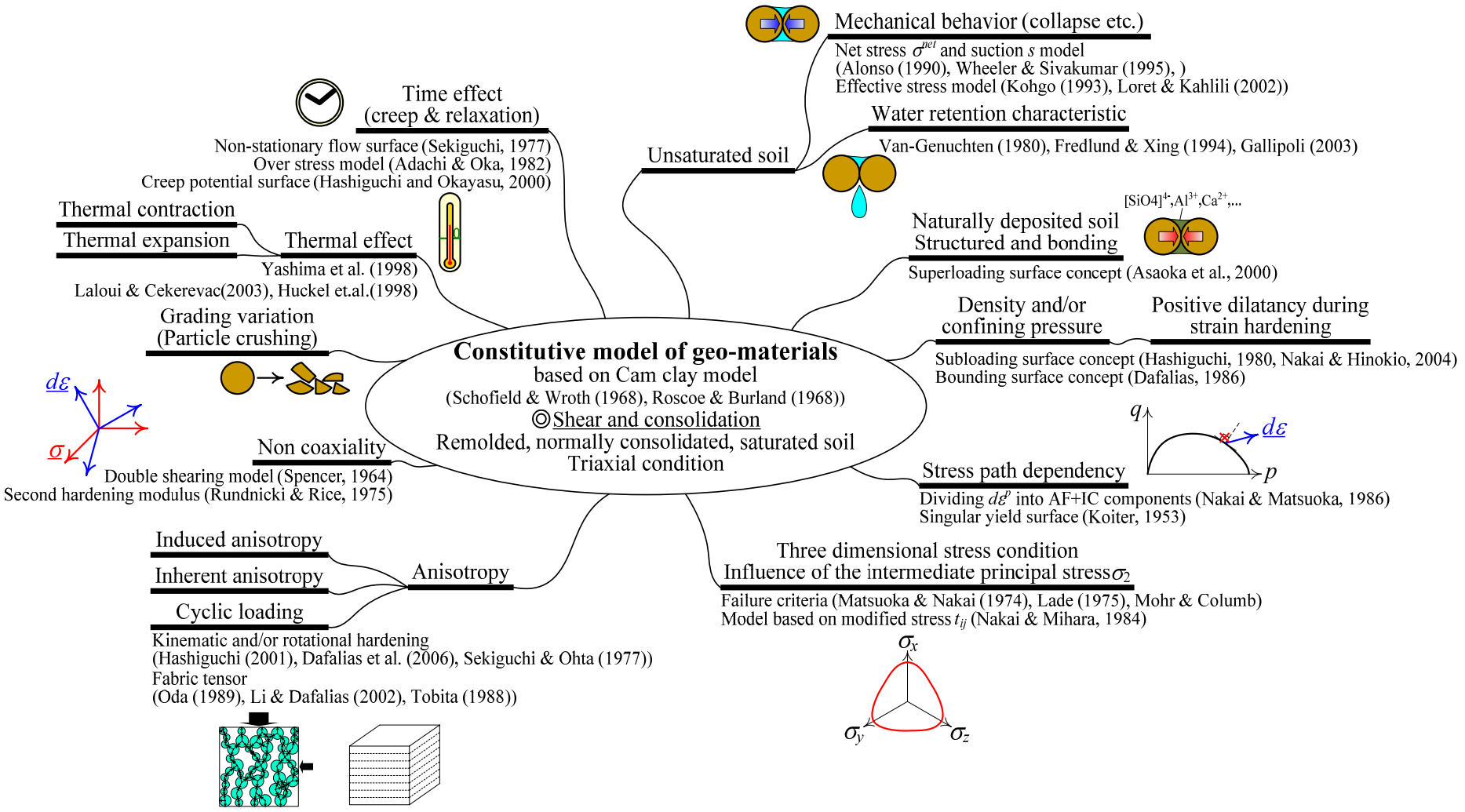


Figure 1.1 The relationships between unified constitutive model for geo-materials and its various features

A number of constitutive model which overcome the limitations of the Cam clay model have ever been developed.

Figure 1.1 with a focus on Cam clay model. As shown in this figure, although many constitutive models have been proposed to overcome the limitations of the Cam clay model, most of them are complex, and/or the applicability of the model is limited.

Nakai and Hinokio (2004) have proposed an elastoplastic isotropic hardening model named subloading $t_{ij}$ model, which can suitably consider the influence of the relative magnitude of intermediate principal stress on deformation and strength characteristics of soil by using modified stress $t_{ij}$, the stress path dependency of plastic flow by dividing the plastic stain increment into two components (i.e. the plastic strain increment $d\varepsilon_{ij}^{p\,\mathrm{AF}}$which satisfies associated flow rule in $t_{ij}$ space and the isotropic plastic strain increment $d\varepsilon_{ij}^{p\,\mathrm{IC}}$ under increasing mean stress), and the positive dilatancy during strain hardening and the influence of density and/or confining pressure on the deformation and strength by introducing subloading surface concept (Hashiguchi and Ueno, 1977; Hashiguchi, 1980). This model has been, furthermore, applied to solve several boundary or initial value problems and the validity of the simulation based on the model are verified by comparing with experimental results of the element tests (triaxial test, hollow cylinder test, true triaxial and others) and those of 1G model experiments on several geotechnical problems such as ground excavation, bearing capacity of foundation and stability of embankment and retaining wall.

Although the subloading $t_{ij}$ model can more properly describe the stress-strain behavior of soils than original Cam clay model, it cannot directly be applied to various types of actual ground yet. This is because that, as shown in Figure 1.1, soil generally lies under a partially saturated state is always changing with temperature and hydraulic condition and because it has a certain interparticle bond which developed during long time process of sedimentation in the field. In addition, soil may experience non-monotonic and complex stress change in practical geotechnical phenomena such as earthquake, i.e., relative difference of three principal stresses, rotation of principal stress axis, cyclic loading and others, which is difficult to be reproduced in laboratory test. Although such complex features are not negligible characteristics in order to predict the actual ground behavior precisely, a unified model considering such features has never been developed. In this study, a constitutive model for the saturated, remolded soil, viz., subloading $t_{ij}$ model, is extended to one taking into account of essential factors which cannot be neglected to predict actual soil behavior, particularly the influence of the bonding, unsaturated condition and an irregular stress path.

These features of soil which have been treated individually should be considered in a unified manner in constitutive model. In addition, it is also important to formulate a model based on simples and widely-accepted assumptions with a small number of material parameters. The outlines of the modeling in this study are shown in following terms.

a) Background of theory is clear and concise – modeling based on meaningful assumptions which can be accepted by many researchers and engineers
b) Objectivity – constitutive parameters have a clear physical meaning and its values are determined easily from general element tests in laboratory.
c) Applicability and versatility – a model can precisely simulate a various actual phenomena and give a valuable result to figure out the mechanism of such phenomena.

If a constitutive model based on above conceptions is developed, it seems that numerical simulation based on

such model can properly predict the deformation and failure of actual ground during multi-hazard such as simultaneous occurrence of earthquake and torrential rainfall.

## 1.2 Framework of the thesis

### Chapter 1 Introduction

Chapter 1 firstly shows the backgrounds and objectives of this study with indicating some features of soils which is not taken into consideration in the Cam clay model and subsequent models overcoming weak points of Cam clay model, and the outlines of this thesis.

### Chapter 2 Constitutive model describing the various isotropic influences on saturated soil

In Chapter 2, the elastoplastic volume behavior of geo-materials firstly considered as simple one-dimensional behavior which is the relation between one dimensional stress $\sigma$ and void ratio $e$ and easy to understand the elastoplastic soil behavior. Moreover, it can be easily extended to one which can consider various characteristics of soil, viz., density, natural deposited bond, temperature dependency, strain rate effect, and others. Firstly, the outline of modeling behavior of normally consolidated soil will be explained, and then this will be extended to one taking account of the influence of density and the bonding effect observed in natural deposited soil in a uniform manner. In addition, one-dimensional constitutive model will be extended to an ordinary multi-dimensional (three-dimensional) model by adding a term of stress ratio to yield function. In order to consider the influence of relative difference of three principal stresses in the multi-dimensional model, then, the modified stress tensor $t_{ij}$ (Nakai and Mihara, 1984) instead of ordinary stress tensor $\sigma_{ij}$ is used for formulating the yield function. As a result of such extension, the isotropic hardening subloading $t_{ij}$ model (Nakai and Hinokio, 2004) will be derived from the one-dimensional model considering the influence of density.

In this chapter, furthermore, a model considering the influence of other factors, which isotropically affect on stress-strain relations of soils as well as the influence of density and bonding, such as temperature, strain rate, partial saturated condition is proposed. Through a careful review of the past experimental results for each external factor, it is assumed that a position of the normally consolidated line (*NCL*), which is regarded as the reference state to evaluate the soil state for density, is shifted to upward / downward according to the variation with each parameter, e.g., degree of saturation, suction, temperature, time and strain rate.

### Chapter 3 Constitutive model describing the influence of the suction and the degree of saturation on unsaturated soil

The mechanical characteristic of unsaturated soils is variously changing due to the magnitude of suction and degree of saturation, and it is more complex than that of saturated soils. It should, however, be described properly as all ground. For unsaturated soil, the experimental and analytical verification have been actively conducted. It is difficult, however, to get the reproducible experimental results due to difficulty of making uniform specimen unsaturated condition even in laboratory elementary test, which also requires a long time

and specialized testing apparatus and procedure. Hence, various types of constitutive model and assumption for modeling of unsaturated soils have ever been proposed. It can be understood for such affairs of modeling that selection of the stress tensor is needed to formulate a model for unsaturated soils: existing model for unsaturated soils are mainly formulated by single effective stress or double stresses of net stress and suction.

In Chapter 3, typical behaviors of unsaturated soils obtained from past experiments are firstly reviewed and summarized in order to discover a determine law and points of concern for modeling, and then the constitutive model is constructed with reference to such results. As a result of such investigating the past experimental results, the proper effective stress for organizing the experimental results and formulating the constitutive equation is selected; a constitutive model for unsaturated soils based on this effective stress is developed in a same manner as modeling of external factors shown in Chapter 1; Ordinary soil water characteristic curve calculating degree of saturation $S_r$ is extended to one considering the influence of drying / wetting history and density. In order to verify the validation of proposed mode, the parametric study in which typical element tests such as compression test, soaking test and triaxial shear test are carried out. In addition, the simulation of compaction behavior of soil is carried out by using the proposed model in this study.

### Chapter 4 Constitutive model describing the induced anisotropy on granular material

The stress-strain characteristic of soil is affected not only by scalar indices such as density, bonding, degree of saturation, suction, temperature, and others, but also by tensorial variable which is caused by the variation in the orientations of particles due to stress change. It is easy to understand that stiffness and strength of soil in depositional direction is generally larger than that in the perpendicular direction, and this effect is called “the inherent anisotropy”. On the other hand, anisotropic stress-strain characteristics of soils exhibited due to the past stress history is widely known as “the (stress) induced anisotropy”. Especially, since the influence of the induced anisotropy can be seen in any stress path, e.g., relative difference of three principal stresses, rotation of principal stress axis, cyclic loading and others, its modeling is essential.

It is well known that the stress induced anisotropy is related closely to the concentration of the interparticle contact normals. In order to represent such situation of microscopic interparticle contact (contact normals and long axis direction of particles) of geomaterials, a second order tensor quantity such as fabric tensor (e.g., Satake (1982)) is widely used. Although the constitutive model using such tensor quantity has been proposed (e.g., Oda (1993) and Dafalias et al. (2004)), the fabric change has never been adequately considered in those models because the prediction of the variation of the fabric due to any stress path is difficult. In Chapter 4, modified stress tensor transformed by such fabric tensor and the isotropic hardening model based on this modified stress are proposed. From referring to the past investigations of the induced anisotropy, then, the evolution of fabric is properly prescribed. The proposed method is verified by the parametric study and comparison with the experimental results of triaxial tests on Toyoura sand, true triaxial tests and directional shear tests on medium dense Leighton Buzzard sand.

### Chapter 5 Conclusion

In Chapter 5, finally, this thesis is concluded with showing the summary of each chapter and the future prospects of this study.

## Reference


Adachi, T. and Oka, F. (1982): Constitutive equations for normally consolidated clay based on elasto-viscoplasticity, *Soils and Foundations*, Vol. 22, No. 4, 57–70.

Alonso, E. E., Gens, A. and Josa, A. (1990): A constitutive model for partially saturated soils, *Geotechnique*, Vol. 40, No. 3, 405-430.

Asaoka, A., Noda, T., Yamada, E., Kaneda, K. and Nakano, M. (2000): Superloading yield surface concept for highly structured soil behavior, *Soil and Foundations*, Vol. 40, No. 2, 99-110.

Dafalias, Y. F. (1986): Bounding Surface Plasticity. I: Mathematical Foundation and Hypoplasticity, *Journal of Engineering Mechanics*, Vol. 112, No. 9, 966-987.

Dafalias, Y. F., Papadimitriou, A. G. and Li, X. S. (2004): Sand plasticity model accounting for inherent fabric anisotropy, *Journal of Engineering Mechanics*, Vol. 130, No. 11, 1319-1333.

Dafalias, Y. F., Manzari, M. T. and Papadimitriou, A. G. (2006): Simple anisotropic clay plasticity model, *Int. J.Numer. Anal. Meth. Geomech*, Vol. 30, No. 12, 1231–1257.

Fredlund, D. G. and Xing, A. (1994): Equation for the soil-water characteristic curve, *Can. Geotech. J*, Vol. 31, No. 3, 521-532.

Gallipoli, D., Wheeler, S. J. and Karstunen, M. (2003): Modelling the variation of degree of saturation in a deformable unsaturated soil, *Geotechnique*, Vol. 53, No. 1, 105-112.

Hashiguchi, K. (1980): Constitutive equation of elastoplastic materials with elasto-plastic transition, *J. of Applied Mech.*, ASME, 102(2), 266-272.

Hashiguchi, K. and Okayasu, T. (2000): Time-dependent elastoplastic constitutive equation based on the subloading surface model and its application to soils, *Soils and Foundations*, Vol. 40, No. 4, 19-36.

Hashiguchi, K. (2001): Description of inherent / induced anisotropy of soils: rotational hardening ruled with

objectivity, *Soils and Foundations*, Vol. 41, No.6, 139-145.

Hueckel, T. and Borsetto, M (1990): Thermoplasticity of saturated soils and clays: constitutive equations, J. Geotech. Engng., Vol. 116, No. 12, 1765-1777.

Kohgo, Y., Nakano, M. and Miyazaki, T. (1993): Theoretical aspects of constitutive modeling for unsaturated soils, *Soils and Foundations*, Vol. 33, No. 4, 49-63.

Koiter, W. T. (1953): Stress-strain relations, uniqueness and variational theorems for elastic-plastic materials with a singular yield surface, *Q. Appl. Math*, Vol. 11, 350–354.

Lade, P. V. and Duncan, J. M. (1975): Elastoplastic stress-strain theory for cohesionless soil, ASCE: *J. Geotech. Eng. Div*, Vol. 101, No. 10, 1037-1053.

Laloui, L. and Cekerevac, C. (2003): Thermo-plasticity of clays: An isotropic yield mechanism, *Computers and Geotechnics*, Vol. 30, No. 8, 649-660.

Li, X. S. and Dafalias, Y. F. (2002): Constitutive modelling of inherently anisotropic sand behaviour, *J. Geotech. Geoenviron. Engng, ASCE*, Vol. 128, No. 10, 868–880.

Loret, B. and Khalili, N. (2002): An effective stress elastic-plastic model for unsaturated porous media, *Mechanics of Materials*, Vol. 34, 97-116.

Matsuoka, H. and Nakai, T. (1974): Stress-strain and strength characteristics of soil under three different principal stresses, *Pro. JSCE*, Vol. 232, 59-70.

Nakai, T. and Mihara, Y. (1984): A new mechanical quantity for soils and its application to elastoplastic constitutive models, *Soils and Foundations*, Vol. 24, No. 2, 82–94.

Nakai, T. and Matsuoka, H. (1986): A generalized elastoplastic constitutive model for clay in three-dimensional stresses, *Soils and Foundations*, Vol. 26, No. 3, 81-98.

Nakai, T. and Hinokio, M. (2004): A simple elastoplastic model for normally and over consolidated soils with unified material parameters, *Soils and Foundation*, Vol. 44, No. 2, 53-70.

Oda, M. (1989): Yield function for soil with anisotropic fabric, *J. Engrg. Mech. Div*, Vol. 115, No. 1, 89-104.

Oda, M. (1993): Inherent and induced anisotropy in plasticity theory of granular soils, *Mechanics of Materials*,

Vol. 16, Issues 1-2, 35-45.

Roscoe, K. H. and Burland, J. B. (1968): On the generalized stress-strain behavior of ‘wet’ clay, *Engineering plasticity (eds J. Heyman and F. A. Leckie)*, Cambridge: Cambridge University Press., 535-609.

Rudnicki, J. W. and Rice, J. R. (1975): Conditions for the localization of deformation in pressure-sensitive dilatant materials, *Journal of the Mechanics and Physics of Solids*, Vol. 23, No. 6, 371-394.

Satake, M. (1982): Fabric tensor in granular materials, *Proc. of IUTAM-Conference on Deformation and Failure of Granular Materials*, pp. 63-68.

Schofield, A. N. and Wroth, C. P. (1968): *Critical State Soil Mechanics*, McGraw Hill, London.

Sekiguchi, H. (1977): Rheological Characteristics of Clays, *Proceedings 9th International Conference on Soil Mechanics and Foundation Engineering*, Japan, 289-292.

Sekiguchi, H. and Ohta, H. (1977): Induced anisotropy and time dependency in clays, Constitutive equations of soils, *Proc., 9th Int. Conf. on Soil Mechanics and Foundation Engineering*, Tokyo, 229–238.

Spencer, A. J. M. (1964): A theory of the kinematics of ideal soils under plane strain conditions, *Journal of the Mechanics and Physics of Solids*, Vol. 12, No. 5, 337–351.

Tobita, Y. (1988): Contact tensor in constitutive model for granular materials. *Proceedings of the US–Japan seminar on micromechanics of granular materials*, Sendai, 263–270.

Van Genuchten, M. Th. (1980): A closed-from equation for predicting the hydraulic conductivity of unsaturated soils, *Soil Sci. Soc. Am. J*, Vol. 44, 892-898.

Wheeler, S. J. and Sivakumar, V. (1995): An elasto-plastic critical state framework for unsaturated soil, *International Journal of Geotechnique*, Vol. 45, No. 1, 35-53.

Yashima, A., Leroueil, S., Oka, F. and Guntoro, I. (1998): Modeling temperature and strain rate dependent behavior of clays: one dimensional consolidation, *Soils and Foundations*, Vol. 38, No. 2, 63-78.

# Chapter 2
# Constitutive model describing the various features of saturated soil

## 2.1 General

The stress-strain behavior of geo-materials is significantly different depending on the magnitude of overconsolidation ratio (OCR): soil having larger OCR exhibits stiffer behavior and soil having smaller OCR (viz., nearly normally consolidated soil) exhibits softer behavior; over consolidated soil shows elastoplastic behavior even in elastic region; positive dilatancy occurs with strain hardening. Such influences of overconsolidation ratio are taken into consideration by introducing the subloading surface concept (Hashiguchi and Ueno, 1977; Hashiguchi, 1980) and the bounding surface concept (Dafalias, 1986). Considering the difference between current void ratio and that on normally consolidated line, subloading $t_{ij}$ model proposed by Nakai and Hinokio (2004) describes such behaviors of overconsolidated soil. This method is similar to subloading surface concept.

The behavior of a natural deposited soil (undisturbed soil) is more complex than that of the remolded soil, even if the density (overconsolidation ratio) of those soils is the same. This is because that a certain interparticle bonding effect (structured) developed during deposition process in natural ground. It is generally known that such structured soil can exist in a region where void ratio is greater than that of non-structured normally consolidated soil under the same stress level. And structured soil exhibits more brittle and more compressive behavior due to reduction of structure than non-structured soil as shown in Figure 2.1. Asaoka et al. (1998 and 2000) developed a model to describe such structured soils by introducing subloading surface and superloading surface concepts to the Cam-clay model. In their modeling, a factor relating to the over consolidation ratio (corresponding to imaginary density) increases the stiffness, and a factor relating to the soil skeleton structure decreases the stiffness. By controlling the evolution rules of these factors, they described various complex behaviors of structured soils.

In this study, however, it is supposed that interparticle bonding which is similar to soil structure just increases the stiffness of soil. And the density and bonding are considered that these factors affect on the

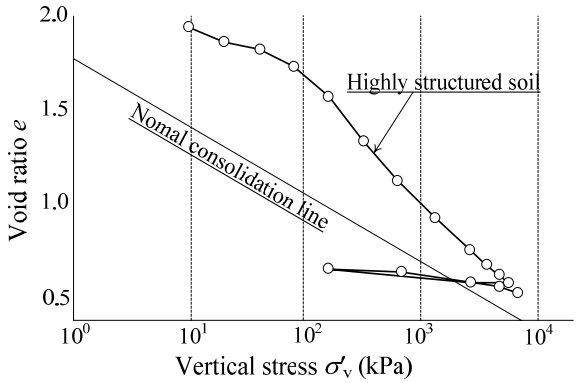


Figure 2.1 Compression behavior of structured soil (Asaoka, 2000)

stress-strain relation of soil isotropically, viz., soil doesn't exhibit anisotropic behavior due to incorporating such factors. In other words, the effects of these factors can be formulated with the variation in scalar quantity (e.g., $R$ in the concept of subloading surface and $R^*$ in the concept of superloading surface) in a modeling. And, isotropic compression behavior (the relation between void ratio $e$ and mean stress $p$) is easy to investigate the characteristic of isotropic material. In this chapter, thus, the modeling of the isotropic characteristic, which is simplified to one-dimensional problem (the relation between one-dimensional stress $\sigma$ and void ratio $e$), is focused on. Firstly, the modeling of behavior of normally consolidated soil will be explained, and this model will be extended to one representing the influence of density and the bonding observed in natural deposit soil in a unified manner. And, a model considering the influences of temperature, strain-rate, partial saturated condition and others which also affect on stress-strain relation of soil isotropically, as well as the influences of density and bonding, are also proposed in this study. Through a careful review of the past experimental results for each external factor, it is supposed that the position of the normally consolidated line is shifted with directly changing of each parameter (e.g., temperature $T$, time $t$ (strain rate $\dot{\varepsilon}$), degree of saturation $S_r$ and suction). Based on this assumption, one-dimensional model considering various external factors is developed. The validity of each one-dimensional model is checked by simulations of one-dimensional consolidation tests for normally consolidated, over consolidated and natural soils. The applicability of modeling for external features of soils is verified by the one-dimensional consolidation with different and changing temperature and strain rate.

Naturally, the multi-dimensional (three-dimensional) relation between ordinary stress tensor $\sigma_{ij}$ and strain tensor $\varepsilon_{ij}$ should be constructed in this study. The one-dimensional model can be extended to such multi-dimensional model easily by formulating the stress function $F$ in yield function based on the parameters of stress tensor. And then, in order to take account of the influence of the relative magnitude of intermediated stress $\sigma_2$, the modified stress $t_{ij}$ (Nakai and Mihara, 1984) is used instead of ordinary stress $\sigma_{ij}$. The validity of the multi-dimensional models is checked by simulations of various shear tests for over consolidated clay with different OCR and for over consolidated and natural clays under drained and undrained conditions, for over consolidated clay with different temperature and strain rates.

The substance of this chapter has been published as follows: Kyokawa et al. (2007), Nakai et al. (2009(a) and (b)) and Shahin et al. (2010).

## 2.2 One-dimensional elastoplastic model for granular materials

### 2.2.1 Modeling of normally consolidated soil and Explanation of one-dimensional behavior of soils

Figure 2.2 shows a typical relation between void ratio $e$ and logarithmic mean effective stress $p'$ of normally consolidated soil during isotropic consolidation (Chowdhury, 1998), which is described in many text books of soli mechanics. In this figure, soil exhibits compression behavior on normally consolidated line (*NCL*) whose gradient is represented as $\lambda$ during loading, and swelling behavior on swelling line whose gradient is $\kappa$ during unloading. These behaviors are appropriately represented in a model. Figure 2.3 schematically illustrates the variation in void ratio when a stress condition moves from the initial state I ($\sigma = \sigma_0$, $e = e_0$) to the current state P ($\sigma = \sigma$, $e = e$) in one-dimensional plane ($\sigma$ vs. $e$). Here, $\sigma_0$ and $\sigma$ represent the initial one-dimensional stress and current one, $e_{N0}$ and $e_N$ are the corresponding void ratio on the normally consolidated line to each stress level, respectively. Then total change in void ratio ($-\Delta e$) of normally consolidated soil is expressed as

$$(-\Delta e) = e_0 - e = e_{N0} - e_N = \lambda \ln \frac{\sigma}{\sigma_0} \tag{2.1}$$

and, its elastic (recoverable) component ($-\Delta e^e$) is assumed to follow the usual nonlinear elastic relationship as given by Equation (2.2).

$$(-\Delta e)^e = \kappa \ln \frac{\sigma}{\sigma_0} \tag{2.2}$$

Here, $\kappa$ is swelling index. The plastic (irrecoverable) component ($-\Delta e^e$) is then given by difference in total change of void ratio and its elastic component as follows

$$(-\Delta e)^p = (-\Delta e) - (-\Delta e)^e = (\lambda - \kappa) \ln \frac{\sigma}{\sigma_0} \tag{2.3}$$

where $\lambda$ is compression index. A yield function $f$ of the general theory of plasticity is expressed as Equation (2.4), if the change in plastic component of void ratio is given as a strain hardening parameter.

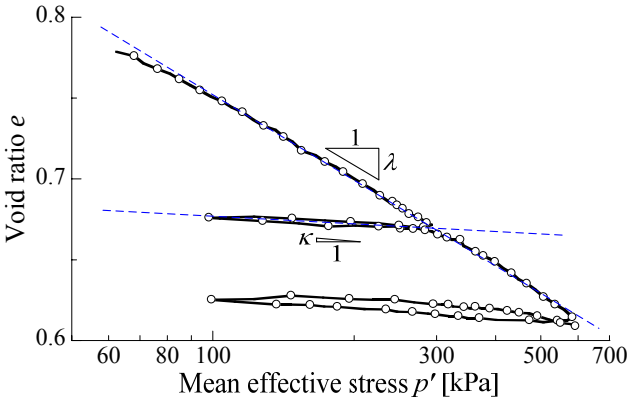


Figure 2.2 Observed results of isotropic consolidation test on Fujinomori clay – loading and unloading path (after Chowdhury, 1998)

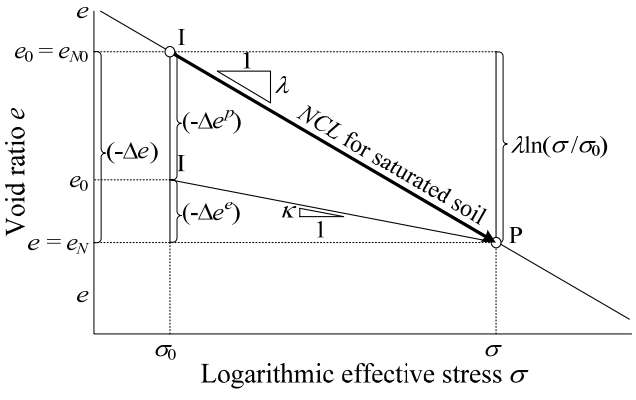


Figure 2.3 Schematic behavior of normally consolidated soil in one-dimensional problem

$$f = F - H = 0 \ \ where \ \ F = (\lambda - \kappa)\ln\frac{\sigma}{\sigma_0}, \ H = (-\Delta e)^p \tag{2.4}$$

Soil behaves perfect elastically, if yield function (2.4) is negative ( $f < 0$). Then, the increment of elastic change in void ratio is expressed as follows from Equation (2.2):

$$d(-e)^e = \kappa \ln\frac{d\sigma}{\sigma} \tag{2.5}$$

On the other hand, the increment of plastic change in void ratio is expressed as following from Prager's consistency condition ( $f = 0$ and $df = 0$), which means the current stress state continually lies on the yield point (surface) when plastic deformation occurs.

$$\begin{aligned} df &= dF - dH = (\lambda - \kappa)\ln\frac{d\sigma}{\sigma} - d(-e)^p = 0 \\ \therefore d(-e)^p &= (\lambda - \kappa)\ln\frac{d\sigma}{\sigma} \end{aligned} \tag{2.6}$$

The increment of total change in void ratio is given by the summation of Equations (2.5) and (2.6), and it is expressed in a form of elastoplasticity as

$$d(-e) = d(-e)^p + d(-e)^e = \{(\lambda - \kappa) + \kappa\}\frac{d\sigma}{\sigma} \tag{2.7}$$

The computed result is shown in Figure 2.4. In reloading path DC, the computed result shows perfect elastic behavior unlike with observed elastoplastic behavior. In early stage of this chapter, the elastoplastic behavior of soil is expressed on the basis of such one-dimensional problem. By explaining the elastoplastic behavior of soil based on one-dimensional problem, it is easy to understand some features of soils effecting on deformation and strength characteristics. And, this one-dimensional model will be extended to the corresponding multi-dimensional one which describes the ordinary stress-strain ($\sigma_{ij}$ - $\varepsilon_{ij}$) relation later.

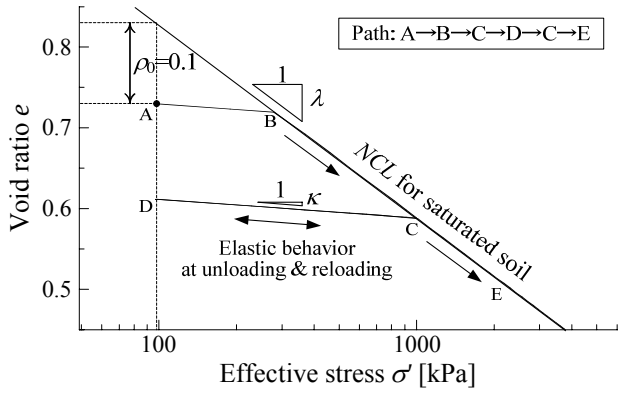


Figure 2.4 Calculated compression behavior of normally consolidated soil in one-dimensional problem

### 2.2.2 Extension of the model for normally consolidated soil to one considering the over consolidated state

It is known that under one-dimensional consolidation (or isotropic consolidation) remolded normally consolidated soil shows typical strain-hardening elastoplastic behavior, so that clay is assumed to be non-linear elastic in the region where the current stress is smaller than the yield stress (over consolidation! region). However, it can be seen from Figure 2.5, which shows a typical behavior of over consolidated saturated soil during consolidation process, that soil behaves elastoplastically even in an over consolidated region. And then, the stiffness of soil is higher than saturated normally consolidated soil. Additionally, soil gradually approaches to *NCL* for saturated soil according to increasing stress level. In the proposed model, these behavior is explained by using the density state variable $\rho$ ($\geq 0$), which is defined as the difference of void ratios of current state and normal consolidation state under the same confining pressure. The heavily overconsolidated soil, therefore, has large magnitude of $\rho$.

Figure 2.6 illustrates the variation in void ratio when the stress condition moves from the initial state I ($\sigma = \sigma_0$, $e = e_0$) to the current state P ($\sigma = \sigma$, $e = e$) on over consolidated state. Here, $e_{N0}$ and $e_N$ are the corresponding void ratio on the normally consolidated line to each stress level as mentioned in former section. The difference of void ratio between over consolidated soil and normally consolidated soil under the same stress level is expressed as the change from $\rho_0 (= e_{N0} - e_0)$ to $\rho (= e_N - e)$. By using the state variable $\rho$, the total change of void ratio $\Delta e$ of over consolidated soil is obtained as follows

$$(-\Delta e) = (e_{N0} - e_N) - (\rho_0 - \rho) = \lambda \ln \frac{\sigma}{\sigma_0} - (\rho_0 - \rho) \tag{2.8}$$

and its plastic component is given as Equation (2.9) by assuming same elastic relation shown in Equation (2.5) for normally consolidated soil.

$$(-\Delta e)^p = (-\Delta e) - (-\Delta e)^e = (\lambda - \kappa) \ln \frac{\sigma}{\sigma_0} - (\rho_0 - \rho) \tag{2.9}$$

By the same way for normally consolidated soil, a yield function $f$ is expressed as follows

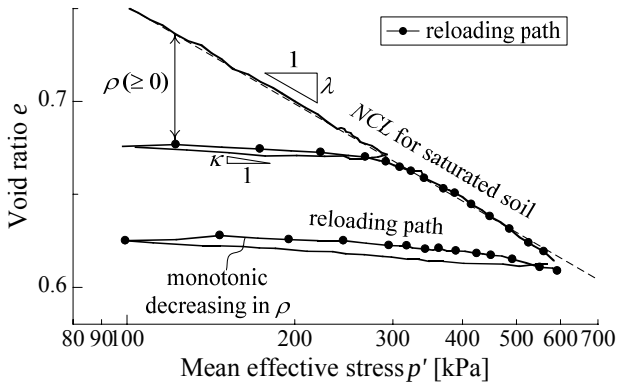


Figure 2.5 Observed results of isotropic consolidation test on Fujinomori clay (after Chowdhury, 1998) - plots represent reloading path and definition of state variable $\rho$

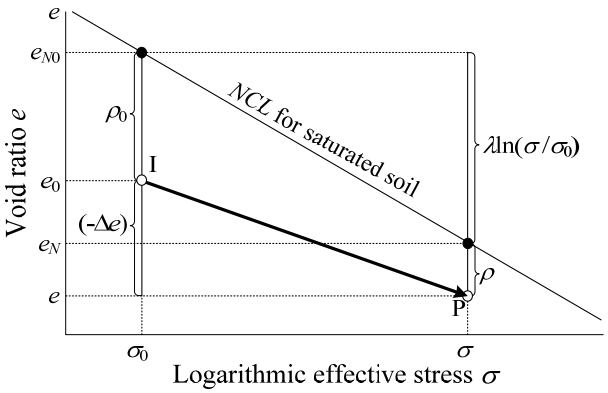


Figure 2.6 Schematic behavior of over consolidated soil in one-dimensional problem

$$f = F - \{H + (\rho_0 - \rho)\} = 0 \ \ where \ \ F = (\lambda - \kappa)\ln\frac{\sigma}{\sigma_0}, H = (-\Delta e)^p \tag{2.10}$$

And now, it can be assumed that the state variable $\rho$ decreases with the development of the plastic deformation (volume contraction) and finally converges to zero, which means soil reaches to the normally consolidated state ($\rho$ = 0). Equation (2.11), which satisfies such requirements, is applied as an evolution law for the state variable $\rho$.

$$d\rho = -G(\rho)\cdot d(-e)^p = -a\rho\cdot d(-e)^p \tag{2.11}$$

Here, the function $G(\rho)$, which satisfies that it is an increasing function and $G(0) = 0$, is given as a simple linear function $G(\rho) = a\rho$. $a$ is a material parameter controlling the effect of density. Finally, the one-dimensional constitutive relationship of saturated over consolidated soil is obtained from the consistency condition ($df = 0$) as follows.

$$\begin{aligned} &df = dF - (dH + d\rho) = (\lambda - \kappa)\ln\frac{d\sigma}{\sigma} - \{d(-e)^p - d\rho\} = (\lambda - \kappa)\ln\frac{d\sigma}{\sigma} - d(-e)^p \cdot \{1 + G(\rho)\} = 0 \\ &\therefore d(-e)^p = \left\{\frac{\lambda - \kappa}{1 + G(\rho)}\right\}\ln\frac{d\sigma}{\sigma} \end{aligned} \tag{2.12}$$

$$d(-e) = d(-e)^p + d(-e)^e = \left[\left\{\frac{\lambda - \kappa}{1 + G(\rho)}\right\} + \kappa\right]\frac{d\sigma}{\sigma} \tag{2.13}$$

As seen from the above equation, $G(\rho)$ has an effect to increases the stiffness of soil, and its effect becomes large with the increase of the value of $\rho$. After $\rho$ becomes zero for decreasing $\rho$, Equation (2.13) corresponds with Equation (2.7) for normally consolidated soil. The method to consider the influence of density presented here, in a sense, corresponds to a one-dimensional interpretation of the subloading surface concept by Hashiguchi (1980).

Figure 2.7 shows the simulations of one-dimensional consolidation for over consolidated soil having different initial void ratio ($e_0$ = 0.63, 0.73). Assuming Fujinomori clay which is used in the previous experimental verification of constitutive models (e.g., Nakai and Hinokio, 2004; Nakai, 2007), following

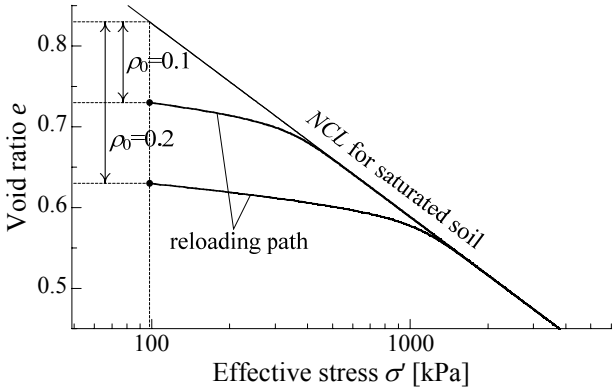


Figure 2.7 Calculated compression behavior of over consolidated soil in one-dimensional problem. Soil shows elastoplastic stiffer behavior in elastic region.

material parameters are employed in the numerical simulations – compression index $\lambda = 0.104$, swelling index $\kappa = 0.010$, void ratio on *NCL* at $\sigma = 98$kPa (atmospheric pressure) $N = 0.83$ and the influence of density $a = 100$. From Figure 2.7, the typical behavior of over consolidated soil as discussed above is suitably described by the proposed model. Furthermore, the proposed model can represent the influence of the difference of initial void ratio which means the stiffness of dense sample is higher.

The state variable $\rho$ is newly added to the model for normally consolidated soil in Equation (2.10), and its evolution rule in Equation (2.11) is reflected on its present value as $G(\rho)$. It should be paid attention that the stiffness of over consolidated soil is affected only by the magnitude of current $\rho$. In next section, the modeling of the influence of the bonding is conducted by considering this relation between the evolution rule of the state variable $\rho$ and the stiffness of soil.

### 2.2.3 Modeling of the natural deposited soil having the bonding effect

Figure 2.8 shows the typical behavior of natural deposited soil in which the stiffness of soil is initially larger than that of the reconstituted remolded soil indicated as solid line, and the natural soil retains a looser void ratio. The large compression behavior, however, occurs from a certain stress level, and then soil gradually approaches to the normally consolidated line (solid line). Such structured soil shows more brittle and more compressive behavior than non-structured soil. It is, therefore, difficult to determine such parameters as the consolidation yielding stress (e.g., $p_f$, $q_f$) and compression index $\lambda$ (or $C_c$) for naturally deposited soil. These complicated behaviors of natural soil are caused by variation in the bonding effect (structured) which develops in the depositional process. Here, a soil structured is different from the particle columns due to the concentration of particles normals which cause the soil anisotropy. So, such bonding effect increases an isotropic stiffness of soil. In this section, the model for saturated over consolidated soil shown in the previous section is extended to one considering this bonding effect.

Figure 2.9 illustrates the variation in void ratio when the stress condition moves from the initial state I ($\sigma = \sigma_0$, $e = e_0$) to the current state P ($\sigma = \sigma$, $e = e$) on over consolidated state with bonding effect. Then,

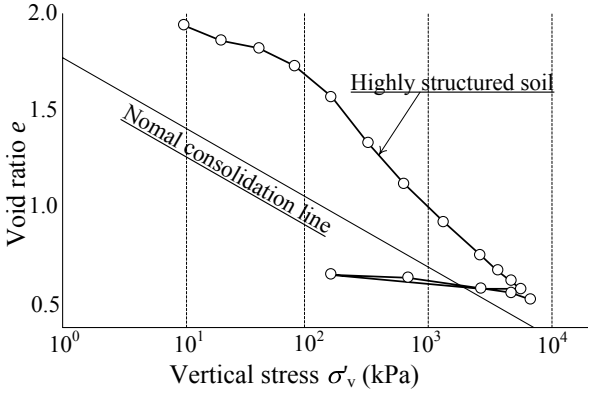


Figure 2.8 Observed results of isotropic consolidation test on highly structured clay (after Asaoka, 2000). Soil can exist in looser state than *NCL*

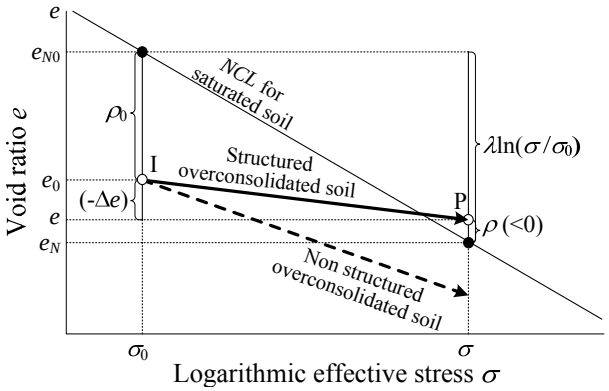


Figure 2.9 Schematic behavior of over consolidated structured soil in one-dimensional problem. Structured soil is stiffer than over consolidated soil having same state variable $\rho$

the variation in void ratio and its plastic component are same as Equation (2.8) and (2.9) considering the change of the state variable $\rho$.

$$(-\Delta e) = (e_{N0} - e_N) - (\rho_0 - \rho) = \lambda \ln \frac{\sigma}{\sigma_0} - (\rho_0 - \rho) \tag{2.14}$$

$$(-\Delta e)^p = (-\Delta e) - (-\Delta e)^e = (\lambda - \kappa) \ln \frac{\sigma}{\sigma_0} - (\rho_0 - \rho) \tag{2.15}$$

A yield function $f$, moreover, is same as Equation (2.10)

$$f = F - \{H + (\rho_0 - \rho)\} = 0 \ \ where \ \ F = (\lambda - \kappa) \ln \frac{\sigma}{\sigma_0}, H = (-\Delta e)^p \tag{2.16}$$

The arrow with broken line, however, denotes the same change of void ratio as that in Figure 2.6 for over consolidated soil. So, it can be understood that the structured soil is stiffer than non-structured over consolidated soil, even if the state variable $\rho$ is the same. The state variable $\rho$, moreover, can be negative value for structured soil as shown in Figure 2.9. This is because that although soil exists on *NCL* ($\rho = 0$), it can show stiffer behavior than normally consolidated soil due to current bonding effect. Consequently, soil can go into a looser region above *NCL* ($\rho < 0$). Considering such change of the state variable $\rho$, it changes under the influence of not only current density $\rho$ but also current bonding which is expressed as $\omega$. And larger value of the state variable $\omega$ has more effect the degradation of $\rho$. Such effect on the evolution rule of $\rho$ is considered as

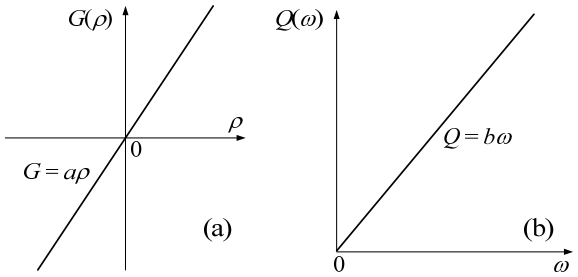

Figure 2.10 The functions $G(\rho)$ and $Q(\omega)$ in the evolution rule of state variables $\rho$ and $\omega$. Both functions are linear function for simple modeling in this study

$$d\rho = -L(\rho, \omega) \cdot d(-e)^p = \{G(\rho) + Q(\omega)\} \cdot d(-e)^p = -(a\rho + b\omega) \cdot d(-e)^p \tag{2.17}$$

Although the function $G(\rho)$ is same function shown in Equation (2.11), its negative region ($\rho < 0$) is considered for structured soil shown in Figure 2.10. On the other hand, the function $Q(\omega)$ is an increasing function and $Q(0) = 0$ and given as a simple linear function $Q(\omega) = b\omega$. $b$ is a material parameter controlling the effect of bonding. For the function $Q(\omega)$, the region of positive value of $\omega$ is treated. Shapes of these functions are shown in Figure 2.10. Since it is assumed that the bonding monotonically diminishes with development of the plastic deformation, the evolution rule of bonding $\omega$ is given as

$$d\omega = -Q(\omega) \cdot d(-e)^p = -b\omega \cdot d(-e)^p \tag{2.18}$$

Here, for simple modeling, the evolution rule of bonding $\omega$ is constructed with function $Q(\omega)$, which is the same function affecting on the evolution of $\rho$. The increment of the plastic change in void ratio for structured soil can be calculated using Prager's consistency condition ($df = 0$) in the same way as above two models.

$$df = dF - (dH + d\rho) = (\lambda - \kappa)\ln\frac{d\sigma}{\sigma} - \{d(-e)^p - d\rho\}$$

$$= (\lambda - \kappa)\ln\frac{d\sigma}{\sigma} - d(-e)^p \cdot \{1 + G(\rho) + Q(\omega)\} = 0 \tag{2.19}$$

$$\therefore d(-e)^p = \left\{\frac{\lambda - \kappa}{1 + G(\rho) + Q(\omega)}\right\}\ln\frac{d\sigma}{\sigma}$$

Finally, assuming the same manner of elastic relationship as that of normally consolidated soil, the one-dimensional constitutive relationship of saturated structured soil is expressed as follows.

$$d(-e) = d(-e)^p + d(-e)^e = \left[\left\{\frac{\lambda - \kappa}{1 + G(\rho) + Q(\omega)}\right\} + \kappa\right]\frac{d\sigma}{\sigma} \tag{2.20}$$

As seen from the above equation, $Q(\omega)$, which consistently indicate positive value, has an effect to increase the stiffness of soil, and its effect becomes large with the increase of the value of $\omega$. On the other hand, the function $G(\rho)$ gives a positive value when the void ratio of soil is downside of the *NCL* ($\rho > 0$), and vice versa. The stiffness soil, thus, intricately changes in response to the magnitude of the state variables $\rho$ and $\omega$, and is divided into three regions as shown in Figure 2.11. Region I ($\rho > 0$ and $\omega > 0$); The stiffness of the soil is much larger than that of normally consolidated soil and over consolidated soil having same value of $\rho$, because of the positive values of $G(\rho)$ and $Q(\omega)$. Moreover, even if the current void ratio becomes the same as that on *NCL* ($\rho = 0$), the stiffness of the soil is still larger than that of NC soil. So, it is possible for the structured soil to have the state which is looser than that on *NCL*. Region II ($\rho < 0$ and $\omega > 0$, $G(\rho) + Q(\omega) > 0$); In this region, the function $G(\rho)$ shows negative value which decreases the stiffness of soil, and the function $Q(\omega)$ consistently shows positive value which increases the stiffness. The effect on increase the stiffness by the positive value of $\omega$ is larger than the effect to decrease the stiffness by the negative value of $\rho$, thus soil keeps a larger stiffness than that of normally consolidated soil. The bonding which increases the stiffness, however, diminishes with the development of plastic deformation. Region III ($\rho < 0$ and $\omega > 0$, $G(\rho) + Q(\omega) < 0$); The effect of $\rho$ to decrease the stiffness becomes prominent because of the negative value of $\rho$, and its effect is larger than increase the stiffness by positive bonding $\omega$. Therefore, the stiffness of soil is

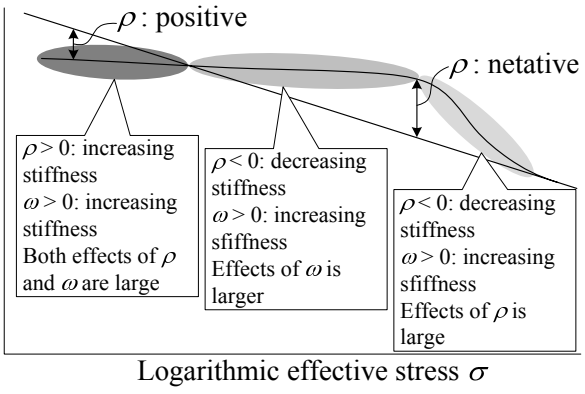


Figure 2.11 Behavior of structured soil affected by the magnitudes of the state variable $\rho$ and $\omega$

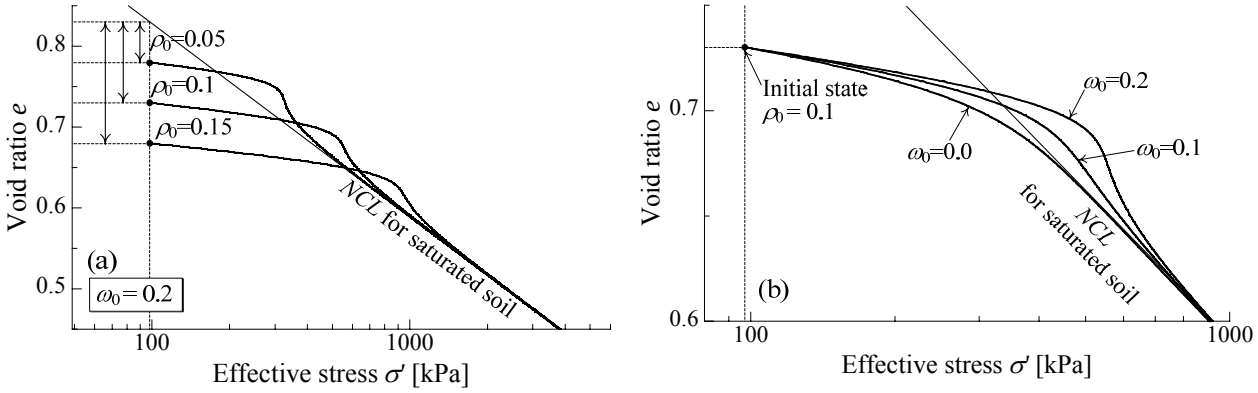


Figure 2.12 Calculated compression behaviors of structured soil having (a) different initial density & same bonding, and (b) different initial bonding & same density – proposed model can represents the influence of bonding on compression behavior of soil and its degradation.

smaller than that of normally consolidated soil, and then the summation of function $G(\rho)$ and $Q(\omega)$ is negative. In this region, the void ratio approaches to that on *NCL*, because $\rho$ and $\omega$ converge to zero. That is to say, though $Q(\omega)$ is approaching to zero with the development of plastic deformation, $G(\rho)$ has an effect for the current void ratio to lie on *NCL*.

In order to verify the performance of the proposed model for structured soil, simulations of one-dimensional compression test on various type of soil with different initial density and bonding have been conducted. Figure 2.12(a) shows the calculated relations between void ratio $e$ and logarithmic stress $ln\sigma$ on the samples with same initial bonding ($\omega_0$ = 0.2) and different initial density. Another diagram (b) shows the calculated results using the same initial void ratio $e_0$ = 0.73 ($\rho_0$ = 0.1) and the different initial bonding. Material parameter representing the influence of bonding $b$ = 40, and other parameters are the same for the calculations of over consolidated soil mentioned above. It is seen from calculated result that the proposed model can describe typical behaviors of structured soil as shown in Figure 2.8. A structured soil has a larger stiffness and can exist in looser state than non-structured soil in early phase of consolidation, after then it shows more brittle and more compressive behavior from certain stress level. Moreover, it can be seen that the void ratio of soil with larger bonding decreases less and enters the looser state above *NCL*, after then, it converges to *NCL* from negative side of $\rho$ with a sharp reduction of the bulk stiffness. In these figures, the parameters ($a$ and $b$) which represent the degradation rate of $\rho$ and $\omega$ are fixed. It can be seen from these figures that the deformation of structured soil is described simply by considering the effect of density and bonding and their evolution rules.

### 2.2.4 Characteristic of the various external influences on the behavior of soils and its modeling

As seen in Figures 2.5 and 2.8, the influences of density and bonding (structured soil) change the stiffness of soil isotropically and those effects decrease, which means the state of soil finally converges to the normally

consolidated line with gradual developing of deformation. In a modeling of those effects, the state variables $\rho$ and $\omega$ representing the density and bonding decrease with the development of plastic deformation by obeying each evolution rule.

On the other hand, it is experimentally known that temperature, strain rate and partial saturation (degree of saturation and suction) effect on the deformation characteristic of soil isotropically as well as density and bonding. In this study, the partial saturation effect among these external effects is minutely discussed and modeled in next chapter. Here, effects of temperature and strain rate on mechanical characteristics of soil, which can be explained in similar manner as the partial saturated characteristic, are briefly organized, more details about such effect and modeling are explained in references (Nakai et al. (2010) and Kikumoto et al. (2010)). Figure 2.13 – 2.16 show typical experimental results for such influences of external factors.

The experimental results for temperature effect are firstly discussed. From Figure 2.13 showing the consolidation test under different temperatures (5, 15, 25, 35 and 45Ⅲ) (Eriksson, 1989), it can be seen that although samples generally show overconsolidated behaviors, and the yield stress of soil depends on the magnitude of temperature, viz., the sample at lower temperature has a higher yield stress. In other word, the position of the normally consolidated line is shifted upward more with keeping its gradient in $e$ - ln$p$ plane. Figure 2.14 shows the result of oedometer tests with changing temperature under constant stress (Tidfors & Sällfors, 1989). Samples are firstly consolidated to prescribed consolidation stress at constant temperature of 25Ⅲ, and then temperature rises to 35, 45 and 55Ⅲ under constant stress. Subsequently, samples are reconsolidated with constant temperature or after temperature falling to 25Ⅲ. It can be observed from this figure that: the samples show not thermal expansion but thermal contraction due to rising temperature, and then samples shift to the normally consolidated line of each temperature; it can be seen from the cases of temperature re-falling to 25Ⅲ before re-consolidation that although the samples once contract due to rising temperature, soil approaches to the normally consolidated line for 25Ⅲ at re-consolidation process.

Figure 2.15 and 2.16 show the typical behavior of soil affected by strain rate effects. Figure 2.15 shows the result of constant strain rate consolidation test including some stress relaxation periods on Osaka Pleistocene clay (Tanaka et al., 2006). Figure 2.16 shows the result of constant strain rate consolidation tests with changing some magnitude of strain rate ($\dot{\varepsilon}_{v1}$ = 2.7 * $10^{-6}$/sec., $\dot{\varepsilon}_{v2}$ = 1.05 * $10^{-7}$/sec. and $\dot{\varepsilon}_{v3}$ = 1.34 * $10^{-5}$/sec.) (Leroueil et al., 1985). It can be observed from these figures that: preconsolidation pressure increases when strain rate is faster; stress relaxation (Figure 2.15) due to changing of strain rate (Figure 2.16) occurs; soil follows to the normally consolidated line of each strain rate at subsequent loading path under constant strain rate. From the experimental results shown in Figure 2.16, it seems that the model should be formulated by prescribing the position of normally consolidated line for each strain rate in the similar manner as the temperature effect.

Figure 2.17 shows exhausted / drained compression behavior of unsaturated soil under constant suction compared with that of saturated one (Honda, 2000). From this figure, as degree of saturation (water content) is lower, soil can retain a loser void ratio under same stress condition. It can be easily understood from the moist-placement method using partial saturated sample to prepare a looser saturated specimen. It is not clear from observed results in Figure 2.17 that the normally consolidated line for unsaturated soil can be described

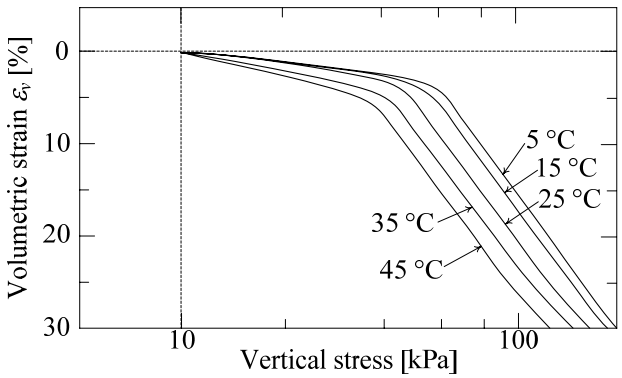


Figure 2.13 Observed results of oedo-meter test at different temperature on undisturbed silty clay (after Eriksson, 1989)

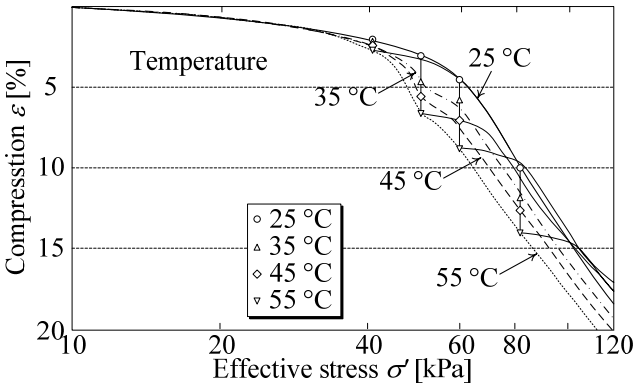


Figure 2.14 Observed results of oedometer test with changing temperature at prescribed stress ($\sigma_v'$ = 40, 50, 60 and 80 kPa) (after Tidfors & Sällfors, 1989)

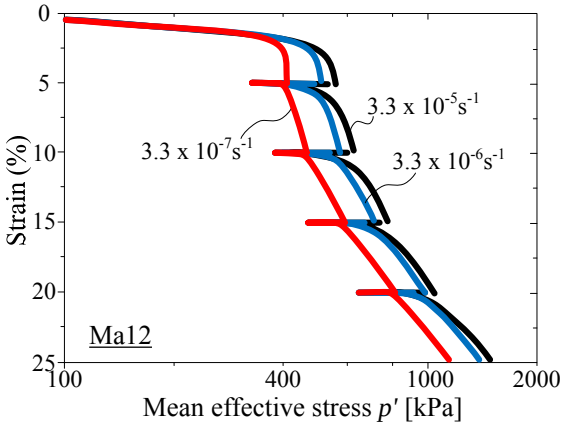


Figure 2.15 Observed results of constant strain rate consolidation tests including some stress relaxation periods on Osaka pleistocene clay (replotted from data in Tanaka et al., 2006)

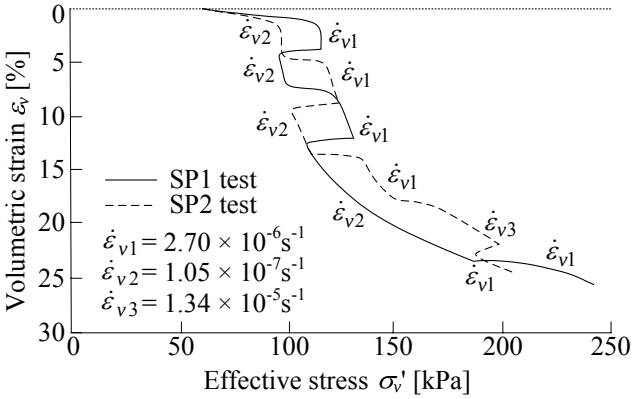


Figure 2.16 Observed result of oedometer test with changing strain rate on Bariscan clay (after Leroueil et. al., 1985)

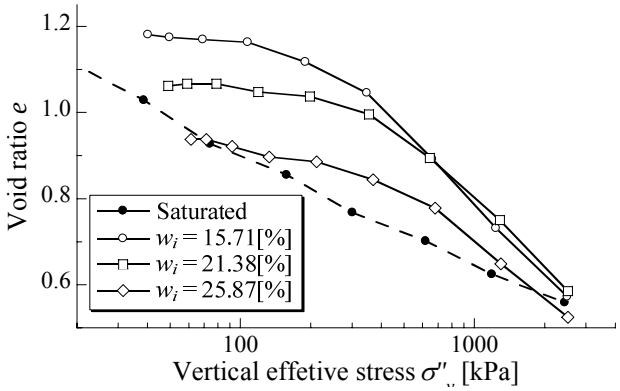


Figure 2.17 Observed results of drained / exhausted oedo-meter tests at constant suction ($s$ = 73.5 kPa) on different water contents Catalpo clay (after Honda, 2000)

as the parallel line to that for saturated soil. As the trend of experimental results, however, it can be supposed that the deformation characteristic of unsaturated soil such as collapse behavior can be represented, if the normally consolidated line for unsaturated soil is shifted due to a variation in degree of saturation. More

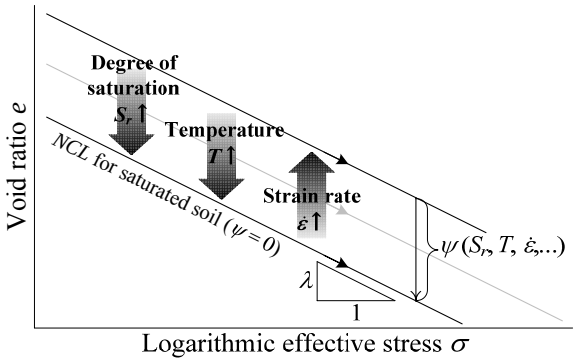


Figure 2.18 Position of normally consolidated line depending on the magnitude of various external influences (e.g., degree of saturation $S_r$, temperature $T$, strain rate $\dot{\varepsilon}$)

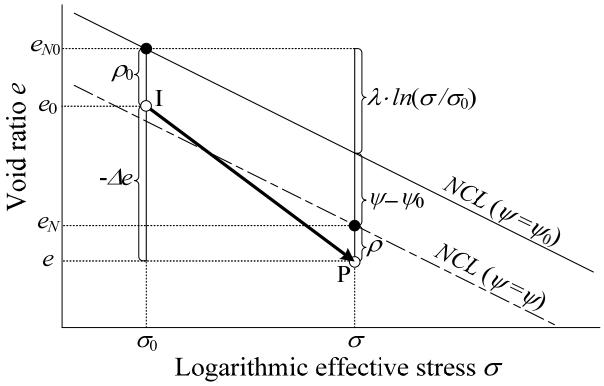


Figure 2.19 Schematic behavior of overconsolidated soil with changing of the magnitude of various external factors

details are shown in next chapter.

Although the influences of density and bonding change with plastic deformation as shown in the previous section, it can be assumed that the features such as temperature-dependent behavior, time-dependent behavior and behavior of unsaturated soils do not depend on the development of plastic deformation but is directly related to the changes of temperature, strain rate and degree of saturation. Those influences change the position of normally consolidated line (*NCL*) upwards / downwards, which is equivalent to changing of a reference state of soil for density. In order to model theses features, a state variable $\psi$, which represents the change of position of normally consolidated line, is defined. It is provided as a function of temperature, strain rate (rate of void ratio change), degree of saturation or others as shown in Figure 2.18.

Figure 2.19 shows the schematic diagram of the modeling considering the various features of soil. Points I ($\sigma = \sigma_0$, $e = e_0$, $\rho = \rho_0$) and P ($\sigma = \sigma$, $e = e$, $\rho = \rho$) represent the initial state and the current state, respectively, in the same way as in Figure 2.5 and 2.8. Here, $\psi_0$ is the initial value of $\psi$. By referring to this figure, the variation in void ratio ($-\Delta e$) of over consolidated soil under the influence of various external factors and its plastic component are represented as follows

$$(-\Delta e) = \{(e_{N0} - e_N) - (\rho_0 - \rho)\} = \lambda \ln \frac{\sigma}{\sigma_0} - (\rho_0 - \rho) - (\psi_0 - \psi) \tag{2.21}$$

$$(-\Delta e)^p = (-\Delta e) - (-\Delta e)^e = (\lambda - \kappa) \ln \frac{\sigma}{\sigma_0} - (\rho_0 - \rho) - (\psi_0 - \psi) \tag{2.22}$$

In comparison with Equation (2.21) and Equation (2.14), the last term ($\psi$ - $\psi_0$) representing the influence of "external factors independent of plastic deformation" through the vertical shift of the *NCL*, is added. This equation can be rewritten and a yield function $f$ of the general elastoplastic theory is defined as Equation (2.23).

$$f = F - \{H + (\rho_0 - \rho) + (\psi_0 - \psi)\} = 0 \quad where \quad F = (\lambda - \kappa) \ln \frac{\sigma}{\sigma_0}, \; H = (-\Delta e)^p \tag{2.23}$$

From Prager's consistency condition ($df$ = 0) and the evolution rule of state variable $\rho$ shown in equation

(2.11), the increment of the plastic component of void ratio is obtained as

$$d(-e)^p = \left\{\frac{\lambda-\kappa}{1+G(\rho)}\right\}\frac{d\sigma}{\sigma} + \left\{\frac{1}{1+G(\rho)}\right\}d\psi \tag{2.24}$$

Here, the evolution rule of $\rho$ is not Equation (2.15) considering the bonding effect but in Equation (2.11), in order to understand briefly the influence of external effect. A one-dimensional elastoplastic constitutive relationship of over consolidated soil affected by external factors is obtained as a sum of Equation (2.5) and Equation (2.24):

$$d(-e) = d(-e)^p + d(-e)^e = \left\{\frac{\lambda-\kappa}{1+G(\rho)} + \kappa\right\}\frac{d\sigma}{\sigma} + \left\{\frac{1}{1+G(\rho)}\right\}d\psi \tag{2.25}$$

Here, the state valuable $\psi$ is a function of temperature $T$, strain rate (rate of plastic void ratio change), time $t$, degree of saturation $S_r$ or others, so that its increment $d\psi$ is given in such forms as $d\psi=(\partial\psi/\partial t)dt$, $(\partial\psi/\partial T)dT$, $(\partial\psi/\partial S_r)dS_r$ or others. Furthermore, when we formulate the model in which multiple soil features should be considered, it is only to define the state valuable $\psi$ as the summation of the corresponding factors in a such way as $\psi = \psi_a + \psi_b + \cdots$.

The loading condition of the proposed models for the normally consolidated soil (Section 2.2.1), the over consolidated soil (Section 2.2.2), structured soil (Section 2.2.3) and soil affected by various types of external factors (present section) is simply given by assuming that the plastic component of the variation in void ratio is always compressive as follow

$$\begin{cases} d(-e)^p \neq 0 & if \quad d(-e)^p > 0 \\ d(-e)^p = 0 & if \quad d(-e)^p \leq 0 \end{cases} \tag{2.26}$$

Henceforth, the modeling of the influence of temperature and strain rate effects is conducted. The modeling of unsaturated soil will be minutely discussed and explained in next chapter.

*Modeling of temperature effect on deformation characteristic of soil in one-dimensional problem*

As seen in Figure 2.14, the amount of volume change due to rising temperature depends on the confining pressure, i.e., it is smaller in over consolidated region than normally consolidated state. Figure 2.20 shows the observed results of rising and falling temperature tests under constant confining pressure on different OCR (over consolidation ratio) Boom clay (Baldi et al., 1991). It can be seen from this figure that the amounts of volume change due to falling temperature are the same regardless of OCR. Heavily over consolidated sample (OCR = 6), especially, shows the same behaviors at rising and falling temperature. It can be regarded as the pure thermal expansion characteristics of soil, which always occurs

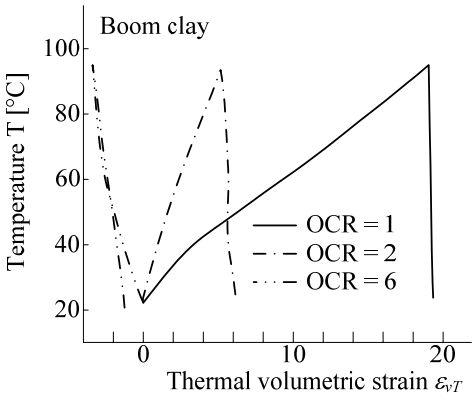


Figure 2.20 Drained rising and falling temperature tests on normally and over consolidated Boom clay (after Baldi, et al., 1991)

among temperature changing. On the other hand, normally consolidated sample (OCR = 1) shows an irrecoverable large volumetric compression, viz., elastoplastic volumetric compression.

From these experimental results, the amount of volume change due to changing temperature: $(-\Delta e)^T$ is given as Equation (2.27) and its elastic component: $(-\Delta e)^{eT}$ is given as Equation (2.28).

$$(-\Delta e)^T = \lambda_T (T - 20.0) = (\psi_0 - \psi) \tag{2.27}$$

$$(-\Delta e)^{eT} = \kappa_T (T - 20.0) \tag{2.28}$$

Here, note that $\lambda_T$ is positive and $\kappa_T$ is negative, and $\kappa_T$ satisfies $\kappa_T = 3\alpha$ ($\alpha$ : coefficient of volumetric expansion). $\lambda_T$ and $\kappa_T$ can be easily determined from the rising and falling temperature test on normally consolidated soil. Equation (2.27) is equivalent to the change of normally consolidated line as mentioned above. So, the plastic component of volume change due to changing temperature: $(-\Delta e)^{pT}$ is obtained from the difference of Equation (2.27) and (2.28) as follows.

$$(-\Delta e)^{pT} = (\lambda_T - \kappa_T)(T - 20.0) \tag{2.29}$$

The yield function considering the temperature effect is, therefore, given as

$$f = F - \{H + (\rho_0 - \rho) + (\lambda_T - \kappa_T)(T - 20.0)\} = 0 \quad where \quad F = (\lambda - \kappa)\ln\frac{\sigma}{\sigma_0},\ H = (-\Delta e)^p \tag{2.30}$$

Applying Prager's consistency condition to Equation (2.30) ($df$ = 0) and considering the elastic thermal expansion expressed as Equation (2.28), finally, the increment of void ratio considering the temperature effect is obtained as

$$d(-e) = d(-e)^p + d(-e)^e = \left\{\frac{\lambda - \kappa}{1 + G(\rho)} + \kappa\right\}\frac{d\sigma}{\sigma} + \left\{\frac{\lambda_T - \kappa_T}{1 + G(\rho)} + \kappa_T\right\}dT \tag{2.31}$$

*Modeling of time - strain rate effect on deformation characteristic of soil in one-dimensional problem*

It is well known that soil shows such creep characteristic as shown in Figure 2.21, which is a linear relation between void ratio and logarithmic time ($e$ – ln$t$ relation) in secondary consolidation phase. Here, $\lambda_\alpha$ is the coefficient of secondary consolidation.

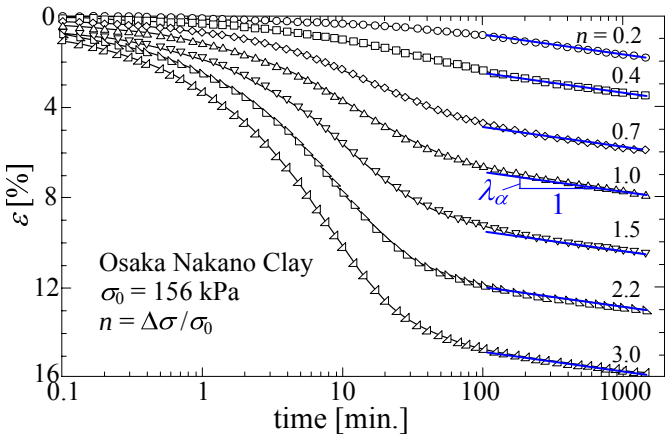


Figure 2.21 Observed results of oedometer tests on remolded normally consolidated Osaka Nanko clay for different stress increment (after Ohshima et al. 2002).

This volume change due to creep characteristic is directly exchanged to the variation in the position of normally consolidated line, because time is irreversible. Considering creep volume change of normally consolidated soil: $(-\Delta e)^{pt}$ shown in Figure 2.21, therefore, the variation in the position of normally consolidated line is give as follows

$$(\psi_0 - \psi) = (-\Delta e)^{pt} = \lambda_\alpha \ln \frac{t}{t_0} \tag{2.32}$$

The time derivative of $(-\Delta e)^{pt}$ is obtained as

$$(-\dot{e})^{pt} = \frac{d(-e)^{pt}}{dt} = \lambda_\alpha \ln \frac{1}{t} dt \tag{2.33}$$

Considering the Equation (2.33), Equation (2.32) is rewritten as follows on basis of the rate of plastic void ratio change.

$$(\psi_0 - \psi) = \lambda_\alpha \ln \frac{(-\dot{e})_0^{pt}}{(-\dot{e})^{pt}} \tag{2.34}$$

The yield function considering the time (strain rate) effect is, therefore, given as

$$f = F - \left\{ H + (\rho_0 - \rho) + \lambda_\alpha \ln \frac{(-\dot{e})_0^{pt}}{(-\dot{e})^{pt}} \right\} = 0 \quad where \quad F = (\lambda - \kappa) \ln \frac{\sigma}{\sigma_0},\ H = (-\Delta e)^p \tag{2.35}$$

Applying Prager's consistency condition to Equation (2.35) ($df = 0$), the increment of void ratio considering the influence of strain rate characteristic is obtained as

$$d(-e) = d(-e)^p + d(-e)^e = \left\{ \frac{\lambda - \kappa}{1 + G(\rho)} \frac{d\sigma}{\sigma} + \frac{\lambda_\alpha}{1 + G(\rho)} \right\} \Bigg/ \left\{ 1 + \frac{\lambda_\alpha}{1 + G(\rho)} \frac{1}{(-\dot{e})_0^{pt} dt} \right\} + \kappa \frac{d\sigma}{\sigma} \tag{2.36}$$

In order to verify the performance of modeling of influence of such external effects, some parametric studies are conducted. Then, parameters for these models are given on the basis of that for Fujinomori clay as well as above calculations. Newly added parameters are: the coefficient of thermal contraction $\lambda_T = 0.0005$ and the coefficient of thermal expansion $\kappa_T = -0.0001$, respectively; the coefficient of secondary consolidation $\lambda_\alpha = 0.003$ and the initial rate of the void ratio change at reference state is $(-\dot{e})^p = 1.0 * 10^{-7}$. Figure 2.22 is the calculated results of one-dimensional consolidation at different temperature, Figure 2.23 is the calculated results of one-dimensional consolidation with changing temperature at prescribed stress levels, and Figure 2.24 shows the calculated results of the rising and falling temperature tests under constant confining pressure on different OCR samples. Comparing the calculated results in Figure 2.22, 2.23, and 2.24 and the observed results in Figure 2.13, 2.14 and 2.22, the proposed model can qualitatively estimate the mechanical characteristics of soil affected by temperature effects and its mechanisms that: the position of the normally consolidated line shifts to upward and downward according to falling and rising temperature; the amount of volume change due to rising temperature depends on current void ratio and confining pressure, viz., over consolidation ratio; heavily over consolidated sample shows volume expansion behavior due rising temperature. This is because that the elastic thermal expansion is more effective than the plastic volume

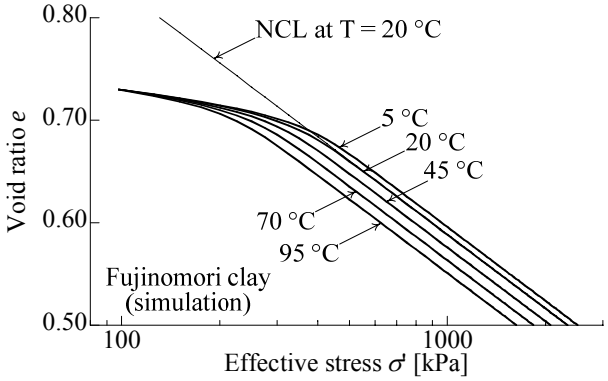


Figure 2.22 Calculated results of one-dimensional consolidation tests at different temperature ($T$ = 5, 20, 45, 70, 95℃)

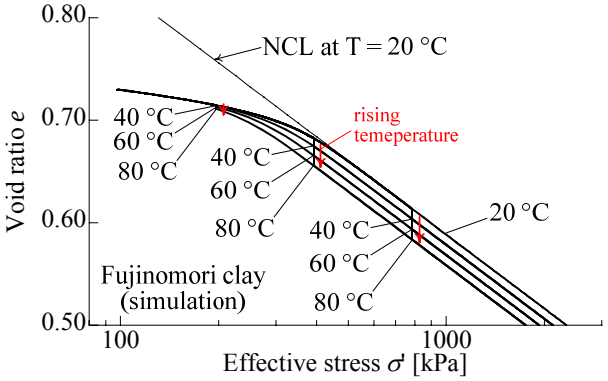


Figure 2.23 Calculated results of one-dimensional consolidation with changing temperature at prescribed stress levels

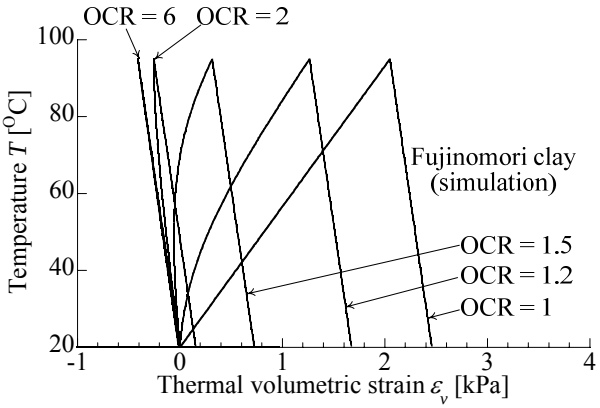


Figure 2.24 Calculated results of rising and falling temperature tests under constant confining pressure on normally consolidated and overconsolidated samples (OCR = 1, 1.2, 1.5, 2 and 6)

contraction due to falling of the normally consolidated line in heavily over consolidated state.

On the other hand, Figure 2.25 shows the calculated results of constant strain rate on one-dimensional consolidation tests. Figures 2.26 and 2.27 show the calculated results of constant strain rate on one-dimensional consolidation tests with changing strain rate and with stress relaxation, respectively. As can be seen from Figure 2.25, the normally consolidated lines of proposed model are prescribed by the magnitude of strain rate, and the reference normally consolidated line whose void ratio is $(-\dot{e})^p = 1.0 * 10^{-7}$ for $N$( = 0.83) in this calculation. It can be seen from comparison with calculated results in Figures 2.26 and 2.27 with observed results in Figure 2.15 and 2.16, moreover, that proposed model can suitably describe the typical behavior of strain-rate characteristics: the position of the normally consolidated line shifts to upward and downward due to accelerating and slow down strain rate; Creep characteristic and stress relaxation occurs with time under constraint condition, viz., constant employing stress and strain, respectively.

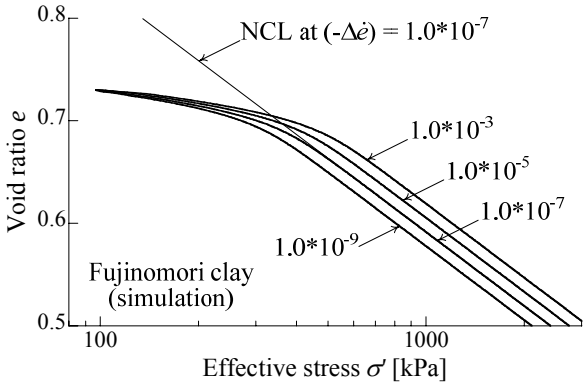


Figure 2.25 Calculated results of one-dimensional consolidation tests at different strain rate ((-Δ$\dot{e}$) = $1.0*10^{-3}$, $1.0*10^{-5}$, $1.0*10^{-7}$ and $1.0*10^{-9}$)

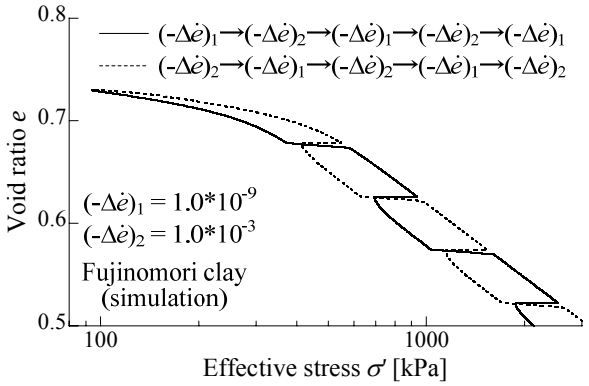


Figure 2.26 Calculated results of one-dimensional consolidation tests with changing strain rate ((-Δ$\dot{e}$)$_1$ = $1.0*10^{-3}$ and (-Δ$\dot{e}$)$_2$ = $1.0*10^{-9}$)

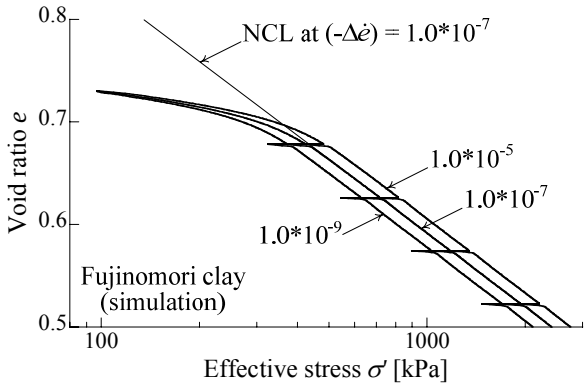


Figure 2.27 Calculated results of one-dimensional consolidation tests with stress relaxation under constant void ratio

The meanings of the state variables ($\rho$, $\omega$ and $\psi$) in the proposed modeling are summarized as follows:

$\rho$ : State valuable representing the density, which is defined by the difference between the current void ratio and the void ratio on current *NCL* at the same stress.

$\omega$ : State valuable considering the effect that is degraded with the development of plastic deformation such as bonding effect in structured soil. The effect is represented by the imaginary increase of density.

$\psi$ : State valuable describing the soil features such as time-dependent behavior, temperature-dependent behavior, unsaturated soil behavior. This variable is not related with the development of plastic deformation. The features are considered by shifting the normally consolidation line (*NCL*) due to the value of this state valuable.

## 2.3 Extension of one-dimensional model to multi-dimensional model and the concept of the modified stress $t_{ij}$

### 2.3.1 The relation between one-dimensional model and multi-dimensional model – Cam clay model

In this section, the one-dimensional model mentioned in the previous section is extended to the multi-dimensional model. The relation between one-dimensional stress $\sigma$ and void ratio $e$ is obtained from one-dimensional model, however, the multi-dimensional model gives the relation between ordinary stress tensor $\sigma_{ij}$ and strain tensor $\varepsilon_{ij}$. One-dimensional model represents the volume change due to (isotropic) compression, because the one dimensional stress $\sigma$ equals to mean stress $p$. Unlike a continuum material such as iron and glass, the volume change of geomaterials occurs due to shear action, which is called the dilatancy. So it must be taken into consideration for modeling of geomaterials. Cam clay model (e.g., Schofield and Wroth, 1968) is first model which describing the deformation and strength characteristic of soil due to "consolidation" and "shear" simultaneously. Afterward, various types of constitutive model based on it have been developed. As the details of Cam clay model are shown in a reference (e.g., Nakai et al., 2009), its yield function and characteristic of dilatancy are discussed here.

The yield function $f$ of Cam clay model is given as the summation of logarithmic of mean stress $p$ and the increasing function of stress ratio $\eta$ (= $q$/$p$):

$$f = \ln p + \zeta(\eta) - \ln p_1 = \ln \frac{p}{p_0} + \zeta(\eta) - \ln \frac{p_1}{p_0} = 0 \tag{2.37}$$

Here, the mean stress $p$ and deviatoric stress $q$ (stress ratio $\eta = q/p$) are defined as follows

$$p = \frac{1}{3}\sigma_{kk} \quad q = \sqrt{\frac{3}{2} s_{ij} s_{ij}} \quad s_{ij} = \sigma_{ij} - p\delta_{ij} \tag{2.38}$$

In Equation (2.37), $p_0$ and $p_1$ are the values of $p$ on $p$-axis for initial and current yield surfaces, respectively, which determine the size of yield surface. And $\zeta(\eta)$ is an increasing function of $\eta$ and satisfies the condition $\zeta(0) = 0$. In original Cam-clay model (Schofield and Wroth, 1968), the stress ratio function $\zeta(\eta)$ is given as follows:

$$\zeta(\eta) = \frac{\eta}{M} \tag{2.39}$$

Here, $M$ is stress ratio $\eta$ at critical state. Figure 2.28 shows the yield surfaces of Cam clay model on $p - q$ plane. The broken curve and solid curve indicate the initial and current yield surfaces when the stress condition moves from the initial state I to the current state P. Equation (2.37) is derived from the following experimental results: Ⓓ Henkel's experimental result – Water content contours from drained tests and effective stress path in undrained test for virgin compressed specimens of Weald clay: From this experimental result, "the volume change of normally consolidated soil is uniquely determined form initial and final stress condition regardless of stress path". Ⓔ The relation between stress ratio and plastic strain increment ratio (stress-dilatancy relation) is given as a linear relation shown in Figure 2.29. Ⓕ Void ratio $e$ and logarithmic mean stress ln $p$ is a linear relation during consolidation.

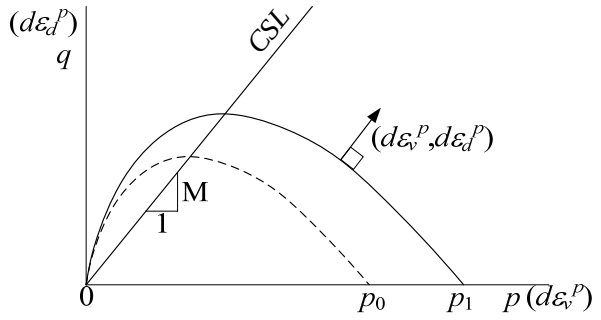


Figure 2.28 Yield surface of original Cam clay model (e.g., Schofield and Wroth, 1968)

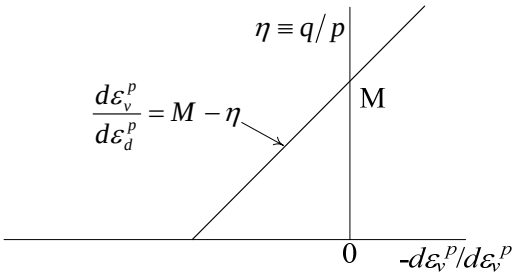


Figure 2.29 Stress-dilatancy relationship (the relation between stress ratio and strain increment ratio) of original Cam clay model

Especially, from experimental results Ⓓ, the plastic volumetric strain $\varepsilon_v^p$ can be used as the plastic potential of soil, i.e., a hardening parameter. Consequently, third term of Equation (2.37) is rewritten as follows by applying the experimental result Ⓕ.

$$\ln\frac{p_1}{p_0} = \frac{1}{C_p}\varepsilon_v^p = \frac{(-\Delta e)^p}{\lambda-\kappa} \;!\quad \left(C_p = \frac{\lambda-\kappa}{1+e_0}\right) \tag{2.40}$$

The yield function $f$ of Cam clay model is rewritten as

$$f = C_p\left\{\ln\frac{p}{p_0} + \zeta(\eta)\right\} - \varepsilon_v^p = 0 \quad or \quad f = (\lambda-\kappa)\left\{\ln\frac{p}{p_0} + \zeta(\eta)\right\} - (-\Delta e)^p = 0 \tag{2.41}$$

In Equation (2.41), first term in middle member represents consolidation behavior, and also second term represents dilatancy behavior. Equation (2.41) is rewritable as

$$f = F - H = 0 \;\; where \;\; F = (\lambda-\kappa)\ln\frac{p_1}{p_0} = (\lambda-\kappa)\left\{\ln\frac{p}{p_0} + \zeta(\eta)\right\},\;\; H = (-\Delta e)^p \tag{2.42}$$

Comparing Equation (2.42) with a yield function $f$ of one-dimensional model shown in Equation (2.4), we can see that $\sigma_0$ and $\sigma$ in the function $F$ of one-dimensional model only replace $p_0$ and $p_1$ which represent the size of yield surfaces. It is, therefore, easy to extend the basic multi-dimensional model expressed in Equation (2.42) to one considering some features of soil such as influences of density, bonding and external factors. And then, the function $F$ in one-dimensional yield function considering some features (Equations (2.10) (, (2.14)) and (2.23)) is replaced in a similar manner as Equation (2.42).

$$f = F - \{H + (\rho_0 - \rho)\} = 0 \;\; where \;\; F = (\lambda-\kappa)\left\{\ln\frac{p}{p_0} + \zeta(\eta)\right\} = (\lambda-\kappa)\ln\frac{p_1}{p_0}, H = (-\Delta e)^p \tag{2.43}$$

$$f = F - \{H + (\rho_0 - \rho) + (\psi_0 - \psi)\} = 0 \;\; where \;\; F = (\lambda-\kappa)\left\{\ln\frac{p}{p_0} + \zeta(\eta)\right\}, H = (-\Delta e)^p \tag{2.44}$$

Equation (2.44) considers the shift of normally consolidated line and also critical state line upwards and downwards on $e - \ln p$ plane. And the vertical distance between those two lines (*NCL* and *CSL*) is constant which means that the stress-dilatancy relation is unaffected by various external factors. Firstly, the factor such as the influence of density, bonding, temperature, strain rate, degree of saturation and others which affect on deformation and strength characteristic of soil isotropically, was considered in simple one-dimensional model.

If those models can be verified in one-dimensional problem, those models can be extended the corresponding multi-dimensional model easily. Then, we have to prescribe the direction of plastic strain increment. It is given by associated flow rule assumed in ordinary stress space as follows;

$$d\varepsilon_{ij}^{p} = \Lambda \frac{\partial f}{\partial \sigma_{ij}} \tag{2.45}$$

The increment of plastic strain, namely, arises in a direction perpendicular to the yield surface. Here, $\Lambda$ is obtained from Prager's consistency condition of yield function $f$ and Equation (2.45) as follows;

$$df = dF - dH = \frac{\partial F}{\partial \sigma_{ij}} d\sigma_{ij} - d(-e)^{p} = \frac{\partial F}{\partial \sigma_{ij}} d\sigma_{ij} - (1+e_0)\Lambda \frac{\partial f}{\partial \sigma_{kk}} = 0 \tag{2.46}$$

$$\Lambda = \left\langle \frac{\dfrac{\partial F}{\partial \sigma_{kl}} d\sigma_{kl}}{(1+e_0)\dfrac{\partial f}{\partial \sigma_{kk}}} \right\rangle = \left\langle \frac{dF}{h^{p}} \right\rangle \tag{2.47}$$

where, the symbol < > which denotes the Macaulay bracket, i.e., $\langle A \rangle = A$ if $A > 0$; otherwise $\langle A \rangle = 0$. And, $h^p$ represents the plastic modulus. The elastic strain increment is given by the generalized Hooke's law

$$d\varepsilon_{ij}^{e} = \frac{1+\nu_e}{E_e} d\sigma_{ij} - \frac{\nu_e}{E_e} d\sigma_{kk}\delta_{ij} \quad \textit{where} \quad E_e = \frac{3(1-2\nu_e)(1+e_0)}{\kappa} p \tag{2.48}$$

Here, $E_e$ is Young's modulus, $\kappa$ is the swelling index and $\nu_e$ is Poisson's ratio respectively. Therefore, the total strain increment is given by

$$d\varepsilon_{ij} = d\varepsilon_{ij}^{e} + d\varepsilon_{ij}^{p} \tag{2.49}$$

### 2.3.2 Concept of the modified stress $t_{ij}$

Figures 2.30 and 2.31 show the stress-strain relation of drained triaxial compression ($\sigma_1 \geq \sigma_2 = \sigma_3$) and extension ($\sigma_1 = \sigma_2 \geq \sigma_3$) tests under constant mean stress on normally consolidated Fujinomori clay and medium dense Toyoura sand, respectively. And Figures 2.32 and 2.33 show the corresponding relations between stress ratio $\eta$ and strain increment ratio (stress-dilatancy relation), respectively. Although the strain increment ratio is arranged including the elastic components, the plastic strain increment ratio can be considered as almost the same as that of the total strain increments, because the elastic strain increments are much smaller than the plastic strain increments under shear loadings. From Figures 2.30 and 2.31, it can be seen that the deformation and strength of soils in multi-dimensional (3D) stress conditions cannot be described uniquely using the invariants based on ordinary stress $\sigma_{ij}$ ($p$ and $q$). There is no unique relation between $d\varepsilon_v/d\varepsilon_d$ and $q/p$ in Figures 2.32 and 2.33, so that the shape of yield surface on $p$-$q$ plane (in triaxial condition) depends on the relative magnitude of the intermediate principal stress $\sigma_2$. Figure 2.34 shows, moreover, the directions and the magnitudes of the observed shear strain increments on the octahedral plane in the true triaxial ($\sigma_1 > \sigma_2 > \sigma_3$) tests ($\theta = 15°$, 30° and 45°). Here, the length of each line is proportional to the value of shear strain increment on the octahedral plane.

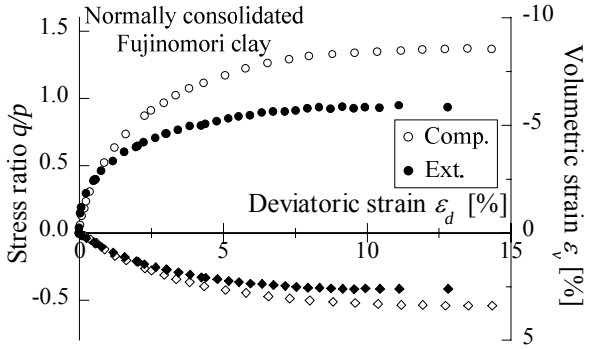


Figure 2.30 Stress-strain relations of triaxial compression / extension tests on normal consolidation Fujinomori clay (after Nakai & Matsuoka, 1986)

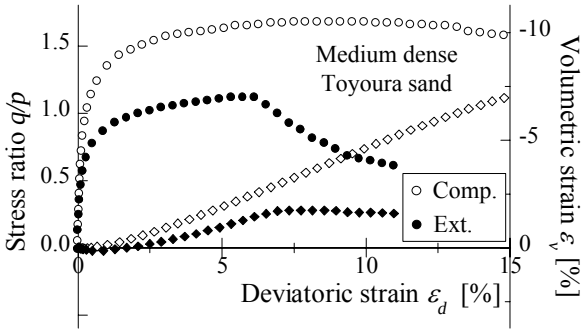


Figure 2.31 Stress-strain relations of triaxial compression / extension tests on medium dense Toyoura sand (after Hinokio, 2000)

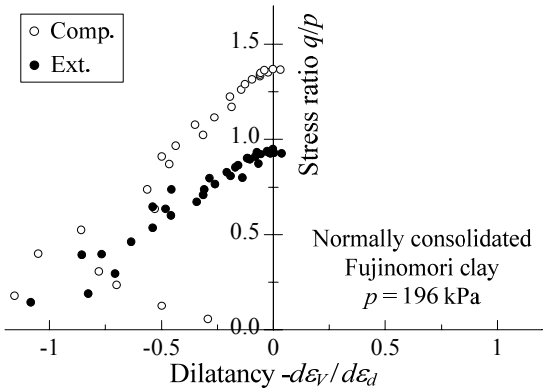


Figure 2.32 Stress-dilatancy relationship of triaxial compression / extension tests on normal consolidation Fujinomori clay (after Nakai & Matsuoka, 1986)

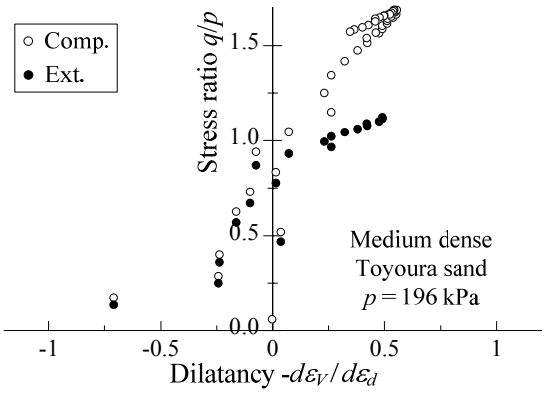


Figure 2.33 Stress-dilatancy relationship of triaxial compression / extension tests on medium dense Toyoura sand (after Hinokio, 2000)

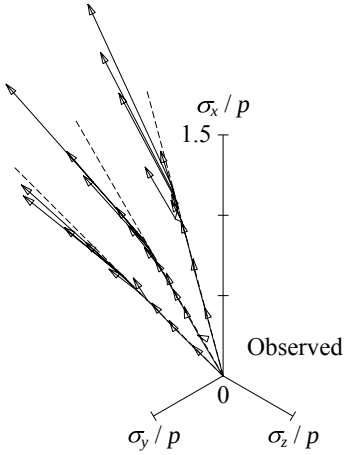


Figure 2.34 Observed strain vectors of true-triaxial test ($\theta$ = 15, 30, 45° const) - strain increments deviates leftward from the direction of shear stress (radial direction). (after Nakai & Hinokio, 2004)

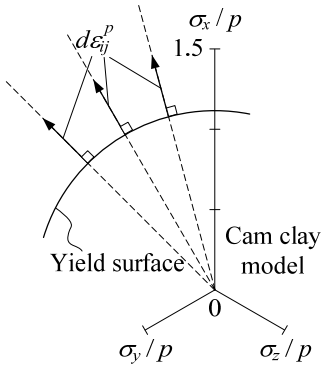


Figure 2.35 Circular yield surface as Cam clay model and assuming strain vectors which occurs in radial direction

In the figures, $\theta$ denotes the angle between $\sigma_1$-axis and the corresponding radial stress path on the octahedral plane, where $\theta = 0°$ and 60° represent the stress path under triaxial compression and triaxial extension conditions, respectively. Note that the direction of the observed shear strain increments deviate leftward from

the direction of shear stress (radial direction) with the increase of stress ratio under three different principal stresses. Since the shape of plastic potential (yield surface) formulated using the stress invariants ($p$ and $q$) is circle on the octahedral plane as shown in Figure 2.35, such deviation of strain increments in the radial cannot be described. Therefore, the constitutive models formulated using these ordinary stress invariants ($p$ and $q$) are not capable of describing the influence of the intermediate principal stress $\sigma_2$ on the deformation and strength characteristics of soils properly.

In order to consider these influences of the intermediate principal stress $\sigma_2$, the method assuming a non-circular shaped yield surface in octahedral plane (or the soil strength depending on the relative magnitude of the intermediate principal stress, i.e., coefficient of intermediate principal stress $b = (\sigma_2-\sigma_3)/(\sigma_1-\sigma_3)$) is proposed. However, physical meaning of such method is not clear. On the other hand, Nakai & Mihara (1984) proposed $t_{ij}$ concept, which can describe uniquely the stress-strain behavior of soils under different three principal stresses. Ordinary stress parameters (mean stress $p$ and deviator stress $q$) and strain parameters (volumetric strain $\varepsilon_v$ and deviator strain $\varepsilon_d$), which is used for formulating ordinary yield function and assuming the stress-dilatancy relation, are obtained as orthogonal and horizontal components of stress and strain to octahedral plane respectively. Meanwhile, the stress and strain parameters of $t_{ij}$ concept are obtained by referring to *SMP* (The Spatially Mobilized Plane).

The modified stress tensor $t_{ij}$ is defined by the product of $a_{ik}$ and $\sigma_{kj}$ as

$$t_{ij} = a_{ik}\sigma_{kj} \tag{2.50}$$

Here, $a_{ij}$ is a symmetric 2 order tensor which is coaxial to ordinary stress tensor $\sigma_{ij}$. And its principal values ($a_1$, $a_2$ and $a_3$) are unit vector normal to the SMP. The $a_{ij}$ are defined as

$$\begin{aligned} a_{ij} &= \sqrt{\frac{I_3}{I_2}} r_{ij}^{-1} \\ &= \sqrt{\frac{I_3}{I_2}} \left(\sigma_{ik} + I_{r2}\delta_{ik}\right)\left(I_{r1}\sigma_{kj} + I_{r3}\delta_{kj}\right)^{-1} \end{aligned} \tag{2.51}$$

where, $\delta_{ij}$ is Kronecker's delta and $r_{ij}$ is square root of $\sigma_{ij}$ ($r_{ik}\, r_{kj} = \sigma_{ij}$). $I_2$ ,$I_3$ and $I_{r1}$, $I_{r2}$, $I_{r3}$ are invariants of $\sigma_{ij}$ and $r_{ij}$ respectively as follows;

$$\left.\begin{aligned} I_2 &= \sigma_1\sigma_2 + \sigma_2\sigma_3 + \sigma_3\sigma_1 = \frac{1}{2}(\sigma_{ii}{}^2 - \sigma_{ij}\sigma_{ji}) \\ I_3 &= \sigma_1\sigma_2\sigma_3 = e_{ijk}\sigma_{i1}\sigma_{j2}\sigma_{k3} \end{aligned}\right\} \tag{2.52}$$

$$\left.\begin{aligned} I_{r1} &= \sqrt{\sigma_1} + \sqrt{\sigma_2} + \sqrt{\sigma_3} = r_{ii} \\ I_{r2} &= \sqrt{\sigma_1\sigma_2} + \sqrt{\sigma_2\sigma_3} + \sqrt{\sigma_3\sigma_1} = \frac{1}{2}(r_{ii}{}^2 - r_{ij}r_{ji}) \\ I_{r3} &= \sqrt{\sigma_1\sigma_2\sigma_3} = e_{ijk}r_{i1}r_{j2}r_{k3} \end{aligned}\right\} \tag{2.53}$$

Here, $e_{ijk}$ is the Edinton's epsilon. That is to say, the modified stress $t_{ij}$, whose principal values ($t_1$, $t_2$ and $t_3$) are three component of traction changing with the relative magnitude of each principal stresses, is symmetric coaxial tensor to $\sigma_{ij}$. The stress and strain parameters on $t_{ij}$ concept are defined as the orthogonal and components of $t_{ij}$ and strain increments to *SMP* respectively. The stress parameters ($t_N$, $t_S$) and

Table 2.1 Comparison stress and strain invariants of modified stress $t_{ij}$ concept with that of ordinary stress $\sigma_{ij}$

| | ordinary concept | $t_{ij}$ concept |
|---|---|---|
| tensor normal to reference plane | $\delta_{ij}$ (unit tensor) | $a_{ij}$ (tensor normal to SMP) |
| stress tensor | $\sigma_{ij}$ | $t_{ij}$ |
| mean stress | $p = \sigma_{ij}\delta_{ij}/3$ | $t_N = t_{ij}a_{ij}$ |
| deviatoric stress tensor | $s_{ij} = \sigma_{ij} - p\delta_{ij}$ | $t'_{ij} = t_{ij} - t_N a_{ij}$ |
| deviatoric stress | $q = \sqrt{(3/2)s_{ij}s_{ij}}$ | $t_S = \sqrt{t'_{ij}t'_{ij}}$ |
| stress ratio tensor | $\eta_{ij} = s_{ij}/p$ | $x_{ij} = t'_{ij}/t_N$ |
| stress ratio | $\eta = q/p$ | $X = t_S/t_N$ |
| strain increment normal to reference plane | $d\varepsilon_v = d\varepsilon_{ij}\delta_{ij}$ | $d\varepsilon_N^* = d\varepsilon_{ij}a_{ij}$ |
| deviatoric strain increment tensor | $de_{ij} = d\varepsilon_{ij} - d\varepsilon_v\delta_{ij}/3$ | $d\varepsilon'_{ij} = d\varepsilon_{ij} - d\varepsilon_N^* a_{ij}$ |
| strain increment parallel to reference plane | $d\varepsilon_d = \sqrt{(2/3)de_{ij}de_{ij}}$ | $d\varepsilon_S^* = \sqrt{d\varepsilon'_{ij}d\varepsilon'_{ij}}$ |

The strain increment parameters ($d\varepsilon_N^*$, $d\varepsilon_S^*$) (*SMP*$^*$: Nakai and Matsuoka) are given as follows, and those are shown in Figure 2.36;

$$t_N = \overline{ON} = t_1 a_1 + t_2 a_2 + t_3 a_3 = t_{ij} a_{ij} \tag{2.54}$$

$$t_S = \overline{NT} = \sqrt{t_1^2 + t_2^2 + t_3^2} = \sqrt{t_{ij}t_{ij} - \left(t_{ij}a_{ij}\right)^2} \tag{2.55}$$

$$d\varepsilon_N^* = \overline{O'N'} = d\varepsilon_1 a_1 + d\varepsilon_2 a_2 + d\varepsilon_3 a_3 = d\varepsilon_{ij} a_{ij} \tag{2.56}$$

$$\begin{aligned} d\varepsilon_S^* = \overline{N'T'} &= \sqrt{d\varepsilon_1^2 + d\varepsilon_2^2 + d\varepsilon_3^2 - \left(d\varepsilon_1 a_1 + d\varepsilon_2 a_2 + d\varepsilon_3 a_3\right)^2} \\ &= \sqrt{d\varepsilon_{ij}d\varepsilon_{ij} - \left(d\varepsilon_{ij}a_{ij}\right)} \end{aligned} \tag{2.57}$$

Table 2.1 compares the stress and strain increment tensors and their variants in ordinary stress $\sigma_{ij}$ space and modified stress $t_{ij}$ space. The plots in Figure 2.37 and 2.38 show the observed stress-dilatancy relation arranged in terms of the relation between stress ratio $t_S/t_N$ (= $X$ ) and strain increment ratio $d\varepsilon_N^*/d\varepsilon_S^*$. These results correspond to Figures 2.30 and 2.31. The stress-dilatancy relations based on $t_{ij}$ concept doesn't depends on the magnitude of intermediate principal stress $\sigma_2$. The yield function derived from stress-dilatancy relation on $t_{ij}$ concept, therefore, can consider the influence of relative magnitude of intermediate principal stress on deformation and strength of soil automatically.

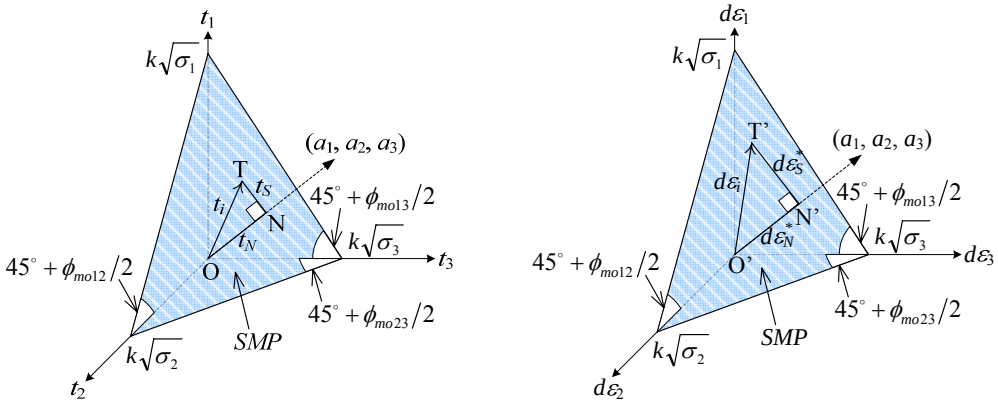


Figure 2.36 Definitions of stress and strain invariants of modified stress $t_{ij}$ concept (left side: stress invariants, right side: strain increment invariants)

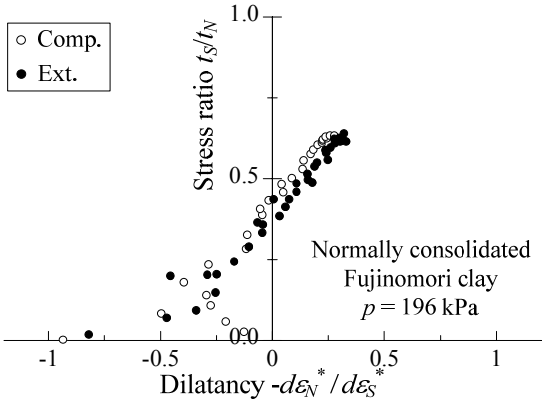


Figure 2.37 Stress-dilatancy relation based on $t_{ij}$ concept of triaxial compression / extension tests on normal consolidation Fujinomori clay (after Nakai & Matsuoka, 1986)

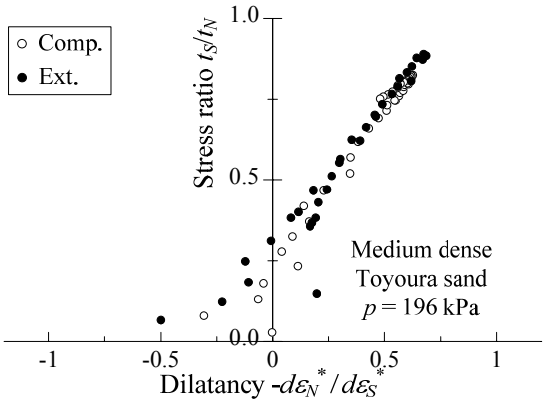


Figure 2.38 Stress-dilatancy relation based on $t_{ij}$ concept of triaxial compression / extension tests on medium dense Toyoura sand (after Hinokio, 2000)

### 2.3.3 Modeling of multi-dimensional model considering the influence of the principal intermediate stress and verification of the model validation

*Multi-dimensional model for normally consolidated soil*

In order to consider the influence of intermediate principal stress on the deformation and strength of soils in constitutive modeling of soils, the yield function is formulated by the stress invariants ($t_N$ and $t_S$) instead of ($p$ and $q$) and assuming the flow rule in the modified stress $t_{ij}$ space instead of the ordinal $\sigma_{ij}$ space (Nakai and Mihara, 1984). The yield function for the normally consolidated soil based on $t_{ij}$ concept is given as follows only by replacing $\sigma_0$ and $\sigma$ in the yield function of one-dimensional models defined as Equation (2.42) with $t_{N0}$ and $t_{N1}$, respectively.

$$f = F - H = 0 \quad where \quad F = (\lambda - \kappa)\ln\frac{t_{N1}}{t_{N0}}, \quad H = (-\Delta e)^p \tag{2.58}$$

Here, the mean stress $t_N$ based on $t_{ij}$ concept coincides with the ordinary mean stress $p$ at isotropic condition ($X$ = 0). And then $F$ equals to the logarithmic function of the mean stress $t_N$ plus an increasing function of stress ratio $X$, which represent volumetric change due to consolidation and dilatancy as well as ordinary constitutive

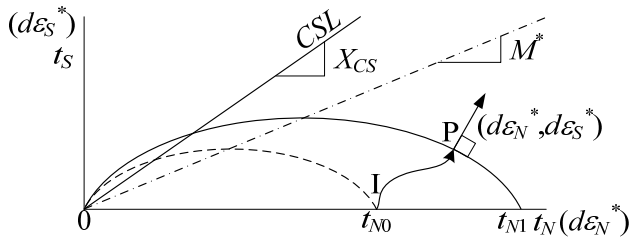


Figure 2.39 Yield surface based on the modified stress $t_{ij}$ concept

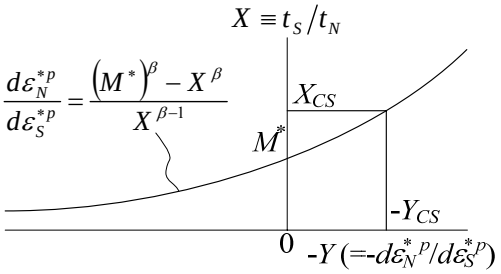


Figure 2.40 Stress-dilatancy relation based on the modified stress $t_{ij}$ concept (after Chowdhury et al., 1999; Nakai and Hinokio, 2004)

model. Therefore, Equation (2.58) can be rewritten as

$$f = F - H = 0 \quad where \quad F = (\lambda - \kappa)\ln\frac{t_{N1}}{t_{N0}} = (\lambda - \kappa)\left\{\ln\frac{t_N}{t_{N0}} + \zeta(X)\right\}, \quad H = (-\Delta e)^p \tag{2.59}$$

where, $\zeta(X)$ is an increasing function of stress ratio $X$ (= $t_S/t_N$) and satisfies the condition $\zeta(0) = 0$, in a similar manner as the ordinary model. Equation (2.59) coincides with the Equation (2.37) formulated by using the modified stress $t_{ij}$ instead of ordinary stress $\sigma_{ij}$. Figure 2.39 shows the yield surfaces on $t_N - t_S$ plane (Equation (2.59)). The broken curve and solid curve indicate the initial and current yield surfaces when the stress condition moves from the initial state I ($t_N = t_{N0}$) to the current state P ($t_N = t_N$, $X = t_S/t_N$). Moreover, $t_{N0}$ and $t_{N1}$ are the values of $t_N$ on $t_N$-axis for initial and current yield surfaces which represent the size of yield surface as well as $p_0$ and $p_1$ in ordinary constitutive model based on ordinary stress $\sigma_{ij}$.

The increment of plastic strain is obtained from associated flow rule assumed in $t_{ij}$ space.

$$d\varepsilon_{ij}^p = \Lambda\frac{\partial F}{\partial t_{ij}} = \Lambda\left(\frac{\partial F}{\partial t_N}\frac{\partial t_N}{\partial t_{ij}} + \frac{\partial F}{\partial X}\frac{\partial X}{\partial t_{ij}}\right) \tag{2.60}$$

The detailed derivation process is shown in reference paper (Nakai & Hinokio, 2004). In the previous section, the stress and strain parameters based on $t_{ij}$ concept can organize the stress-dilatancy relation uniquely. In recent models (Chowdhury et al., 1999; Nakai and Hinokio, 2004), the following equation is adopted for the function of stress ratio $\zeta(X)$ in Equation (2.59)

$$\zeta(X) = \frac{1}{\beta}\left(\frac{X}{M^*}\right)^\beta \tag{2.61}$$

Because the following stress-dilatancy relation holds

$$\frac{d\varepsilon_N^{*p}}{d\varepsilon_S^{*p}} = \frac{\dfrac{\partial F}{\partial t_N} + \dfrac{\partial F}{\partial X}\dfrac{\partial X}{\partial t_N}}{\dfrac{\partial F}{\partial X}\dfrac{\partial X}{\partial t_S}} = \frac{1 - \zeta'(X)\cdot X}{\zeta'(X)} = \frac{M^{*\beta} - X^\beta}{X^{\beta-1}} \tag{2.62}$$

Figure 2.40 illustrates this equation in terms of the relation between $X = t_S/t_N$ and $Y = d\varepsilon_N{}^{*p}/d\varepsilon_S{}^{*p}$. Here, $M^*$ is the intercept with the vertical axis and is expressed as follows

$$M^* = \left(X_{CS}{}^\beta + X_{CS}{}^{\beta-1}Y_{CS}\right)^{1/\beta} \tag{2.63}$$

where, $X_{CS}$ and $Y_{CS}$ are the stress ratio $X$ and the plastic strain increment ratio $Y$ at critical state ($d\varepsilon_v^{\,p} = 0$), respectively. Those are expressed as follows using the principal stress ratio at critical state in triaxial compression $R_{CS} = (\sigma_1/\sigma_3)_{CS(comp)}$ (Nakai and Mihara, 1984):

$$X_{CS} = \frac{\sqrt{2}}{3}\left(\sqrt{R_{CS}} - \frac{1}{\sqrt{R_{CS}}}\right) \tag{2.64}$$

$$Y_{CS} = \frac{1-\sqrt{R_{CS}}}{\sqrt{2}(\sqrt{R_{CS}} + 0.5)} \tag{2.65}$$

It can be seen that the shape of Equation (2.62) (Figure 2.40) is similar to the experimental stress-dilatancy relation as shown in Figures 2.37 and 2.38. Applying Prager's consistency condition ($df = 0$) and flow rule shown in Equation (2.60) to the yield function, The proportionality constant $\Lambda$ is obtained as follows

$$df = dF - dH = \frac{\partial F}{\partial \sigma_{ij}} d\sigma_{ij} - d(-e)^p = \frac{\partial F}{\partial \sigma_{ij}} d\sigma_{ij} - (1+e_0)\Lambda \frac{\partial f}{\partial t_{kk}} = 0 \tag{2.66}$$

$$\Lambda = \left\langle \frac{\dfrac{\partial F}{\partial \sigma_{kl}} d\sigma_{kl}}{(1+e_0)\dfrac{\partial f}{\partial t_{kk}}} \right\rangle = \left\langle \frac{dF}{h^p} \right\rangle \tag{2.67}$$

Substituting $\Lambda$ expressed as above into Equation (2.60), the plastic strain increment can be calculated. Assuming same elastic relation as Equation (2.48) in $t_{ij}$ concept, total strain increment is similarly obtained from Equation (2.49).

*Modeling of the influence of density in multi-dimensional problem*

Here, the above-mentioned elastoplastic model based on $t_{ij}$ concept for normally consolidated soil is extended to the model for over consolidated soil. The multi-dimensional model for normally consolidated soil can be extended to one considering the influence of density in the similar manner as that for one-dimensional model, even if the multi-dimensional model is based on $t_{ij}$ concept. The yield function for the model of over consolidated soil based on $t_{ij}$ concept is given as follows only by replacing $\sigma_0$ and $\sigma$ in the yield function of one-dimensional models defined as Equation (2.10) with $t_{N0}$ and $t_{N1}$, respectively.

$$f = F - \{H + (\rho_0 - \rho)\} = 0 \;\; where \;\; F = (\lambda - \kappa)\ln\frac{t_{N1}}{t_{N0}}, H = (-\Delta e)^p \tag{2.68}$$

Assuming the shape of yield function, Equation (2.68) can be rewritten as follows in similar manner as Equation (2.59)

$$f = F - \{H + (\rho_0 - \rho)\} = 0 \;\; where \;\; F = (\lambda - \kappa)\ln\frac{t_{N1}}{t_{N0}} = (\lambda - \kappa)\left\{\ln\frac{t_N}{t_{N0}} + \zeta(X)\right\}, \; H = (-\Delta e)^p \tag{2.69}$$

Especially, the yield function whose function $\zeta(X)$ is given as Equation (2.61) coincides with the yield function for subloading $t_{ij}$ model (Nakai and Hinokio, 2004). The consistency condition ($df = 0$) and the flow

rule in Equation (2.60) give

$$df = dF - (dH - d\rho) = \frac{\partial F}{\partial \sigma_{ij}} d\sigma_{ij} - \left\{ (1+e_0)\Lambda \frac{\partial f}{\partial t_{kk}} - d\rho \right\} = 0 \tag{2.70}$$

It can be assumed that positive value of $\rho$ decreases with development of plastic strain in a similar manner as the one-dimensional model. The proportionality constant $\Lambda$ (> 0) which represents the magnitude of the plastic deformation has the dimension of stress, because $F$ is a dimensionless function. Then, $(\partial F/\partial t_{kk})$ has the dimension of the inverse of stress. To satisfy these conditions, the following evolution rule of $\rho$ is given using monotonous increasing function $G(\rho)$ which satisfies $G(0) = 0$:

$$d\rho = -\Lambda \cdot (1+e_0) \cdot L(\rho, t_N) = \Lambda \cdot (1+e_0) \cdot \frac{-G(\rho)}{t_N} \tag{2.71}$$

In the present 3D model, the increasing function $G(\rho)$, which was given as linear function for one-dimensional model, is given as the following quadratic function of state variable $\rho$ in order to describe the observed behavior precisely.

$$G(\rho) = a\rho^2 \tag{2.72}$$

Substituting Equation (2.71) into Equation (2.70), the proportional constant $\Lambda$ is expressed as

$$\Lambda = \left\langle \frac{\dfrac{\partial F}{\partial \sigma_{kl}} d\sigma_{kl}}{(1+e_0)\left\{ \dfrac{\partial f}{\partial t_{kk}} + \dfrac{G(\rho)}{t_N} \right\}} \right\rangle = \left\langle \frac{dF}{h^p} \right\rangle \tag{2.73}$$

Then, the plastic strain increment is calculated by substituting the proportional constant $\Lambda$ into Equation (2.60). Figure 2.41 shows the observed (symbols) and calculated (curves) results of triaxial compression and extension tests on remolded Fujinomori clay with different over consolidation ratios (OCR=1, 2, 4 and 8). The model is capable of describing uniquely not only the influence of over consolidation ratio (density) on the deformation, dilatancy and strength of clay but also the influence of intermediate principal stress on them with unified material parameters. The values of material parameters for Fujinomori clay is shown in Table 2.2.

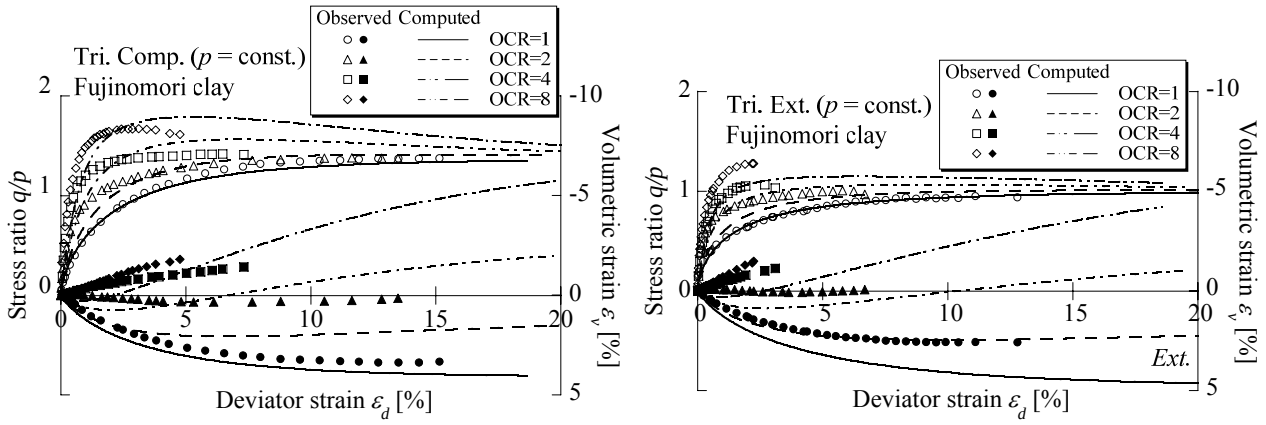


Figure 2.41 Comparison observed stress-strain relation of triaxial compression / extension tests on different OCR samples with computed one by subloading $t_{ij}$ model (experimental results from Nakai & Hinokio, 2004)

Table 2.2 Material parameters for Fujinomori clay

| | | |
|---|---|---|
| $\lambda$ | 0.104 | Same parameters as Cam clay model |
| $\kappa$ | 0.010 | |
| $N = e_{NC}$ at $p = 98$ kPa & $q = 0$ kPa | 0.83 | |
| $R_{cs} = (\sigma_1/\sigma_3)_{cs(comp)}$ | 3.5 | |
| $\nu_e$ | 0.2 | |
| $\beta$ | 1.5 | Shape of yield surface (same as original Cam clay at $\beta = 1$) |
| $a / (\lambda-\kappa)$ | 500 | Influence of density and confining pressure |

*Modeling of the influence of bonding in multi-dimensional problem*

Next, the multi-dimensional model for over consolidated soil is subsequently extended to one taking into consideration the influence of bonding in a similar manner as one-dimensional model. The yield function of multi-dimensional model for structured soil is same as that for over consolidated soil expressed in Equation (2.68) and (2.69).

$$f = F - \{H + (\rho_0 - \rho)\} = 0 \quad where \quad F = (\lambda - \kappa)\ln\frac{t_{N1}}{t_{N0}} = (\lambda - \kappa)\left\{\ln\frac{t_N}{t_{N0}} + \zeta(X)\right\}, H = (-\Delta e)^p \tag{2.74}$$

However, as mentioned in former section, the variation in state variable $\rho$ is affected by not only current density but also current bonding $\omega$, and larger value of the state variable $\omega$ has more effect for the degradation of $\rho$. Then the evolution rule of $\rho$ for non-structured over consolidated soil expressed in Equation (2.71) is extended to following equation added the bonding effect $\omega$.

$$d\rho = -\Lambda \cdot (1 + e_0) \cdot L(\rho, \omega, t_N) = -\Lambda \cdot (1 + e_0) \cdot \left\{\frac{G(\rho) + Q(\omega)}{t_N}\right\} \tag{2.75}$$

In Equation (2.75), the increasing function $G(\rho)$ is given as follows which is an extended function of Equation (2.72) considering the negative region of $\rho$, because $\rho$ becomes negative value due to bonding effect. Therefore, Positive value of $\rho$ increases the plastic modulus, but negative value of $\rho$ decreases the plastic modulus.

$$G(\rho) = a\rho \cdot |\rho| \tag{2.76}$$

Meanwhile, the function $Q(\omega)$ in Equation (2.75) is the same function for one-dimensional model, given as $Q(\omega) = b\omega$. And, although the evolution rule of $\omega$ is here given as follows using the same function $Q(\omega)$, it is possible to express it using other high dimension function:

$$d\omega = -\Lambda \cdot (1 + e_0) \cdot \frac{Q(\omega)}{t_N} = -\Lambda \cdot (1 + e_0) \cdot \frac{b\omega}{t_N} \tag{2.77}$$

Substituting Equation (2.75) into Equation (2.70), which is equivalent to the consistency condition of Equation (2.74), and assuming the associated flow rule in $t_{ij}$ space expressed as Equation (2.60), the proportionality constant $\Lambda$ is give as

$$\Lambda = \left\langle \frac{\dfrac{\partial F}{\partial \sigma_{kl}} d\sigma_{kl}}{(1+e_0)\left\{ \dfrac{\partial f}{\partial t_{kk}} + \dfrac{G(\rho)}{t_N} + \dfrac{Q(\omega)}{t_N} \right\}} \right\rangle = \left\langle \frac{dF}{h^p} \right\rangle \tag{2.78}$$

Then, the plastic strain increment is calculated by substituting the proportional constant Λ above into Equation (2.60).

Simulation for structured clay is carried out to confirm the performance of the present model. The values of the material parameters used in the simulations are the same as those for Fujinomori clay in Table 2.2. One added parameter *b* for the bonding effect is shown in Table 2.3. Figure 2.42 shows the results of simulations using the three-dimensional model for the oedometer tests on structured clays which have the same initial void ratio but have different initial bonding effects, and it is arranged in terms of the relations between void ratio and vertical stress in log scale. Here, the solid line with $\omega_0$=0.0 is the result for non-structured soil. It is seen that three-dimensional model can also describe the typical one-dimensional consolidation behavior of structured soils in the same way as those by the one-dimensional model in the previous section. Figure 2.43 shows the results of simulation in constant mean principal stress tests ($p$ = 98kPa) on the same clay under triaxial compression and extension conditions. The initial stiffness, peak strength and dilatancy become large with the increase of the bonding effect, even if the initial void ratio is the same. Figure 2.44 shows the results of numerical simulations of undrained triaxial compression and extension tests ($p'_0$ = 98kPa) on the same clay. Diagram (a) is the results of effective stress paths, and diagram (b) is the results of stress-stain curves. In these figures, upper part is the results under triaxial compression condition, and lower part is the results under triaxial extension condition. The straight lines from the origin in diagram (a) represent the critical state lines (*CSL*) in $p'$-$q$ plane. Under undrained shear loadings, clays with bonding are stiffer and have higher strength than clay without bonding. It is also seen that over consolidated clay without bonding ($\omega_0$ = 0.0) shows strain hardening with the decrease and the subsequent increase of mean stress, whereas clays with bonding ($\omega_0$ = 0.2, 0.4) show not only strain hardening with the decrease and the increase of mean stress but also strain softening with the decrease of mean stress and deviatoric stress under undrained condition. These are the typical undrained behaviors of structured soil.

Figure 2.45 shows the results of numerical simulations of isotropic compression and the succeeding undrained shear tests on the structured clay. Diagram (a) shows the consolidation curve of a structured clay (initial state: $e_0$ = 0.73 ($\rho_0$ = 0.1), $\omega_0$ = 0.4 at $p_0$ = 98kPa) from stress condition (A). Diagrams (b) and (c) show the result of effective stress paths and stress-strain curves in undrained triaxial compression tests on the clay which are sheared from stress conditions (A), (B) and (C) in diagram (a). Figure 2.46 shows the observed results of undrained shear tests on undisturbed Osaka Pleistocene clay (Ma12) by Asaoka et al., (2000a). Here, OC is the results under initial confining pressure $p_0'$ = 98kPa (over consolidation state), and NC is the results under $p_0'$ = 490kPa (almost the same stress as the overburden pressure in site). They also carried out the simulations of structured soils using the SYS Cam clay model (Asaoka et al., 2000a; Asaoka et al., 2000b; Asaoka, 2005), in which subloading surface concept (to increase the plastic modulus) and superloading surface concept (to decrease the plastic modulus) are introduced to the Cam clay model. On the other hand, as

Table 2.3 Material parameters assuming Fujinomori clay – new parameter b represents the bonding effect

| | | |
|---|---|---|
| $\lambda$ | 0.104 | Same parameters as Cam clay model |
| $\kappa$ | 0.010 | |
| $N = e_{NC}$ at $p = 98$ kPa & $q = 0$ kPa | 0.83 | |
| $R_{cs} = (\sigma_1/\sigma_3)_{cs(comp.)}$ | 3.5 | |
| $\nu_e$ | 0.2 | |
| $\beta$ | 1.5 | Shape of yield surface (same as original Cam clay at $\beta = 1$) |
| $a / (\lambda\text{-}\kappa)$ | 500 | Influence of density and confining pressure |
| $b / (\lambda\text{-}\kappa)$ | 40 | Degradation parameters of bonding |

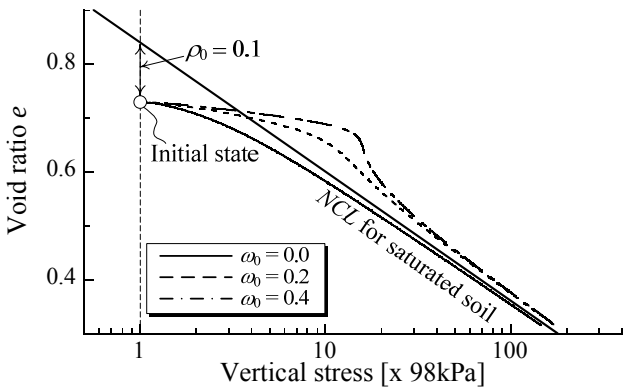


Figure 2.42 Simulations of oedometer tests on clay with same initial void ratio but different initial bonding

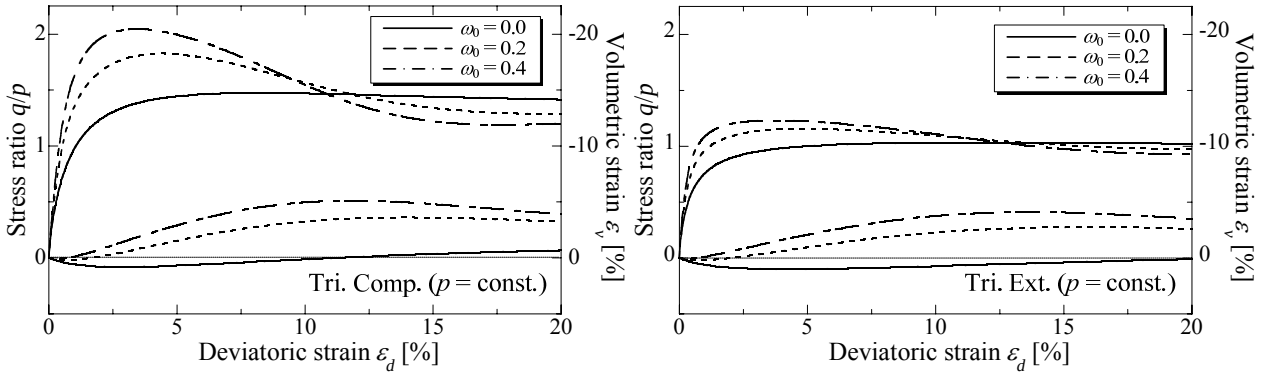


Figure 2.43 Simulations of drained triaxial compression and extension tests ($p$ = 98kPa) on clay with same initial void ratio but different initial bonding

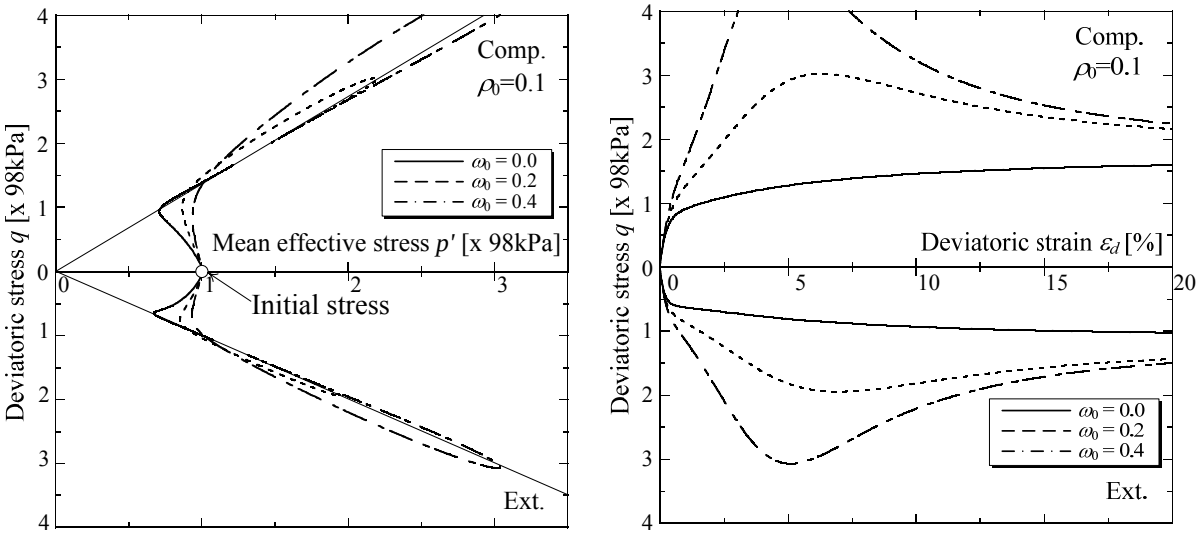


Figure 2.44 Simulation of undrained triaxial compression and extension tests on clay with same initial void ratio but different initial bonding

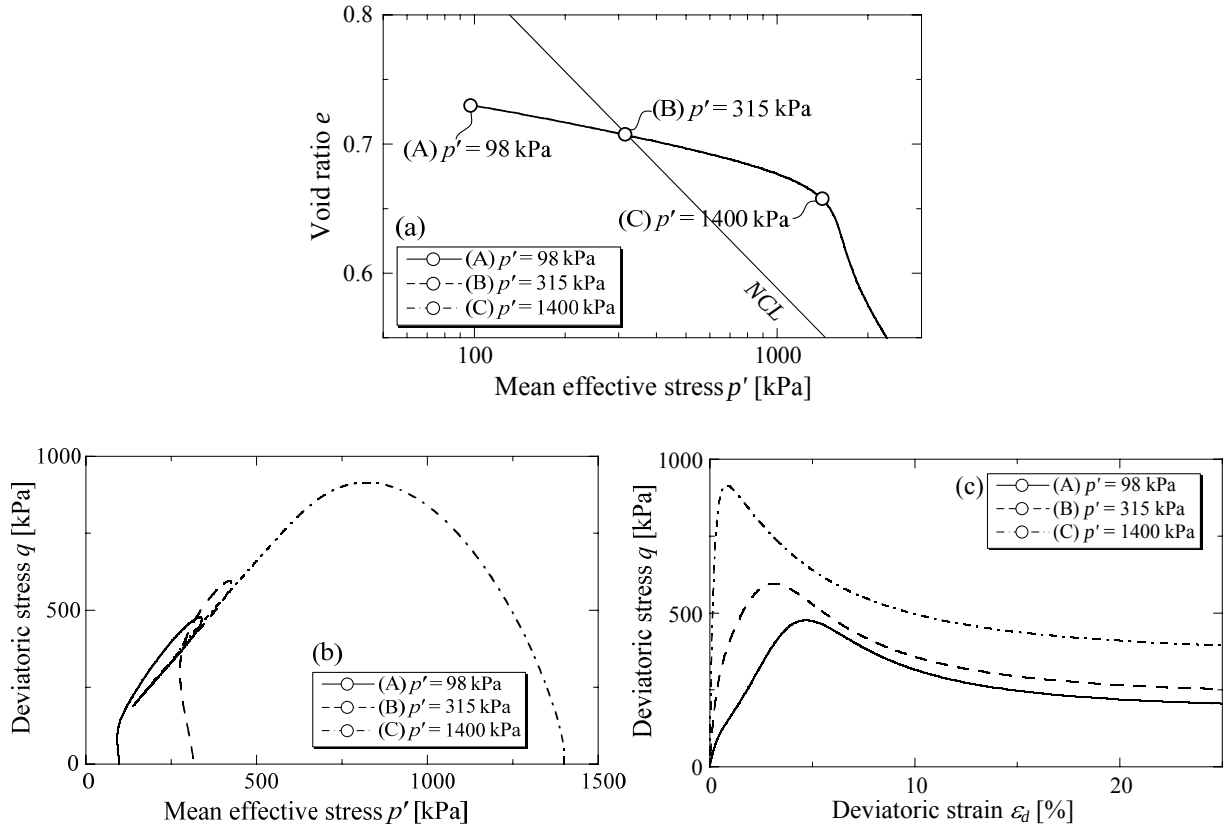


Figure 2.45 Calculated results of isotropic compression and succeeding undrained shear tests on structured clay ((a): isotropic consolidation test and undrained triaxial compression test – (b) effective stress path, (c) stress-strain curve)

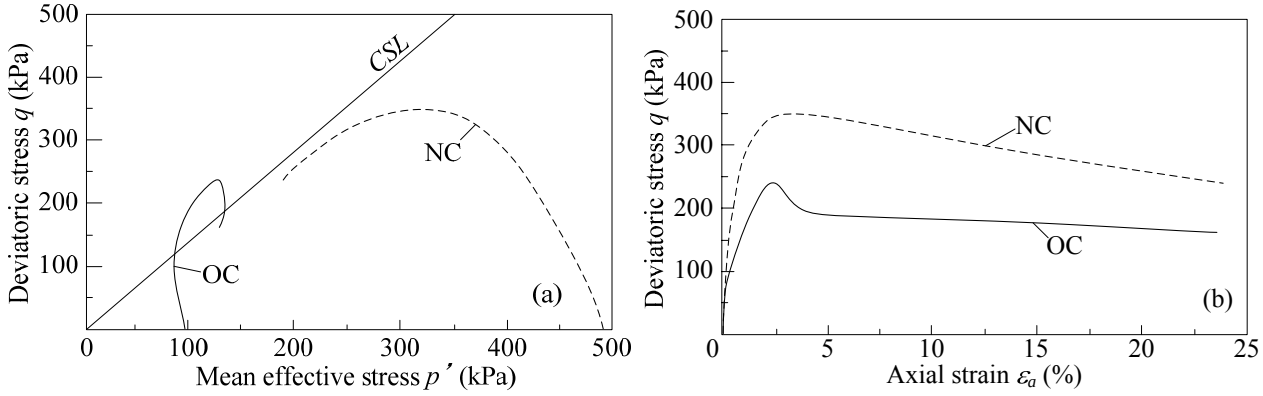


Figure 2.46 Observed results of undrained shear tests on overconsolidated (OC) and normally consolidated (NC), undisturbed Osaka Pleistocene clay (Ma12) (after Asaoka et al., 2000). ((a)effective stress path, (b)stress-strain curve)

can be seen from Equation (2.75) in the present model, $G(\rho)$ and $Q(\omega)$ have effects to increase the plastic modulus in the case that $\rho$ and $\omega$ are positive. Only when $\rho$ becomes negative (the current void ratio is larger than that on *NCL*), $G(\rho)$ has an effect to decrease the plastic modulus. The model simulates well typical undrained shear behavior of structured soil under different confining pressure, i.e., the differences of stress paths and stress-strain curves depending on the magnitude of confining pressure, rewinding of stress path after increasing of mean stress and deviatoric stress and others.

*Modeling of the influence of external factor*

As shown in former section, the external factors, e.g., temperature, strain-rate, degree of saturation and others, affect on the stress-strain behavior of soil in one-dimensional problem. As a matter of course, those external factors have to be considered for modeling of the multi-dimensional model. Figure 2.47 shows the results of drained triaxial compression test on clay under different temperatures (Hueckel & Baldi, 1990), Figure 2.48 shows the results of undrained triaxial compression test on normally and over consolidated clay with different strain rate, and Figure 2.49 shows the results of drained / exhausted triaxial compression tests on DL-clay with different suctions (degree of saturation) (Toyota et al., 2007). It can be seen from these experimental results that specimens with lower temperature, faster strain rate and lower degree of saturation represent stiffer behavior, higher strength and more dilative, even if having the same density and same value of mean stress. It seems that those deformation and strength characteristics of soil in the multi-dimensional problem is closely related to that in one-dimensional problem for these isotropic effects, thus the influences of those external factors for multidimensional problem can be considered to change the position of normally consolidated line

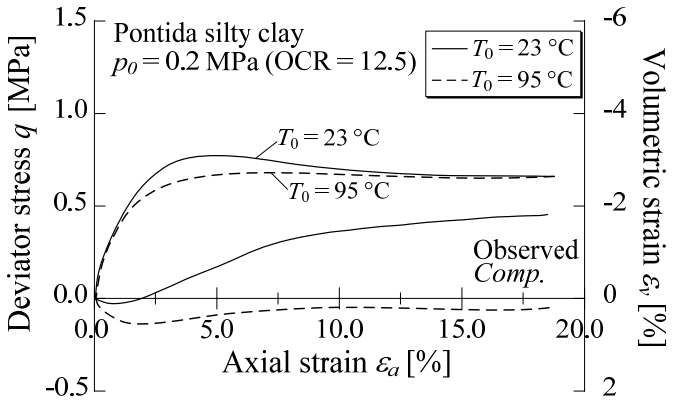


Figure 2.47 Observed results of drained shear tests on clay at different temperature (after Hueckel & Baldi, 1990)

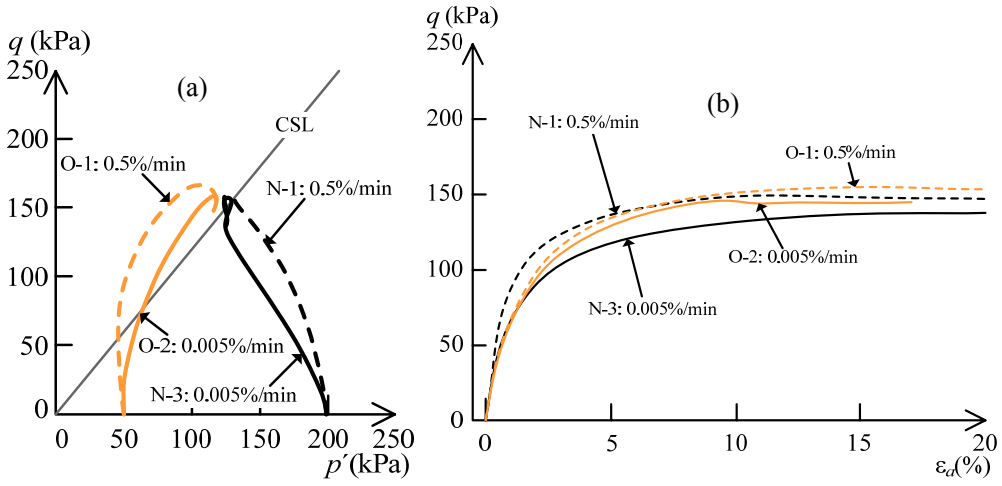


Figure 2.48 Observed results of undrained triaxial compression tests on normally consolidated and over consolidated clays with different strain rates ((a) effective stress path, (b) axial strain $\varepsilon_a$ and deviatoric stress $q$ relation) (after Oka et al., 2003)

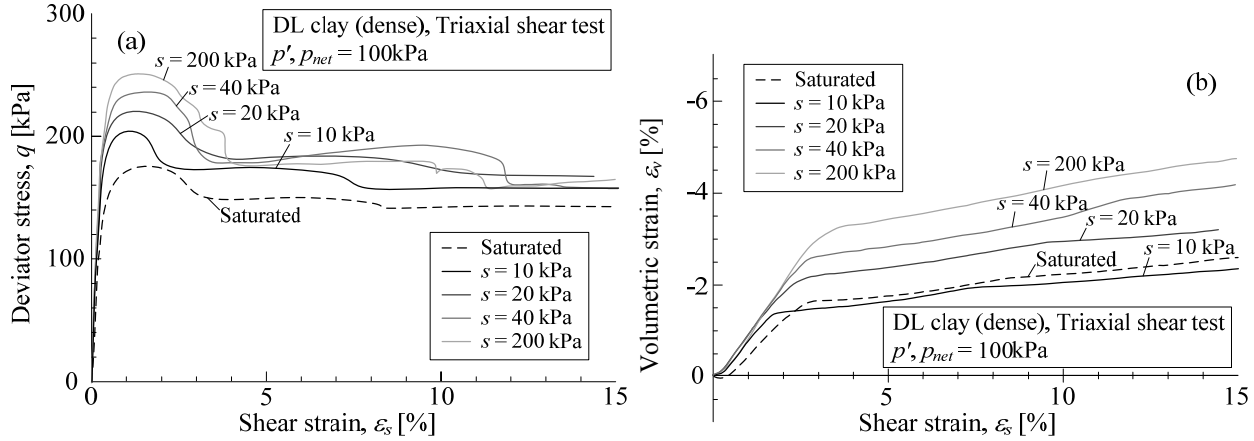


Figure 2.49 Observed results of exhausted / drained triaxial compression tests under different suction on unsaturated DL-clay ((a) deviatoric strain $\varepsilon_d$ and deviatoric stress $q$ relation, (b) deviatoric strain $\varepsilon_d$ and volumetric strain $\varepsilon_v$ relation) (after Toyota et al., 2007)

(and critical state line) in a similar manner as one-dimensional problem. Then, the following aspects are assumed: Ⓓ The residual strength of soil is determined only by the value of effective stress regardless of the magnitude of external factors. Ⓔ The variation in position of critical state line (CSL) on $e$-ln $p$ plane changes due to the magnitude of external factors with keeping the vertical distance between CSL and NCL.

In a same manner as the extension of one-dimensional model considering the influence density and bonding to its multi-dimensional model above mentioned, the yield function of multi-dimensional model considering the influence of external factors is formulated by replacing $\sigma_0$ and $\sigma$ in the yield function of one-dimensional models (Equation (2.23)) by $t_{N0}$ and $t_{N1}$, respectively.

$$f = F - \{H + (\rho_0 - \rho) + (\psi_0 - \psi)\} = 0$$
$$where\ F = (\lambda - \kappa)\ln\frac{t_{N1}}{t_{N0}} = (\lambda - \kappa)\left\{\ln\frac{t_N}{t_{N0}} + \zeta(X)\right\},\ H = (-\Delta e)^p \tag{2.79}$$

Here, $\psi$, which is the state variable to determines the position of *NCL*, is related with strain rate, temperature, degree of saturation and others in the same way as one-dimensional model, and $\psi_0$ is the initial value of $\psi$. Note that it is automatically provided from above second assumption, i.e., the constant vertical distance between *NCL* and *CSL*, which means the stress-dilatancy relation is determined uniquely regardless of the magnitude of external factors. From the consistency condition ($df$ = 0) of Equation (2.79) and flow rule in Equation (2.60), we can obtain

$$df = dF - (dH - d\rho - d\psi)$$
$$= \frac{\partial F}{\partial \sigma_{ij}} d\sigma_{ij} - \{d(-e)^p - d\rho - d\psi\} = \frac{\partial F}{\partial \sigma_{ij}} d\sigma_{ij} - \left\{(1 + e_0)\Lambda \frac{\partial f}{\partial t_{kk}} - d\rho - d\psi\right\} = 0 \tag{2.80}$$

Since $d\rho$ is simply considered only density effect in Equation (2.71), $\Lambda$ is expressed as

$$\Lambda = \left\langle \frac{\dfrac{\partial F}{\partial \sigma_{ij}} d\sigma_{ij} + d\psi}{\left(1+e_0\right)\left\{\dfrac{\partial f}{\partial t_{kk}} + \dfrac{G(\rho)}{t_N}\right\}} \right\rangle = \left\langle \frac{dF}{h^p} \right\rangle \tag{2.81}$$

Then, the plastic strain increment is calculated by substituting the proportional constant Λ above into Equation (2.60).

*Modeling of temperature effect on deformation and strength characteristic of soil in multi-dimensional problem*

In a similar manner as modeling of temperature effect on deformation characteristic of soil in one-dimensional problem, the state variable $\psi$ which prescribes the position of normally consolidated line and critical state line in $e$-ln $p$ plane is given as function of temperature and it is same as Equation (2.27) in multi-dimensional modeling. The proportionality constant Λ shown in Equation (2.81), therefore, is developed to follows.

$$\Lambda = \left\langle \frac{\dfrac{\partial F}{\partial \sigma_{ij}} d\sigma_{ij} + \left(\lambda_T - \kappa_T\right) dT}{\left(1+e_0\right)\left\{\dfrac{\partial f}{\partial t_{kk}} + \dfrac{G(\rho)}{t_N}\right\}} \right\rangle = \left\langle \frac{dF}{h^p} \right\rangle \tag{2.82}$$

The plastic strain increment is calculated by substituting Equation (2.82) into Equation (2.60), and also the elastic strain increment obeying the Hooke's law is developed as follows by considering thermal expansion.

$$d\varepsilon_{ij}^e = \frac{1+\nu_e}{E_e} d\sigma_{ij} - \frac{\nu_e}{E_e} d\sigma_{kk}\delta_{ij} + \frac{\kappa_T}{3\left(1+e_0\right)} dT\delta_{ij} \quad \textit{where} \quad E_e = \frac{3\left(1-2\nu_e\right)\left(1+e_0\right)}{\kappa} p \tag{2.83}$$

*Modeling of time - strain rate effect on deformation characteristic of soil in one-dimensional problem*

In the one-dimensional time-dependent model, the state variable $\psi$ is related with the rate of plastic void ratio change $(-\dot{e})^{pt}$ as described in Equation (2.33). However, in multi-dimensional stress condition, $(-\dot{e})^{pt}$ (or plastic volumetric strain rate) is not necessarily positive during plastic deformation because of soil dilatancy, and then the rate of plastic void ratio change (or plastic volumetric strain rate) is not suitable for the measure of time-dependent behavior. Since the norm of plastic strain rate $\|d\dot{\varepsilon}_{ij}^p\|$ is always positive during plastic deformation even in multi-dimensional condition and gives the magnitude of the plastic stain rate, it seems reasonable that $\psi$ is related with some quantity using the norm of the plastic stain rate. Now, under isotropic compression, the norm of plastic strain rate $\|d\dot{\varepsilon}_{ij}^p\|$ is expressed as follows using the rate of plastic void ratio change $(-\dot{e})^{pt}$:

$$\left\|d\dot{\varepsilon}_{ij}^p\right\| = \sqrt{d\dot{\varepsilon}_{ij}^p d\dot{\varepsilon}_{ij}^p} = \sqrt{d\dot{\varepsilon}_1^{p\,2} + d\dot{\varepsilon}_2^{p\,2} + d\dot{\varepsilon}_3^{p\,2}} = \sqrt{3} d\dot{\varepsilon}_1^p = \frac{\left(-\dot{e}\right)^p}{\sqrt{3}\left(1+e_0\right)} \quad \textit{at isotropic stress condition} \tag{2.84}$$

It is assumed that $(-\dot{e})^{pt}_{(equ)}$ is a rate of equivalent plastic void ratio change, which is defined by Equation (2.84) not only under isotropic compression but also under any kinds of stress conditions.

$$\left(-\dot{e}\right)_{(equ)}^{pt} = \sqrt{3}\left(1+e_0\right)\left\|d\dot{\varepsilon}_{ij}^p\right\| \tag{2.85}$$

Therefore, the state variable $\psi$ is given as function of the rate of equivalent plastic void ratio in order to the influence of strain rate on deformation and strength characteristics of soil in multi-dimensional problem.

$$\left(\psi_0 - \psi\right) = \lambda_\alpha \ln \frac{\left(-\dot{e}\right)^{pt}_{(equ)_0}}{\left(-\dot{e}\right)^{pt}_{(equ)}} \tag{2.86}$$

And the proportionality constant Λ shown in Equation (2.81) is developed to follows.

$$\Lambda = \left\langle \frac{\dfrac{\partial F}{\partial \sigma_{ij}} d\sigma_{ij} + \lambda_\alpha}{\left(1+e_0\right)\left\{\dfrac{\partial f}{\partial t_{kk}} + \dfrac{G(\rho)}{t_N} + \dfrac{\lambda_\alpha}{\left(-\Delta\dot{e}\right)^{pt}_{(equ)} dt}\sqrt{3}\left\|\dfrac{\partial f}{\partial t_{ij}}\right\|\right\}} \right\rangle = \left\langle \frac{dF}{h^p} \right\rangle \tag{2.87}$$

Then, the plastic strain increment is calculated by substituting the proportional constant Λ above into Equation (2.60), and the elastic strain increment is given as Equation (2.47).

Then, parameters for these models are given on the basis of that for Fujinomori clay as well as above calculations shown in Table 2.2. Newly added parameters are: the coefficient of thermal contraction $\lambda_T$ = 0.0005 and the coefficient of thermal expansion $\kappa_T$ = -0.0001, respectively; the coefficient of secondary consolidation $\lambda_\alpha$ = 0.003 and the initial rate of the void ratio change at reference state is $(-\dot{e})^p$ = 1.0 * $10^{-7}$. Figure 2.50 shows the calculated results of drained triaxial compression tests at different temperature ($T$ = 20 and 80℃). Comparing this figure and observed results shown in Figure 2.47, it is indicated that the present model can qualitatively estimate the mechanical characteristics of soil depending on temperature: the sample under higher temperature has higher strength and more dilative than lower temperature one. Figure 2.51 shows the calculated results of undrained triaxial compression tests with different axial strain rate ($\dot{\varepsilon}_a$ /min. = 2.0 %/min. and 0.002 %/min.) on normally consolidated and over consolidated samples ((a) effective stress

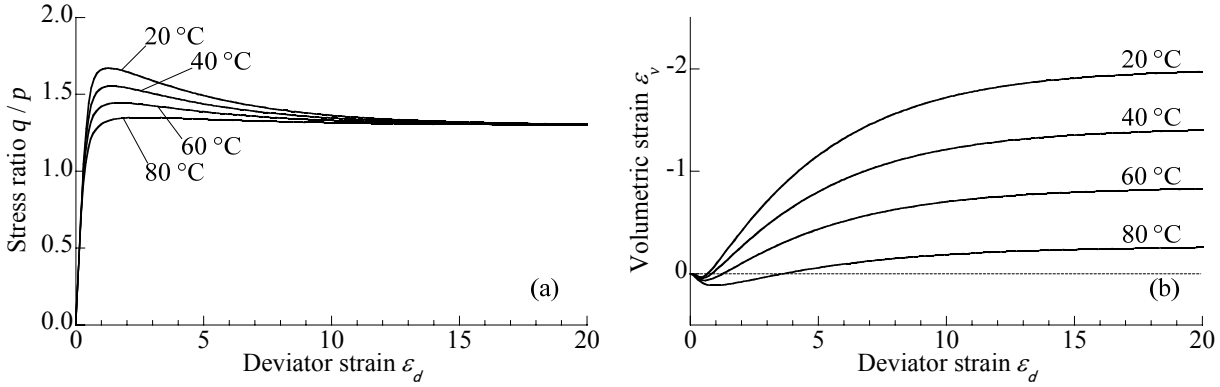


Figure 2.50 Calculated results of drained triaxial compression tests on overconsolidated soil at different temperature. ((a) deviatoric strain $\varepsilon_d$ and deviatoric stress $q$ relation, (b) deviatoric strain $\varepsilon_d$ and volumetric strain $\varepsilon_v$ relation)

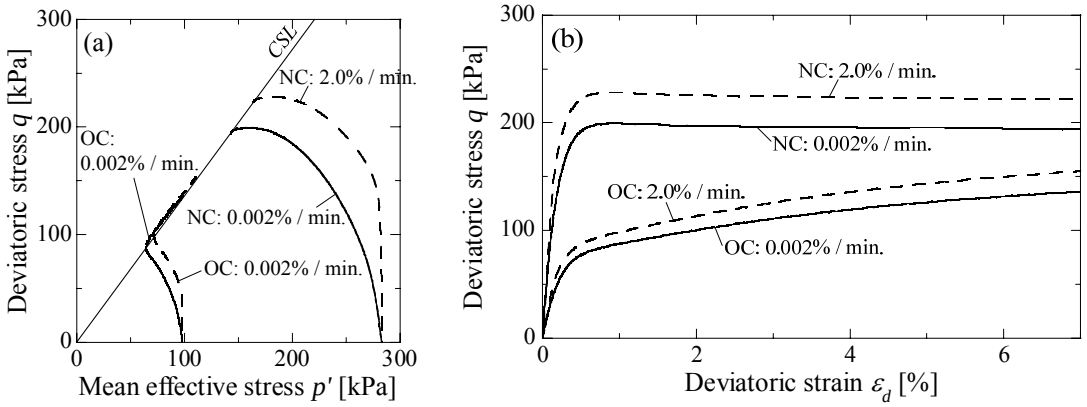


Figure 2.51 Calculated results of undrained triaxial compression tests on normally and over consolidated soil with different strain rate ($\dot{\varepsilon}_a$ /min. = 2.0 %/min. and 0.002 %/min.) ((a) effective stress path, (b) deviatoric strain $\varepsilon_d$ and deviatoric stress $q$ relation)

paths, (b) stress-strain curves). The present model can describe well-known strain rate effects on strength of soil and development of pore water pressure – higher undrained shear strength and less pore pressure development with increasing strain rate as can be seen in observed results shown in Figure 2.48.

## 2.5 Summary

In this chapter, in order to construct the elastoplastic constitutive model of soil considering the various features of soil behavior, the one-dimensional model which describes the relation between one-dimensional stress $\sigma$ and void ratio $e$ was firstly formulated. The simple model for normally consolidated soil was extended to one considering the influence of density, bonding, external factors (i.e. temperature, strain-rate, degree of saturation and so on). Those one-dimensional models are, subsequently, extended to the multi-dimensional models, which describe the relation between stress tensor $\sigma_{ij}$ and strain tensor $\varepsilon_{ij}$. The main results of this paper are summarized as follows:

*One dimensional elastoplastic constitutive model*

(1) Normally consolidated soil; The fundamental one dimensional yield function was derived from general experimental result on normally consolidated soil, which is the linear relation between void ratio and logarithmic mean stress under consolidation. The hardening parameter, then, was given as the plastic change of void ratio $(-\Delta e)^p$.

(2) Over consolidated soil; A simple method to describe the behavior of over consolidated soil, which is elastoplastic behavior even in elastic region and stiffer behavior with larger over consolidated ratio, is presented by introducing one state variable "$\rho$". The state variable "$\rho$" relates to density and was given monotonous evolution rule. This formulation is, in a sense, one-dimensional comprehension of the

subloading surface concept by Hashiguchi (1980).

(3) Structured soil (Bonding effect); The structured soil is stiffer than non-structured over consolidated soil, even if the state variable $\rho$ is the same. By considering the bonding effect "$\omega$" on the evolution rule of "$\rho$", the behavior of structured soil which shows the complex stiffness change with dissipation of bonding is modeled.

(4) Various external factors (temperature, strain rate, degree of saturation and so on); It is experimentally known that temperature, strain rate and partial saturation (degree of saturation and suction) isotropically effect on the deformation characteristic of soil as well as density and bonding, and also the normally consolidated line shifts due to change of value of those parameters. In order to model theses features, by introducing a state valuable $\psi$ given as function of strain rate (rate of void ratio change), temperature, degree of saturation or others, the position of *NCL* is shifted.

*Multi-dimensional model elastoplastic model*

(1) The yield function for the multi-dimensional model of normally consolidated soil, e.g., Cam clay model, is given only by replacing $\sigma_0$ and $\sigma$ in the yield function of one-dimensional model with $p_0$ and $p_1$, which represent the size of yield surface. And the associated flow rule is assumed in ordinary stress space to determine direction of plastic strain increment.

(2) The ordinary constitutive model formulated by using the invariants ($p$ and $q$) based on ordinary stress $\sigma_{ij}$, such as Cam clay model, cannot consider the influence of intermediate stress $\sigma_2$ on the deformation and strength characteristics of soil. The concept of $t_{ij}$ can take account of the influence of intermediate principal stress $\sigma_2$ automatically. The general method to extend any one-dimensional model to three-dimensional one based on the $t_{ij}$ concept was presented.

(3) One-dimensional model considering the influence of density by using the state variable "$\rho$" is extended to the corresponding multi-dimensional model based on modified stress $t_{ij}$. It was shown that the present model can describe the stress-strain behavior of soils including positive and negative dilatancy under different void ratio by using the material parameters common with the one-dimensional model.

(4) Multi-dimensional model for structured soil based on modified stress $t_{ij}$ was extended in a similar manner as the case of over consolidated soil. This model can describe well-known drained and undrained shear behavior of structured soils in three-dimensional stresses as well as consolidation behavior of natural deposited soil by adding only one extra material parameter.

(5) It is experimentally known that specimen with lower temperature, faster strain rate and lower degree of saturation represent stiffer behavior and higher strength, even if having the same density and value of

mean stress. Since those deformation and strength characteristics of soil in the multi-dimensional problem is related to that in one-dimensional problem, the influences of external factors can be considered by changing the position of normally consolidated line (and critical state line) in the same way as one-dimensional model. For describing other features of soil in three-dimensional stress condition, one-dimensional models were extended to the corresponding three-dimensional models by introducing the state variable $\psi$.

## Reference


Asaoka, A., Nakano, M. and Noda. T. (1998): Super loading yield surface concept for the saturated structured soils, *Proc. of the Fourth European Conference on Numerical Methods in Geotechnical Engineering-NUMGE98*, pp.232-242.

Asaoka, A., Noda, T., Yamada, E., Kaneda, K. and Nakano, M. (2000a): Superloading yield surface concept for highly structured soil behavior, *Soil and Foundations*, Vol. 40, No. 2, 99-110.

Asaoka, A., Nakano. M and Noda, T. (2000b): Elasto-plastic behavior of structured overconsolidated soils, J. Appl. Mech. JSCE, Vol. 3, 335-342.

Asaoka, A (2005): Consolidation of clay and compaction of sand – an elastoplastic description, *Proc. of 12th Asian Regional Conf. on Soil Mech. and Geotechnical Eng.*, Keynote Paper, Singapore, Vol. 2, 1157-1195.

Chowdhury, E. Q. (1998): *Ph.D Thesis*, Nagoya Institute of Technology.

Chowdhury, E. Q. & Nakai, T. (1999): Consequence of the $t_{ij}$-concept and a new modeling approach, *Computers and Geotechnics*, Vol. 23, 131-164.

Dafalias, Y. F. (1986): Bounding Surface Plasticity. I: Mathematical Foundation and Hypoplasticity, *Journal of Engineering Mechanics*, Vol. 112, No. 9, 966-987.

Eriksson, L.G. (1989): Temperature effects on consolidation properties of sulphide clays, *Proc. of the 12th int. conf. on Soil Mech. and Foundation Engrg.*, 3, 2087-2090.

Hashiguchi, K. and Ueno, M. (1977): Elastoplastic constitutive laws of granular material, Constitutive Equations of Soils, *Pro. 9th Int. Conf. Soil Mech. Found. Engrg.*, *Spec. Ses.9*, Murayama, S. and Schofield, A. N. (eds.), Tokyo, JSSMFE, pp.73-82.

Hashiguchi, K. (1980): Constitutive equation of elastoplastic materials with elasto-plastic transition, *J. of Applied Mech.*, ASME, 102(2), 266-272.

Henkel, D. J. (1960): The shear strength of saturated remoulded clay, *Proc. of Research Conf. on Shear Strength of Cohesive Soils at Boulder*, Colorado, 533-540.

Hinokio, M. (2004): *ph.D Thesis, Nagoya Institute of Technology*. (in Japanese)

Shahin, H. M., Nakai, T., Kikumoto, M., Kyokawa, H. and Miyahara, Y. (2010): Modeling of time-dependent behavior of clay in one-dimensional consolidation, *Proc. of the 4th Sino-Japan Geotechnical Symposium*, 54-61.

Honda, M. (2000): *Ph.D Thesis, Kobe univ.* (in Japanese).

Kyokawa, H., Nakai, T., Zhang, F. and Kikumoto, M. (2007)‡ A method of modeling of geomaterials considering density and bonding of soils, *Proc. of APCOM '07 in conjunction with EPMESC XI*, MS29-1-3.

Matsuoka, H. and Nakai, T. (1974): Stress-deformation and strength characteristic of soil under three different principal stresses, *Proc. JSCE*, **232**, pp.59-70.

Nakai, T. (2007): Modeling of soil behavior based on $t_{ij}$ concept, *Proc. of 13th Asian Regional Conf. on Soil Mech. and Geotechnical Eng*., Keynote Paper, Kolkata, Vol. 2, 69-89.

Nakai, T., Kyokawa, H., Kikumoto, M., Shahin, H. M. and Zhang, F. (2009(a)): Elastoplastic modeling of geomaterials considering the influence of density and bonding, *Proc. of the international symposium on Prediction and Simulation Methods for Geohazard Mitigation*, Kyoto, Japan, 367-374.

Nakai, T. and Hinokio, M. (2004): A simple elastoplastic model for normally and over consolidated soils with unified material parameters, *Soils and Foundation*, Vol. 44, No. 2, 53-70.

Nakai, T. and Matsuoka, H. (1986): A generalized elastoplastic constitutive model for clay in three-dimensional stresses, *Soils and Foundations*, Vol. 26, No. 3, 81-98.

Nakai, T., M., Shahin, H. M., Kikumoto, Kyokawa, H. and Zhang, F. (2009(b)): Simple and unified method for describing various characteristics of geomaterials - Influences of density, bonding, time effects and others -, *Journal of Applied Mechanics JSCE*, Vol. 12, 371-382. (in Japanese)

Nakai, T. and Mihara, Y. (1984): A new mechanical quantity for soils and its application to elastoplastic constitutive models, *Soils and Foundations*, Vol. 24, No. 2, 82–94.

Oshima, A., Ikeda, Y. and Masuda, S. (2002): Effects of load increment ratio on step loading consolidation test of clay, *Proc. of 37th Annual Meeting on JGS*, Vol. 1, 289-290 (in Japanese)

Schofield, A. N. and Wroth, C. P. (1968): *Critical State Soil Mechanics*, McGraw Hill, London.

Tidfors, M. and Sällfors, G. (1989): Temperature effect on preconsolidation pressure, *Geotechnical testing journal*, 12(1), 93-97.

Tanaka, H., Udaka, K. and Nosaka, T. (2006): Strain rate dependency of cohesive soils in consolidation settlement, *Soils and Foundations*, 46(3), 315-322.

# Chapter 3
# Constitutive model considering the influence of suction and degree of saturation

## 3.1 General

Stress-strain behavior of unsaturated soil seems rather different from that of saturated soil whose void is filled up with water. Since the capillary stress arising within the meniscus water in internal particles inhibits the interparticle slippage, it is well known that unsaturated soil shows stiffer behavior and higher strength than saturated one. Those stiffer behaviors are essentially similar to retain a larger void ratio (looser state) than saturated soil under same stress level. Once interparticle connection with capillary stress diminishes (or weakens) due to soaking process, however, unsaturated soil cannot retain its soil skeleton, and then soaking collapse behavior occurs. Thus stress-stain behavior of soil is closely and intricately related to moisture content (capillary stress). Unsaturated soils exist widely in the form of compacted fills and natural soils generally above the water table, and moisture content of soils changes due to drying and swelling processes such as rainfall. For any geotechnical problems, therefore, understanding of mechanical behavior of unsaturated soil and its modeling are absolutely essential.

Early investigations of the mechanical behavior of unsaturated soils focused on attempts to combine total stress $\sigma$, pore air pressure $u_a$ and pore water pressure $u_w$ within a single effective stress tensor $\sigma''$. The relationship most widely quoted was that suggested by Bishop (1959):

$$\sigma''_{ij} = \sigma_{ij} - u_a\delta_{ij} + \chi(u_a - u_w)\delta_{ij} \tag{3.1}$$

where $\chi$ was a factor varying with the degree of saturation $S_r$, from zero for dry soil to unity for fully saturated conditions. However, Jennings and Burland (1962), and subsequent authors indicated that while it is relatively easy to relate the shear strength of unsaturated soil to a single effective stress parameter involving $\sigma$, $u_a$ and $u_w$, the volumetric behavior is not controlled by the same stress parameter or by any other single stress variable. In particular, it has proved impossible to represent the complex wetting transition induced swelling and collapse behavior by single effective stress. Fredlund and Morgenstern (1977) argue that any two of the three stress parameters $\sigma - u_a$, $\sigma - u_w$ and $u_a - u_w$ would be sufficient to describe fully the stress state of an unsaturated soil. The most common choice is to use net stress $\sigma - u_a$ and matric suction $s$ (= $u_a$ - $u_w$) as two independent stress state variables. This approach, which was firstly used by Coleman (1962) and Bishop and Blight (1963), has formed the main basis for developments in constitutive modeling of unsaturated soils during the last 40 years. An elastoplastic critical state framework for unsaturated soil based on net stress $\sigma - u_a$ and matric suction $u_a - u_w$ was presented in qualitative form by Alonso et al. (1987). By using two independent stress variables, there is a lot of flexibility for modeling; Loading Collapse (LC) yield curve and Suction Increase (SI) yield surface are introduced in order to represent the swelling collapse and higher strength of unsaturated soil, and the volume change due to increasing of suction. Wheeler & Sivakumar (1995) and other authors

proposed further modifications, in the light of experimental data. Although such model can describe the diverse mechanical behaviors of unsaturated soil, its formulation is complicated and it is difficult to apply some ordinary modeling techniques which have ever developed for saturated soil (e.g., kinematic hardening law, subloading surface concept, and others) to such model based on two independent stress variables. Moreover, unsaturated state and fully saturated state have to be distinguished in such models using net stress and suction independently.

In modeling based on single effective stress (Bishop's effective stress), meanwhile, it is common that suction (degree of saturation) is used for not only effective stress shown in Equation (3.1) but also soil hardening parameter in order to describe typical behaviors of unsaturated (e.g., swelling collapse, higher strength and others). Moreover, it is easy and simple to apply ordinary modeling technique for saturated soil to unsaturated model based on single effective stress, and such model can consider from dry soil to fully saturated soil continuously. Some models were already applied to initial and boundary value problem (Iizuka, 2000). In modeling based on single effective stress, however, it is important issue to select an appropriate hardening parameter, which is ordinary linked with suction $s$ and degree of saturation $S_r$, and describe variation of its hardening parameter.

In the beginning of this chapter, general mechanical behaviors of unsaturated soil are discussed and organized by reviewing past experimental results. And then the schemes of modeling are shown. Especially, referring to a typical compression behavior of unsaturated soil which is generally known that the unsaturated soil is able to stay in a looser state above normally consolidated line in $e$-ln$p''$ plane, the modeling of unsaturated soil is carried out. In the present study, such effects of "partial saturation" are described by extending an existing constitutive model for saturated ones based on Bishop's effective stress. Then modeling of one-dimensional behavior considering the influence of various external factors shown in Chapter 2 is applied to the unsaturated soil, and the present one-dimensional model is extended to that of multi-dimensional model based on $t_{ij}$ concept subsequently. In the model, the increase (/ decrease) in degree of saturation is linked with downward (/ upward) movement of the normally consolidated line in the void ratio $e$ - logarithmic stress $\sigma$ (mean stress $p$) plane which controls the volumetric behavior and the peak strength of unsaturated soil. That is to say, the state variable $\psi$ representing the position of normally consolidated line proposed in Chapter 2 is given as function of degree of saturation. And the variation in degree of saturation is estimated by a newly proposed model for water retention curve considering the effects of hydraulic hysteresis and density. The validation of proposed model is verified by parametric study and comparison with experimental results, and then mechanisms of consolidation, soaking and compaction behavior of unsaturated soils are discussed through the simulations by the proposed model. Moreover, the simulation of compaction behavior of unsaturated soil is carried out by proposed model. As a result of calculation, the mechanical meanings of the compaction curve which represents the relation between dry density and moisture contents and the optimum moisture content are discussed.

! The substance of this chapter has been published as follows: Kyokawa et al. (2009, 2010(a), (b) and (c)), Kikumoto et al. (2009 and 2010).

## 3.2 Review the past research - various features of unsaturated soil

Here, some typical mechanical features of unsaturated soil are shown and discussed, and the schemes of modeling are shown in next section.

*Water retention curve – relation between suction and degree of saturation*

Suction, which is defined as the difference between pore air pressure $u_a$ and pore water pressure $u_w$, and degree of saturation are dominant factors on the mechanical and hydraulic characteristic of unsaturated soil. Physical meaning of suction is a force pulling water away from void of soil, and consequently surface tension (capillary stress) arises within the meniscus water in internal particles. And it is well known that suction generally correlate with degree of saturation through soil water characteristic curve (SWCC). A proper model for soil water characteristic curve, thus, is necessary to formulate a constitutive model for unsaturated soils.

Soil water characteristic curve on drying and wetting process is ordinarily S-shaped curve as shown in Figure 3.1 (e.g., Huang et al., 2005) regardless of type of soil such as sand, clay and others. In addition, it can be seen from Figure 3.1 the hydraulic hysteresis, which means that SWCC usually follows different paths according to drying and wetting suction histories. It is also shown through the past experimental studies Figure 3.2 (Kawai et al., 2000) that volumetric behavior also affects on SWCC, which indicate denser soil tends to retain higher $S_r$, and a variation in degree of saturation is caused by volume change even if suction is constant. It is also reported that temperature and magnitude of fine content affect on SWCC. Degree of saturation, therefore, does not have uniquely relationship with suction as describe by classical SWCC model (van-Genuchten, 1980 and Fredlund & Xing, 1994).

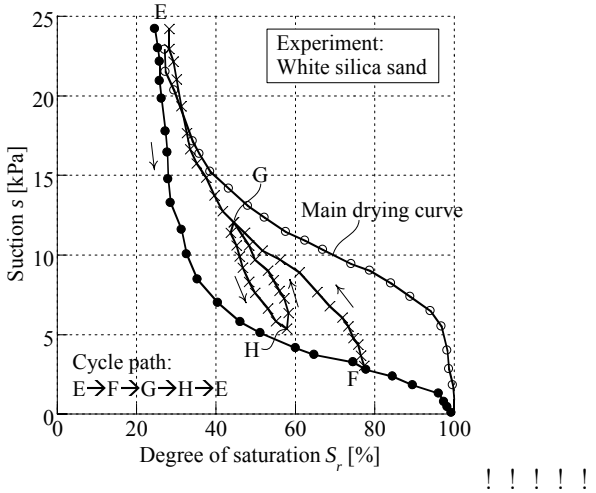


Figure 3.1 one instance of water retention and scanning curve on white silica sand (after Huang et al., 2005)

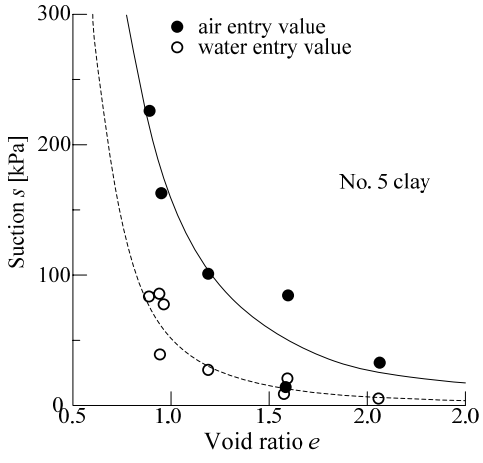


Figure 3.2 The experimental relation between void ratio $e$ and air entry / water entry value of suction (after Kawai et al., 2000) – denser soil has higher air / water entry value.

! ! ! ! !

*Effective stress of unsaturated soil*

In modeling of features of soil and organizing experimental results, it is important what type of effective stress to use. Bishop (1959) extended the effective stress for saturated soil proposed by Terzaghi to one considering the influence of suction defined as

$$\sigma''_{ij} = \sigma_{ij} - u_a\delta_{ij} + \chi(u_a - u_w)\delta_{ij} = \sigma^{net}_{ij} + S_r s\delta_{ij} \tag{3.2}$$

The parameter $\chi$ is imposed to vary from 0 for dry soils to 1 for saturated soils, enabling a simple transition from partially to fully saturated states, and recovering Terzaghi's effective stress for the saturated state. The investigation for how to define the parameter $\chi$ has ever been actively conducted (e.g., Nuth, 2008), and results of each investigations are summarized as a relation between parameter $\chi$ and degree of saturation in Figure 3.3. It can be seen that the parameter $\chi$ is positive correlative to degree of saturation, although a certain amount of variation can be seen. Therefore, $\chi$ is a variable given as a function of $S_r$, which is assumed to be equal to $S_r$ here for simplicity in this study.

Figures 3.4(a) and (b) mirror two stress interpretations at critical state on unsaturated soil ((a)Sivakumar (1993), (b)Geiser, Laloui and Vulleit (2006)), namely the deviator stress $q$ – mean net stress $p^{net}$

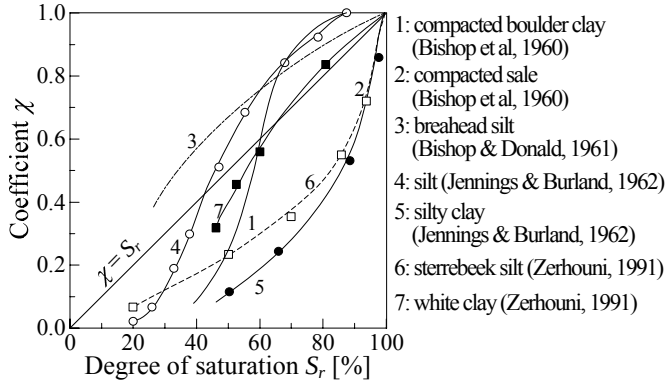


Figure 3.3 Observed relations between degree of saturation $S_r$ and parameter $\chi$ (after Nuth, 2008)

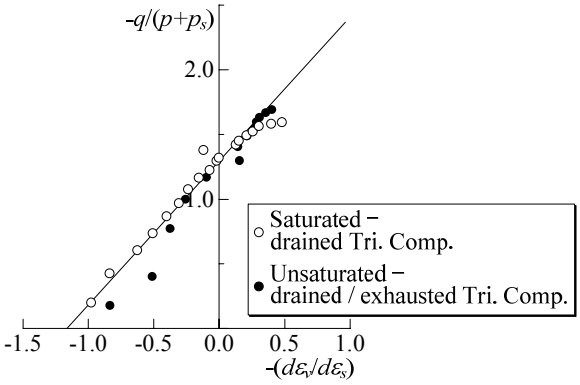


Figure 3.5 Stress-dilatancy relation organized by using effective degree of saturation $S_{re}$ (after Kawai et al., 2000)

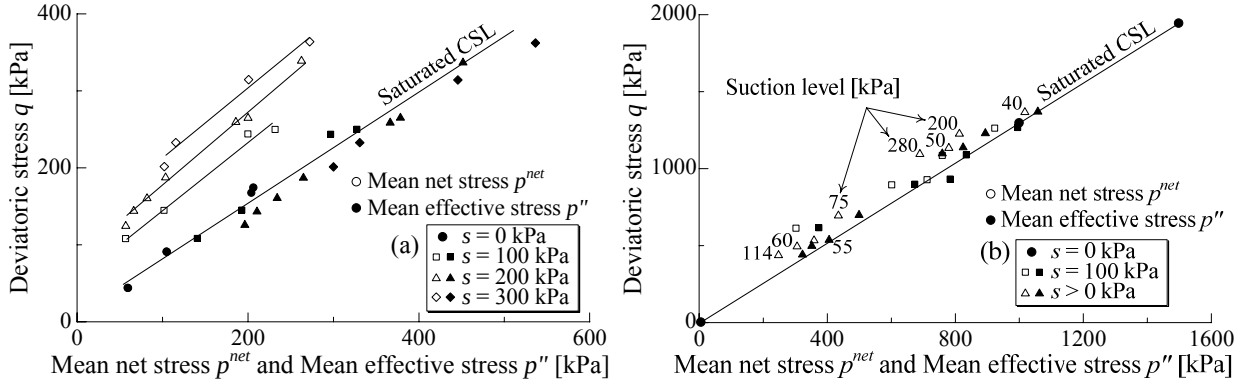


Figure 3.4 The residual strength organized by deviatoric stress $q$ – mean net stress $p^{net}$ and mean effective stress $p''$ whose $\chi$ is degree of saturation $S_r$ (left is form Sivakumar (1993), right one is from Geise et al. (2006))- $p''$ can uniquely determine the strength of soil.

plane and the deviator stress $q$ – mean effective stress $p''$ plane. And, Figure 3.5 shows stress-dilatancy relation (Kawai et. al., 1996) organized by using the effective stress in which parameter $\chi$ is given as effective degree of saturation $S_{re}$ (= $(S_r - S_{rc})/(1 - S_{rc})$) (Karube, 1996). Here, $S_{rc}$ is the degree of saturation on main wetting curve under same current suction level. From both Figures 3.4 and 3.5, it can be seen that Bishop's effective stress $p''$ can uniquely determine the critical state strength regardless of degree of saturation $S_r$. Moreover, the stress dilatancy relation of unsaturated soil coincides with that of saturated soil by using Bishop's effective stress whose parameter $\chi$ is defined as $S_{re}$. It is, thus, very simple and briefness to formulate a constitutive model for unsaturated soil based on Bishop's effective stress, since the critical strength, stress-dilatancy relation and shape of yield surface (if the associated flow rule is assumed) of saturated soil can be applied to modeling the unsaturated soil directly.

Jennings & Burland (1962) note that Bishop's effective stress cannot represent swelling collapse behavior, because it shows elastic behavior due to unloading during swelling path. And, Alonso (1990) proposed an elastoplastic constitutive model for unsaturated soil, in which stress parameters $\sigma_{ij}^{net}$ (=$\sigma_{ij} - u_a\delta_{ij}$) and suction $s$ are independently treated for flexibility modeling, and it can describe swelling collapse phenomena. On the other hand, some effective stress based on Bishop's one is newly proposed, e.g. Kohgo (1993), Karube (1996), Aitchson (1960), Kahlili & Khabbaz (1998) and Khalili et.al. (2004) define the parameter $\chi$ in Bishop's effective stress as a function of suction, through precisely fitting with a number of experimental results (e.g., compression index and shear strength). Even these newly proposed stresses cannot explain all of mechanical behaviors of unsaturated soil. In this paper, recognizing that such existing effective stress as Bishop's one cannot describe a whole mechanical behavior of unsaturated soil, the rest of mechanical behaviors are taken into consideration as various features of elastoplastic constitutive relations (model).

*Consolidation behavior of unsaturated soil*

Figures 3.6(a), (b) show compression behaviors of unsaturated Catalpo clay which are compared with that of saturated one (Honda, 2000); Diagram (a) shows the relation between vertical effective stress $\sigma'_v$ and void ratio $e$, Diagram (b) shows the relation between vertical effective stress $\sigma'_v$ and degree of saturation

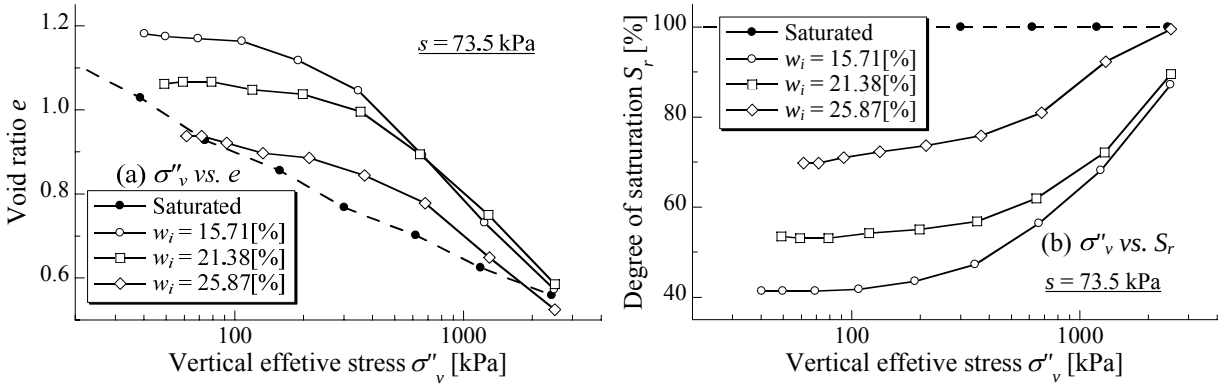


Figure 3.6 Observed results of exhausted / drained oedo-meter test under constant suction (s = 73.5 kPa) on various water contents unsaturated samples (after Honda, 2000) ((a) relation between vertical effective stress $\sigma_v''$ and void ratio $e$, (b) relation between vertical effective stress $\sigma_v''$ and degree of saturation $S_r$)

$S_r$. It is seen from Figure 3.6 that the unsaturated samples (solid line) initially show relatively higher stiffness and retain a larger void ratio than the saturated one (break line) under same stress level. Water content (degree of saturation) is lower, compression stiffness becomes higher. The stiffness of unsaturated samples, however, decreases form a certain stress level and these samples asymptotically approach to the normally consolidated line of the saturated sample ($NCL_{sat}$). It can be assumed that a capillary stress diminishes or weakens according to increasing of degree of saturation (water content) due to soil compression under constant suction, so that the stiffness of soil decreases. From this compression result, it can also be seen that the degree of saturation varies with density even though suction is constant.

*Swelling collapse behavior*

Figure 3.7 shows the volumetric compression behavior of air dried silt due to compression and swelling (Jennings and Burland, 1962). Air dried samples similarly behave that it stay in a looser region above the compression line of initially swelling sample (saturated sample) during the consolidation phase. In the subsequent soaking process with keeping respective confining pressures or respective volume $v$ ( = 1 + $e$), they show the swelling induced collapse or stress relaxation behavior until they come close to the compression line of saturated one. Moreover, the recompression behavior of these soaked samples traces the compression line of saturated one. As reasons for these swelling collapse phenomena and stress relaxation, it seems that soil reaches from unstable looser region above *NCL* for saturated soil to saturated stable state due to disappearance of capillary stress due to increasing of water content (degree of saturation).

Figure 3.8 shows the experimental observations in soaking tests on Kaolin clay conducted under constant applied stress varying initial void ratio and stress level (Sun et al., 2007). It is revealed from this figure that the amount of volume change due to swelling induced collapse is highly dependent on density and confining pressure. Especially, it can be observed from the results of lower confining pressure on denser sample ($e_0$ = 1.05) that soil shows volumetric expansive behavior due to soaking.

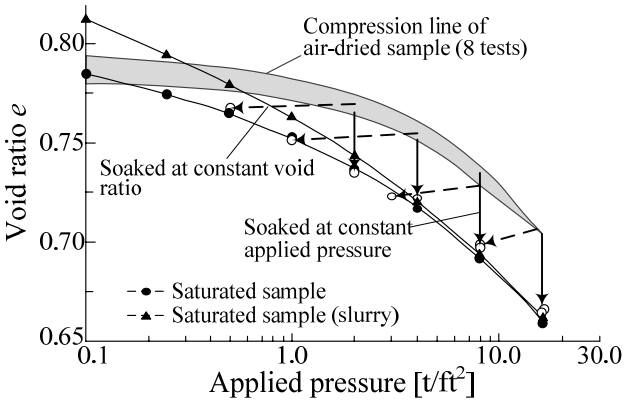


Figure 3.7 One-dimensional compression and subsequent soaking tests under constant void ratio and constant applied pressure on air dried silt (after Jennings and Burland, 1962)

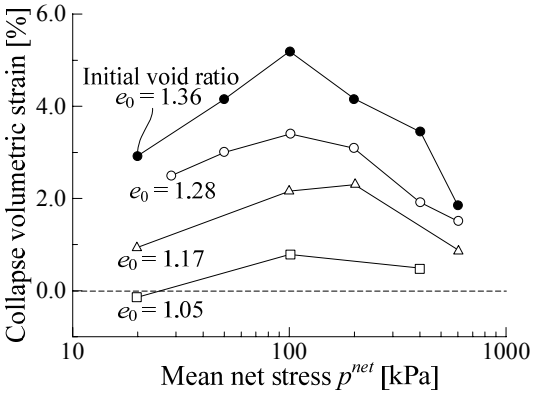


Figure 3.8 Soaking-induced volumetric strains at different mean total stresses for compacted Pearl clays with different initial densities (after Sun et al., 2007)

*Shear strength and deformation characteristics of unsaturated soil*

As generally known, it can be seen from Figures 3.9(a), (b) which are the results of drained and exhausted triaxial compression tests on DL clay with different suctions (Toyota et al., 2007), that unsaturated sample applied larger suction has higher shear strength. The possible explanation for this higher strength is shown as follows: The residual strength of soil is uniquely determined from effective stress shown in Equation (3.2), which gives higher value of mean stress due to higher capillary stress (suction); Unsaturated soil exhibits stiffer behavior due to lower water content (degree of saturation) in the same mechanism as compression behavior mentioned above.

Focusing on dilatancy characteristic sample having higher suction shows more dilative behavior as over consolidated soil, even if initial void ratio of each samples are the same. It is supposed, thus, that the critical state line on *e*-ln*p″* plane moves upward with increasing suctions (decreasing degree of saturation). From Figure 3.10(a) and (b) in which critical states of soil obtained from triaxial compression tests at

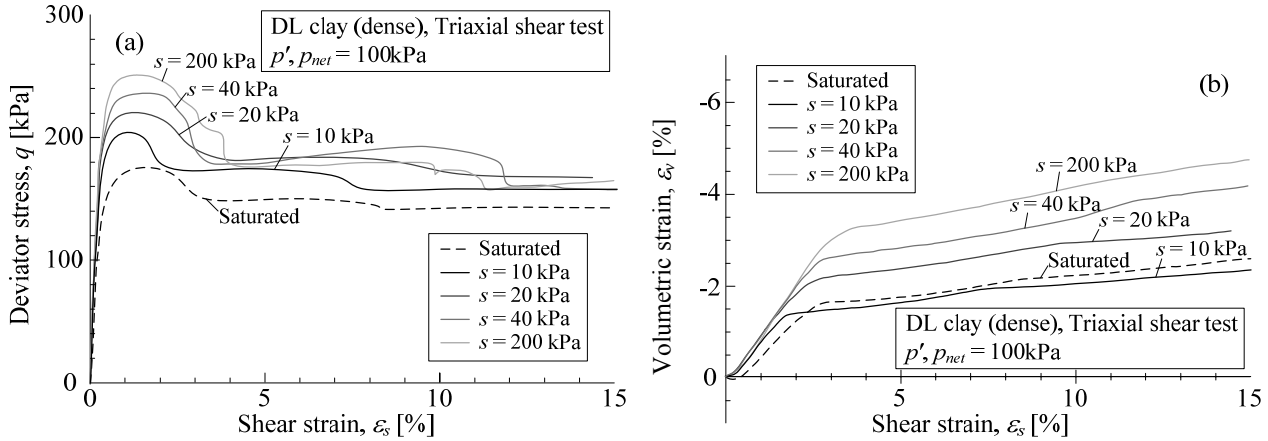


Figure 3.9 Observed results of exhausted / drained triaxial compression tests under different suction on unsaturated DL-clay ((a) deviatoric strain $\varepsilon_d$ and deviatoric stress $q$ relation, (b) deviatoric strain $\varepsilon_d$ and volumetric strain $\varepsilon_v$ relation) (after Toyota et al., 2007) – Sample applied higher suction (and lower degree of saturation ) shows higher strength and more dilative behavior, although initial void ratio of samples are the same.

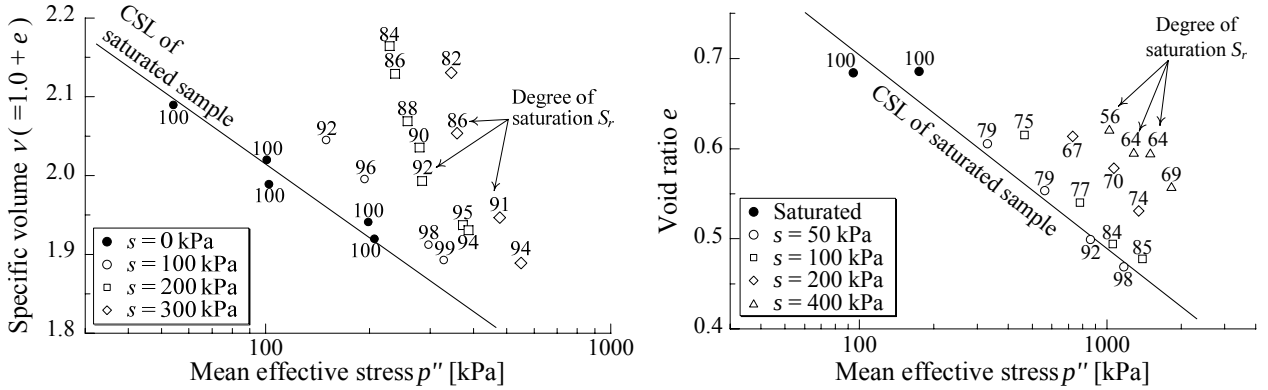


Figure 3.10 Critical state of saturated soil and unsaturated soil organized in e– ln*p″* plane (left one is from Sivakumar (1993), right one is from Cui (1996)) – It seems that *CSL* for sample having lower degree of saturation $S_r$ lies on looser state of e-ln*p″* plane.

different suction are plotted on $e$-ln$p''$ plane (Sivakumar, 1993 and Cui, 1996), it can be seen that the position of critical state line is uniquely determined in terms of not suction but degree of saturation.

## 3.3 Modeling of unsaturated soil

In this chapter, elastoplastic constitutive model for unsaturated soil will be formulated to capture the experimental results shown in former section. Knowledge about mechanical behaviors of unsaturated soil is summarized and corresponding modeling ideas are shown in follows;

(1) By using Bishop's effective stress, the critical state strength, stress-dilatancy relation and shape of yield surface (if the associated flow rule is assumed) of saturated soil can be applied to modeling of stress-strain relation of unsaturated soil directly.

∫∫ Based on Bishop's effective stress, organizing experimental results and formulating the constitutive model are conducted.

(2) Classical models of SWCC cannot consider the hydraulic hysteresis and the influence of density, temperature and others.

∫∫ A newly method extending easily all sort of SWCC model to one suitably considering these effects is proposed. In addition, in order to keep the formulation of the model as simple as possible, a well-known classical Equation for SWCC proposed by van Genuchten (1980) is extended.

(3) Compression behavior of unsaturated samples initially shows relatively higher stiffness and retains a larger void ratio than the saturated one under same stress level.

(4) In the swelling process with keeping confining pressures or respective volume ( = void ratio), unsaturated soils exhibit the hydraulic collapse or stress relaxation behavior until they come close to the compression line of saturated one. These swelling phenomena, additionally, are affected by the influence of density and confining pressure.

(5) Unsaturated sample applied larger suction has higher shear strength and shows larger dilative behavior as over consolidated soil, even if initial void ratio of each samples are the same.

(3), (4) and (5) ∫∫ Such influences of degree of saturation can be incorporated relatively simple way by shifting both normally consolidated line (*NCL*) and critical state line (*CSL*) of unsaturated soil downward (or upward) in the plane of void ratio $e$ and logarithm of effective mean stress $p''$ depending on the increase (or decrease) of degree of saturation.

### 3.3.1 Modeling of soil water characteristic curve considering the hydraulic hysteresis and the influence of density

The stress-strain behavior of unsaturated soil is remarkably affected by the variation in degree of saturation $S_r$. Therefore, a proper modeling of soil water characteristic curve (herein after called SWCC) is necessary in order to extend a constitutive model for saturated soils to that for unsaturated soils. The ordinary SWCC

model such as van Genuchten model (1980) can not consider, however, some features of SWCC: the hydraulic hysteresis effect, viz., SWCC of soil usually trace a different paths according to drying and wetting histories; the influence of density means that degree of saturation increase and decrease due to the volumetric compression and expansion even under constant suction as shown in Figure 3.6 (b). In this study, a new methods (models) extending all sort of SWCC model to one suitably considering these features are proposed, and it is introduced into the proposed elastoplastic constitutive model for the unsaturated soil. In order to keep the formulation of the model as simple as possible, a well-known classical Equation for water retention curves proposed by van Genuchten (1980) as an example is extended. The newly proposed method can be applied to any kind of classical SWCC model such as one proposed by Fredlund and Xing (1994) (Kikumoto et al., 2009).

*Modeling of hydraulic hysteresis on SWCC*

Some of method for considering hydraulic hysteresis on SWCC due to cyclic suction (or water content) histories have ever proposed, e.g., Poulovassilis (1962), Mualem (1974), Scott et al. (1983), Kool and Parker (1987), Li (2004), Huang et al (2005)., Liu and Muraleetharan (2006), Wei and Dewoolkar (2006), Kohgo (2008). Formulation and calculation of those existing models, in which scanning curve (intermediate route between drying curve and wetting curve) is obtained by interpolating position or gradient of main drying and wetting curve, is complicated. It is, therefore, difficult to extend those models to one considering other factors, e.g. density, temperature and others. The newly proposed method applied to simple classical model can be easily extended to one considering some effects.

Figure 3.11 shows the schematic diagram of the modeling. Two break line curves representing the highest and the lowest boundaries of degrees of saturation, which are usually called as the main drying curve and the main wetting curve respectively, are given by the classical non-hysteretic SWCC model taken van Genuchten's model as an example. Two boundaries of main curves ($f_d = 0$ and $f_w = 0$) are given as follows;

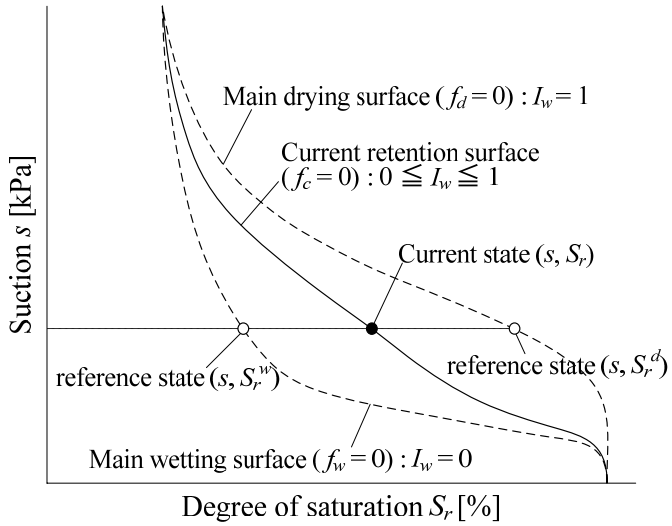


Figure 3.11 Modeling of the hysteresis by hydraulic state variable $I_w$ considering the suction histories.

Table 3.1 Material parameters for soil water characteristic curve (van Genuchten's model, 1980)

| | | |
|---|---|---|
| $S_{max}$ | 0.85 | maximum degree of saturation |
| $S_{min}$ | 0.02 | minimum (residual) degree of saturation |
| $\alpha$ | 0.25 | position of main drying curve |
| $\beta$ | 0.42 | position of main wetting curve |
| $m$ | 0.2 | shape of main drying / wetting curves |
| $n$ | 19.0 | |

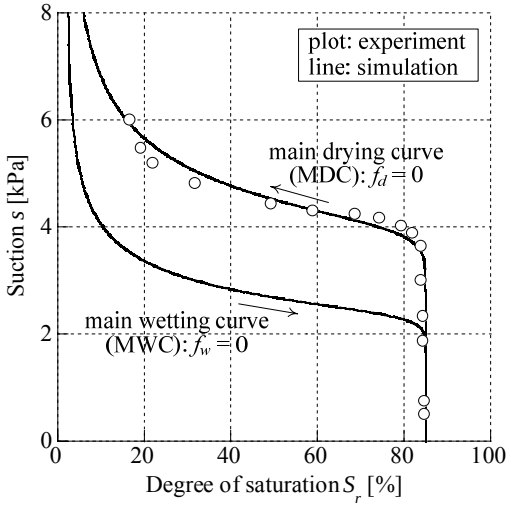


Figure 3.12 Calculated main drying and main wetting curves of soil water characteristic curve (experiment (Huang, 2005)).

$$f_d(S_r, s) = S_{\min} + (S_{\max} - S_{\min})\left[1 + (\alpha_d s)^n\right]^{-m} - S_r = F_d(s) - S_r = 0 \tag{3.3}$$

$$f_w(S_r, s) = S_{\min} + (S_{\max} - S_{\min})\left[1 + (\alpha_w s)^n\right]^{-m} - S_r = F_w(s) - S_r = 0 \tag{3.4}$$

Here, $S_{min}$, $S_{max}$, $n$, $m$ and $\alpha$ are material parameters for van Genuchten's equation and the subscripts $d$ and $w$ of the parameter $\alpha$ denote that for the main drying and wetting curves, respectively. Figure 3.12 shows comparison between observed main drying and wetting curve on uniform glass beads and the corresponding calculated results whose parameters are shown in Table 3.1. It can be seen from this figure that classical SWCC model can properly describe the observed monotonic main drying and wetting curves.

Even if soil undergoes any suction histories, it can be conceived that any state of water retention ($s$, $S_r$) lies at least between two main curves. A state variable $I_w$ defined as the ratio of interior division of the current state between two reference states on the main curves, therefore, is introduced as an intermediary of the model.

$$I_w = \frac{S_r - S_r^w}{S_r^d - S_r^w} \tag{3.5}$$

where $S_r^d$ and $S_r^w$ are degrees of saturation of the reference states on the main drying and wetting curves under current suction, respectively. $I_w$ bound by 0 for the main wetting curve and 1 for the main drying curve provides a simplified, scalar representation of the current state of hydraulic hysteresis ($0 \le I_w \le 1$). By using Equations (3.3), (3.4) and (3.5), any water retention state including scanning curve affected by hydraulic hysteresis is represented as unified function $f_c(S_r, s, I_w) = 0$ expressed as Equation (3.6).

$$f_c(s, S_r, I_w) = I_w F_d(s) + (1 - I_w) F_w(s) - S_r = 0 \tag{3.6}$$

In Figure 3.11, "current retention surface (CRS)" is represented by Equation (3.6), here any current water retention state ($S_r$, $s$, $I_w$) always exists on CRS.

Figures 3.13(a), (b) show the schematic diagram for describing scanning curve on drying and

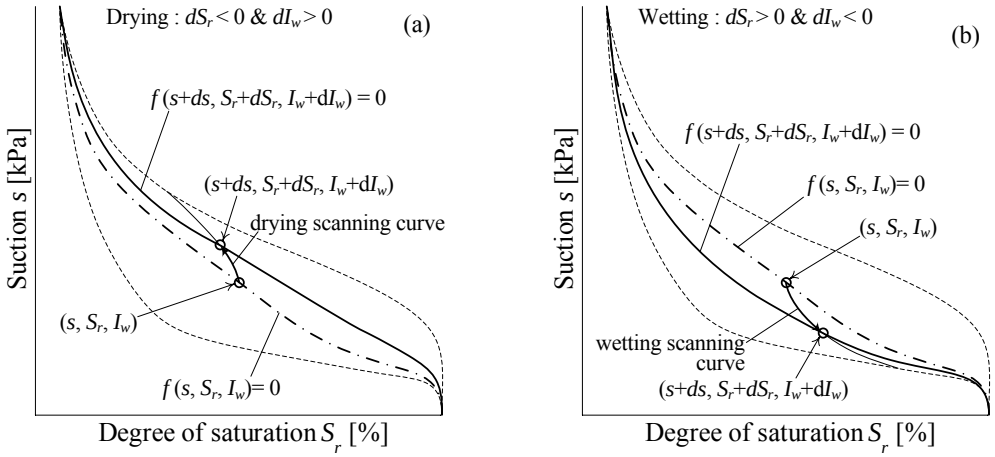


Figure 3.13 Relation between current degree of saturation $S_r$, suction $s$, and state variable $I_w$ at drying and wetting path.((a) scanning curve at drying path ($dS_r < 0$ & $dI_w > 0$)), (b) scanning curve at wetting path ($dS_r > 0$ & $dI_w < 0$))

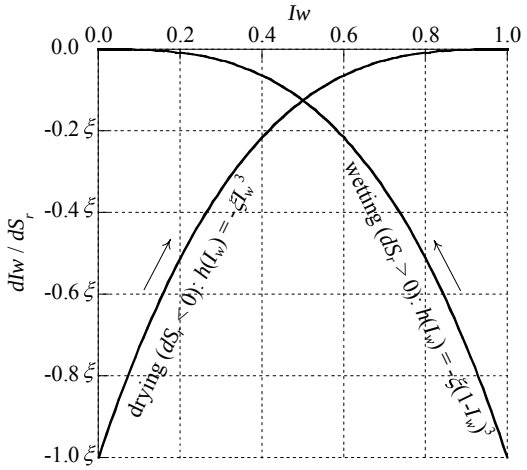


Figure 3.14 Evolution law for the hydraulic state index $I_w$ during drying and wetting processes.

wetting paths, respectively. It can be seen from Figure 3.13(a) that current state ($S_r$, $s$, $I_w$) moves on CRS towards the main drying curve during drying path, and then $I_w$ increases monotonically to 1 as degree of saturation decreases. On the other hand, from Figure 3.13(b), current state ($S_r$, $s$, $I_w$) moves on CRS towards the main wetting curve during wetting path, and then $I_w$ decreases monotonically to 0 as degree of saturation increases. An evolution law of state variable $I_w$ satisfying above conditions, thus, is given as follows;

$$dI_w = h(I_w)dS_r = \begin{cases} -\xi(1-I_w)^3 dS_r & when \;\; dS_r \le 0 \\ -\xi I_w{}^3 dS_r & when \;\; dS_r > 0 \end{cases} \tag{3.7}$$

where $\xi$ (> 0) is material parameter representing the characteristic hydraulic hysteresis, and its value determines the shape of scanning curve between main drying and wetting curves. Figure 3.14 shows the relation between $I_w$ and function $h(I_w)$ (= $dI_w$ / $dS_r$) in Equation (3.7). In order to satisfy that $I_w$ monotonically increases to 1 during drying ($dS_r < 0$), and vice versa, function $h(I_w)$ has to satisfy the conditions of $h(0) = h(1) = 0$ and $h(I_w) < 0$ within $0 < I_w < 1$. It is possible to exchange the evolution rule $I_w$ in Equation (3.7) with other expression satisfying the condition above mentioned.

Any hydraulic state of unsaturated soil always locates on CRS ($f_c = 0$), the consistency condition of Equation (3.6) ($df_c = 0$) gives

$$df_c = \frac{\partial f_c}{\partial S_r} dS_r + \frac{\partial f_c}{\partial s} ds + \frac{\partial f_c}{\partial I_w} dI_w = 0 \tag{3.8}$$

From Equations (3.3), (3.4), (3.7) and (3.8), the incremental form of SWCC model considering the influence of hydraulic hysteresis is obtained as

$$dS_r = \frac{\frac{\partial f_c}{\partial s} ds}{1 + \frac{\partial f_c}{\partial I_w} h(I_w)} \tag{3.9}$$

Applying the evolution rule of state variable $I_w$ according to the variation of degree of saturation, the increment of degree of saturation is easily obtained from Equation (3.9) in any situation. Unlike the existing model, therefore, calculation of the position and gradient of scanning curve according to switch of drying and wetting path are not necessary.

Figure 3.15 shows the comparison experiment results, which are obtained from water retentively test with cyclic suction loading on white silica sand (Huang, 2005), and corresponding calculated results by proposed model. White silica sand, whose grain size is 0.074 - 0.297 mm, is sample, and the average void ratio of samples is produced by compaction is approximately 0.56. Parameters used in this simulation are

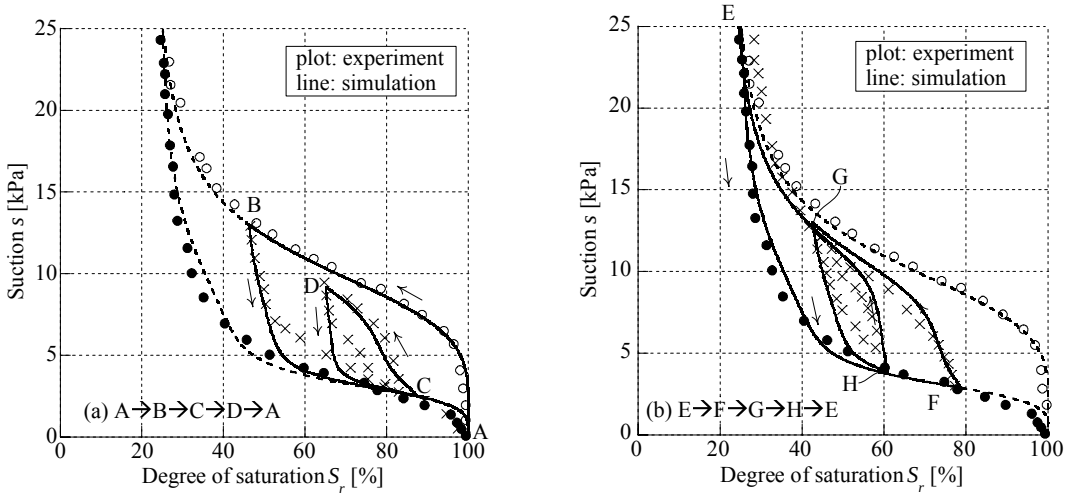


Figure 3.15 Hysteretic soil water characteristic curves of White silica sand (after Huang, 2005) and corresponding results of calculations (a) path ABCDA; (b) path EFGHE

Table 3.2 Material parameters for soil water characteristic curve considering the hydraulic hysteresis

| | | | |
|---|---|---|---|
| $S_{max}$ | 1.00 | maximum degree of saturation | parameters for van Genuchten model |
| $S_{min}$ | 0.20 | minimum (residual) degree of saturation | |
| $\alpha$ | 0.10 | position of main drying curve | |
| $\beta$ | 0.30 | position of main wetting curve | |
| $m$ | 0.70 | shape of main drying / wetting curves | |
| $n$ | 4.70 | | |
| $\xi$ | 70.0 | influence of suction histories | |

summarized in Table 3.2. Diagrams (a) and (b) in Figure 3.15 show results of cyclic path "drying, wetting, drying and wetting" and "wetting, drying, wetting and drying path" respectively, and the main drying and wetting curves are shown in each figures simultaneously. It is indicated from this figure that the proposed model can accurately describe not only the main drying and wetting curve represented by ordinary van Genuchten model, but also hysteretic water retention characteristic under complicated suction histories. Only adding one material parameter $\xi$ considering the influence of hydraulic hysteresis, scanning curve due to complicated suction histories can be rationally described by simple SWCC model based on proposed method.

*Modeling of the influence of density on SWCC*

SWCC model describing hydraulic hysteresis proposed in former section is extended to one considering the influence of density (void ratio). It is indicated from past experiment results that degree of saturation increase (or decrease) due to volumetric compression (or expansion) under constant suction (Figure 3.6), and denser soil tends to show a higher air entry value of suction, over which air can enter into void of saturated soil, and also show a higher water entry value, below which water can enter into void of dried soil (Figure 3.2). That is to say, denser soil can retain a larger degree of saturation than that of looser one under the same suction. Under same degree of saturation, meanwhile, denser sample shows a larger suction than that of loose one. In order to consider such influence of density (void ratio), the equation which is extended from van Genuchten model was proposed (Gallipoli, 2003 and Tarantino, 2005).

$$S_r = \left[1 + \left(\alpha^* s\right)^n\right]^{-m} \quad where \quad \alpha^* = \alpha e^{\psi} \tag{3.10}$$

Equation (3.10) is essentially the same as Equations (3.3) and (3.4), although it doesn't use the estimation of maximum and minimum degree of saturations. $\alpha$ and $\psi$ are material parameters. This method, however, lacks versatility for extending other classical SWCC model, because equations and material parameters of each model need to be modified.

The new method which is easily applicable to all sorts of SWCC models is proposed in this section. Transforming Equation (3.10) to equivalent Equation (3.11), it can be understood that the modified suction $s^*$ expressed in Equation (3.11) can consider the influence of density on SWCC.

$$S_r = \left[1 + \left(\alpha s^*\right)^n\right]^{-m} \quad where \quad s^* = e^{\psi} s \tag{3.11}$$

In a similar manner as Equation (3.11), it is possible to extend the ordinary SWCC model by replacing its ordinary suction $s$ with the modified suction $s^*$ to consider the influence of density. Modified suction $s^*$ in Equation (3.11) is redefined as follows;

$$s^* = s\left(\frac{e}{N_{sat}}\right)^{\xi_e} \tag{3.12}$$

$\xi_e$ is a material parameter controlling the influence of density and $N_{sat}$ represents the reference void ratio of saturated, normally consolidated soil under atmospheric pressure, which means that $s^*$ in Equation (3.12) corresponds to ordinary suction $s$ in the reference state ($e = N_{sat}$). The definition of modified suction $s^*$

expressed as Equation (3.12) is verified through comparison with various experimental results (Kyokawa et al., 2010). The modified suction $s^*$ is applied to ordinary SWCC model instead of the ordinary suction $s$ in order to describe the influence of the volume change. In the present study, the ordinary suction in Equation (3.6) is replaced by the modified suction $s^*$ as follows;

$$f\left(S_r, s^*, I_w\right) = I_w f_d\left(S_r, s^*\right) + \left(1 - I_w\right) f_w\left(S_r, s^*\right) = I_w F_d\left(s^*\right) + \left(1 - I_w\right) F_w\left(s^*\right) - S_r = 0 \tag{3.13}$$

The response of Equation (3.13) corresponds to that of Equation (3.6) in the reference state ($e = N_{sat}$), since the modified suction $s^*$ in Equation (3.12) is equal to ordinary suction $s$. The evolution rule of state parameter $I_w$ is given as the same Equation (3.7). As any hydraulic state ($S_r$, $s^*$) of unsaturated soil always locates on CRS, which means that Equation (3.13) is satisfied, the consistency condition ($df_c = 0$) as Equation (3.14) is imposed.

$$df = \frac{\partial f}{\partial S_r} dS_r + \frac{\partial f}{\partial s^*} ds^* + \frac{\partial f}{\partial I_w} dI_w = 0 \tag{3.14}$$

The increment of modified suction, which is the dependent variable of ordinary suction and void ratio, is obtained as

$$ds^* = \frac{\partial s^*}{\partial s} ds + \frac{\partial s^*}{\partial e} de \tag{3.15}$$

Substituting Equations (3.7), (3.13) and (3.15) into Equation (3.14), the incremental form of SWCC model considering the influence of hydraulic hysteresis and volumetric change is obtained as

$$dS_r = \frac{\dfrac{\partial f}{\partial s^*} ds^*}{1 + \dfrac{\partial f}{\partial I_w} h\left(I_w\right)} = \frac{\dfrac{\partial f}{\partial s^*}\left(\dfrac{\partial s^*}{\partial s} ds + \dfrac{\partial s^*}{\partial e} de\right)}{1 + \dfrac{\partial f}{\partial I_w} h\left(I_w\right)} \tag{3.16}$$

Here, other interpretation of modified suction is discussed. Figure 3.16 shows the relation between degree of saturation and specific volume $v$ (= 1 + $e$). Diagram (a) shows observed results in which plot is hydraulic state at critical state with different suction (Sivakumar, 1993), and solid lines represents changing of hydraulic states during isotropic consolidation with different suction, respectively. It can be seen from diagram (a) that degree of saturation $S_r$ increase with decreasing of specific volume $v$ (void ratio $e$) under constant suction, and denser soils show higher degree of saturation $S_r$ under same suction level. Diagram (b) shows the explanation of modified suction $s^*$ in which the arrowed solid line indicates the variation in degree of saturation due to compression under constant suction ($s$ = 300kPa). The arrowed broken line, meanwhile, shows the same amount of variation in degree of saturation due to suction change under constant specific volume, which can be described by ordinary SWCC model such as van Genuchten model. In other word, the modified suction expressed as Equation (3.12) can be regarded as one substituting a volume change (arrowed solid line) with the equivalent suction change (arrowed broken line). It is important for proposed method that ordinary SWCC model can be easily extended to one considering the influence of density only by replacing ordinary suction $s$ by modified suction $s^*$. The description of SWCC based on modified suction $s^*$ is nothing but extending two-dimensional soil water characteristic "curve" ($s$-$S_r$ plane) to multi-dimensional soil water

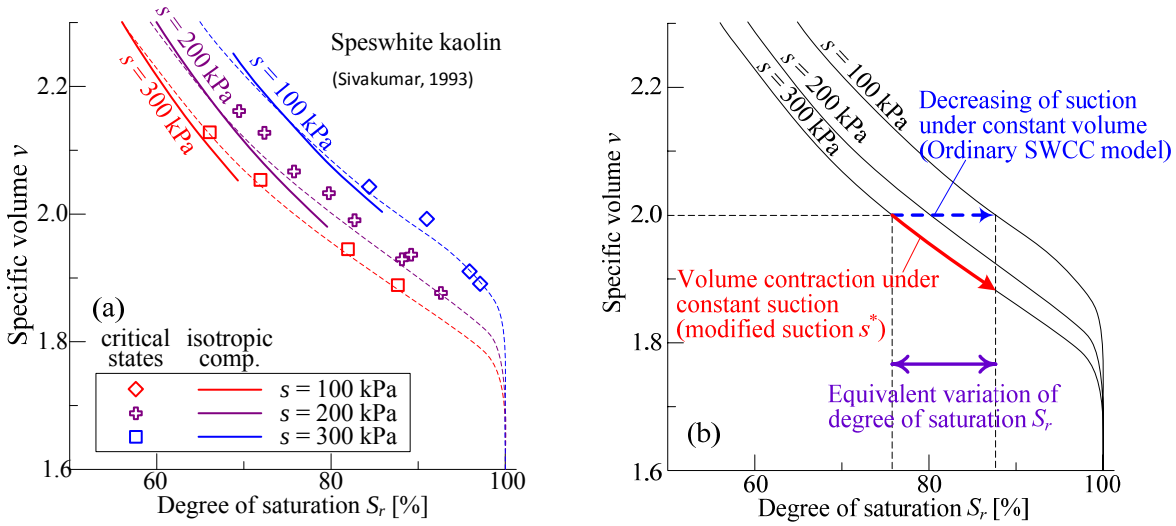


Figure 3.16 Modeling of the influence of density (volume change) on SWCC by using modified suction $s^*$ - degree of saturation $S_r$ increase due to volumetric contraction
(a) Observed results (after Sivakumar, 1993) (b) explanation drawing of modified suction $s^*$

characteristic "surface" considering the influence of density ($s$-$S_r$-$e$ surface).

The validation of proposed method is verified by parametric studies, assuming the water retentivity test of soil under different densities and compression test under constant suction. Material parameters are shown in Table 3.3, in which the new parameter $\xi_e$ representing the influence of density on SWCC is added to Table 3.2, and two kinds of parameters for White silica sand and Fujinomori clay are summarized, respectively. It is generally known that the air-entry value on drying path and the water-entry value on wetting path are larger than those of looser indicated as experimental results as shown in Figure 3.2 (Kawai et al., 2000). In a denser state, the modified suction represents lower value than current ordinary suction. The proposed SWCC model based on the modified suction, therefore, can describe those effects as shown in Figure 3.17 which is the calculated result of SWCC on the samples of different initial densities. Figure 3.18 shows the simulation of compression tests under constant suction on saturated Fujinomori clay. Firstly, suction increase to a prescribed value (B: 49 kPa, C: 98 kPa, D: 196 kPa and E: 392 kPa) from initial saturated state, and then compression tests are carried out. In addition to the proposed SWCC model, the stress-strain relation (constitutive model) of unsaturated soil is required for these simulations. Here, only the simulation results are shown, the details of constitutive model will be explained and proposed in the following section. It can be seen from Figure 3.18 that proposed model can describe the increase in degree of saturation with the decrease in void ratio due to compression. On the other hand, almost existing SWCC models cannot describe such variations in degree of saturation with the change of density (volume). Description of the relation between suction, degree of saturation and density, however, is necessary for explanation of mechanical behavior of unsaturated soil. Moreover, this concept of modified suction $s^*$ can be extended to one considering the influence of temperature, fine contents, and others on SWCC easily. Then, the modified suction $s^*$ is give as variable of not only suction, void ratio and also temperature, fine contents and other parameters.

Table 3.3 Material parameters for soil water characteristic curve considering the hydraulic hysteresis and the influence of density

| | White silica sand | Fujinomori clay | |
|---|---|---|---|
| $S_{max}$ | 1.00 | 1.00 | |
| $S_{min}$ | 0.20 | 0.1 | |
| $\alpha$ | 0.1 | 0.03 | parameters for van Genuchten model |
| $\beta$ | 0.3 | 0.10 | |
| $m$ | 0.7 | 0.1 | |
| $n$ | 4.7 | 2.0 | |
| $\xi$ | 70.0 | 100.0 | influence of suction histories |
| $\xi_e$ | 1.2 | 5.0 | influence of void ratio |

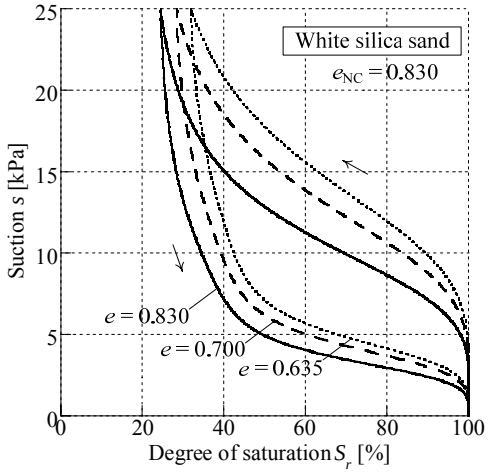


Figure 3.17 Calculated water retention curves of White silica sands of different densities

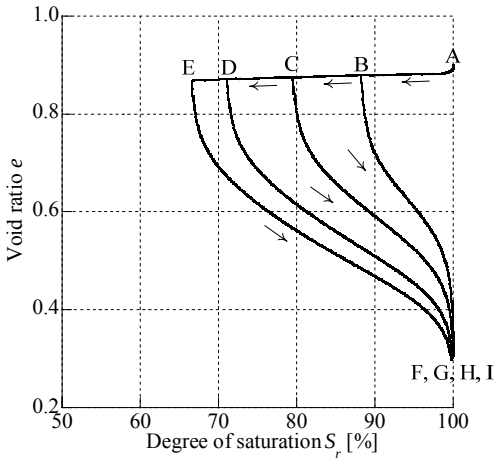


Figure 3.18 Simulation of drying path (increasing of suction: AB, AC, AD, AE) and wetting path (increasing of degree of saturation $S_r$) (volumetric contraction: BF, CG, DH, EI)

The details of extension of $s^*$ and the verification of such extension is shown in reference paper (Kikumoto et al., 2009).

### 3.3.2 Modeling of one dimensional behavior of unsaturated soil and its verification

It is shown from past experimental results explained in former section 3.2 that the positions of normally consolidated line (*NCL*) and critical state line (*CSL*) on *e*-ln*p''* plane, in which the effective stress is given as Bishop's effective stress in Equation (3.2), can be uniquely provided depending on degree of saturation. In this section, firstly, one-dimensional model proposed in Chapter 2, which can take account of the influence of external factors by introducing the state variable $\psi$, is applied to stress-strain relation of unsaturated soil. Subsequently, one-dimensional is extended to multi-dimensional model in a similar manner as explained above. (In extending to multi-dimensional model by introducing the state variable $\psi$, it is assumed automatically that the vertical distance between *NCL* and *CSL* is constant, which means that the stress-dilatancy relation of unsaturated soil corresponds to that of saturated one.)

The position of normally consolidated line (*NCL*) is shifted downward / upward in the plane of void

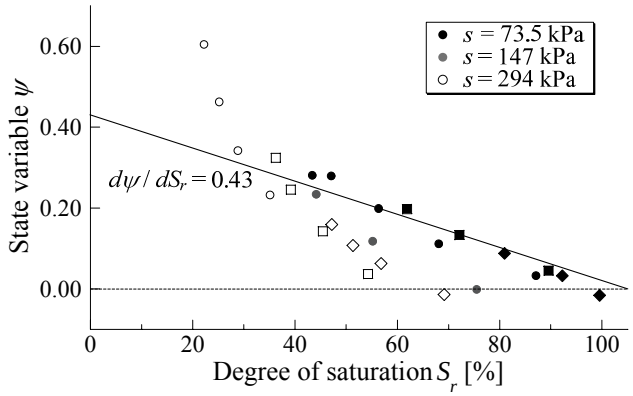


Figure 3.19 The relation between degree of saturation $S_r$ and state variable y representing the position of *NCL* (observed plots are obtained from experimental results of exhausted / drained oedometer tests under constant suction (after Honda, 2000))

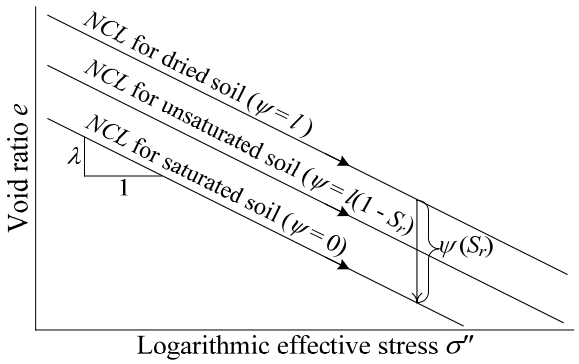


Figure 3.20 Effect of $S_r$ on the position of *NCL* and its description through the state variable $\psi(S_r)$

ratio $e$ and effective confining stress $p''$ depending on the decrease / increase of degree of saturation $S_r$ without changing its shape as derived from Figure 3.6. And, Figure 3.19 shows the relation between degree of saturation and state variable $\psi$ defined as vertical distance of the current *NCL* from that of the saturated sample. This relations are obtained from organizing the various test result of drained water and exhausted air one-dimensional consolidation tests with different water contents and different suctions ($s$ = 73.5, 147, 294 kPa) on Catalpo clay (Honda, 2000), in which normal consolidation state of soil is determined by Casagrande method. A negative correlation between degree of saturation $S_r$ and the state variable $\psi$ can be seen from Figure 3.19. The state variable $\psi$, therefore, varies with the change of $S_r$ and is assumed to be incrementally proportional to $S_r$ with satisfying $\psi = 0$ at saturated condition (Figure 3.20);

$$\psi(S_r) = -l(1 - S_r) \tag{3.17}$$

where $l$ is a material parameter representing the vertical distance of the *NCL* for dried and saturated samples in the compression plane. Although the state variable $\psi$ is given as a linear function (Equation (3.17)) for simple modeling, it is possible to change with other high order functions to fit various experimental results. In reference to formulation of one-dimensional model shown in Chapter 2, modeling of stress-strain relation of unsaturated soil is conducted. Figure 3.21 shows the outline of the modeling of unsaturated soils considering the influence of the variation of the degree of saturation. Horizontal axis in Figure 3.21 shows the one-dimensional Bishop's effective stress given as

$$\sigma'' = \sigma - u_a + \chi(u_a - u_w) = \sigma^{net} + S_r s \tag{3.18}$$

By the referring to this figure, the variation in void ratio ($-\Delta e$) of overconsolidated, unsaturated soil, when the stress condition moves from the initial state I ($\sigma'' = \sigma''_0$, $e = e_0$, $\rho = \rho_0$) to the current state P ($\sigma'' = \sigma''$, $e = e$, $\rho = \rho$), is given as follows

$$(-\Delta e) = \{(e_{N0} - e_N) - (\rho_0 - \rho)\} = \lambda \ln \frac{\sigma''}{\sigma''_0} - (\rho_0 - \rho) - (\psi_0 - \psi) \tag{3.19}$$

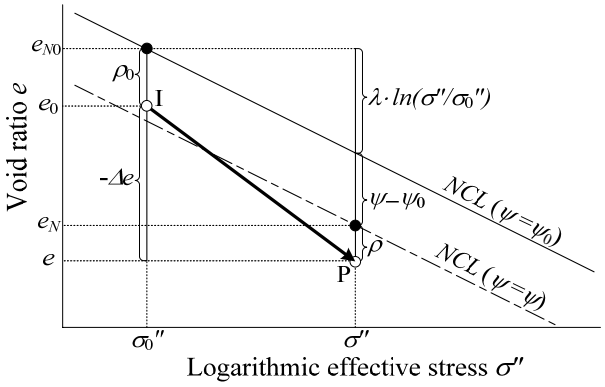

Figure 3.21 Modeling of the volumetric behaviour of unsaturated soil

Here, the last term ($\psi$ - $\psi_0$) represents the influence of "partial saturation" through the vertical shift of the *NCL*. Assuming a usual nonlinear elastic relation on effective stress $\sigma''$ the same as that for saturated soil given as Equation (2.2), the plastic component of the change of void ratio $(-\Delta e)^p$ is obtained as

$$\begin{aligned}(-\Delta e)^p &= (-\Delta e)-(-\Delta e)^e \\ &= \lambda \ln\frac{\sigma''}{\sigma_0''}-(\rho_0-\rho)-(\psi_0-\psi)-\kappa\ln\frac{\sigma''}{\sigma_0''} = (\lambda-\kappa)\ln\frac{\sigma''}{\sigma_0''}-(\rho_0-\rho)-(\psi_0-\psi)\end{aligned} \tag{3.20}$$

Considering the plastically changing of void ratio as hardening parameter, the yield function of unsaturated soil is defined as follows:

$$f = F-\{H+(\rho_0-\rho)+(\psi_0-\psi)\} = 0 \;\; where \;\; F = (\lambda-\kappa)\ln\frac{\sigma''}{\sigma_0''},\; H = (-\Delta e)^p \tag{3.21}$$

From the consistency condition ($df = 0$), evolution rule of $\rho$ given as Equation (2.11) for non-stuructured over consolidated soil and Equation (3.17), the increment of the plastic component of void ratio is obtained as

$$d(-e)^p = \left(\frac{\lambda-\kappa}{1+G(\rho)}\right)\frac{d\sigma''}{\sigma''}+\frac{1}{1+G(\rho)}\frac{d\psi}{dS_r}dS_r \tag{3.22}$$

Finally, a one-dimensional elastoplastic constitutive relationship for over consolidated unsaturated soils is obtained as a sum of Equation (2.2) based on effective stress $\sigma''$ (Equation 3.2) and Equation (3.22):

$$d(-e) = d(-e)^p + d(-e)^e = \left\{\frac{\lambda-\kappa}{1+G(\rho)}+\kappa\right\}\frac{d\sigma''}{\sigma''}+\frac{1}{1+G(\rho)}\frac{d\psi}{dS_r}dS_r \tag{3.23}$$

The loading condition is given simply by assuming that the plastic component of the variation of void ratio is always compressive as follow

$$\begin{cases} d(-e) = d(-e)^e + d(-e)^p \quad if \quad d(-e)^p > 0 \\ d(-e) = d(-e)^e \quad if \quad d(-e)^p \le 0 \end{cases} \tag{3.24}$$

*Verification of proposed model – the parametric study and comparison with observed phenomena*

The validity of the proposed one dimensional model for unsaturated soil is verified by a series of parametric studies: consolidation tests under constant suction and subsequent wetting tests. Table 3.4 shows the material parameters for mechanical stress-strain characteristic in one-dimensional model assuming Fujinomori clay.

Table 3.4 Material parameter for mechanical stress-strain characteristic in one-dimensional problem

| *Parameter of constitutive model* (1D) | |
|---|---|
| $\lambda$: Compression Index | 0.104 |
| $\kappa$: Swelling Index | 0.01 |
| N: void ratio under 98kPa | 0.83 |
| $a$: Effect of over consolidated | 100 |
| $l$: Effect of unsaturated | 0.5 |

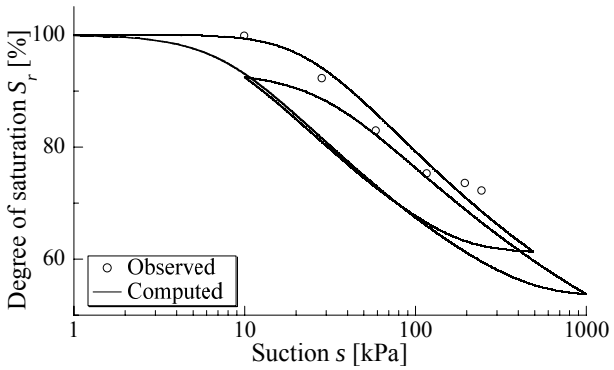


Figure 3.22 Soil water characteristic curve of Fujinomori clay (after Shimizu, 2000) and corresponding calculated results

Material parameters for SWCC are the same as shown in Table 3.3. Figure 3.22 shows the experimental result of water retention characteristics of Fujinomori clay (Shimizu, 2003) and the corresponding calculated result. From this figure, the proposed model properly estimates the experimental result, while it can represent the influence of the hydraulic hysteresis. Firstly, the parametric study of consolidation tests under constant suction ($s$ = 49, 98, 196, 294 kPa) on initially saturated and normally consolidated soil ($e_0$ = 0.9, $\sigma^{net}$ = 49 kPa, $s$ = 0 kPa) and initially saturated and over consolidated soil ($e_0$ = 0.8, $\sigma^{net}$ = 49 kPa, $s$ = 0 kPa), are carried out. In the calculation, as shown in Figure 3.23, suction is firstly increased to a prescribed value (point A, B, C and D) from saturated initial state, after then consolidation tests are carried out. The calculated results are shown in Figure 3.24 and 3.25, in which diagrams (a) and (b) show the relation between net stress $\sigma_{net}$ (= $\sigma$ - $u_a$) and void ratio $e$ and degree of saturation $S_r$, respectively, and diagram (c) shows the relation between one-dimensional effective stress $\sigma'$ and void ratio $e$. It is indicated from these figures that the proposed model can describe a typical behaviors of unsaturated soil such as: unsaturated soil initially shows relatively higher stiffness and it can stay in a looser region than saturated one; unsaturated soil undergoes a significant compression from a certain stress level, and then degree of saturation increases in response to the volumetric compression; Compression line of unsaturated soil finally converges to the *NCL* for saturated one. The proposed SWCC model represents increasing of degree of saturation with contraction, and the *NCL* for the unsaturated soil shifts downwards due to increase of degree of saturation. The proposed model can represent typical mechanical and hydraulic compression behaviors of unsaturated soil with similar mechanism as observed result in Figure 3.6. It is also known that the sample having larger suction and lower degree of saturation shows stiffer behavior, as shown in a former experimental data. However, even if the sample undergoes the same magnitude of suction, its degree of saturation is different depending on density as shown in both calculated results. Applying the same suction to both normally and over consolidated samples, higher value of degree of saturation is obtained from over consolidated sample. Therefore, the position of compression line determined by Equation (3.17) of over consolidated sample is lower than normally consolidated one.

Figure 3.25(a) shows an experimental result of cyclic consolidation test under constant suction which is shown as the relation between mean net stress $p_{net}$ and void ratio $e$ (Wheeler et al., 2003), and its

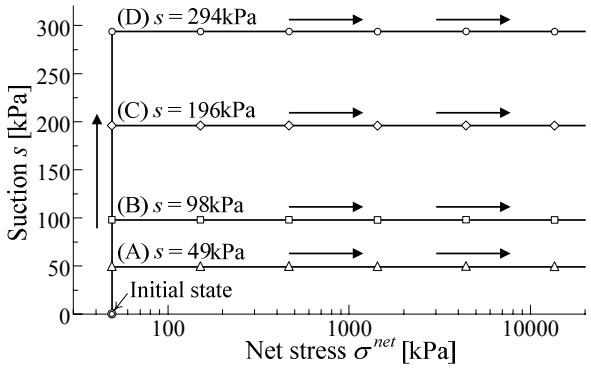


Figure 3.23 Stress path of simulation of exhausted / drained consolidation tests under constant suction ($s$ = 0, 49, 98, 196 and 294 kPa)

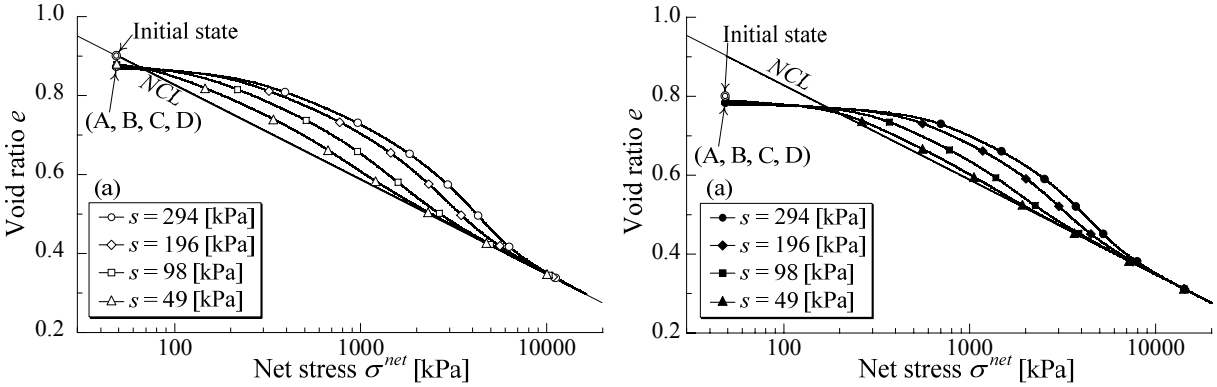


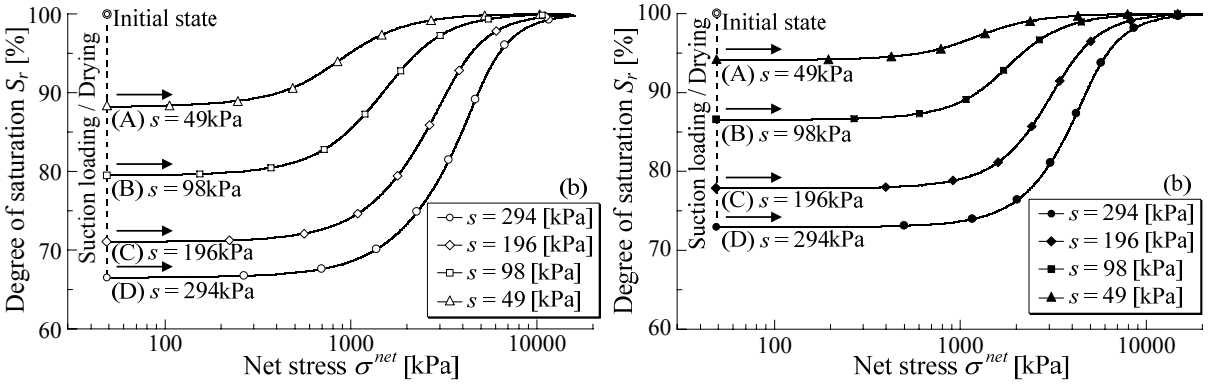


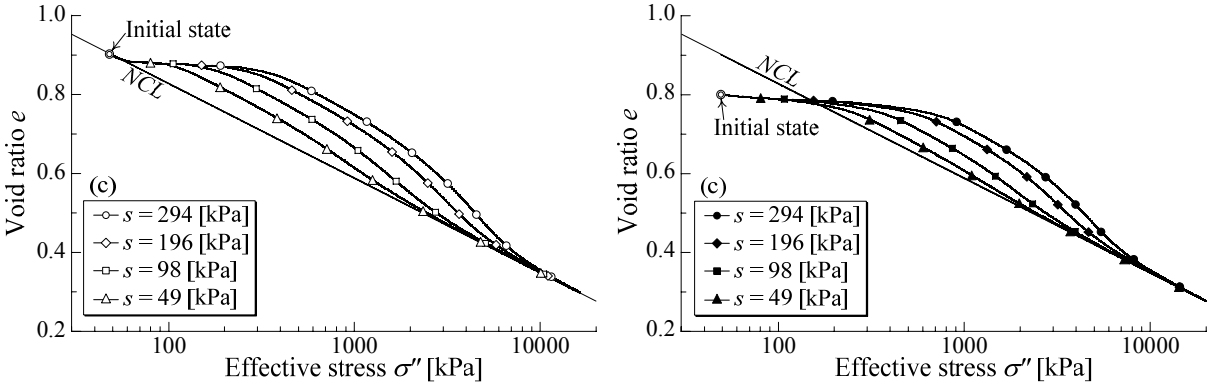


Figure 3.24 Simulations of constant suction consolidation tests on initially saturated, normally consolidated sample ($e_0$ = 0.9) (a) $\sigma^{net}$ vs. $e$; (b) $\sigma^{net}$ vs. $S_r$; (c) $\sigma''$ vs. $e$










Figure 3.25 Simulations of constant suction consolidation tests on initially saturated, over consolidated sample ($e_0$ = 0.8) (a) $\sigma^{net}$ vs. $e$; (b) $\sigma^{net}$ vs. $S_r$; (c) $\sigma''$ vs. $e$

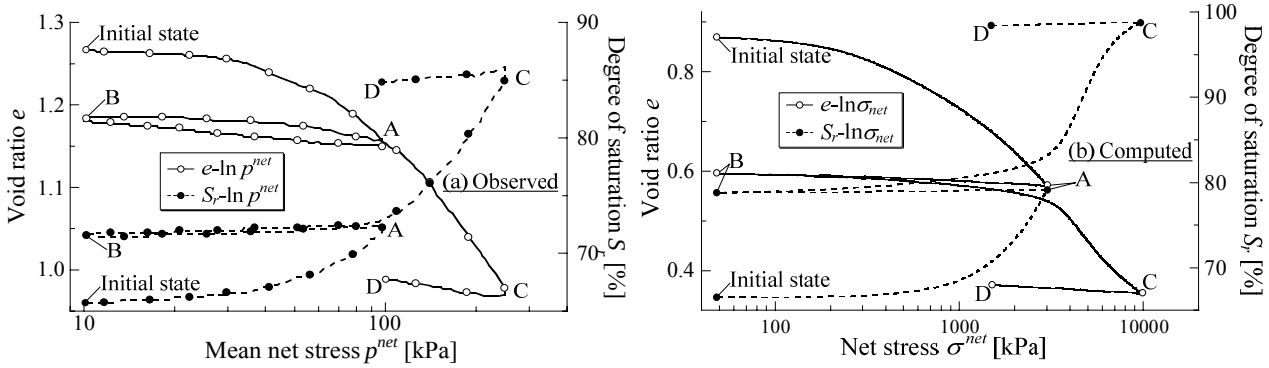


Figure 3.26 (a) Observed results of drained / exhausted cyclic consolidation test (Initial→ A→ B→ A→ C→ D) (after Wheeler et al., 2003) and (b) corresponding calculated result. Both figures show the relation between net stress and void ratio $e$, degree of saturation $S_r$, simultaneously.

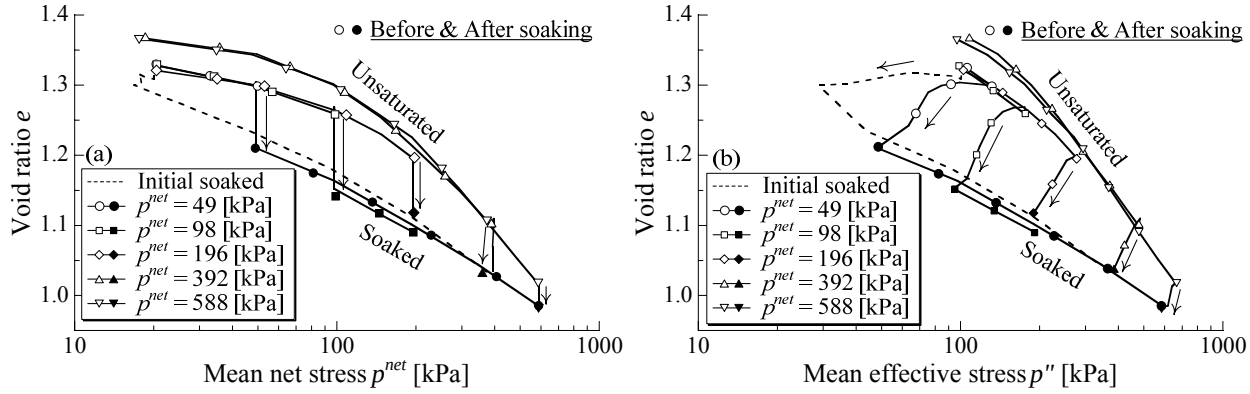


Figure 3.27 Observed results of constant suction consolidation and subsequent soaking tests (after Sun et al., 2007)
(a) relation between mean net stress $p^{net}$ and void ratio $e$, (b) relation between mean effective stress $p''$ and void ratio $e$

corresponding calculation result are shown in Figure 3.25 (b). From comparison with these results, it is seen that the proposed model can adequately describe the mechanical and hydraulic behavior of unsaturated soil on not only monotonic loading but also on cyclic loading condition.

The experimental results of compression under constant suction and subsequent wetting test are shown in Figure 3.27 (Sun et al., 2007), in which the diagram (a) is the relation between mean net stress $p_{net}$ and void ratio $e$ and the diagram (b) is the relation between mean effective stress $p''$ decreases, i.e., unloading path, during a wetting collapse. Taking up this unloading path, Jennings and Burland (1962) pointed out that the Bishop's effective stress cannot describe the swelling collapse phenomena. The corresponding calculations, in which the normally consolidated soil ($e_0$ =0.9, $\sigma^{net}$ = 49 kPa, $s$ = 0 kPa) and over consolidated soil ($e_0$ = 0.8, $\sigma^{net}$ = 49 kPa, $s$ = 0 kPa) are taken as soil samples, are carried out. Samples are firstly compressed to a prescribed net stress ($\sigma^{net}$ = 49, 294, 588, 1017, 1960, 2940, 9800 kPa) under constant suction of 294kPa and they are saturated by decreasing suction to zero. These stress paths are summarized in Figure 3.28. Figures 3.29 and 3.30 show the calculated results, in which diagram (a) shows the relationship between net stress $\sigma^{net}$ and void ratio $e$, (b) shows the relationship between suction $s$ and degree of saturation $S_r$ during wetting path, and (c) shows the relationship between effective stress $\sigma''$ and void ratio $e$. In these diagrams, the degree of

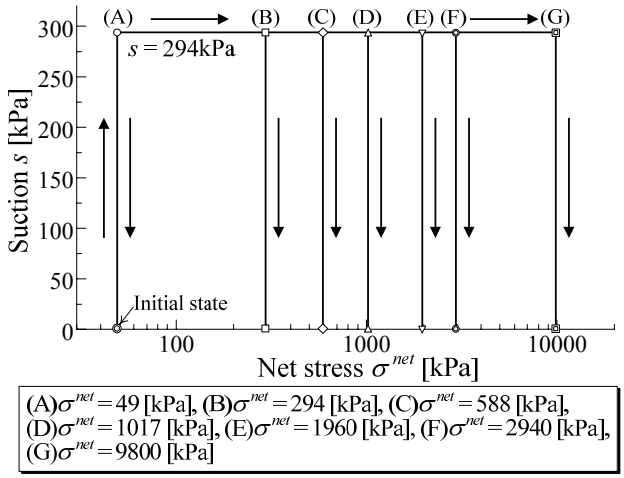


Figure 3.28 Stress path of simulation of constant suction consolidation and subsequent soaking tests

saturation before wetting is depicted in each plot.

It is seen from these figures that the proposed model suitably reproduces a typical wetting collapse behaviors of unsaturated soils: the samples contract due to wetting and finally come close to the normally consolidated line of saturated soil. It can be seen from diagram (b) that effective stress decreases during contraction due to wetting as shown in experimental result (Figure 3.27 (b)). The calculation result also represents the softening behavior which indicates the elastoplastic behavior during unloading path. The variation in volumetric compression is different for each initial soaking point on consolidation line, because the compression line makes convex line changing with a variation in degree of saturation. The observed collapse volume changes of Pearl clays with different densities at different consolidation stress state (after Sun et al., 2007) are summarized in Figure 3.31 (after Sun et al., 2004), and the corresponding calculated results are summarized in Figure 3.32 which is obtained from organizing the calculated results shown in Figure 3.29 and 3.30. Comparing with those observed and calculated results, the proposed model suitably describes the difference of the collapsing volume change depending on the stress level and initial density. The proposed model, especially, can describe the soaking-induced expansive behavior of unsaturated-over consolidated sample as can be seen in experimental results.

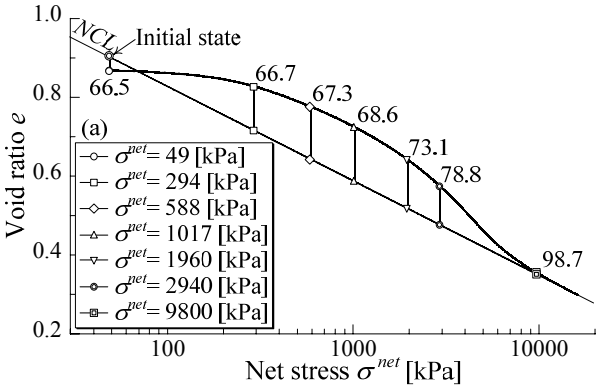


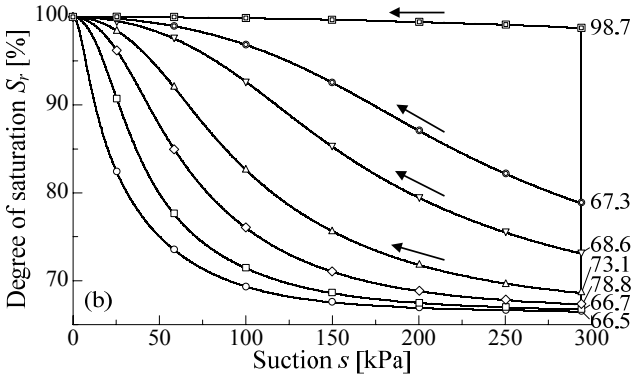


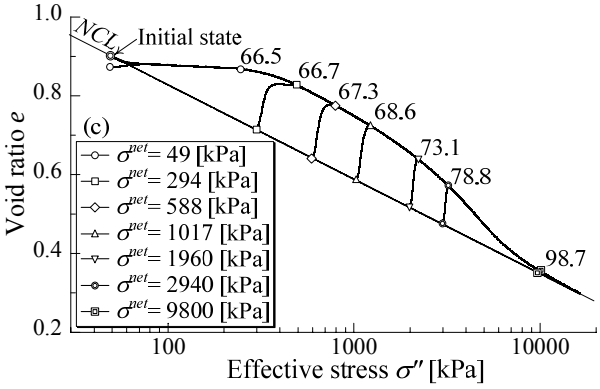


Figure 3.29 Simulations of constant suction consolidation and subsequent soaking tests on initially saturated, normally consolidated sample ($e_0$ = 0.9) (a) $\sigma^{net}$ vs. $e$; (b) $\sigma^{net}$ vs. $S_r$; (c) $\sigma'$ vs. $e$

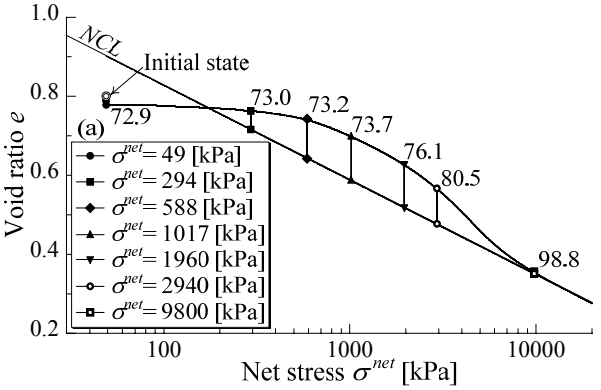


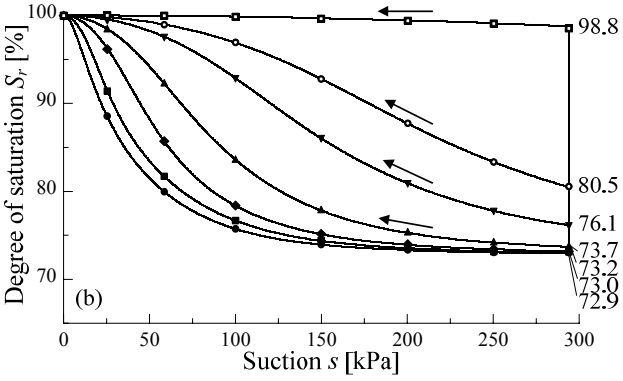


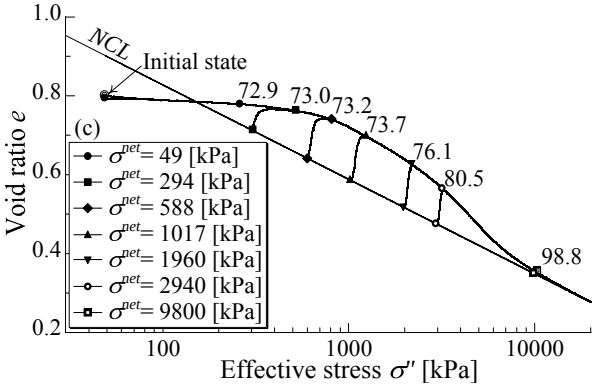


Figure 3.30 Simulations of constant suction consolidation and subsequent soaking tests on initially saturated, over consolidated sample ($e_0$ = 0.8) (a) $\sigma^{net}$ vs. $e$; (b) $\sigma^{net}$ vs. $S_r$; (c) $\sigma'$ vs. $e$

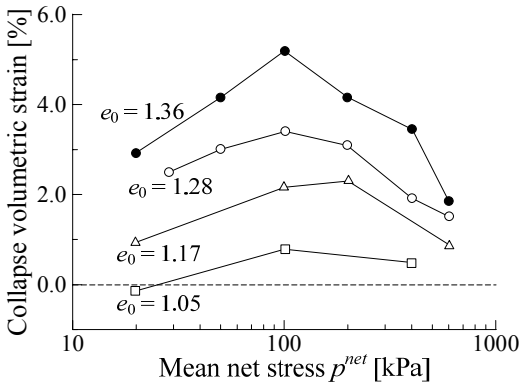


Figure 3.31 Soaking-induced volumetric strains at different mean total stresses for compacted Pearl clays with different initial densities (after Sun et al., 2007)

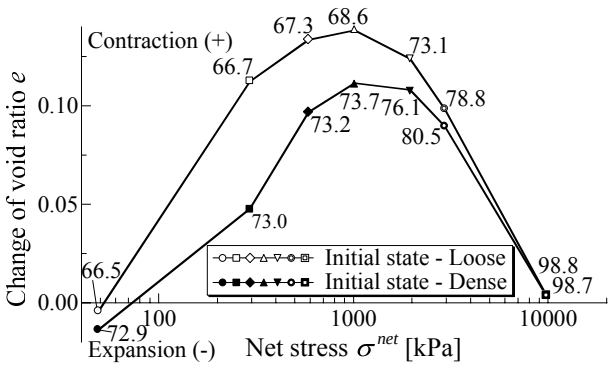


Figure 3.32 Decreases in void ratio of dense and loose samples ($e_0$ = 0.8, 0.9) during soaking process depending on confining pressure

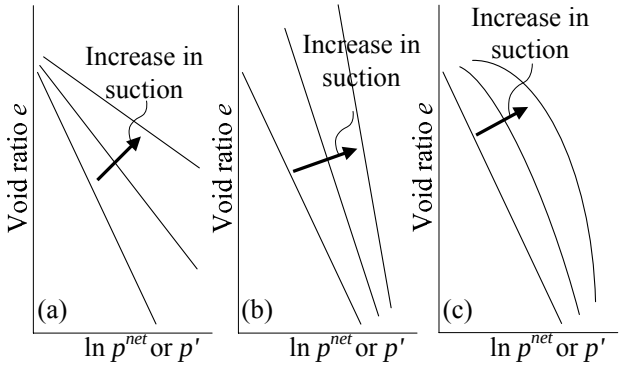


Figure 3.33 Various types of normal consolidation line, particularly its gradient and intercept, have been proposed in past research.

Some ideas about the position and gradient of normally consolidated line, i.e., compression index $\lambda$ and intercept $N$, for unsaturated soil have been argued and proposed by referring to the experimental and analytical results. Those ideas are classified as shown in Figure 3.33: (a) Alonso (1990) and Kohgo (1993), for instance, proposed that the compression index of *NCL* for unsaturated soil is defined as function of suction and it is smaller than the saturated one. The intercept of *NCL*, furthermore, depends on the value of suction too; (b) Conversely, the compression index depending on value of suction, which is larger than the saturated one, is given by Wheeler and Sivakumar (1995) and Benjamin & Khalili (2002). ; (c) In reference to the volumetric compression behavior depending on confining pressure under swelling process, Josa et al. (1992) give the normally consolidated line whose shape is convex for linear *NCL* of saturated one. On the other hand, as can be seen from calculated results in Figure 3.23 and 3.24, the compression line of proposed model can describe the characteristic of various experimental compression behavior and also those existing models inclusively by shifting the position of *NCL* with degree of saturation, which changes due to not only suction but also volume change. Additionally, the proposed model can properly describe the difference of swelling collapse behavior depending on stress level as can be seen in the observed results.

### 3.3.3 Extension of one dimensional model to multi dimensional model for unsaturated soil and its verification

Regarding the strength and deformation characteristics of unsaturated soil, it was indicated from Figure 3.5 in former section that the stress-dilatancy relation of saturated soil corresponds to that of unsaturated one by using the effective stress, in which the parameter $\chi$ is given as the residual degree of saturation $S_{re}$. In other word, the vertical distance between normally consolidated line shifting upward / downward with variation in degree of saturation and critical state line is constant, so that modeling of multi-dimensional model for unsaturated soil can be conducted only by replacing the one dimensional stress function $F$ in Equation (3.21) with newly formulated by invariants of the modified stress $t_{ij}$ as shown in Chapter 1. The yield function of multi dimensional model for unsaturated soil is expressed as

$$f = F - \{H + (\rho_0 - \rho) + (\psi_0 - \psi)\} = 0 \quad where \quad F = (\lambda - \kappa)\left\{\ln\frac{t_N}{t_{N0}} + \zeta(X)\right\},\ H = (-\Delta e)^p \tag{3.25}$$

In proposed model, the following equation given in Equation (2.61) is adopted for the function of stress ratio $\zeta(X)$ in Equation (3.25).

$$\zeta(X) = \frac{1}{\beta}\left(\frac{X}{M^*}\right)^{\beta} \tag{3.26}$$

Needless to say, the modified stress tensor $t_{ij}$ in Equations (3.25) and (3.26) is defined by Equation (2.50) on the basis of Bishop's effective stress tensor $\sigma''_{ij}$ expressed as Equation (3.2). The increment of plastic strain is obtained from associated flow rule assumed in $t_{ij}$ space.

$$d\varepsilon_{ij}^p = \Lambda\frac{\partial F}{\partial t_{ij}} = \Lambda\left(\frac{\partial F}{\partial t_N}\frac{\partial t_N}{\partial t_{ij}} + \frac{\partial F}{\partial X}\frac{\partial X}{\partial t_{ij}}\right) \tag{3.27}$$

From the consistency condition ($df$ = 0), evolution rule of $\rho$ given as Equation (2.72), flow rule in Equation (3.27) and Equation (3.25), we can obtain

$$\begin{aligned} df &= dF - (dH - d\rho) \\ &= \frac{\partial F}{\partial \sigma''_{ij}} d\sigma''_{ij} - \{d(-e)^p - d\rho - d\psi\} \\ &= \frac{\partial F}{\partial \sigma''_{ij}} d\sigma''_{ij} - \left\{(1+e_0)\Lambda\frac{\partial f}{\partial t_{kk}} + (1+e_0)\Lambda\frac{G(\rho)}{t_N} - \frac{d\psi}{dS_r}dS_r\right\} = 0 \end{aligned} \tag{3.28}$$

The proportional constant Λ, therefore, is expressed as

$$\Lambda = \left\langle \frac{\dfrac{\partial F}{\partial \sigma''_{ij}} d\sigma'' + \dfrac{d\psi}{dS_r}dS_r}{(1+e_0)\left\{\dfrac{\partial F}{\partial t_{kk}} + \dfrac{G(\rho)}{t_N}\right\}} \right\rangle = \left\langle \frac{\dfrac{\partial F}{\partial \sigma''_{ij}} d\sigma'' + \dfrac{d\psi}{dS_r}dS_r}{h_p} \right\rangle \tag{3.29}$$

The plastic strain increment is calculated by substituting the proportional constant Λ into Equation (3.27). The elastic strain increment is given by the generalized Hooke's law based on Bishop's effective stress (Equation

(3.2))

$$d\varepsilon_{ij}^{e} = \frac{1+\nu_e}{E_e} d\sigma_{ij}'' - \frac{\nu_e}{E_e} d\sigma_{kk}'' \delta_{ij} \quad where \quad E_e = \frac{3(1-2\nu_e)(1+e_0)}{\kappa} p'' \tag{3.30}$$

Here, $E_e$ is the Young's modulus, $\kappa$ is the swelling index and $\nu_e$ is the Poisson's ratio respectively. Finally, the total strain increment is given by the sum of elastic and plastic strain increments.

$$d\varepsilon_{ij} = d\varepsilon_{ij}^{e} + d\varepsilon_{ij}^{p} \tag{3.31}$$

*Verification of proposed model – parametric study and comparison with observed phenomena*

The validity of the proposed multi dimensional model for unsaturated soil is verified by comparing a series of simulations of shear test and wetting test on anisotropic stress state with observed phenomena. The additional parameters for multi-dimensional model are shown in Table 3.5. Other parameters are the same as that of Fujinomori clay shown in Table 3.4, and parameters for SWCC model are the same as listed in Table 3.3. Firstly, the simulation of drained water and exhausted air triaxial compression test on unsaturated sample is conducted. Firstly, initial unsaturated over consolidated soil ($e_0$ = 0.36, $p^{net}$ = 196 kPa, $s$ = 10 kPa, $S_r$ = 92 %) is subjected to increasing or decreasing suction to each predetermined value ($s$ = 0(saturated), 10, 20, 40, 80 kPa), and then triaxial compression tests under constant mean net stress $p^{net}$ and constant suction are carried out. The calculated stress-strain relation (relation $q$ - $\varepsilon_d$, $\varepsilon_v$ - $\varepsilon_d$, and $q/p''$ - $\varepsilon_d$) is shown in Figures 3.34 (a) , (b) and (c), respectively. As can be seen in these figures, the proposed model can properly describe the typical shear behavior of unsaturated soil as shown in observed shear behavior (Figure 3.9 (a) and (b)); increasing in stiffness and strength of soil, and development of dilative tendency with increasing in suction (or decreasing in degree of saturation). Proposed model represents these typical behaviors like over consolidated soil, since soil is in the relative over consolidated state due to shifting of *NCL* and *CSL* upward with decreasing in degree of saturation. From Figure 3.33(b), it can be seen that stress ratio $q/p''$ converges to the residual strength based on Bishop's effective stress. As concerns about critical state defined as steady state with non plastic volume change, any simulation behaviors still show expansive behavior at over 25% of deviator strain $\varepsilon_d$, since the critical state line shifts continuously due to change of degree of saturation depending on volume change.

Table 3.5 Material parameters for stress-strain relation in multi-dimensional problem and for soil water characteristic curve

| *Parameters for mechanical model* | | | *Parameters for SWCC* | | |
|---|---|---|---|---|---|
| $\lambda$ | 0.104 | same parameters as Cam clay model | $S_{min}$ | 0.10 | parameters for van Genuchten's equation |
| $\kappa$ | 0.0100 | | $S_{max}$ | 1.00 | |
| $N_{sat}$ | 0.83 | | $\alpha_{wet}$ | 0.03 | |
| $R_{cs}$ | 3.5 | | $\alpha_{dry}$ | 0.10 | |
| $\nu$ | 0.2 | | $m$ | 0.1 | |
| $\beta$ | 1.5 | shape of yield surface | $n$ | 2.0 | |
| $a$ | 500 | effect of density and confining pressure | $\xi$ | 100 | effect of suction history |
| $l$ | 0.50 | effect of $S_r$ on the position of *NCL* | $\xi_e$ | 5.0 | effect of void ratio |

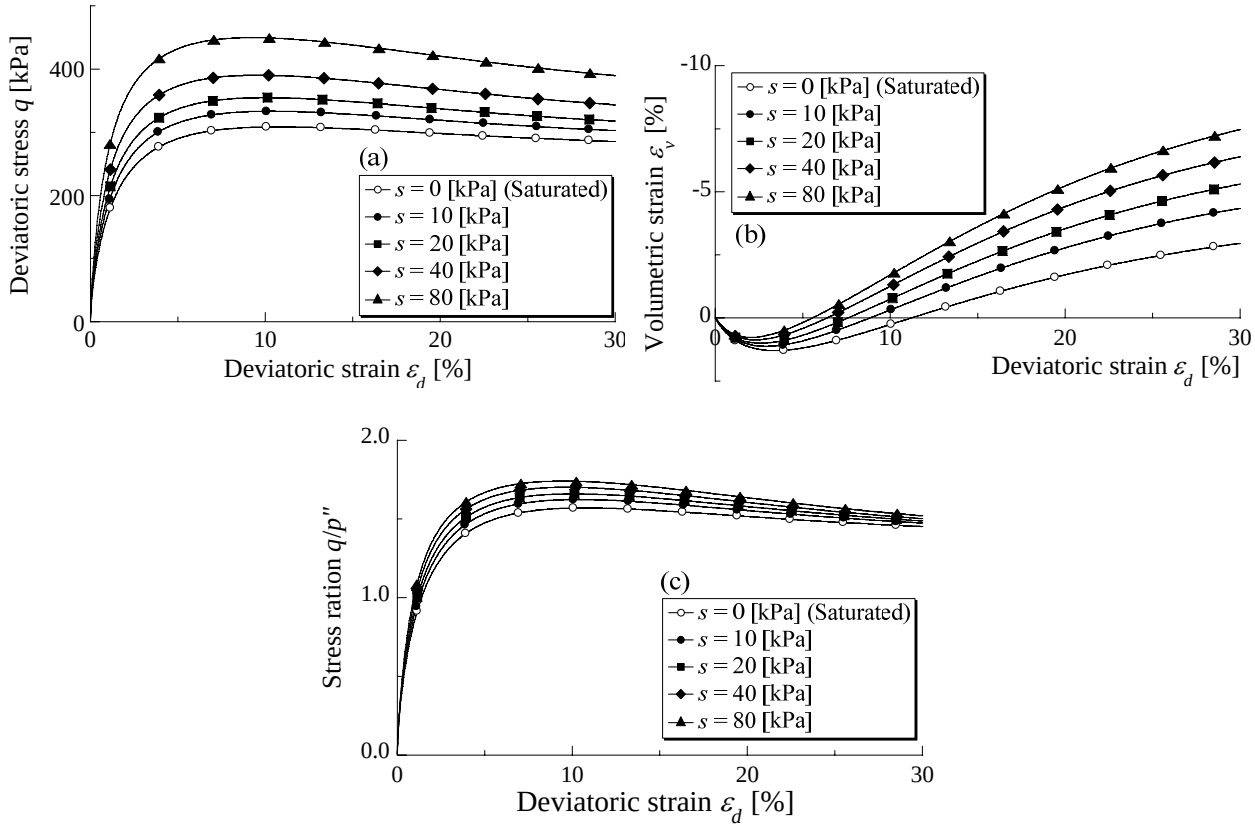


Figure 3.34 Calculated results of exhausted / drained triaxial compression tests under constant suction ($s$ = 0, 10, 20, 40 and 80 kPa) on initial unsaturated, overconsolidated samples. ((a) $\varepsilon_d$ vs. $q$ relation, (b) $\varepsilon_d$ vs. $\varepsilon_v$ relation, (c) $\varepsilon_d$ vs. $q/p''$ relation)

Next, details of critical state line represented by proposed model are discussed. Figure 3.35 shows stress path to describe the calculated critical state lines. Figure 3.36 shows the calculated relations between void ratio $e$ and logarithmic mean effective stress $p''$, in which circular plots represents the result of saturated samples, diamond and inverse triangular plots represent results of unsaturated samples under constant suction s = 98, 294 kPa, respectively. And, plots with open circle represent the conditions before shear and plots with close circle represent the conditions after shear, i.e., critical state. So, soil state moves from the plots with open circle to the plots with close circle during shear. Critical states of unsaturated samples represented with black diamond and black inverse triangle where the values of degree of saturation are depicted. From this figure, compression behavior represented as the plots with open circle indicates that soil approaches to normally consolidated line for saturated soil due to volumetric contraction in a similar way as one-dimensional compression behavior. As regard with critical state line (*CSL*), *CSL* of saturated sample can be drawn as a linear line parallel to the *NCL* of saturated one. On the other hand, both *CSLs* of unsaturated sample which is organized by each value of suction ($s$ = 98, 294 kPa) are not parallel to the *NCL* of saturated one, and the *CSL* of unsaturated sample having larger suction ($s$ = 294 kPa) exists in looser state, because *CSL* of unsaturated soil shifts with keeping distance from *NCL* given as Equation (3.17). Therefore, the shape of *CSL* of unsaturated soil organized by degree of saturation is linear and parallel to the NCL of saturated sample.

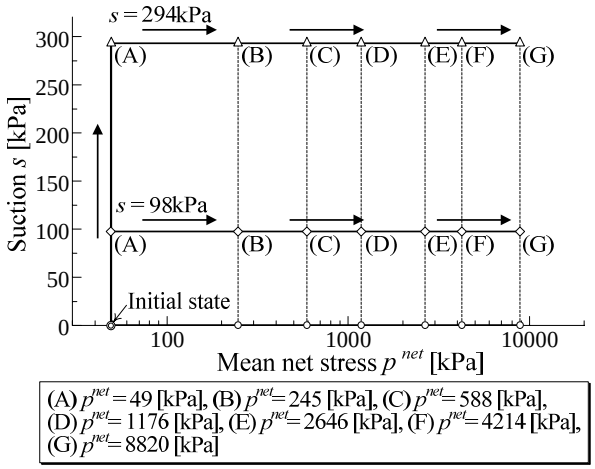


Figure 3.35 Stress paths for describing the *CSL* of unsaturated samples

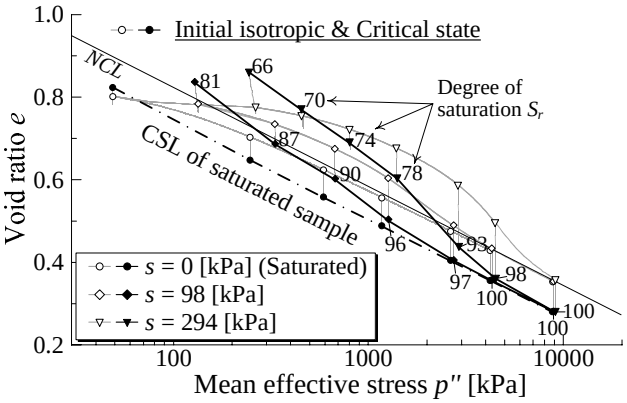


Figure 3.36 Calculated critical state line of unsaturated soil organized by each suction ($s$ = 0(saturated), 98, 294 kPa)

It was indicated from the observed results (Figure 3.9), in which critical states on $e$-ln$p''$ plane are obtained from the drained / exhausted triaxial compression tests at different suctions (Sivakumar, 1993 and Cui, 1996), that *CSL* of unsaturated soil is not parallel to *CSL* (and *NCL*) for saturated soil and its shape is similar with the calculated one. Moreover, the position of *CSL* shifts upward according to increasing in suction (and decreasing in degree of saturation). From comparing the calculated results with the observed phenomena about *CSL*, it is found that the proposed model in which the positions of *NCL* and *CSL* change with variation degree of saturation can describe unsaturated compression behavior and shear behavior, inclusively.

Swelling collapse behavior in one-dimensional problem corresponds to that of isotropic stress condition in multi-dimensional problem. Here, swelling collapse simulation under anisotropic condition is conducted. Two types of samples are assumed, one is normally consolidated soil ($e_0$ = 0.83) and another one is over consolidated soil ($e_0$ = 0.68), the degree of saturation of both samples is the same (80 %) in this simulation. Figure 3.37 shows stress path of the tests. Firstly, the samples are sheared (triaxial compression and extension) from initial condition ($p_{net}$ = 98 kPa and $s$ = 110 kPa) to a prescribed value of deviator stress under constant mean net stress, and then subsequent swelling path is simulated by decreasing suction under constant deviator stress. Samples which don't reach to failure state by initial swelling are sheared again until its critical state (residual strength). Figures 3.38(a) and (b) show the results of anisotropic swelling test under triaxial compression states ((a): 49, 98, 147 kPa) and extension states ((b): 49, 98 kPa) on normally consolidated soil, respectively. In both diagrams, dash lines represent the result of monotonically compression and extension sheared at constant suction without swelling path. It can be seen that proposed model based on the modified stress $t_{ij}$ can consider the influence of relative magnitude of the intermediate principal stress $\sigma_2$, viz., difference in strength and deformation characteristics under triaxial compression ($\sigma_1 > \sigma_2 = \sigma_3$) and extension ($\sigma_1 = \sigma_2 > \sigma_3$) conditions, not only on saturated condition but also on unsaturated condition. It can be seen from this figure that behaviors during swelling are significantly different depending on the magnitude of deviator stress and stress condition (compression / extension). This is because that stress ratio ($q/p''$)

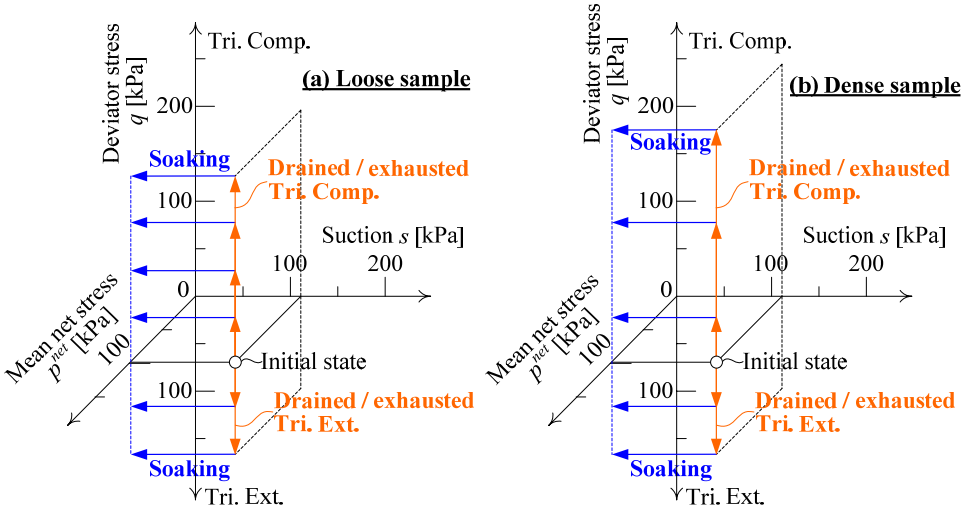


Figure 3.37 Stress paths for simulation of exhausted / drained triaxial compression and extension tests and subsequent soaking test with keeping deviatoric stress on initial unsaturated, normally and over consolidated samples

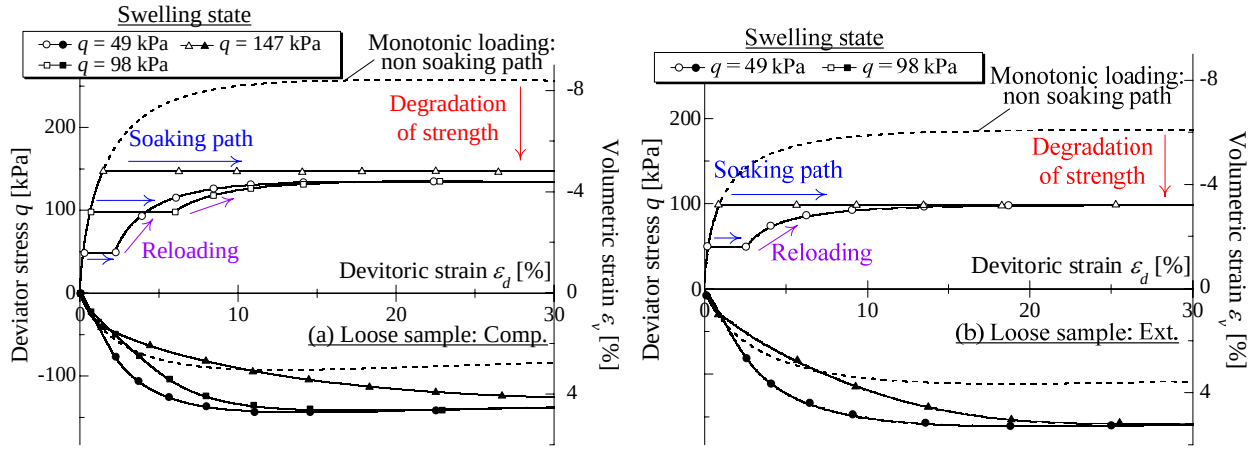


Figure 3.38 Simulation results of exhausted / drained shear tests and subsequent soaking test with keeping deviatoric stress on initial unsaturated, normally consolidated (Loose) samples. (a) results of triaxial compression states, (b) results of triaxial extension states

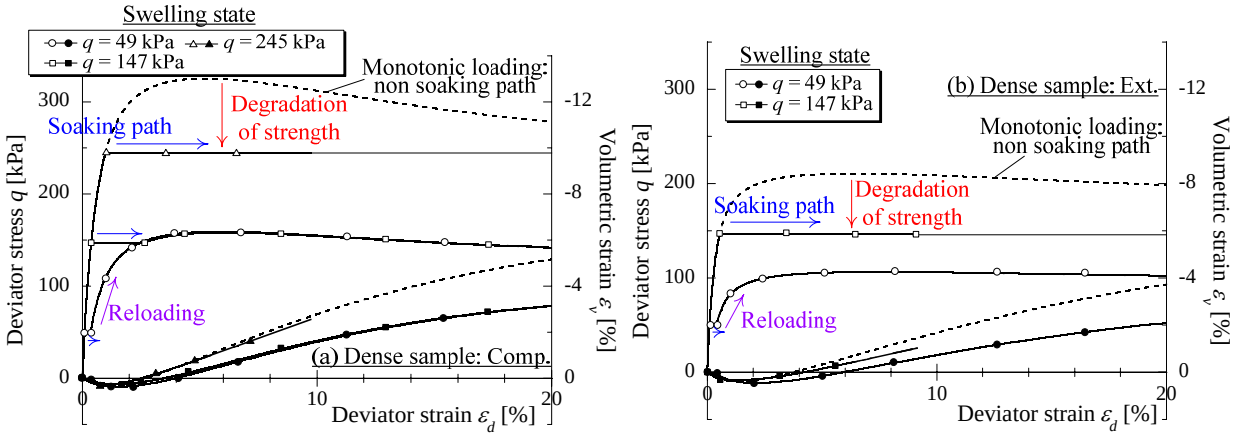


Figure 3.39 Simulation results of exhausted / drained shear tests and subsequent soaking test with keeping deviatoric stress on initial unsaturated, over consolidated (Dense) samples. (a) results of triaxial compression states, (b) results of triaxial extension states

increases due to decreasing of mean effective stress $p''$ (= $p^{net}$ + $S_r s$) in swelling path ($s$ 0 kPa), so that samples are subjected to larger stress ratio during swelling path. Consequently, it can be seen from the result of swelling at higher deviatoric stress condition ($q$ = 147 kPa on Comp. and $q$ = 98 kPa on Ext.) that the significant deformation occurs during swelling. Such soils, then, approach to failure conditions in which plastic coefficient $\Lambda$ equals to the infinite due to increasing in stress ratio $q/p''$. For the result of other cases, although soils exhibit a little development of deviatoric deformation and volumetric compression, soils approach not to failure state ($\Lambda$ ) but to saturated anisotropic stress condition. And then, some samples are sheared to residual strength of saturated soil. It is generally indicated that the larger deformation occurs due to swelling in the higher stress ratio. Especially, in the case of higher stress ratio than saturated residual strength, soil approaches to failure state. Similar behaviors during anisotropic swelling can be seen in the experimental results on Pearl clay conducted by De'an Sun et al. (2007). On the other hand, the volumetric behaviors due to swelling on anisotropic stress condition are more complicated than that on isotropic condition, i.e., general swelling test (swelling collapse), because the dilatancy characteristics obey a flow rule in the model.

It can be seen from the influence of stress condition on anisotropic swelling behavior in Figures 3.38 (a) and (b), that the swelling behaviors at about $q$ 100 kPa in each figure are remarkably different. This difference can be explained as the influence of intermediate stress $\sigma_2$, which means strength of triaxial extension condition is smaller than that of triaxial compression condition. The swelling behavior on anisotropic stress condition is, therefore, affected by not only magnitude of stress ratio, but also three dimensional stress conditions. Figures 3.39 (a) and (b) show the results of swelling tests under triaxial compression ((a): $q$ = 49, 147, 245 kPa) and extension states ((b): $q$ = 49, 147 kPa) on heavily over consolidated soil, respectively. As regards the influence of difference in stress condition (triaxial compression / extension), it is found from diagrams (a) and (b) in Figure 3.39 that the behaviors are wholly similar to the one for normally consolidated soil mentioned above. It is expected that the volumetric expansive behavior during swelling can be seen at higher stress ratio ($q$ = 245 kPa at comp. and $q$ = 147 kPa at ext.) on over consolidated samples. Since the direction of plastic strain increment is given by a flow rule in $t_{ij}$ space, viz., it is uniquely determined by stress state. Such expansive behavior occurs at higher stress ratio. It can be supposed, therefore, that swelling causes not only the compression collapse behavior at isotropic condition but also the development of deformation with negative and positive dilatancy behaviors at anisotropic stress condition (stress ratio $q/p''$). Discussing about influence of density on swelling behavior from Figures 3.38 and 3.39, it can be seen that swelling deformation of over consolidated soil is generally smaller than that of normally consolidated soil.

## 3.4 Application to the soil compaction

The volumetric behavior of soils due to external loading is divided into consolidation (discharging void water), compaction (discharging void air) and dilatancy (shear). Although the ordinary constitutive models such as Cam clay model (Roscoe et al, 1958) can describe consolidation and shear behavior of soils, compaction behavior has not been described by any constitutive model and the mechanism of soil compaction has not been fully understood. Soil compaction is a method of mechanically decreasing the void ratio and increasing the density, which is quite significant from an engineering point of view as increasing strength and decreasing permeability of several geo-structures. While consolidation occurs for the drainage of void water which can be properly described by constitutive models for saturated soils, mechanism of soil compaction needs to be discussed within the framework of unsaturated soil mechanics. This is because soil compaction occurs primarily for the discharge of void air and the compaction efficiency is strongly dependent on degree of saturation (or water content). From the simulation of compaction behavior of unsaturated soil carried out by proposed model, the mechanical meanings of the compaction curve which represents the relation between dry density and moisture contents, and the optimum moisture content are discussed in this section.

It was indicated from experimental theory by Proctor that the soil compacted at near optimum moisture content shows higher stiffness and strength, and little variation in strength due to wetting, since its density is very large and the degree of saturation hardly change due to wetting. Based on Proctor's theory, the soil compaction at optimum content is conventionally conducted in a present working level. The variation of stress-strain relation of compacted soil due to subsequent mechanical and hydraulic effects, however, has also never been argued theoretically. In this study, the subsequent mechanical (compression and shear) and hydraulic (soaking) behaviors are explained by analytical knowledge. A permanent mechanical quality of compacted soil can be investigated from such simulations, because the hydraulic problem is equivalent to the behavior of soil at rainfall condition which is a worse condition for geo-structures such as embankment.

### 3.4.1 Mechanical interpretation of the compaction behavior of soil

In this calculation, a set of material parameters assuming Fujinomori clay (Table 3.5) is used in common with above parametric studies. The initial unsaturated sample (void ratio: $e_0$ = 0.9, water content: $w_0$ = 13.6%, degree of saturation: $S_{r0}$ = 40%), which is under mean stress $p$ = 49kPa, pore air pressure $u_a$ = 0 kPa (atmosphere pressure) and pore water pressure $u_w$ = -2000 kPa, is firstly adjusted to prescribed water content $w$ by increasing pore water pressure $u_w$. This process assumes the wetting method for soil compaction. Since the compaction of soil is generally regarded as the mechanical discharge of void air without significant drainage of void water, total stress $p$ is statically increased from 49 kPa to predetermined maximum value ($p_{\max}$ = 100, 200, 400, 800, 1600, 3200, 6400 kPa) with keeping constant water content and back again to the original stress $p$ = 49 kPa in this calculation. Whereas compaction energy or compactive effort is usually increased by increasing the number of rammer drop in the laboratory compaction test, maximum applied pressure is increased in this calculation.

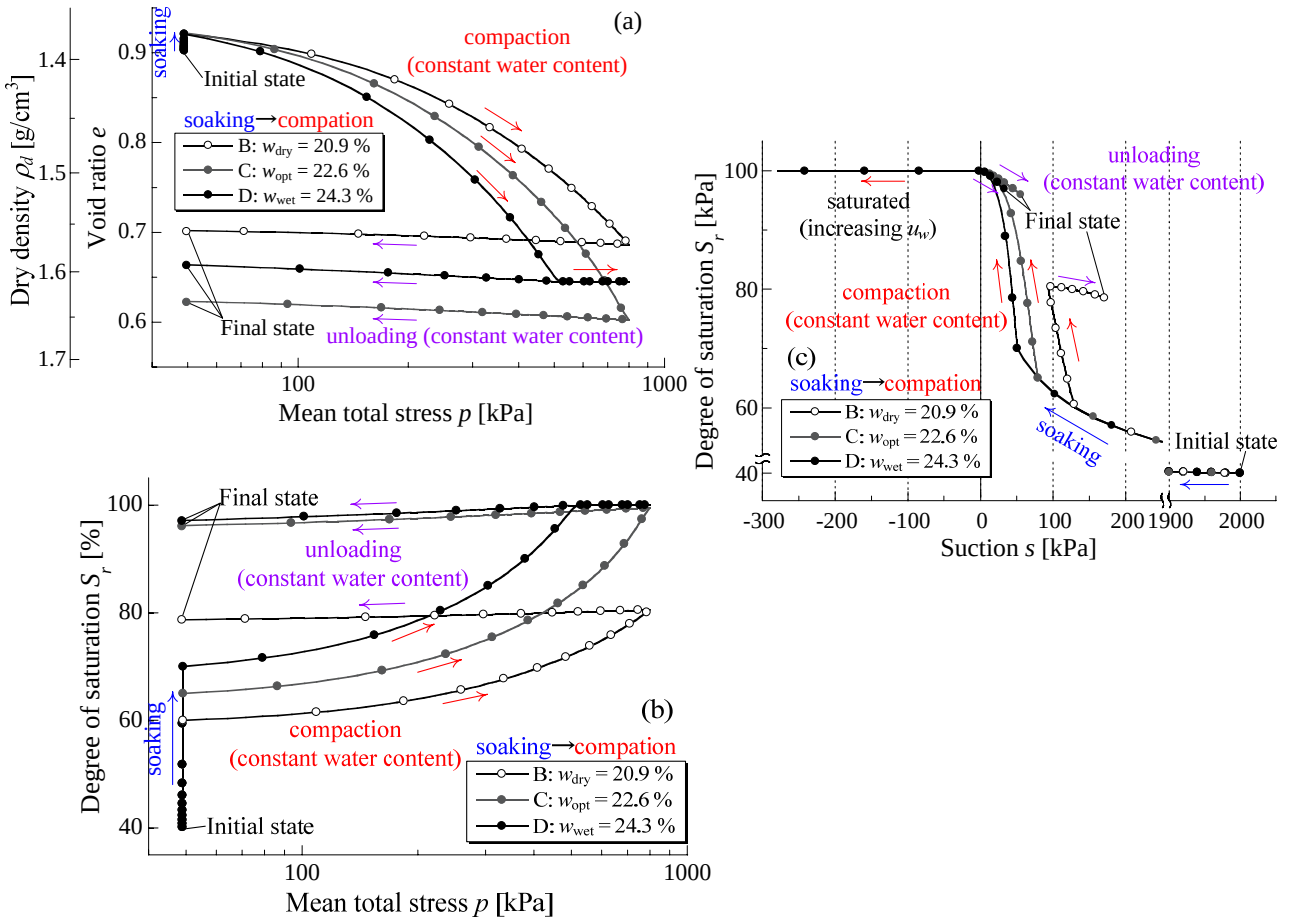


Figure 3.40 Simulations of compaction tests under constant water content ($p_{max}$ = 800 kPa, $w$ = 20.9, 22.6, 24.3 %)
(a) total stress $p$ vs. void ratio $e$; (b) total stress $p$ vs. degree of saturation $S_r$; (c) suction $s$ vs. degree of saturation $S_r$

Figure 3.40 shows static compaction behaviors ($p_{max}$ = 800 kPa) of three samples with different water contents ($w$ = 20.9, 22.6, 24.3 %). Diagrams (a) and (b) show the variation in void ratio $e$ (dry density $\rho_d$) and degree of saturation against applied mean stress $p$, respectively. It can be seen from these diagrams that the soil compresses with discharging void air due to increasing of applied stress regardless of water content, and the dry density increases. Soil sample having lower water content shows higher stiffness, so the volume change of such soil during compaction is smaller. In contrast, soil sample having larger water content is more compressible in the early stage of compaction. This is quite reasonable with actual soil behaviour because it is intuitively accepted that moisture acts as a lubricant within soil particles. However, once soil is saturated with water, soil is hardly compressed regardless of its water content. This is because that the applied pressure is cancelled out by excess pore water pressure in nearly saturated condition. It can be seen from diagram (c) representing the relation between suction and degree of saturation $S_r$ that suction decreases with the increase of applied pressure under exhausted and undrained conditions. Therefore, it seems that the increasing of degree of saturation $S_r$ during compaction is caused due to decreasing of suction and volumetric contraction which is represented by the proposed SWCC considering the influence of density. So, it is

concluded from this figure that water content of the soil is critical for the mechanism of soil compaction, viz., lack of void water results in inadequate compaction as drier soil is more resistant to compaction; on the other hand, too much moisture also leads to insufficient compaction as applied pressure is cancelled out by excess pore water pressure and hence effective stress hardly increases. Therefore, in Figure 3.40, soil having intermediate water content is effectively compacted and highest dry density is achieved.

Calculations of 84 static compaction tests have been carried out under varied water content $w$ (12 kinds) and maximum applied stress $p_{max}$ (7 kinds: 50, 100, 200, 400, 800, 1600, 3200 kPa). The results of compaction tests are summarised in Figure 3.41 (a) (the relation between dry density and water content), in which different curves are drawn for different applied pressures (compactive effort). As is already mentioned

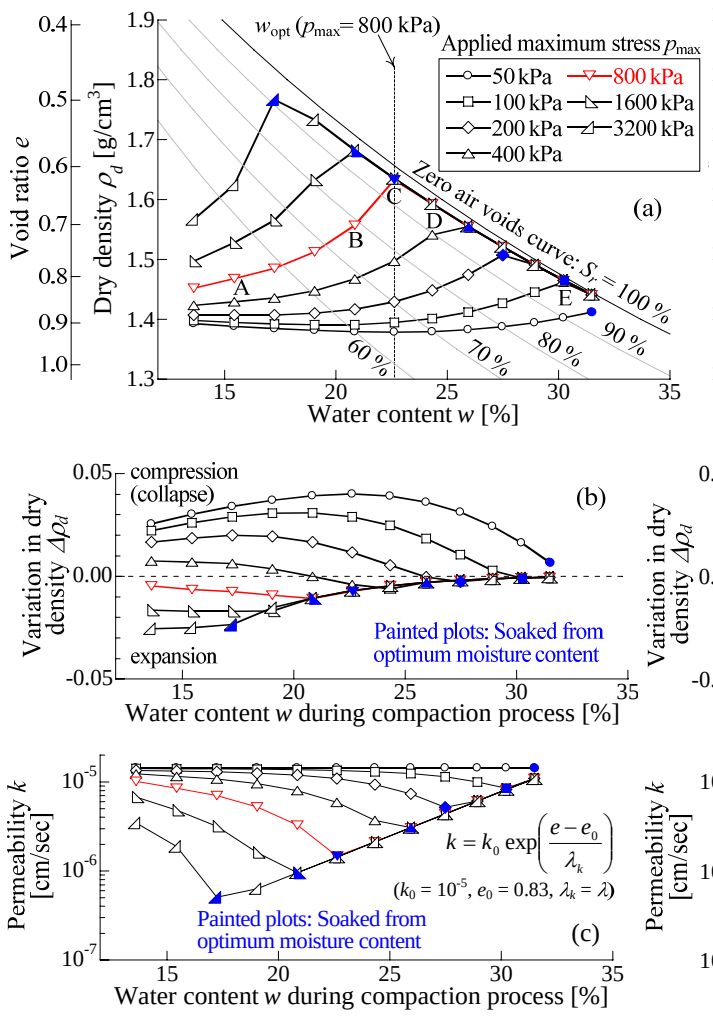


Figure 3.41 Compaction curves for different applied maximum stresses (a) water content vs. dry density after compaction (final states of compaction tests); (b) initial water content vs. variation in dry density during subsequent soaking test; (c) initial water content vs. permeability of soil saturated with water after compaction tests

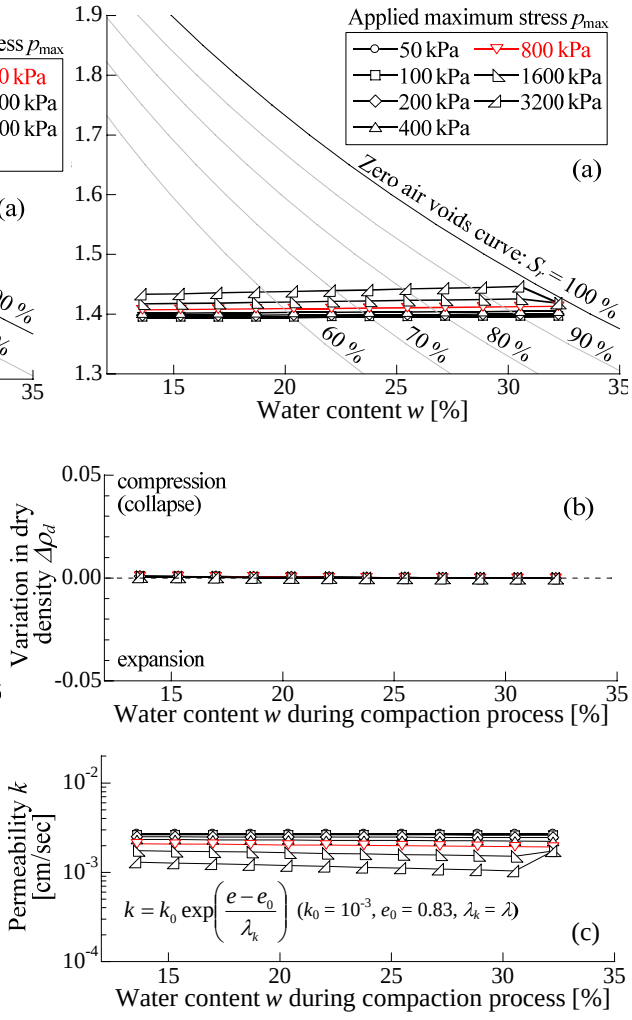


Figure 3.42 Simulations of static compaction of Toyoura sand (a) water content vs. dry density after compaction (final states of compaction tests); (b) initial water content vs. variation in dry density during soaking tests; (c) initial water content vs. permeability after compaction and subsequent soaking

Table 3.6 Material parameters for stress-strain relation and soil water characteristic curve on Toyoura sand

| *Parameters for mechanical model* | | | *Parameters for SWCC* | | |
|---|---|---|---|---|---|
| $\lambda$ | 0.070 | same parameters as Cam clay model | $S_{min}$ | 0.10 | parameters for van Genuchten's equation |
| $\kappa$ | 0.0045 | | $S_{max}$ | 1.00 | |
| $N_{sat}$ | 1.10 | | $\alpha_{wet}$ | 0.03 | |
| $R_{cs}$ | 3.2 | | $\alpha_{dry}$ | 0.10 | |
| $\nu$ | 0.2 | | $m$ | 0.1 | |
| $\beta$ | 2.0 | shape of yield surface | $n$ | 2.0 | |
| $a$ | 500 | effect of density and confining pressure | $\xi$ | 100 | effect of suction history |
| $l$ | 0.05 | effect of $S_r$ on the position of *NCL* | $\xi_e$ | 5.0 | effect of void ratio |

from Figure 3.40, soil with intermediate amount of water content is effectively compacted and hence upward-convex compaction curve having maximum dry density (or lowest void ratio) at optimum water content is properly described by the proposed model. It is also pointed out from Figure 3.41 (a) that the increase of the maximum applied pressure in lower optimum water content gives higher maximum dry density. The proposed model, therefore, can exhibit the well-known transition of the compaction curves with increase of the applied pressure.

In order to investigate the effectiveness of soil compaction, 84 compacted soil samples are subsequently soaked under constant total stress of 49 kPa. Variations in dry density during soaking process are compared in Figure 3.41 (b), and permeability of soaked sample is plotted against initial water content in Figure 3.41 (c). It is known that: soil packed densely at optimum water content is quite resistant to the soaking-induced volumetric compression; compaction at optimum water content achieves the lowest permeability and provides good resistance against flooding. Simulations of the same series of compaction and subsequent soaking tests are conducted using material parameters for Toyoura sand listed in Table 3.6. Toyoura sand has a rather uniform grain size distribution. The results of calculations are summarised in Figures 3.42 (a), (b) and (c). In contrast to the simulations of Fujinomori clay, compaction curves of Toyoura sand are rather flat and the maximum dry density and optimum water content cannot be clearly determined. This seems to be reasonable as it is widely known that well-classified (or poorly-graded) uniform soil is hardly compacted and distinctive maximum dry density is not seen in such soil. So, it can be said that the proposed model can precisely consider the difference of compaction behavior of different soils by adjusting the material parameters.

### 3.4.2 Mechanical quality evaluation of the compacted soil

*Evaluation of compression characteristic of compacted soil*

The compression and shear characteristics of compacted soils after wetting are discussed here. Compression tests under exhausted and drained conditions, and soaking test with keeping constant confining pressure were carried out on three kinds of compacted samples A, C and E at $p_{max}$ = 800 kPa shown in Figure 3.40 (a). These simulations predict the mechanical stability of geo-structures such as embankment in the condition

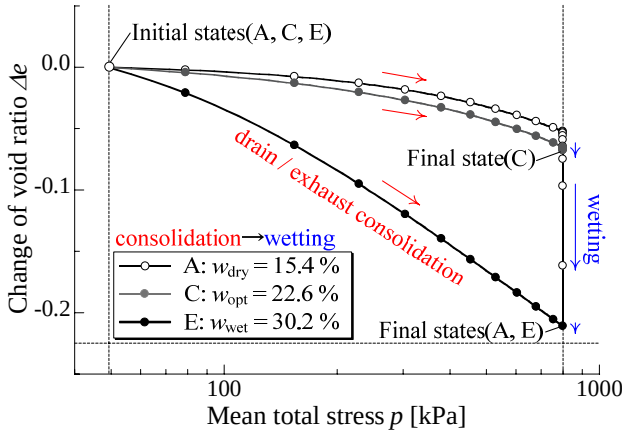


Figure 3.43 Simulation results of exhausted / drained compression and subsequent soaking tests on compaction samples A($w_{dry}$= 15.4%), B($w_{opt}$= 22.6%) and C($w_{wet}$= 15.4%) in Figure 3.41

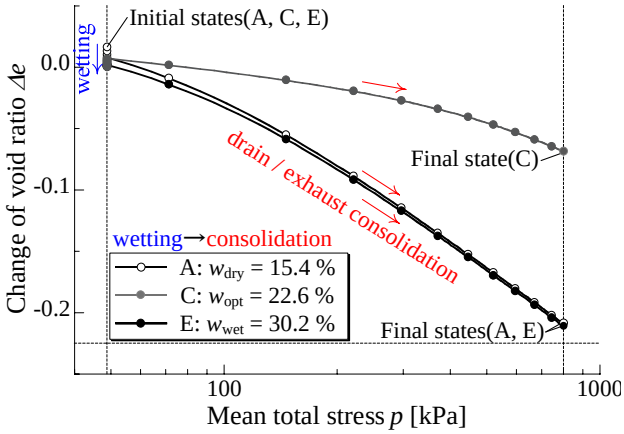


Figure 3.44 Simulation results of soaking and subsequent exhausted / drained compression tests and subsequent on compaction samples A($w_{dry}$= 15.4%), B($w_{opt}$= 22.6%) and C($w_{wet}$= 15.4%) in Figure 3.41

of soaking during rainfall. Soil samples are firstly re-compressed until pre-compaction pressure $p$ = 800 kPa, and then are soaked under constant mean stress. Soaking path is simulated by increasing pore water pressure $u_w$ (decreasing suction $s$) until zero in this calculation. Figure 3.43 shows the relation between total mean stress $p$ and change of void ratio $\Delta e$ during this process. It can be observed from Figure 3.43 that the sample (C) compacted at optimum water content shows higher stiffness along with compression path and hardly compressive also during wetting path. It is well known that soil compacted at optimum water content achieves densely and nearly saturated packing, so that sample is quite resistant to the soaking-induced volumetric compression (soaking collapse). In contrast, although sample (A) compacted at smaller water content than $w_{opt}$ (at dry side) shows stiffer behavior due to partial saturated effect (capillary stress) during compression, the significant volumetric compression behavior can be observed in the subsequent soaking process. On the other hand, sample (E) compacted at larger water content than $w_{opt}$ (at wet side) is compressible at the compression process, since such sample could not achieve a sufficient density due to insufficiently compacted. Such wet side sample is nearly saturated, so that it hardly compresses due to soaking.

Contrary to the former simulations, same soil samples A, C and E are initially soaked at mean stress $p$ = 49 kPa, and then total mean stress $p$ is increased from 49 kPa to pre-compaction pressure 800 kPa. From these simulation results shown in Figure 3.44, it can be observed that: looser sample (E) compacted at wet side is affected by initial wetting path and shows compressive behavior as well as the former simulation (Figure 3.43); sample (C) compacted at the optimum water content also shows the same mechanical and hydraulic resistance as seen in Figure 3.44; In contrast to the simulation result of Figure 3.43, although sample (A) compacted at dry side hardly compresses due to soaking at low confining pressure, such sample shows the large volume change at subsequent compression process. This is because sample (A) having lower density and smaller water content loses the capillary stress at soaking process, and then it is just insufficient compacted sample.

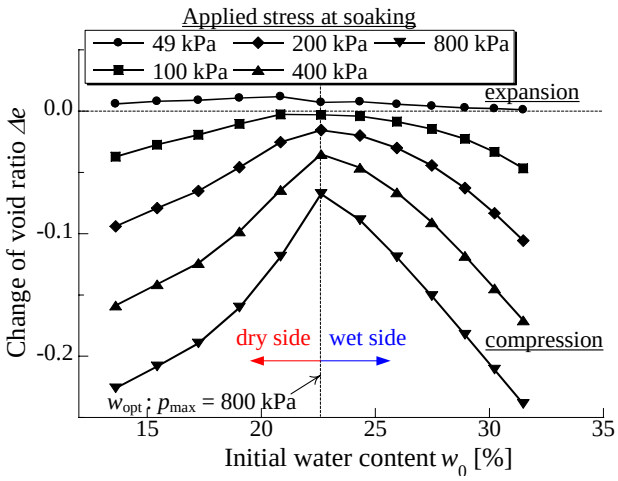


Figure 3.45 The relation between the compaction water contents and amount of volume change due to soaking collapse after loading stress from $p$ = 49 kPa to prescribed mean stress ($p$ = 49, 100, 200, 400 and 800 kPa)

The induced-soaking volumetric change $\Delta e$ under different applied pressures ($p$ = 49, 100, 200, 400, 800 kPa) on 12 samples, which were previously compacted until $p_{max}$ = 800 kPa with various 12 water contents, are summarized in Figure 3.45. It can be seen from this figure that although all 12 samples show a little soaking expansive behavior under lower confining pressure ($p$ = 49kPa), the amount of volume compression increases with the increasing applied stress. The relation between initial water content and change of void ratio, therefore, draws the upward-convex curve, viz., the soil compacted at the optimum moisture content is stable for the compression behavior due to applying stress and soaking. Although samples compacted at dry side and wet side are compressive during soaking (collapse) and compression after soaking process, the mechanisms of such volumetric change are different, i.e., produces soaking collapse and lower stiffness due to insufficient compaction.

*Evaluation of shear characteristic of compacted soil*

Figure 3.46 shows the stress-strain behaviors of drained conventional triaxial tests ($p_0$ = 49 kPa) on soaked samples which were prepared by soaking compacted samples A, B, C, D and E in Figure 3.41 under constant mean stress $p$ = 49 kPa. It can be observed from this figure that the sample (C) compacted at optimum moisture content shows larger initial stiffness and peak strength. Samples (C) and (E) insufficiently compacted at wet side show lower stiffness and strength than sample (C). It is generally expected that unsaturated soil samples compacted at dry side show stiffer behavior and higher strength than saturated one having the same density, as shown in parametric studies (Figure 3.33). Once soaking, however, such unsaturated soil diminishes the influence of partial saturation (interparticle bonding with meniscus water (capillary stress)), hence its strength and shear stiffness decrease to that of saturated sample having same density ((A) and (B)). Concerning dilatancy behavior, all samples show the dilative behavior commensurate with its density regardless of initial water content. The relation between compaction curve and a peak strength after soaking, which is plotted at water content before soaking, are organized in Figure 3.47. The proposed model can represent such distribution of strength having a peak at optimum moisture content which has been indicated

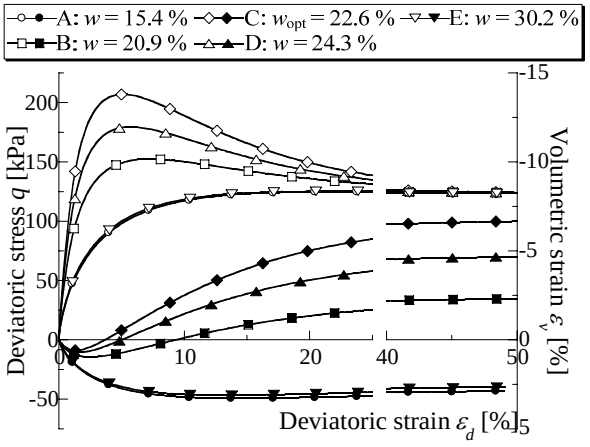


Figure 3.46 Simulation results of exhausted / drained triaxial compression tests ($p_0$ = 49 kPa) after soaking at $p$ = 49 kPa on compaction samples A – E in Figure 3.41.

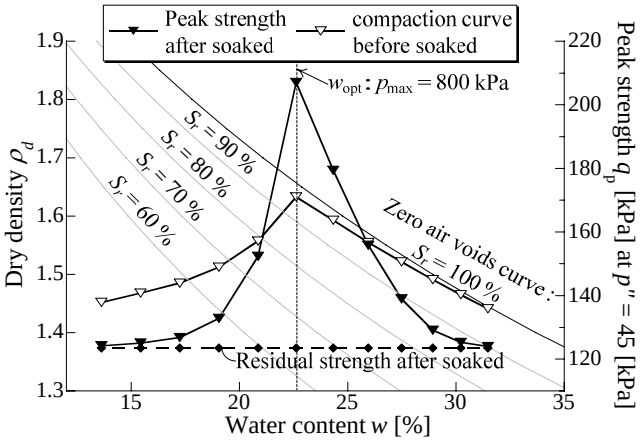


Figure 3.47 The relationship between compaction samples at different water content and its residual strength after soaking plotted on water content $w$ – dry density $\rho_d$ plane

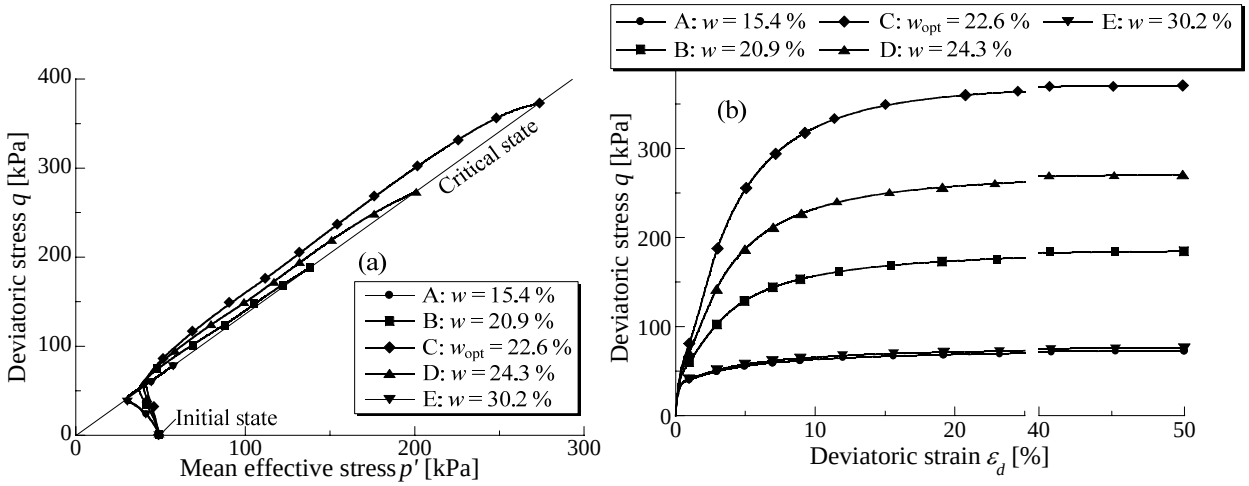


Figure 3.48 Simulation results of undrained triaxial compression tests after soaking at $p$ = 49 kPa on compaction samples A – E in Figure 3.41.
(a) effective stress path, (b) stress-strain relations (deviatoric strain $\varepsilon_d$ – deviatoric stress $q$)

from Proctor's theory. Figures 3.48 (a) and (b) shows the results of undrained shear tests on the same five kinds of samples which were used in Figure 3.46. In the same manner as Figure 3.46, each sample show the deformation and strength characteristics commensurate with its density, thus it can be indicate that optimum moisture content sample (C) having the larger undrained shear strength is the most stable sample.

It was shown by the proposed model that soil compacted at the optimum moisture content shows higher stiffness and strength even after soaking as indicated by Proctor's theory. Soil compaction is mainly applied for constructing the geo-structures such as embankment. Therefore, the proposed model can investigate the prolonged stability of geo-structures such as embankment in consideration of its construction phase and bad condition such as rainfall.

## 3.5 Summary

The constitutive model for saturated soil considering the various external effects, which is proposed in Chapter 1, was extended to one applicable to the partial saturated state in this chapter. A large number of constitutive models for unsaturated soil have ever been proposed based on a wide range of theoretical assumptions. About the stress tensor, for instance, we have to determine that we use either the single stress (effective stress) or net stress $\sigma^{net}$ and suction $s$, and we have to discuss various types of effective stress tensor. A model representing inclusively various mechanical and hydraulic behaviors of unsaturated soil has not been proposed yet. With reference to past experimental results of unsaturated soil, the model based on simple assumption which is applicable to a broad range of observed behavior was proposed in this chapter. The main results of this paper are summarized as follows:

(1) Bishop's effective stress tensor was used for organizing experimental results and formulating the constitutive model in this study, since the critical state strength, the stress-dilatancy relation and the shape of yield surface (if the associated flow rule is assumed) of saturated soil can be applied to that of unsaturated soil directly by using this effective stress tensor.

(2) Soil water characteristic curve (SWCC), which is ordinary represented as the unique relation between degree of saturation $S_r$ and suction $s$, is affected by suction history (hydraulic hysteresis), density, temperature and others. Classical models of SWCC cannot consider such hydraulic features of soils. In this study, two new simple methods considering such influences on SWCC were proposed. The new state variable $I_w$ defined as the ratio of interior division of the current hydraulic state ($s$, $S_r$) between two reference states on the main drying and wetting curves and its evolution rule were applied to classical SWCC model. It was shown that such extended SWCC model suitably represents the scanning curves (hydraulic hysteresis). On the other hand, in order to consider the influence of density and other external effects, the modified suction $s^*$ formulated by not only suction but also void ratio, temperature and other variables is proposed. The SWCC model formulated on the basis of $s^*$ instead of ordinary $s$ can represents the influence of density on SWCC: degree of saturation increases with decreasing of void ratio (volumetric compression) even under constant suction.

(3) Unsaturated soils can exist in looser state than saturated sample under same confining pressure. Once unsaturated soil is soaked, it rapidly converges to compression line of saturated one, viz., soaking collapse occurs. Sample having lower degree of saturation has higher shear strength and shows larger dilative behavior similar to over consolidated soil. Such influence of degree of saturation on compression and shear characteristics of unsaturated soil can be incorporated simply by shifting both normally consolidated line (*NCL*) and critical state line (*CSL*) of unsaturated soil downward (or upward) in the plane of void ratio $e$ and effective mean stress $p''$ depending on the increase (or decrease) of degree of saturation $S_r$. Introducing the state variable $\psi$ explained in Chapter 2, which was given as a function of degree of saturation, we shifted the position of *NCL*. In a similar manner as Chapter 2, one-dimensional

model and three-dimensional for unsaturated soil based on Bishop's $\sigma''_{ij}$ were formulated. Note that changing position of *NCL* is equivalent to changing position of *CSL* in this method.

(4) It was indicated through the simulations that the proposed model suitably describes typical behaviors of unsaturated soils. The compression line calculated by proposed model represented the various compression lines obtained from experiments inclusively. The proposed model, furthermore, properly considered the soaking collapse phenomena depending on confining pressure and density. Concerning the shear behavior, it could be seen that the proposed model can describe the strength, deformation, dilatancy characteristics depending on degree of saturation $S_r$, and the development of deviatoric deformation during soaking under anisotropic stress condition as can be seen in observed results.

(5) The proposed model was applied to describe the compaction of soil. It was seen from calculation that the proposed model can express the well-known compaction curves of soil including their transition due to the increase of the applied stress. It was concluded that water content of the soil is critical for the mechanism of soil compaction, viz., lack of void water results in inadequate compaction as drier soil is more resistant to compaction; on the other hand, too much moisture also leads to insufficient compaction as applied pressure is cancelled out by excess pore water pressure and hence effective stress hardly increases. Soil having intermediate water content, accordingly, is effectively compacted and the highest dry density is achieved. It was shown from calculated results that: the difference in compaction curves is due to the distribution of grain size; sample having optimum water content shows the mechanical stability for both compression and shear behaviors.

# Reference


Alonso, E.E., Gens, A. and Hight, D. W. (1987): Special problems soils, General report, Proc. 9th Eur. Conf. Soil Mech., Dublin, Vol. 3, 1087-1146.

Alonso, E. E., Gens, A. and Josa, A. A. (1990): A constitutive model for partially saturated soils, Geotechnique, Vol. 40, No. 3, 405-430.

Atchison, G. D. (1960): Relationships of moisture stress and effective stress functions in unsaturated soils, *Pore Pressure and Suction in Soils*, Butterworths, London.

Bishop, A.W., Alpan, I., Blight, G.E. and Donald, I.B. (1960): Factors controlling the strength of partly saturated cohesive soils, *In ASCE Res. Conf. Shear Strength of Cohesive Soils (Univ. of Colorado, Boulder)*, 503-532.

Bishop, A.W. and Blight, G. E. (1963): Some aspects of effective stress in saturated and partly saturated soils, Geotechnique, Vol. 13, No. 3, 177-197.

Bishop A.W., Donald I. (1961): The experimental study of partly saturated soil in the triaxial apparatus. *5th International Conference on Soil Mechanics and Foundation Engineering*, Paris, 13–21.

Coleman, J. D. (1962): Stress strain relations for partly saturated soil, Geotechnique, Vol. 12, No. 4, 348-350.

De'an Sun, Daichao Sheng and Yongfu Xu (2007): Collapse behaviour of unsaturated compacted soil with different initial densities, *Canadian Geotechnical Journal*, 44, 673-686.

Fredlund, D. G. and Morgenstern, N. R. (1977): Stress state variables for unsaturated soils, Canadian Geotechnical Journal, Vol. 15, No. 3, 313-321.

Fredlund, D. G. and Xing, A. (1994): Equation for the soil-water characteristic curve, *Can. Geotech. J.* 31(3), 521-532.

Gallipoli, D., Wheeler, S.J. and Karstunen, M.: Modelling the variation of degree of saturation in a deformable unsaturated soil, Géotechnique 53(1), 105-112, 2003.

Geiser F, Laloui L, Vulliet L. (2000): Modelling the behaviour of unsaturated silt. *Experimental Evidence and Theoretical Approaches in Unsaturated Soils*; *Proceedings of an International Workshop*, Trento, 155–175.

Honda, M. (2000): *PhD Thesis*, Kobe University, Japan.

Huang, H.C., Tan Y.C., Liu, C.W. and Chen, C.H. (2005): A novel hysteresis model in unsaturated soils, Hydrol. Process. 19, 1653-1665.

Iizuka, A., Honda, M., Nishida, H., Kawai, K. and Karube, D. (2000): Soil / water coupled analysis considering unsaturated pore water distribution, *Journal of Geotechnical Engineering(III), JSCE*, Vol. III-52, No. 659, 165-178. (in Japanese)

Jennings, J. E. B. and Burland, J. B. (1962): Limitations to the use of effective stresses in partly saturated soils, *Geotechnique*, Vol. 12, No. 2, 125-144.

Josa, A., Balmaceda, A., Gens A. and Alonso, E.E. (1992): An elasto-plastic model for partially saturated soils exhibiting a maximum of collapse, *Proceeding of 3rd International Conference Computational Plasticity (Barcelona)*, vol. 1, 815-826.

Karube, D., Kato, S., Hamada, K. and Honda, M. (1996): The relation between pore water and mechanical behavior of soil mass on unsaturated soil, *Journal of Geotechnical Engineering(III), JSCE*, Vol. III-34, No. 535, 83-92. (in Japanese)

Kawai, K., Karube, D., Kato, S. and Kado, Y. (2000): Behavior of unsaturated soil and water characteristics in undrained shear, *Research paper of research center for urban safety and security, Kobe univ.* 4, 231-239 (in Japanese).

Khalili, N. and Khabbaz, M. H. (1998): A unique relationship for $\chi$ for the determination of the shear strength of unsaturated soils, Geotechnique, Vol. 48, No. 2. 1-7.

Khalili, N., Geiser F. and Blight G. E. (2004): Effective stress in usaturated soils: review with new evidence, *International Journal of Geomechanics*, Vol. 4, No. 2, 115-126.

Kikumoto, M., Kyokawa, H. and Nakai, T. (2009): Comprehensive modeling of the water retention curve considering the influences of suction histories, void ratio and temperature, *Journal of Applied Mechanics JSCE*, Vol. 12, 343-352. (in Japanese)

Kikumoto, M., Kyokawa, H., Nakai, T. and Shahin, H. M. (2010): A simple elasto-plastic model for unsaturated soils and interpretations of collapse and compaction behaviours, *Proc. of the 5th International Conf. on Unsaturated Soils* (UNSAT 2010), Barcelona, Spain, 849-855.

Kohgo, Y., Nakano, M., and Miyazaki, T. (1993): THEORETICAL ASPECTS OF CONSTITUTIVE MODELING FOR UNSATURATED SOILS, *Soils and Foundations* 33(4), 49-63.

Kohgo, Y. (2008): A hysteresis model of soil water retention curves based on bounding surface concept, Soils and Foundations 48(5), 633-640.

Kool, J.B. and Parker, J.C.: Development and evaluation of closed-form expressions for hysteretic soil hydraulic properties, Water Resour. Res. 23(1), 105-114, 1987.

Kyokawa, H., Kikumoto, M. and Nakai, T. (2010(a)): A simple description of stress-strain and hydraulic behaviours of unsaturated soil, *Proc. of the 4th Sino-Japan Geotechnical Symposium*, 74-81.

Kyokawa, H., Kikumoto, M., Nakai, T. and Shahin, H. M. (2009): An elasto-plastic constitutive model for unsaturated soil unified considering the relation between suction, degree of saturation and density, *Journal of Applied Mechanics JSCE*, Vol. 12, 331-342. (in Japanese)

Kyokawa, H., Kikumoto, M., Nakai, T. and Shahin, H. M. (2010(b)): Simple modeling of stress-strain relation for unsaturated soil, *Experimental and Applied Modeling of Unsaturated Soils* (*Geotechnical Special Publication No.202*), American Society of Civil Engineers, Shanghai, China, 17-25.

Kyokawa, H., Kikumoto, M., Nakai, T., Tatematsu, K. and Koike, M. (2010(c)): Extension of ordinary water retention curve model by using the modified suction, *Proceedings of the 65th Annual Conference of the Japan Society of Civil Engineers*, III-085.

Li, X.S. (2004): Modelling of hysteresis response for arbitrary wetting / drying paths, Computers and Geotech. 32, 133-137.

Liu, C. and Muraleetharan, K.K. (2006): Description of soil water characteristic curve using the bounding surface plasticity theory, Unsat. Soils, Geotech. Special Publication, ASCE, 147, 2432-2440.

Loret, B. and Khalili, N. (2002): An effective stress elastic-plastic model for unsaturated porous media, Mechanics of Materials, Vol. 34, 97-116.

Nakamura, K. and Toyota, H. (2007): Influence of suction on strength of unsaturated sandy soil, *Proceedings of the 62 th Annual Conference of the Japan Society of Civil Engineers*, Vol. III, 191-192.

Kawai, K., Karube, D., Ashida, W. and Kido, Y. (2000): Model of water retention curve considering the influence of void ratio, *Journal of Geotechnical Engineering(III), JSCE,* Vol. 666, No. III-53, 291-302. (in Japanese)

Nuth, M. and Laloui, L. (2008): Effective stress concept in unsaturated soils: Clarification and validation of a unified framework, *International J. Numer. and Anal. Meth. in Geomech.*, 32, 771-801.

Mualem, Y.: A conceptual model of hysteresis, Water Resour. Res. 10(3), 514-520, 1974.

Poulovassilis, A.: Hysteresis of pore water, an application of the concept of independent domains, Soil Sci. 93, 405-412, 1962.

Proctor, R. R. (1933): Four Article on the design and construction of rolled-earth dams, *Eng. News Record*, Vol. 111, 245-248, 286-289, 348-351, 372-376.

Schofield, A. N. and Wroth, C. P. (1968): *Critical State Soil Mechanics*, McGraw Hill, London.

Scott, P.S., Farquhar, G.J. and Kouwen, N.: Hysteretic effects on net infiltration, Advance in Infiltration, Am. Soc. Agric. Eng., 163-170, 1983.

Sivakumar, V. (1993): A critical state frame work for unsaturated soil, *Ph.D thesis*, University of Sheffield.

Shimizu, M., Fukuda, N. and Nambu, K. (2003): Behavior of unsaturated soil under constant volume at exhausted and undrained conditions, *Research report of engineering department of Tottori university*, Vol. 34, 49-54.

Tarantino, A. and Tombolato, S.: Coupling of hydraulic and mechanical behaviour in unsaturated compacted clay, Géotechnique 55(4), 307-317, 2005.

Terzaghi, K. (1936): The shearing resistance of saturated soils and the angle between the planes of shear. *InternationalConference on Soil Mechanics and Foundation Engineering*. Harvard University Press: Cambridge, MA, 54–56.

van Genuchten, M. Th. (1980): A closed-form equation for predicting the hydraulic conductivity of unsaturated soils, *Soil Sci. Soc. Am. J.* 44, 892-898.

Wei, C. and Dewoolkar, M.M.: A deductive scheme for modeling hysteresis of capillarity, Unsat. Soils, Geotech. Special Publication, ASCE, 147, 2420-2431, 2006.

Wheeler, S. J., Sharma, R. J. and Buisson, M. S. R. (2003): Coupling of hydraulic hysteresis and stress-strain behaviour in unsaturated soils, *Geotechnique*, Vol. 53, No. 1, 41-54.

Wheeler, S. J. and Sivakumar, V. (1995): An elasto-plastic critical state framework for unsaturated soil, *Geotechnique*, 45(1), 35-53.

Y. J. Cui and P. Delage (1996): Yielding and plastic behavior of an unsaturated compacted silt, *Geotechnique*, 46(2), 291-311.

# Chapter 4
# Constitutive model describing the induced anisotropy on granular material

## 4.1 General

In soil mechanics, void is one of the important characteristics of soil for a long time. And its state variable quantity, viz., void ratio $e$ (= $V_v / V$ ), plays an essential role in interpreting the mechanical behavior of soil and its modeling. The modeling of normally consolidated soil for both one-dimensional and multi-dimensional expressed in Chapter 2 is exactly derived from relation between “void ratio $e$” and one-dimensional stress $\sigma$ (mean stress $p$). As considering the various features of soil (i.e., density, structure (bonding), temperature and partial saturated state), the normally consolidated line and the critical state line on $e$-ln$\sigma$ ($p$) plane, which are relative state to evaluate the condition of void of soil (void ratio $e$), are shifted in a modeling. Void ratio $e$, therefore, is just an important factor of soils. In other word, such modeling based on void ratio $e$ and relative position of it treats soil as a homogeneous isotropic material, and such features of soil affect on deformation and strength of soil isotropically. It is well known, however, that geomaterials represented as an assembly of granular materials shows anisotropic deformation characteristic due to geometric influence such as particle orientation and arrangement, and this is called “soil anisotropy”. These anisotropic behaviors cannot be considered only by void ratio $e$.

Soil anisotropy can be discriminated between the inherent anisotropy and the induced anisotropy. The former is produced during deposition process, while the latter is induced by the change of orientation of particles (fabric) due to loading (non-elastic deformation). These anisotropies cannot be negligible and should be considered properly in a constitutive model of soils in order to predict the behavior of actual ground. Especially, since the influence of the induced anisotropy can be seen as “the influence of different three-dimensional stresses condition” and “the influence of stress histories” in any stress path (e.g., relative difference of three principal stresses, rotation of principal stress axis, cyclic loading and others), its modeling is absolutely essential.

In the ordinary models, the influence of different three-dimensional stresses condition is usually modeled by assuming a non-circular shaped yield surface in octahedral plane (or by changing the strength depending on the relative magnitude of the intermediate principal stress) (e.g., Yoshimine, 2006), and that of the stress histories is considered by applying kinematic / rotational hardening rule in ordinary stress space (e.g., Dafalias et al. (1986) and Hashiguchi (2001)). Kinematic / rotational hardening rule, however, is more complicated than isotropic hardening model, and mechanical meanings of constitutive variable such as back stress and its evolution rule are not clear. Even if the material parameter for strength is modified to accommodate the observed results by using such parameter as the coefficient of principal intermediate stress $b$ (= ($\sigma_2$ - $\sigma_3$) / ($\sigma_1$ - $\sigma_3$)), it is hard to say that such model can suitably consider the deformation characteristics of soil under any three dimensional stress conditions. Moreover, it is a part of reason for modeling

complicatedness that the state variable representing the magnitude of development of anisotropy is not defined clearly in these methods.

Anisotropic tensor reflecting on the situation of microscopic interparticle contact (contact normals and long axis direction of non-spherical particle) of geomaterials, e.g., fabric tensor (Satake (1982), Kanatani (1981) and Oda et al. (1982)), is used for soil anisotropy from a long time ago. Considering such anisotropic tensor, modeling of soil behavior from the aspect of micromechanics in which soils are treated as assemblies of discrete particles is conducted (e.g., Iai (1993), Gardiner & Todesillas (2005), Chang & Hicher (2005)). In continuum mechanics, Oda (1993) represents the influence of (inherent) anisotropy on sand by introducing the invariants of fabric tensor into both the yield function and the potential function. Dafalias et al. (2004) also proposed the anisotropy model, in which strength parameter and critical state line are varied with the anisotropic state parameter "A" depending on the fabric tensor and current stress condition. Moreover, Tobita (1988), Tobita and Yanagisawa (1992), Li and Dafalias (2002, 2004) and Yang et al. (2008) formulated the yield function based on the modified stress, which is ordinary defined as multiplication fabric tensor $F_{ij}$ by current stress tensor $\sigma_{ij}$, instead of ordinary stress tensor $\sigma_{ij}$. However, it is difficult to quantitatively estimate the variation of the fabric, so that the fabric is constant which means only the influence of the inherent anisotropy is considered in these models. Therefore, the model applicable to the induced anisotropy in which the fabric changes in response to any applied stress has never been developed.

A new method, in which the influences of the induced anisotropy (i.e., the influences of intermediate principal stress and stress histories) on the strength and deformation characteristics of soil is described inclusively by applying modified stress $t_{ij}^{*}$, is developed in this study. Considering a character of the transformation tensor $a_{ij}$ based on $t_{ij}$ concept (Nakai & Mihara, 1984) which intrinsically corresponds to the fabric tensor $F_{ij}$ on monotonic loading condition, the transformation tensor $a_{ij}$ is extended to new tensor $a_{ij}^{*}$ applicable to more wide range of fabric change. Therefore, although proposed method obeys simple and general isotropic hardening rule in the modified stress space, it can suitably consider the influence of stress histories and the relative magnitude of intermediate stress $\sigma_2$, simultaneously. In this chapter, the outline of the proposed method is presented and it is verified through the parametric study and comparisons of the experimental results of not only simple triaxial test but also complicated true triaxial tests and directional shear tests with the corresponding computed results.

! The substance of this chapter has been published as follows: Kyokawa et al. (2008 and 2010), Kikumoto et al. (2007, 2008 and 2009).

## 4.2 Experimental and analytical investigation for the induced anisotropy Description of the induced anisotropy by using the modified stress $t_{ij}^*$

*Inherent anisotropy*

Concerning the soil anisotropy, Casagrande and Carillo (1994) first discriminated between the inherent anisotropy and the induced anisotropy. Practically all soil structures, natural or man-made, are formed under a gravitational field which induces an anisotropic soil fabric with transverse isotropy on the bedding plane, and such anisotropy affects on the mechanical response of soils. It is common knowledge, additionally, indicated by Arthur and Menzies (1972), Oda (1972) and Tatsuoka et al. (1986) that strength of granular soils is different depending on the direction of stress path, because non-spherical particles are deposited more or less parallel to the horizontal plane under the gravitational force. Yoshimine et al. (1998) and Nakata et al. (1998) showed from the results of hollow cylinder undrained torsional shear tests on Toyoura sand that the undrained stress paths and stress-strain relation dramatically depends on the direction of the principal stress relative to the deposition axes. This is an evidence of the strong effect of initial sand fabric anisotropy created by the sample preparation method, mimicking in the laboratory the soil deposition process with the sample axis along the gravity direction. According to the micromechanical investigations by Oda, Nemat-Masser & Konishi (1985), and Oda & Nakayama (1988), anisotropic initial fabric characteristics associated with the preferred orientation of particles undergo limited change at very large macroscopic shear deformation. On the whole, some inherent fabric descriptor persists until critical failure.

The influence of such persistent anisotropy (the inherent anisotropy) has simply been considered in constitutive model, for example, by changing the shape and position of yield surface according to the magnitude of anisotropy (e.g., Dafalias et.al. (2004)). However, it is difficult to evaluate the magnitude of the development of (inherent) anisotropy and to select a proper parameter evaluating the anisotropy quantitatively. Such evaluation of fabric change is essential for modeling of "the induced anisotropy" in which fabric change associates with any stress change. In this study, with reference to the past experimental results, proper state variable representing fabric change is given and a new constitutive relation considering the induced anisotropy is proposed.

*Induced anisotropy*

It is generally known that anisotropy strongly concerns with the situation of interparticle contact. Oda (1972) has shown that the concept of fabric, if the assembly is macroscopically homogeneous, should include not only a measure showing the preferred orientation of individual particles (the orientation fabric) but also two measures which reflect the mutual relationship of individual particles, i.e., the number of contacts and the orientation of contact normals. Figure 4.1 shows the stress-strain behavior of sand in a drained triaxial compress tests and the rose diagrams of contact normals in each loading condition (Oda, 1972). Here, E($n$) denotes a density function of unit vectors, $n$, parallel to contact normals. It can be seen from Figure 4.1 that distribution of contact normals progressively changes during a triaxial compression test. Initial isotropic consolidated sample (a) shows the no clear concentrated distribution of contact normals. As increasing the

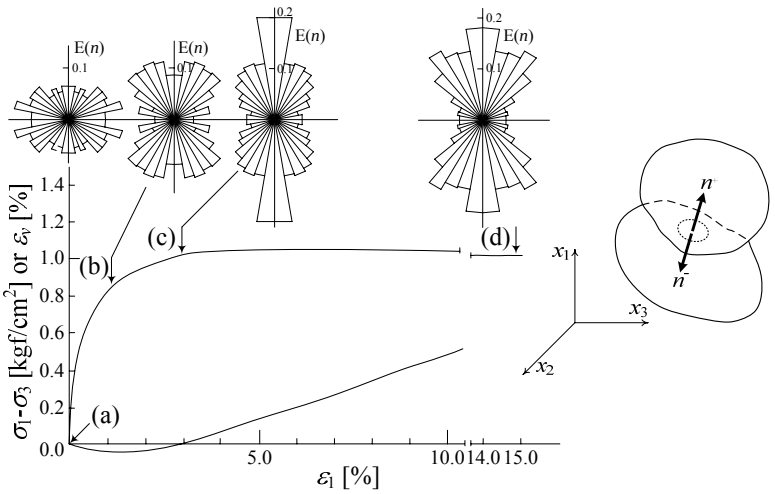


Figure 4.1 Stress-strain behavior of sand in a drained triaxial compress tests and the rose diagrams of contact normals in each loading condition (after Oda, 1972)

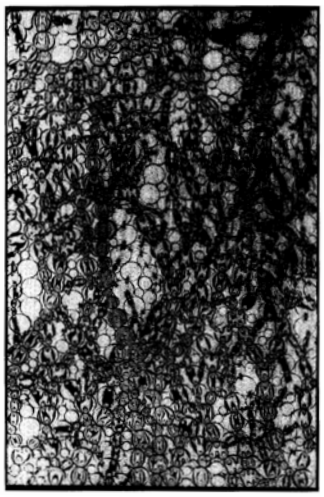

Figure 4.2 photo-elastic picture taken at around peak strength at biaxial compression test on an assembly of photo-elastic sensitive rods (after Oda et al. 1985)

axial stress $\sigma_1$, contact normals tend to concentrate toward the axial direction (b), and come to a maximum concentration around the peak strength (c). After peak strength, however, the tendency of concentration is lost even though the deviator strain is accumulating (d). It seems, therefore, that the preferred direction of the concentration of interparticle normals is not determined by the magnitude of applied shear displacement but by the intensity of mobilized stress ratio. Figure 4.2 shows a photo-elastic picture which is taken at around peak strength at biaxial compression test on an assembly of photo-elastic sensitive rods (Oda et al., 1985). As can be seen this figure, some rows of rods (called the "columns"), whose elongation axes are oriented roughly parallel to the vertical direction (maximum principal stress $\sigma_1$), arise, and these arising the columns harden the assemblies. The new occurrence of the columns leads necessarily to the concentration of contact normals. Finally, these columns begin to collapse at failure. Similar fabric change is observed in numerical simulations of biaxial compression tests, and the details of such fabric phenomena are investigated (e.g., Majmudar & Behriger (2005), Maeda et al. (2006) and Yimsiri et al. (2010)).

On the other hand, in order to investigate the effect of the rotation of the principal stress axes on the fabric change, experimental and analytical investigations were conducted (e.g., Miura et al. (1986) and Nakata et al. (1998) for experimental investigations, and Tanaka et al. (2009) for analytical investigations by DEM simulations). It can be commonly observed from these experimental and analytical results that the preferred direction of contact normals gradually rotates with the rotation of principal stress axes during shear deformation (applying shear stress).

*The influence of the induced anisotropy on the strength and deformation characteristic of soil*

Next, it is investigated from the experimental results of consolidation and shear tests on sand how the induced anisotropy affects on the strength and deformation of characteristic of soil. The typical consolidation behaviors of Toyoura sand ($e_{max}$ = 0.95, $e_{min}$ = 0.58, $G_s$ = 2.65, $D_r$ ⊗ 73 %) with shear history and without

history are firstly compared in Figure 4.3 (Nagai, 2003). Sample with shear history which was sheared to principal stress ratio $R$ ($\sigma_1/\sigma_3$) = 4 is represented as circlur plot, another one without shear history is represented as square plot. It can be seen from this figure that the sample having initial sheared history shows such anisotropic deformation as stiffer in the axial direction ($d\varepsilon_a < d\varepsilon_v/3$) in spite of under isotropic loading condition, and it gradually behave isotropically ($d\varepsilon_a = d\varepsilon_v/3$) due to subsequent increase of consolidation stress. Such anisotropic deformation on isotropic loading path is literally derived from the influence of the stress induced anisotropy. Since the column formed in axial direction with concentrating of contact normals by former triaxial compression test ($\sigma_a = \sigma_1$) doesn't diminishes during subsequent elastic unloading path to isotropic condition, sample with sheared history exhibits such anisotropic behavior. This is because that soil behaves isotropically with the progression of consolidation, however, it seems that the columns in the axial direction diminish due to development of plastic deformation.

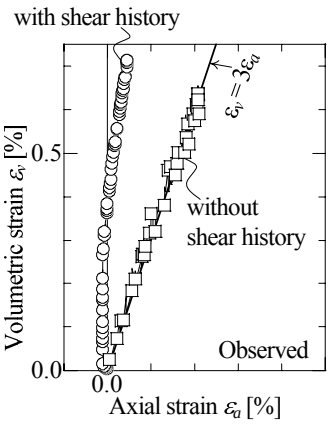


Figure 4.3 Observed results of isotropic consolidation tests on samples (Toyoura sand) with / without past shear history (after Nagai, 2003)

Next, the results of triaxial compression and extension tests on medium dense Toyoura sand ($e_{max}$ = 0.95, $e_{min}$ = 0.58, $G_s$ = 2.65, $D_r$ ⊗ 73 %) with stress histories and without stress histories are shown in Figure 4.4. Diagram (a) shows stress paths; circular plots represent the stress-strain behavior (: $q/p$ - $\varepsilon_a$, : $\varepsilon_v$ - $\varepsilon_a$) of isotropic sample without stress histories, square plots represent that of sample with stress histories which was once sheared to principal stress ratio $R$ = 3.5 on triaxial compression state (: $q/p$ - $\varepsilon_a$, : $\varepsilon_v$ - $\varepsilon_a$), and triangle plots represent that of another sample with stress histories which was once sheared to principal stress ratio $R$ = 3.5 on triaxial extension state (: $q/p$ - $\varepsilon_a$, : $\varepsilon_v$ - $\varepsilon_a$), respectively in diagrams (b) and (c). As compared with the result of the sample without shear history, the sample with sheared history shows stiffer / softer behavior in the same / opposite direction as the previous sheared direction, in spite of the identical initial void ratio. The differences of peak strengths in each test are not clear, and it seems that the residual strength is unaffected by the magnitude and direction of the (induced) anisotropy. As regards the dilatancy characteristic, the sample with sheared history shows more dilative behavior in the same direction as the previous sheared direction, and also shows less dilative behavior in the opposite direction than the isotropic sample without shear history.

It can be easily understood from the similar interpretation of the induced anisotropy to the consolidation behavior mentioned above that the behavior of sample having the columns in axial stress $\sigma_a$ ($\sigma_1$) direction is hard to compress in the same direction. It is natural to expect that the column developed in the axial stress $\sigma_a$ ($\sigma_1$) direction can collapse under an additional lateral stress $\sigma_r$ (other direction stress) or the reduction of the axial stress $\sigma_a$ ($\sigma_1$). Such collapse of the developed columns during reversal loading may be a contributing factor in producing large volumetric strain changes if the sample is drained, or large changes in excess pore pressure if the sample is saturated and undrained. Therefore, the sample with extension shear history, which has the column in lateral direction, is easy to show large axial compression in subsequent

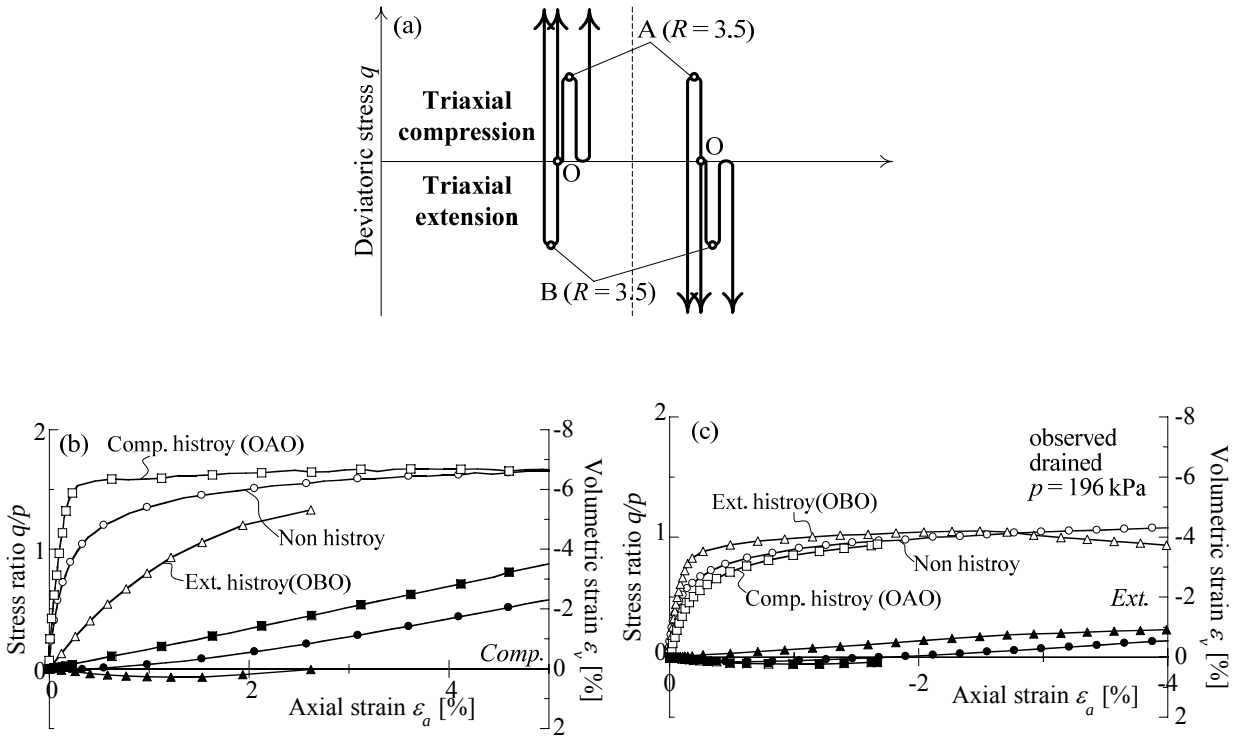


Figure 4.4 Observed results of drained triaxial compression and extension tests on samples (Toyoura sand) with Comp. history, Ext. history and non history (a) stress path under mean stress $p$ = 196 kPa const., (b) stress-strain relation ($\varepsilon_a - q/p - \varepsilon_v$) of triaxial compression tests, (c) stress – strain relation ($\varepsilon_a - q/p - \varepsilon_v$) of triaxial extension test

triaxial compression test.

From the observed result about residual strength, it seems that the influence of the induced anisotropy diminishes at the failure state, and then soil fabric of sample with stress history corresponds to that of sample without history at failure state. Every strain components of sample with shear history intricately varies due to the induced anisotropy. In order to explain the details of the influence of the induced anisotropy on dilatancy characteristics, therefore, further investigation of the induced anisotropy is required from henceforth. Note, however, it can be seen from the observed results that the sample having the column in the subsequent loading direction shows more dilative behavior.

These anisotropic behaviors observed in laboratory tests are not very different to the behaviors of soil having the sedimentation effect, i.e., the inherent anisotropy. That is to say, it seems that the anisotropy developing in sedimentation process is similar to a kind of the induced anisotropy produced by the gravity. It is indicated that, however, the inherent anisotropy tends to retain the initial fabric situation until critical state or unless very large deformation occurs, as compared with the induced anisotropy. The induced anisotropy is continuously developed by changing the distribution of contact normals, and a greater concentration of contact normals is produced along the orientation parallel to the direction of the maximum principal axis. It is conceivable that more complicated anisotropy develops in actual ground, because stress condition in actual ground is not necessarily triaxial (axisymmetric stress) condition but under different three principal stresses with rotating principal stress axis. Moreover, the induced anisotropy becomes very important in dealing with

the non-elastic behavior of soils subjected to cyclic stresses. The induced anisotropy, therefore, cannot be negligible and should be considered properly in a constitutive model of soils in order to conduct the deformation and failure prediction in actual ground.

*State variable representing the situation of soil fabric – fabric tensor*

Considering the results of stress probe tests by which the yield surface of soil having the anisotropy is drawn, the kinematic / rotating hardening law is used for changing the center and central axis of yield surface in ordinary modeling (Figure 4.5). Although these methods can more or less represent such observed phenomena as exhibition of anisotropic deformation and cyclic behavior, its formulation is more complicated than isotropic hardening model, and the variables determining the position of yield surface and its evolution rule have no physical meaning and are determined by juts fitting to experimental results.

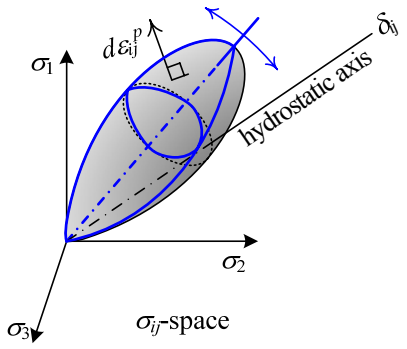


Figure 4.5 Ordinary kinematic / rotational hardening model with changing shape of yield surface according to the intermediate principal stress coefficient *b* value

So, what kind of a physical quantity is proper to organize the experimental results and modeling of soil? It is easily understood from above investigation that the evaluation of the situation of interpaticle contacts is suitable. The geometric anisotropy representing the situation of interparticle contacts is microscopic mechanical behavior, while the macroscopic mechanical behavior is normally treated in practical problem. In order to connect with microscopic and macroscopic mechanical behaviors, therefore, the macroscopic anisotropy is represented as what the geometric microscopic anisotropy is statistically averaged. Therefore, a tensor quantity is used to express the situation of interparticle contact, i.e., anisotropy, in general. Satake (1978) and Oda et al. (1982) proposed the fabric tensor given as follows

$$F_{ij} = \frac{1}{2N}\sum n_i \otimes n_j \tag{4.1}$$

$n_i$ is a $x_i$ component of a unit vector $\boldsymbol{n}$ normal to a contact plane (Figure 4.1). $N$ is the total number of contact points in a given volume. As considering that $N$ is sufficiently-large, the density function $E(\boldsymbol{n})$ describing the statistical distribution of contact normal $\boldsymbol{n}$ is used. Then, Equation 4.1 is statistically averaged as

$$F_{ij} = \int E(n) n_i \otimes n_j d\Omega \tag{4.2}$$

$\Omega$ is a solid angle corresponding to the entire surface of a unit sphere ($\Omega = 4\pi$). It is worthy of note that $F_{ij}$ is symmetric, i.e., $F_{ij} = F_{ji}$ with the trace $F_{kk}$ being equal to unity. $F_{ij}$ is an index measure showing the anisotropy due to the particle orientation.

*Describing the induced anisotropy by using the modified stress*

With the fabric tensor appropriately evaluating the orientation of the interpaticle (contact normals), the modeling of stress-strain behavior of soil is conducted in continuum mechanics. Figure 4.6 shows the schematically description of the induced anisotropy and its modeling based on ordinary stress and modified

stress in the simplified 2-dimendional condition, respectively. As mentioned above, the distribution of the interparticle contact normals gradually concentrate towards the direction of the major principal stress ($\sigma_1$) under the anisotropic stress condition ($\sigma_1 > \sigma_2$) as shown in diagram (a). Considering an equivalent continuum, such material exhibits anisotropy since the stiffness in the $\sigma_1$ direction should be larger than that in the $\sigma_2$ direction with the increase of stress ratio as shown in diagram (b). Some models considering such anisotropic stiffness are proposed by using fabric tensor $F_{ij}$. Oda (1989) assumes the anisotropic yield function formulated based on invariants of $\sigma_{ij}$ and also fabric tensor $F_{ij}$. Li & Dafalias (2002) and Dafalias (2004) change the strength and the critical state line in $e$-ln$p$ plane with a state variable based on fabric tensor $F_{ij}$. It is reasonable to treat the soil as an isotropic material by introducing the modified stress, in which induced anisotropy is already taken into consideration. This means that stress ratio based on modified stress is smaller than ordinary stress ratio $\sigma_1/\sigma_2$ as shown in diagram (c). Although number of descriptions and theories of the modified stress have been proposed, e.g., Satake (1982), Mehrabadi & Nemat-Nasser (1983) and Tobita (1988), these modified stress tensor are similar.

$$\sigma_{ij}^{*} = F_{ik}^{-1}\sigma_{kj} \tag{4.3}$$

These models are applicable to only the inherent anisotropy with hardly fabric change, however, since it is difficult to evaluate the fabric tensor determined by the orientation of contact normals under with every-changing stress condition. In other words, the model considering the induced anisotropy properly with changing the fabric tensor has never been proposed.

It is problem that how does the fabric tensor $F_{ij}$ change due to the particle orientation? As shown previously in Figure 4.1, it is supposed that the orientation of contact normals changes due to not accumulating of shear strain but stress ratio. Satake (1984) indicated from the result of two-dimensional compression test on photo-elastic material that the principal axes of $\sigma_{ij}$ and $F_{ij}$ are consistent under monotonic loading condition without rotation of principal stress axis, and then following relation is prescribed.

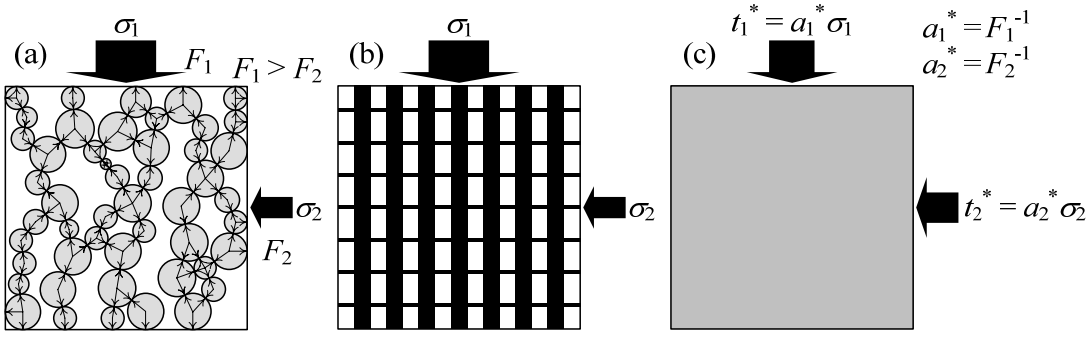


Figure 4.6 Concept of constitutive modeling of stress-induced anisotropy of soils using modified stress (a) Increase of the interparticle contact normals in the direction of major principal stress due to the increase in stress ratio (b) Anisotropic continuum considering the concentration of contact normals (ordinary method) (c) Isotropic continuum equivalently transformed by modified stress (proposed method)

$$\frac{F_1}{F_2} = \left( \frac{\sigma_1}{\sigma_2} \right)^{\alpha} \tag{4.4}$$

Above equation whose coefficient $\alpha$ is called the inductivity degree of anisotropy represents the magnitude of anisotropy. $\alpha = 0$ represents the isotropy, and $\alpha = 1$ represents the perfect anisotropy. Satake (1984) gives $\alpha = 0.4$ - $0.6$ from biaxial compression test on photo-elastic material, and also Maeda (2006) obtains $\alpha = 0.5$ from the biaxial test of DEM simulation shown in Figure 4.7.

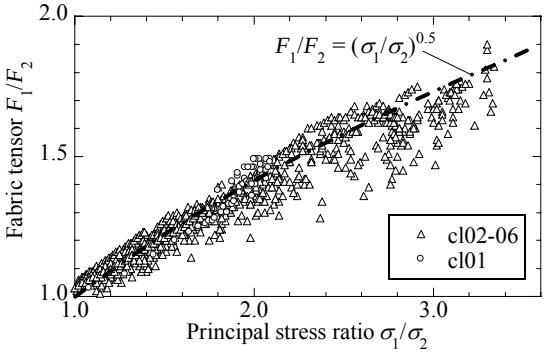


Figure 4.7 Variation in the ratio of principal values of fabric tensor due to the increase in principal stress ratio during biaxial monotonic loading tests using 2d-DEM (after Maeda et al., 2006)

On the other hand, Nakai and Mihara (1984) proposed the modified stress $t_{ij}$ to take account of the influence of relative magnitude of intermediate principal stress on the strength and deformation characteristic of soil. The modified stress tensor $t_{ij}$ is given as follows, and its details have already been discussed in Chapter 2.

$$t_{ij} = a_{ik}\sigma_{kj} \tag{4.5}$$

Here, transformation tensor of second order $a_{ij}$ whose principal values ($a_1$, $a_2$ and $a_3$) are unit vector normal to the *SMP* is coaxial with $\sigma_{ij}$, and has following relation with principal stress in a similar manner as $F_{ij}$.

$$\frac{a_1}{a_2} = \left( \frac{\sigma_1}{\sigma_2} \right)^{-0.5} \tag{4.6}$$

By comparison with Equation (4.6) and Equation (4.4), the inverse tensor of $a_{ij}$ ($a_{ij}^{-1}$) corresponds to $F_{ij}$ whose the inductivity degree of anisotropy $\alpha$ is 0.5. Therefore, it can suitably evaluate variation of the orientation of contact normals, i.e., the induced anisotropy, under the monotonic loading condition. It is indicated, moreover, that the spatially mobilized plane (*SMP*) corresponds to the averaged plane of interparticle contacts, which is perpendicular to the orientation of contact normals (fabric tensor $F_{ij}$). So, the anisotropic strength and deformation characteristics of soil depending on the relative magnitude of intermediate principal stress described by such transformation tensor $a_{ij}$ (and the modified stress $t_{ij}$) are essentially regarded as a part of the induced anisotropy under monotonic loading.

In this chapter, the modified stress $t_{ij}$ and the transformation tensor $a_{ij}$ describing the induced anisotropy under monotonic loading condition are extended to new modified stress $t_{ij}^*$ and the transformation tensor $a_{ij}^*$, respectively, which can consider the fabric change due to the variation of the intermediate principal stress and the stress histories under any stress paths. As considering the anisotropy under various stress state and stress history, however, the principal axes of stress tensors $\sigma_{ij}$ and the transformation tensor $a_{ij}^*$ (fabric tensor) are not necessarily coincident. The new modified stress $t_{ij}^*$, therefore, is defined as follows

$$t_{ij}^{*} = \frac{a_{ik}^{*}\sigma_{kj} + \sigma_{ik}a_{kj}^{*}}{2} \tag{4.7}$$

The elastoplastic constitutive model of soil based on such modified stress tensor $t_{ij}^{*}$ ($t_1^{*}/\ t_2^{*} < \sigma_1/\sigma_2$) can describe the induced anisotropy under various stress condition and stress histories with obeying a simple isotropic hardening rule as shown in diagram (c) in Figure 4.6.

## 4.3 Evolution rule of transformation tensor $a_{ij}^{*}$

In the previous section, it was indicated that the simple isotropic hardening model with the modified stress can be applied to describing the induced anisotropy. The evolution rule of transformation tensor $a_{ij}^{*}$ is determined from following assumptions based on the past experimental results.

(a) The newly proposed transformation tensor $a_{ij}^{*}$ corresponds to ordinary transformation tensor $a_{ij}$ under monotonic loading condition.

$$a_{ij}^{*} = a_{ij}\ \&\ da_{ij}^{*} = da_{ij} \quad when\ monotonic\ loading \quad \left(d\varepsilon_{ij}^{p} \neq 0\right) \tag{4.8}$$

This assumption is obvious from that the modified stress $t_{ij}$ (and transformation tensor $a_{ij}$) can suitably describe the influence of the relative magnitude of the intermediate principal stress $\sigma_2$, which is equivalent to the induced anisotropy under the monotonic loading condition as mentioned in section 4.2. In this condition, $a_{ij}^{*}$ is given as equation (2.51), and it is coaxial to ordinary stress tensor $\sigma_{ij}$.

(b) $a_{ij}^{*}$ is constant during unloading as the fabric of interparticle contact hardly changes under unloading condition.

$$da_{ij}^{*} = 0 \quad when\ reversal\ loading \quad \left(d\varepsilon_{ij}^{p} = 0\right) \tag{4.9}$$

Figure 4.8 shows the result of anisotropic consolidation ($R = \sigma_1 / \sigma_3 = 2$) tests on sample with shear history $R_{max} = 4$ (Nagai, 2004). The sample was firstly sheared until principal stress ratio $R_{max} = 4$, and then unloaded to square root of $R_{max}$, i.e., $R = 2$. Subsequently anisotropic consolidation with $R = 2$ is conducted. It can be seen from Figure 4.8 that soil initially shows isotropic behavior (⏢-plots) in spite of the anisotropic condition. In order to represent such isotropic condition by using the modified stress $t_{ij}^{*}$, $a_{ij}^{*}$ which corresponds to $a_{ij}$ under monotonic loading to $R = 4$ is fixed during an elastic unloading path until $R = 2$. So, $a_{ij}^{*}$ at principal stress ratio $R = 2$ corresponds to the ordinary $a_{ij}$ in $R_{max} = 4$ before unloading path, and $t_{ij}^{*}$ explained as Equation (4.7) represents the isotropic stress condition as shown in follows, which is the simplified representation of Equation (4.7) under triaxial condition.

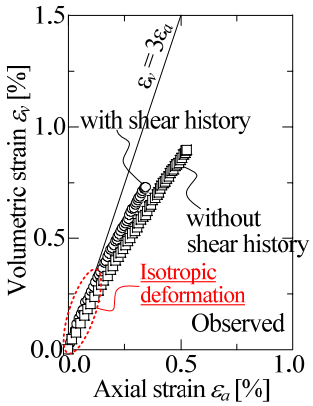


Figure 4.8 Observed results of anisotropic consolidation tests at $\sigma_1/\sigma_3 = 2$ on samples (Toyoura sand) with past shear history ($\sigma_1/\sigma_3 = 4$) and without history (after Nagai, 2003)

$$\left(t_1^*, t_2^*, t_3^*\right) = \left(a_1^* \sigma_1, a_2^* \sigma_2, a_3^* \sigma_3\right) = \left(\sqrt{1/R_{\max}} \cdot \sqrt{R_{\max}},\ 1,\ 1\right) = (1,\ 1,\ 1) \tag{4.10}$$

In other words, the fabric of interparticle contact hardly changes under unloading condition. Cassagrande & Carillo (1944), Oda (1989) and other authors said, moreover, that "When a granular assembly undergoes "plastic deformation", neighboring particles may form new contacts and, at the same time, some existing contacts may disappear. Also, particles may rotate rigidly to make a new appearance of the orientation of fabric.". Second assumption can be understood also from above interpretation of the induced anisotropy, because soils show "elastic deformation" at unloading path.

(c) After the non-monotonic loading path (changing the direction of stress path in octahedral plane), soil is affected by the influence of the stress histories.

$$da_{ij}^* \neq da_{ij} \quad when\ non-monotonic\ loading \quad \left(d\varepsilon_{ij}^p \neq 0\right) \tag{4.11}$$

Above second assumption is obtained from a limited stress path, viz., the direction of stress path in the octahedral plane (lode angle $\theta$) is fixed. However, direction of stress path on the octahedral plane arbitrarily changes with the rotation of principal stress axis, and then soil fabric is not fixed but more or less affected by such changing stress path.

(d) The strength and deformation characteristics of soils are independent of the stress histories at failure state even if soils had the complex stress path histories. Soils with anisotropic stress histories, moreover, eventually show isotropic behavior with progression of isotropic consolidation. That is to say, $a_{ij}^*$ gradually approaches to $a_{ij}$ with the development of plastic deformation although $a_{ij}^*$ differs from $a_{ij}$ under complex loading paths.

$$da_{ij}^* \supset \left\| d\varepsilon_{ij}^p \right\| \cdot \left(a_{ij} - a_{ij}^*\right)$$
$$wiht\ development\ of\ plastic\ deformation \quad \left(d\varepsilon_{ij}^p \neq 0\right) ! \ ! \ ! \tag{4.12}$$

Here, the symbol "A⋈ B" means that A includes the term of B. From Figure 4.5 representing the results of triaxial compression tests on samples with and without shear histories, it can be seen that both samples with compression and extension histories finally reach to the residual strength of sample without stress history. Figure 4.9 shows the vectors of shear strain increment along two different stress paths on octahedral plane of true triaxial tests (Nakai et al. 2001). Although the direction of vectors of sample with non-monotonic stress path (BC) deviate from the radial direction due to the influence of the stress histories (the induced anisotropy), it finally corresponds to the vectors of the sample with monotonic loading (AC) at critical state. It can be

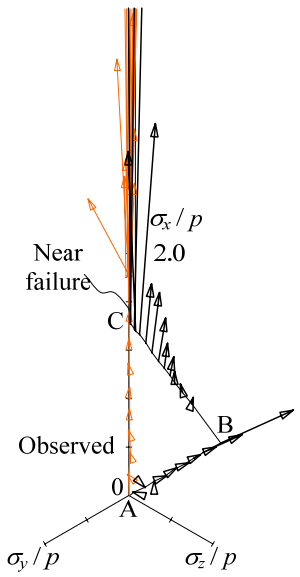


Figure 4.9 Observed vectors of shear strain increment along two different stress paths: AC (triaxial compression test) and ABC (after Nakai et al., 2001)

indicated from these experimental results that the influences of stress history not only on the strength but also on the deformation of soil diminish at the critical state. So, soil is affected only by the influence of the intermediate principal stress $\sigma_2$, viz., $a_{ij}^* = a_{ij}$, at critical state. From the consolidation behavior of sample with anisotropic stress history as shown in Figure 4.4, moreover, it seems that such sample eventually show isotropic behavior with development of the plastic deformation. Ordinary kinematic / rotational hardening model defined in stress ratio space cannot describe such degradation of the influence of the induced anisotropy due to consolidation.

An evolution rule of $a_{ij}^*$ satisfying conditions (a) - (d) is, finally, given as equation (4.13).

$$da_{ij}^* = k\, da_{ij} + l\left(a_{ij} - a_{ij}^*\right) \tag{4.13}$$

Here, the right side first term is given on the basis of assumptions (a), (b) and (c), viz., Equations (4.8), (4.9) and (4.11). The coefficient "$k$" represents loading directions, namely, $k = 1$ in monotonic loading, $0 < k < 1$ in non-monotonic loading ($d\theta \perp 0$) and $k = 0$ in reversal loading ($d\theta = 0$). And also "$k$" considers the existence or nonexistence of the influence of stress history and its magnitude. Since $a_{ij}^*$ changes as $a_{ij}$ ($da_{ij}^* = da_{ij}$) in monotonic loading condition ($k = 1$), $t_{ij}^*$ corresponds ordinary modified stress $t_{ij}$. In non-monotonic loading condition ($0 < k < 1$), development of the influence of stress history is described as the difference between $da_{ij}^*$ and $da_{ij}$. A coefficient "$k$" satisfying above conditions, therefore, is given as

$$k = \cos\frac{\alpha}{2} \tag{4.14}$$

Here, $\alpha$ represents the angle of stress ratio tensor $x_{ij}^*$ based on the modified stress tensor $t_{ij}^*$ (Table 4.1 after mentioned) and its increment $dx_{ij}^*$ (Figure 4.10), and it is given as follows.

$$\alpha = \cos^{-1}\left(\frac{x_{ij}^* dx_{ij}^*}{\sqrt{x_{kl}^* x_{kl}^* dx_{mn}^* dx_{mn}^*}}\right) \tag{4.15}$$

As shown in Figure 4.10, the monotonic loading is given when directions of $x_{ij}^*$ is coincident with that of $dx_{ij}^*$ ($\alpha = 0 \leftrightarrow k = 1$); the reversal loading which means unloading with $d\theta = 0$ is given when directions of $x_{ij}^*$ is opposite to that of $dx_{ij}^*$ ($\alpha = \pi \leftrightarrow k = 0$); other loading condition is given as non-monotonic loading ($0 < \alpha < \pi \leftrightarrow 0 < k < 1$). Note that Equation (4.14) giving a judgment of change of stress path is different from the bracket sign in after mentioned Equation (4.35) which determines the occurrence of the plastic deformation (loading condition).

The second term in the right side of Equation (4.13) describing the diminishing of the influence of stress history, reduce the gap between $a_{ij}^*$ and $a_{ij}$. Considering the assumption (d) and Equation (4.12) which mean that the influence of stress history dissipates with the development of the plastic deformation, the coefficient "$l$" is given as follows by using the norm of the plastic strain increment, while $\mu$ is a newly added constitutive parameter and it represents the rate of the decay of the influence of stress histories.

$$l = \mu\sqrt{d\varepsilon_{kl}^p d\varepsilon_{kl}^p} \tag{4.16}$$

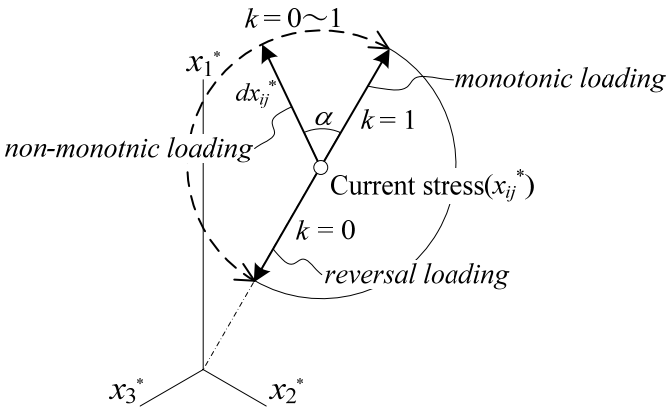


Figure 4.10 Judgment of loading condition by stress ratio tensor $x_{ij}^*$ and incremental stress ratio tensor $dx_{ij}^*$

So, the first term in the right side of Equation (4.13) represents the development of the influence of stress history and the second term represents decay of it. An increment of $a_{ij}$ in Equation (4.13) is given as follows from Equation (2.51).

$$\begin{aligned} da_{ij} &\equiv \frac{\partial a_{ij}}{\partial \sigma_{kl}} d\sigma_{kl} \\ &\equiv \left( \frac{\partial a_{ij}}{\partial I_2}\frac{\partial I_2}{\partial \sigma_{kl}} + \frac{\partial a_{ij}}{\partial I_3}\frac{\partial I_3}{\partial \sigma_{kl}} + \frac{\partial a_{ij}}{\partial r_{mn}}\frac{\partial r_{mn}}{\partial \sigma_{kl}} \right) d\sigma_{kl} \end{aligned} \tag{4.17}$$

$$\left.\begin{aligned} &\frac{\partial a_{ij}}{\partial I_2} \equiv -\frac{a_{ij}}{2I_2}, && \frac{\partial I_2}{\partial \sigma_{ij}} \equiv \sigma_{kk}\delta_{ij} - \sigma_{ji} \\ &\frac{\partial a_{ij}}{\partial I_3} \equiv \frac{a_{ij}}{2I_3}, && \frac{\partial I_3}{\partial \sigma_{ij}} \equiv \frac{1}{2} e_{ikl} e_{jst} \sigma_{ks} \sigma_{lt} \\ &\frac{\partial a_{ij}}{\partial r_{kl}} \equiv \sqrt{\frac{I_3}{I_2}} \delta_{ik}\delta_{jl}, && \frac{\partial r_{ij}}{\partial \sigma_{kl}} \equiv \left( \delta_{ik} r_{jl} + \delta_{jl} r_{ik} \right)^{-1} \end{aligned}\right\} \tag{4.18}$$

The newly modified stress tensor $t_{ij}^*$ considering the influence of the intermediate principal stress $\sigma_2$ and stress history simultaneously is, finally, obtained from substituting the increment of $a_{ij}^*$ determined here and ordinary stress tensor $\sigma_{ij}$ for Equation (4.7).

## 4.4 Application of the modified stress $t_{ij}^*$ to isotropic hardening model

The essential parts of modeling of the induced anisotropy were already constructed in previous section 4.2 and 4.3: a mechanical tensor quantity considering the situation of interparticle contact (anisotropy), viz., fabric tensor $F_{ij}$; the mechanical meaning of the describing the anisotropy of soil in continuum mechanics with the modified stress $t_{ij}^*$; the newly transformation tensor $a_{ij}^*$ based on $a_{ij}$ in $t_{ij}$ concept and its evolution rule. In this section, the newly modified stress $t_{ij}^*$ is applied to ordinary elastoplastic constitutive model – subloading $t_{ij}$ model as an example, and the induced anisotropy is described in isotropic hardening model.

*The stress and strain parameters based on the concept of the modified stress $t_{ij}^*$*

In the concept of the ordinary modified stress $t_{ij}$, $a_{ij}$ is applied not only for converting $\sigma_{ij}$ into $t_{ij}$ but also for dividing $t_{ij}$ and strain increment tensor $d\varepsilon_{ij}^p$ into their parameters in $t_{ij}$-space ($t_N$, $t_S$) and ($d\varepsilon_N^*$, $d\varepsilon_S^*$) as shown in Table 2.1 in Chapter 2. In the newly method for $t_{ij}^*$, the transformation tensor $a_{ij}^*$ is not necessarily coaxial with $t_{ij}^*$. Thus, a unit tensor $a_{ij}^{\#}$ coaxial with $t_{ij}^*$ is newly employed for dividing $t_{ij}^*$ and $d\varepsilon_{ij}^p$ into their components. In consideration of the relation between $t_{ij}$ and $a_{ij}$, $a_{ij}^{\#}$ can be expressed in the same form as $a_{ij}$.

$$a_{ij}^{\#} = \frac{I_{t3}^*}{\sqrt{I_{t2}^{*\,2} - 2I_{t1}^* I_{t3}^*}} t_{ij}^{*\,-1} \tag{4.19}$$

where $I_{t1}^*$, $I_{t2}^*$, $I_{t3}^*$ are invariants of the modified stress $t_{ij}^*$ shown in follows

$$\left.\begin{aligned} I_{t1}^* &= t_1^* + t_2^* + t_3^* = t_{ii}^* \\ I_{t2}^* &= t_1^* t_2^* + t_2^* t_3^* + t_3^* t_1^* = \frac{1}{2}\left(t_{ii}^{*\,2} - t_{ij}^* t_{ji}^*\right) \\ I_{t3}^* &= t_1^* t_2^* t_3^* = e_{ijk} t_{i1}^* t_{j2}^* t_{k3}^* \end{aligned}\right\} \tag{4.20}$$

Table 4.1 Tensors and scalars related to stress and stain increment in ordinary concept, $t_{ij}$ concept and proposed $t_{ij}^*$ concept

| | Ordinary concept | $t_{ij}$ concept | $t_{ij}^*$ concept |
|---|---|---|---|
| Transform tensor to modified stress | - | $a_{ij}$ | $a_{ij}^*$ |
| Stress tensor | $\sigma_{ij}$ | $t_{ij} = a_{ik}\sigma_{kj}$ | $t_{ij}^* = (a_{ik}^*\sigma_{kj} + \sigma_{ik}a_{kj}^*)/2$ |
| Unit tensor normal to reference plane | $\delta_{ij}$ (Oct. plane) | $a_{ij}$ (*SMP*) | $a_{ij}^{\#}$ |
| Mean stress | $p = \sigma_{ij}\delta_{ij}/3$ | $t_N = t_{ij}a_{ij}$ | $t_N^* = t_{ij}^* a_{ij}^{\#}$ |
| Deviatoric stress tensor | $s_{ij} = \sigma_{ij} - p\delta_{ij}$ | $t'_{ij} = t_{ij} - t_N a_{ij}$ | $t'^*_{ij} = t_{ij}^* - t_N^* a_{ij}^{\#}$ |
| Deviatoric stress | $q = \sqrt{(3/2)s_{ij}s_{ij}}$ | $t_S = \sqrt{t'_{ij}t'_{ij}}$ | $t_S^* = \sqrt{t'^*_{ij}t'^*_{ij}}$ |
| Stress ratio tensor | $\eta_{ij} = s_{ij}/p$ | $x_{ij} = t'_{ij}/t_N$ | $x_{ij}^* = t'^*_{ij}/t_N^*$ |
| Stress ratio | $\eta = q/p = \sqrt{\eta_{ij}\eta_{ij}}$ | $X = t_S/t_N = \sqrt{x_{ij}x_{ij}}$ | $X^* = t_S^*/t_N^* = \sqrt{x_{ij}^*x_{ij}^*}$ |
| Strain increment normal to reference plane | $d\varepsilon_v = d\varepsilon_{ij}\delta_{ij}$ | $d\varepsilon_N = d\varepsilon_{ij}a_{ij}$ | $d\varepsilon_N^* = d\varepsilon_{ij}a_{ij}^{\#}$ |
| Deviatoric strain increment tensor | $de_{ij} = d\varepsilon_{ij} - d\varepsilon_v\delta_{ij}/3$ | $d\varepsilon'_{ij} = d\varepsilon_{ij} - d\varepsilon_N a_{ij}$ | $d\varepsilon'^*_{ij} = d\varepsilon_{ij} - d\varepsilon_N^* a_{ij}^{\#}$ |
| Strain increment parallel to reference plane | $d\varepsilon_d = \sqrt{(2/3)de_{ij}de_{ij}}$ | $d\varepsilon_S = \sqrt{d\varepsilon'_{ij}d\varepsilon'_{ij}}$ | $d\varepsilon_S^* = \sqrt{d\varepsilon'^*_{ij}d\varepsilon'^*_{ij}}$ |
| Flow rule | $d\varepsilon_{ij}^p = \Lambda\dfrac{\partial f}{\partial\sigma_{ij}}$ | $d\varepsilon_{ij}^p = \Lambda\dfrac{\partial f}{\partial t_{ij}}$ | $d\varepsilon_{ij}^p = \Lambda\dfrac{\partial f}{\partial t_{ij}^*}$ |

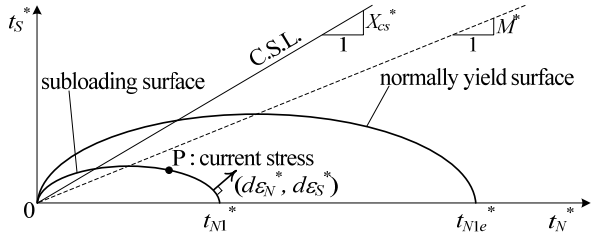


Figure 4.11 Yield surface on $t_N^*$ - $t_S^*$ plane

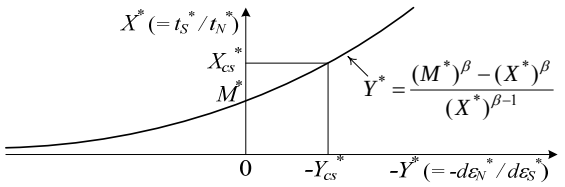


Figure 4.12 Stress-dilatancy relation based on modified stress $t_{ij}^*$

Using the unit tensor $a_{ij}^{\#}$ coaxial to the modified stress $t_{ij}^*$, $t_{ij}^*$ and the plastic strain increment $d\varepsilon_{ij}^p$ are divided into those components as organized in Table 4.1.

*The application of the modified stress $t_{ij}^*$ into the ordinary elastoplastic constitutive model of soil*

The proposed concept of the modified stress $t_{ij}^*$ can be applied to any isotropic hardening model. Subloading $t_{ij}$ model (Nakai & Hinokio, 2004) shown in Chapter 2 is extended to one taking account of the induced anisotropy of soils by applying the new stress tensor $t_{ij}^*$ in this study. Since the details of the original model were explained in Chapter 2, application of $t_{ij}^*$ to the subloading $t_{ij}$ model is mainly presented here. The method of applying $t_{ij}^*$ is quite simple, viz., defining the yield function $f$ based on the parameters of $t_{ij}^*$ and assuming associated flow rule in $t_{ij}^*$-space. The yield function of soil is usually formulated as a logarithmic function of the mean stress plus an increasing function of stress ratio. Using the parameters of $t_{ij}^*$ shown in Table 4.1, the yield function is presented in the same form as the subloading $t_{ij}$ model.

$$\begin{aligned} f &= \ln t_N^* + \zeta\left(X^*\right) - \ln t_{N1}^* \\ &= \ln\frac{t_N^*}{t_{N0}^*} + \frac{1}{\beta}\left(\frac{X^*}{M^*}\right)^\beta - \ln\frac{t_{N1}^*}{t_{N0}^*} = \ln\frac{t_N^*}{t_{N0}^*} + \frac{1}{\beta}\left(\frac{X^*}{M^*}\right)^\beta - \ln\frac{t_{N1e}^*}{t_{N0}^*} - \ln\frac{t_{N1}^*}{t_{N1e}^*} = 0 \end{aligned} \tag{4.21}$$

$\beta$ is a material parameter which determines the shape of the yield surface. Figure 4.11 illustrates the yield surface on $t_N^*$-$t_S^*$ plane. $t_{N1e}^*$ and $t_{N1}^*$ determine the size of the normal yield surface (*NYS*) and the subloading yield surface (*SYS*), respectively, and these parameters are linked with the plastic volumetric strain and state variable $\rho$ as

$$\varepsilon_v^p = \frac{\lambda-\kappa}{1+e_0}\ln\frac{t_{N1e}^*}{t_{N0}^*} \tag{4.22}$$

$$\frac{\rho}{1+e_0} = \frac{\lambda-\kappa}{1+e_0}\ln\frac{t_{N1e}^*}{t_{N1}^*} \tag{4.23}$$

Substituting Equations (4.22) and (4.23) for Equation (4.21), the yield function is rewritten as

$$f = \ln\frac{t_N^*}{t_{N0}^*} + \frac{1}{\beta}\left(\frac{X^*}{M^*}\right)^\beta - \frac{1}{C_p}\left(\varepsilon_v^p + \frac{\rho}{1+e_0}\right) = 0 \tag{4.24}$$

Equation (4.24) is essentially equivalent to Equation (2.68) and (2.69) which are multidimensional model considering the influence of density in Chapter 2. $M^*$ is expressed using stress ratio $X_{CS}^* = (t_S^*/t_N^*)_{CS}$ and

plastic strain increment ratio $Y_{CS}^{*} = (d\varepsilon_N^{*}/d\varepsilon_S^{*})_{CS}$ at critical state as Equation (4.25).

$$M^{*} = \left( X_{CS}^{*\,\beta} + X_{CS}^{*\,\beta-1} Y_{CS}^{*} \right)^{1/\beta} \tag{4.25}$$

The ratios $X_{CS}^{*}$ and $Y_{CS}^{*}$ are represented by the principal stress ratio at critical state in triaxial compression: $R_{CS} = (\sigma_1/\sigma_3)_{CS\,(\mathrm{comp.})}$ as follows

$$X_{CS}^{*} = \frac{\sqrt{2}}{3}\left( \sqrt{R_{CS}} - \frac{1}{\sqrt{R_{CS}}} \right), \quad Y_{CS}^{*} = \frac{1-\sqrt{R_{CS}}}{\sqrt{2}(\sqrt{R_{CS}} + 0.5)} \tag{4.26}$$

Assuming the coaxiality between $t_{ij}^{*}$ and $d\varepsilon_{ij}^{p}$, the stress-dilatancy relation based on $t_{ij}^{*}$ concept is obtained (Figure 4.12).

$$Y = \frac{M^{*\beta} - X^{*\beta}}{X^{*\beta-1}} \tag{4.27}$$

The plastic strain increment is obtained by assuming the associated flow rule in $t_{ij}^{*}$-space as follow.

$$d\varepsilon_{ij}^{p} = \Lambda \frac{\partial f(t_{ij}^{*}, a_{ij}^{\#})}{\partial t_{ij}^{*}} \tag{4.28}$$

And the consistency condition ($df = 0$) give

$$df = \frac{\partial f}{\partial \sigma_{ij}} d\sigma_{ij} + \frac{\partial f}{\partial a_{ij}^{*}} da_{ij}^{*} - \frac{1}{C_p}\left\{ d\varepsilon_v^{p} + d\left( \frac{\rho}{1+e_0} \right) \right\} = 0 \tag{4.29}$$

Note that $a_{ij}^{*}$ is a function of $\sigma_{ij}$ and the stress histories although ordinary $a_{ij}$ is only dependent on $\sigma_{ij}$, thus an evolution rule of $a_{ij}^{*}$ is given as follows by substituting Equations (4.14), (4.16) and (4.28) to Equation (4.13).

$$da_{ij}^{*} = k\, da_{ij} + l\left(a_{ij} - a_{ij}^{*}\right) = \left( \cos\frac{\theta}{2} \right) \frac{\partial a_{ij}}{\partial \sigma_{kl}} d\sigma_{kl} + \mu\Lambda \left\| \frac{\partial f}{\partial t_{kl}^{*}} \right\| \left( a_{ij} - a_{ij}^{*} \right) \tag{4.30}$$

Paying attention that the proportionality constant $\Lambda$ is a dimensionless, the evolution rule of $\rho$ based on $t_{ij}^{*}$ concept is given in a similar manner as original subloading $t_{ij}$ model.

$$d\rho = -\Lambda \cdot (1+e_0) \cdot L\left(\rho, t_N^{*}\right) = \Lambda \cdot (1+e_0) \cdot \frac{-G(\rho)}{t_N^{*}} = -\Lambda \cdot (1+e_0) \cdot \frac{a\rho^2}{t_N^{*}} \tag{4.31}$$

The proportionality constant $\Lambda$ representing the magnitude of the plastic strain increment is obtained by Equations (4.7), (4.24), (4.29), (4.30) and (4.31).

$$\Lambda = \left\langle \frac{\left( \dfrac{\partial f}{\partial \sigma_{ij}} + \dfrac{\partial f}{\partial a_{kl}^{*}} \dfrac{\partial a_{kl}^{*}}{\partial \sigma_{ij}} \right) d\sigma_{ij}}{\dfrac{1}{C_p}\left\{ \dfrac{\partial f}{\partial t_{kk}^{*}} + \dfrac{G(\rho)}{t_N^{*}} \right\} - \mu \dfrac{\partial f}{\partial a_{ij}^{*}} \left( a_{ij}^{*} - a_{ij} \right) \left\| \dfrac{\partial f}{\partial t_{lm}^{*}} \right\|} \right\rangle = \left\langle \frac{n_{ij}^{*} d\sigma_{ij}}{h_p} \right\rangle \tag{4.32}$$

Here, denominator $h^p$ is the plastic modulus representing the stiffness of plastic components. The plastic strain

increment is obtained by substituting the equations (4.32) into (4.28). On the other hand, the elastic strain increment is given by the generalized Hooke's law as

$$d\varepsilon_{ij}^{e} = \frac{1+\nu_e}{E_e} d\sigma_{ij} - \frac{\nu_e}{E_e} d\sigma_{kk}\delta_{ij} \quad where \quad E_e = \frac{3(1-2\nu_e)(1+e_0)}{\kappa} p \tag{4.33}$$

Here, $E_e$ is the Young's modulus, $\kappa$ is the swelling index and $\nu_e$ is the Poisson's ratio respectively. Thus, the total strain increment is given by

$$d\varepsilon_{ij} = d\varepsilon_{ij}^{e} + d\varepsilon_{ij}^{p} \tag{4.34}$$

The proportionality constant $\Lambda$ can be, furthermore, expressed by strain increment as follows

$$\Lambda = \left\langle \frac{D_{ijmn}^{e} \dfrac{\partial f}{\partial t_{mn}^{*}} d\varepsilon_{mn}}{h_p + n_{qr}^{*} D_{qrst}^{e} \dfrac{\partial f}{\partial t_{st}^{*}}} \right\rangle \tag{4.35}$$

where, $D^{e}_{ijkl}$ is the elastic stiffness tensor represented as

$$D_{ijkl}^{e} = \frac{E_e}{1+\nu_e}\delta_{ik}\delta_{jl} + \frac{\nu_e E_e}{(1+\nu_e)(1-2\nu_e)}\delta_{ij}\delta_{kl} \tag{4.36}$$

Finally, the stress-strain relation is given as follows

$$d\sigma_{ij} = D_{ijkl}^{ep} d\varepsilon_{kl} = \left( D_{ijkl}^{e} - \frac{D_{ijmn}^{e} \dfrac{\partial f}{\partial t_{mn}^{*}} n_{op}^{*} D_{opkl}^{e}}{h_p + n_{qr}^{*} D_{qrst}^{e} \dfrac{\partial f}{\partial t_{st}^{*}}} \right) d\varepsilon_{kl} \tag{4.37}$$

Here, $D^{ep}_{ijkl}$ is the elastoplastic stiffness tensor.

*The characteristics and advantages of the proposed model*

The comparisons with the proposed model based on the newly modified stress $t_{ij}^{*}$ reflecting on the induced anisotropy and the other ordinary constitutive model are organized in Table 4.2 and Figure 4.13. The influence of the intermediate principal stress and stress histories are described inclusively by a simple isotropic hardening model based on the modified stress $t_{ij}^{*}$ in which the induced anisotropy is already considered. In the proposed method, a non-circular shaped yield surface in octahedral plane (or by changing the strength depending on the relative magnitude of the intermediate principal stress) and kinematic / rotational hardening rule are no longer necessary for considering the induced anisotropy. Hence,

Table 4.2 Comparison the proposed model with ordinary models: Proposed model can consider the influences of relative magnitude of intermediated stress $\sigma_2$ and stress histories, simultaneously.

| Influence of intermediate principal stress | Influence of stress histories: not considered | Influence of stress histories: considered |
|---|---|---|
| not considered | Ordinary isotropic model as Cam clay model<br>$\sigma_{ij}$ ○ $d\varepsilon_{ij}^{p}$ | Kinematic / rotational hardening model<br>$\sigma_{ij}$ ☆ $d\varepsilon_{ij}^{p}$ |
| considered | Modified stress $t_{ij}$ (Subloading $t_{ij}$ model)<br>$\sigma_{ij}$ ○ $d\varepsilon_{ij}^{p}$, $a_{ij}$ ○ $t_{ij}$ | Modified stress $t_{ij}^{*}$ (proposed model)<br>$\sigma_{ij}$ ☆ $d\varepsilon_{ij}^{p}$, $a_{ij}^{\#}$, $a_{ij}^{*}$ ☆ $t_{ij}^{*}$ |

○: coaxial, ☆: non-coaxial

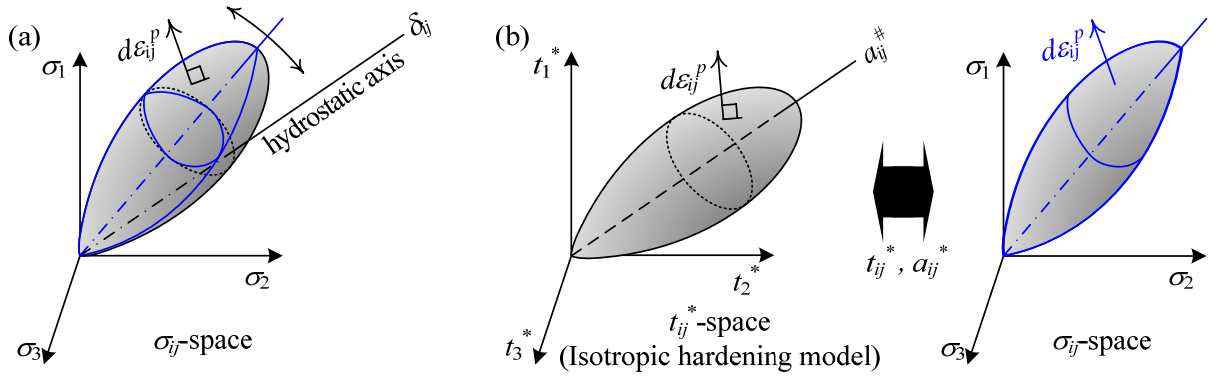


Figure 4.13 Comparison of the method for describing the influence of stress history (a) ordinary kinematic / rotational hardening model with changing shape of yield surface according to the intermediate principal stress coefficient *b* value (b) proposed method can consider the influence of the induced anisotropy by obeying isotropic hardening rule and following associated flow rule in modified stress $t_{ij}^*$ space

hardening parameters and constitutive parameters！ for such modeling are not required. Although the proposed model obeys isotropic hardening rule in the $t_{ij}^*$ space, moreover, the non-coaxiality between $\sigma_{ij}$ and $d\varepsilon_{ij}^p$ can also be described. Even though the relation between ordinary stress tensor $\sigma_{ij}$ and the transformation tensor $a_{ij}^*$ is non-coaxial, the coaxiality between the modified stress $t_{ij}^*$ which is product of these tensors and the plastic strain increment is ensured by the flow rule assumed in $t_{ij}^*$-space. The non-coaxiality between $\sigma_{ij}$ and $d\varepsilon_{ij}^p$ can, therefore, also be described by the proposed model, while it obeys isotropic hardening rule based on $t_{ij}^*$ and $d\varepsilon_{ij}^p$.

In addition, the proposed method can extend the ordinary model to one considering the induced anisotropy only by replacing the ordinary stress tensor $\sigma_{ij}$ by the newly modified stress tensor $t_{ij}^*$, and then the original features of ordinary models are remained. In the present case extending subloading $t_{ij}$ model, follows features are remained: Stress path dependency on the direction of plastic flow is considered by dividing the plastic strain increment $d\varepsilon_{ij}^p$ into the component $d\varepsilon_{ij}^{p(\mathrm{AF})}$ which is determined by the flow rule in modified stress space and the component $d\varepsilon_{ij}^{p(\mathrm{IC})}$ representing the isotropic behavior, and details of this method is shown in APPENDIX; Influence of density and/or confining pressure on the deformation and strength can be described by the concept of the subloading surface. For such modeling of the induced anistorpy, a new parameter $\mu$ controlling the dissipative rate of the influence of stress histories due to the magnitude of the plastic strain increment $d\varepsilon_{ij}^p$ is added. And its value is determined easily from the simple cyclic shear test as the triaxial compression and extension test.

## 4.5 Verification of the validation of the proposed model
### The comparison with the experimental results and the parametric study

In this section, the performance of the proposed model representing the induced anisotropy is verified through the parametric studies and comparison of the calculated results with the experimental results: triaxial test on medium dense Toyoura sand; true triaxial test and directional shear test on medium dense Leighton Buzzard sand.

*Typical triaxial and true triaxial tests under constant lode angle on Toyoura sand*

Firstly, the validation of the proposed model is checked by comparison with the typical triaxial and true-triaxial tests, which are isotropic consolidation test, shearing test under constant lode angle ($\theta$ = 0°, 15°, 30°, 45° and 60°) and others on Toyoura sand (mean diameter $D_{50}$ = 0.2mm, uniformity coefficient $U_c$ = 1.3, specific gravity $G_s$ = 2.65, maximum void ratio $e_{max}$ = 0.95, and minimum void ratio $e_{min}$ = 0.58). In these tests, two types of samples with different densities ($e_{initial}$ ∪ 0.68, 0.92) are used, and these have quasi-isotropic structures. Table 4.3 shows the values of material parameters for Toyoura sand. As indicated in this table, one parameter $\mu$ controlling the influence of past stress history is newly added to the original parameters which are fundamentally the same as those of the Cam clay model with the exception of parameter $a$ representing the influence of density. The values of parameters except for $\mu$ can be determined from consolidation and triaxial compression tests on normally and over consolidated soils in approximately a similar manner as Cam clay model. The value of $\mu$ is easily determined from fitting the calculated curve to the observed result of stress-strain behavior on triaxial cyclic compression and extension test after shown in Figure 4.18.

Figure 4.14 shows the observed results (Nakai & Hinokio, 2004) and calculated results of isotropic consolidation tests on dense and loose sands, arranged in terms of the relation between void ratio $e$ and confining pressure $p$ in logarithmic scale. Henceforth, the calculated results of original subloading $t_{ij}$ model will be shown together with that of the proposed model and experimental results. It can be observed from this

Table 4.3 Material parameters of proposed model for Toyoura sand in which $\mu$ representing the influence of stress history is newly added to parameters of original subloading $t_{ij}$ model

| | | | |
|---|---|---|---|
| $\lambda$ | | 0.0700 | Same parameters as Cam clay model |
| $\kappa$ | | 0.0045 | |
| $e_{NC}$ at $p$ = 98 kPa & $q$ = 0 kPa | | 1.1 | |
| $R_{cs} = (\sigma_1/\sigma_3)_{cs(comp.)}$ | | 3.2 | |
| $\nu_e$ | | 0.2 | |
| $\beta$ | | 2.0 | Shape of yield surface (same as original Cam clay if $\beta$ = 1) |
| $a$ | $a_{AF}$ | 33 | Influence of density and confining pressure |
| | $a_{IC}$ | 500 | |
| $\mu$ | | 40.0 | Influence of stress history |

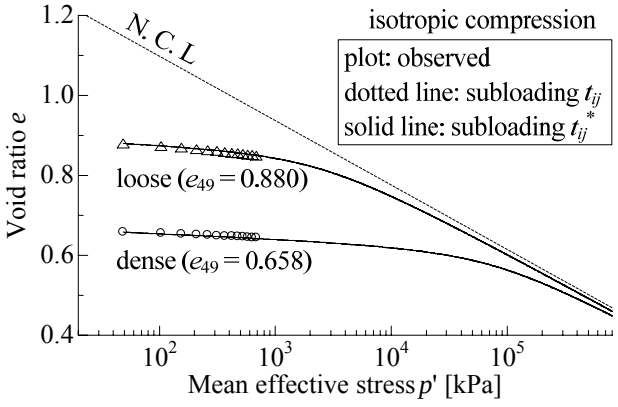


Figure 4.14 Observed and calculated results (subloading $t_{ij}$ model and proposed model) of isotropic consolidation tests on loose and dense samples (after Nakai & Hinokio, 2004)

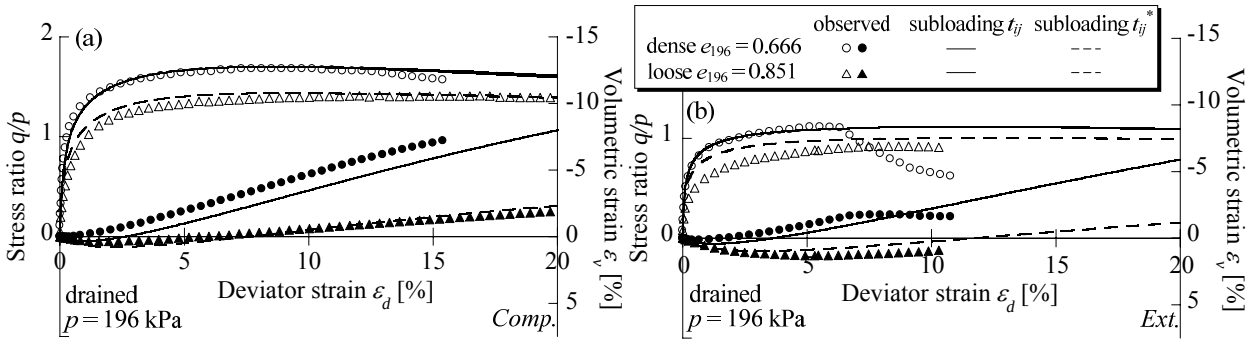


Table 4.15 Experimental results of drained triaxial compression and extension tests under constant mean stress $p$ on dense and loose sand (after Nakai & Hinokio, 2004) and their simulations using subloading $t_{ij}$ model and subloading $t_{ij}^*$ model

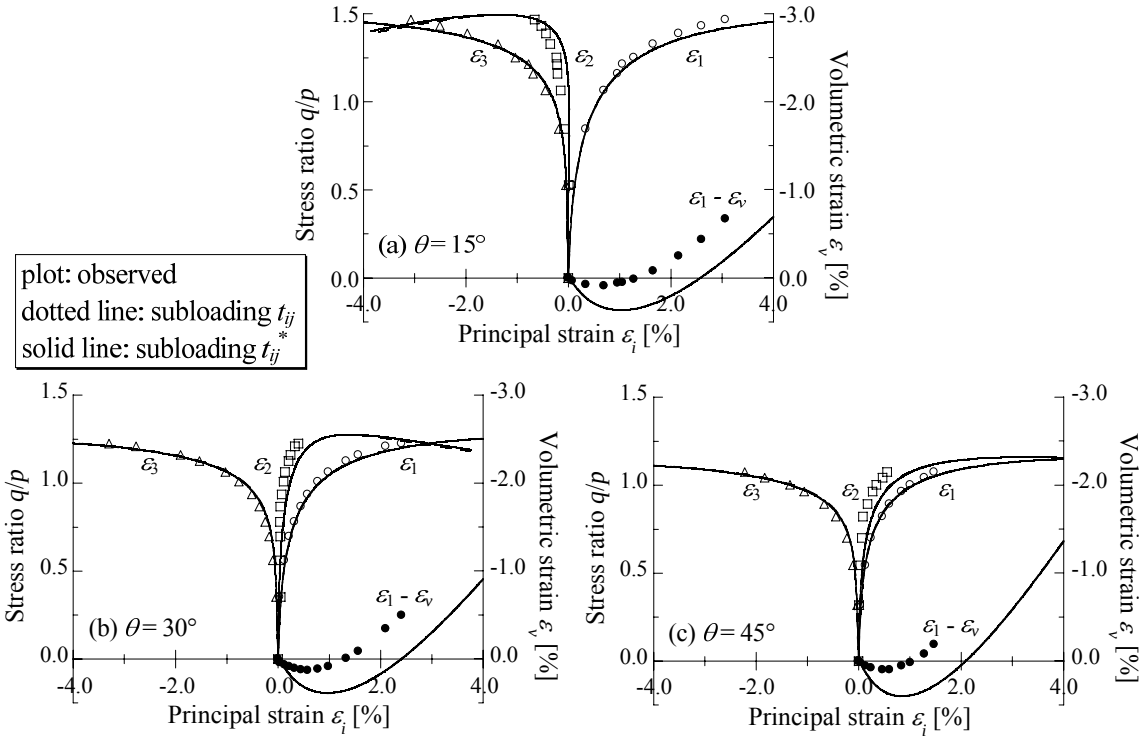


Figure 4.16 Comparison between experimental results of true triaxial tests under constant mean stress and constant Lode angle $\theta$ on Toyoura sand (after Nakai & Hinokio, 2004) with calculated results by subloading $t_{ij}$ model and subloading $t_{ij}^*$ model (a) $\theta$= 15° (b) $\theta$= 30° (c) $\theta$= 45 °

figure that, since the soil fabric is constant ($a_{ij}^* = a_{ij}$ : isotropic fabric) and stress path doesn't change (monotonic loading) in this isotropic consolidation path, the calculated result by the proposed model is completely the same as the calculated result by subloading $t_{ij}$ model, and both results agree well with the experimental result. From comparison with analytical and experimental consolidation behaviors, the values of $\lambda$, $\kappa$, $N$ are determined.

Figures 4.15 (a) and (b) show the observed results of drained triaxial compression and extension tests under constant mean stress (symbols) (Nakai & Hinokio, 2004) and the corresponding calculated curves by the proposed model and subloading $t_{ij}$ model. It can be seen that the proposed model whose result corresponds to that of subloading $t_{ij}$ model in the monotonic loading ($t_{ij}^* = t_{ij}$ when $a_{ij}^* = a_{ij}$) can

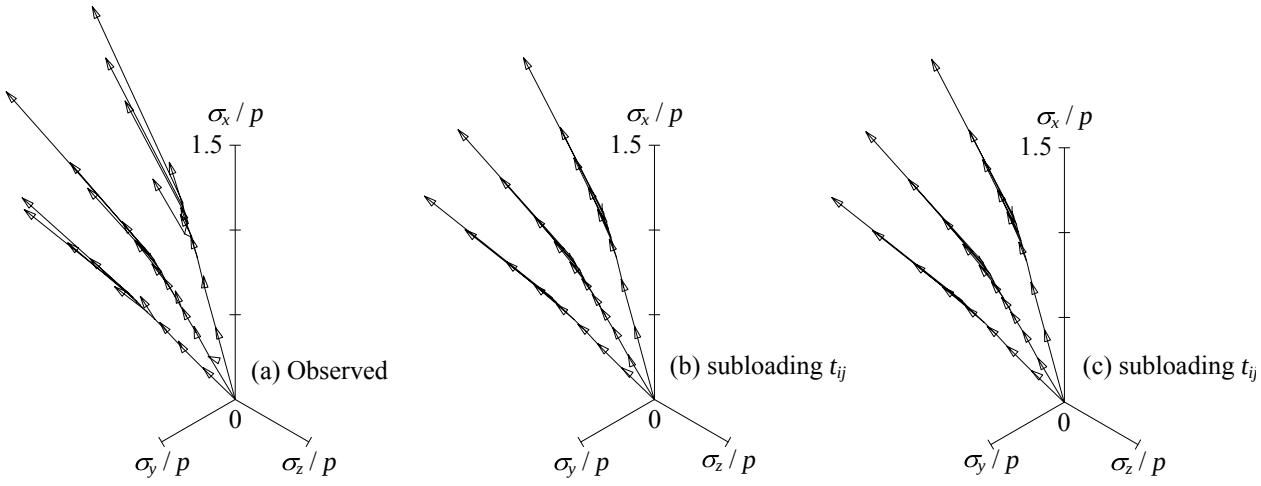


Figure 4.17 Stress paths and strain increment vectors in stress ratio plane obtained from the simulations of drained true triaxial tests under constant mean stress :(a) experiments (after Nakai & Hinokio, 2004) (b) subloading $t_{ij}$ model (c) subloading $t_{ij}^*$ model

suitably describes not only the influence of density on the deformation and strength of soils but also the influence of the intermediate principal stress on them. Furthermore, in order to check the applicability of the proposed model to the different principal stresses conditions, the simulations of the monotonic shearing test under constant lode angle $\theta$ are carried out. The lode angle $\theta$ indicates the angle between $\sigma_1$-axis and the corresponding radial stress path on the octahedral plane, where $\theta = 0°$ and 60° represent the stress path under triaxial compression and extension condition, respectively. Figures 4.16(a), (b) and (c) show the observed (symbols) (Nakai & Hinokio, 2004) and calculated (curves) variations of the three principal strains ($\varepsilon_1$, $\varepsilon_2$ and $\varepsilon_3$) against stress ratio $q/p$ and the volumetric strain $\varepsilon_v$ against the major principal strain $\varepsilon_1$ in true-triaxial tests ($\theta = 15°$, 30° and 45°) on dense sand under constant mean principal stress ( $p$ = 196 kPa). Figures 4.17(a), (b) and (c) show the observed and calculated vectors of shear strain increment along such monotonic stress paths on octahedral plane. As can be seen in Figure 4.16, the stress-strain behavior of the proposed model (and subloading $t_{ij}$ model) under different three principal stresses conditions are good agreement with that of the observed behavior. It can be seen, moreover, from Figure 4.17 that the proposed model also predicts the observed tendency that the direction of strain increment vectors deviate from the direction of shear stress path with the increasing of stress ratio.

Next, an applicability of the proposed model to typical anisotropic behaviors due to the influences of past stress history on triaxial condition is discussed. 11 kinds of stress paths shown in Figure 4.18 are conducted. In Figure 4.19, the experimental results obtained from triaxial compression and extension tests under a constant mean stress (path OCOD) are compared with the calculated results by the proposed model and original subloading $t_{ij}$ model. The value of parameter $\mu$ is determined by fitting calculated curve to this experimental result. Diagram (a) in Figure 4.19 shows the relation between axial strain and stress ratio, while diagram (b) illustrates the relation between stress ratio and volumetric strain along reversal path (C→O→D). It can be observed from this figure that, during triaxial compression test (O→C), the result obtained by the

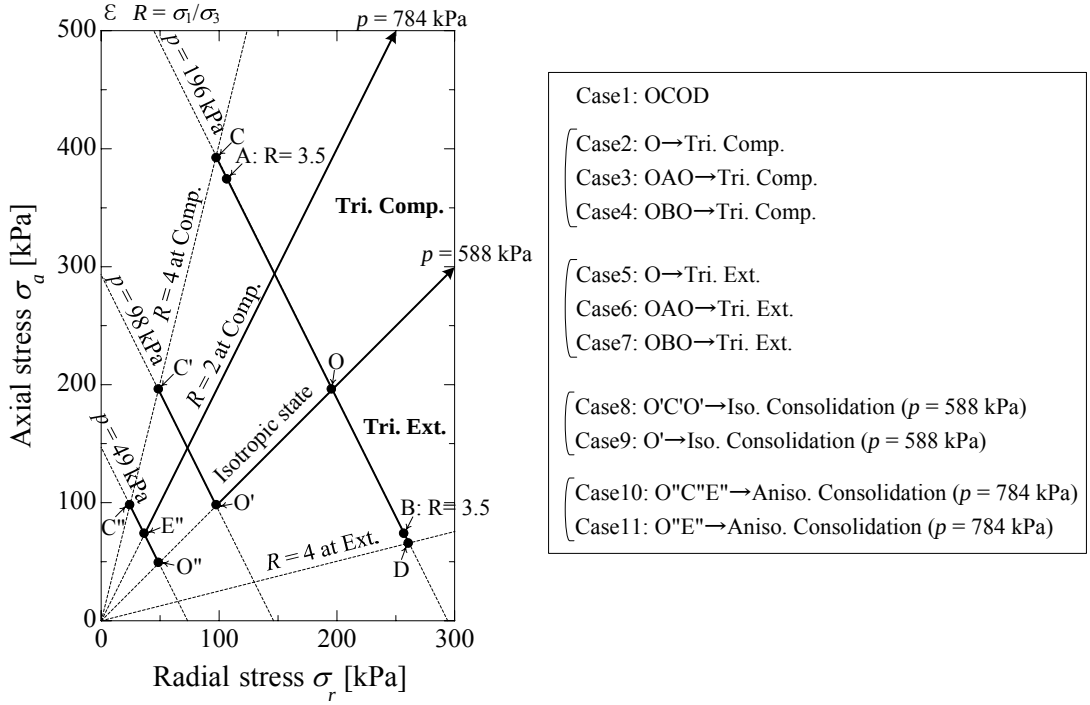


Figure 4.18 Stress paths of 11 kinds of tests investigating the influence of stress histories on mechanical behavior of Toyoura sand

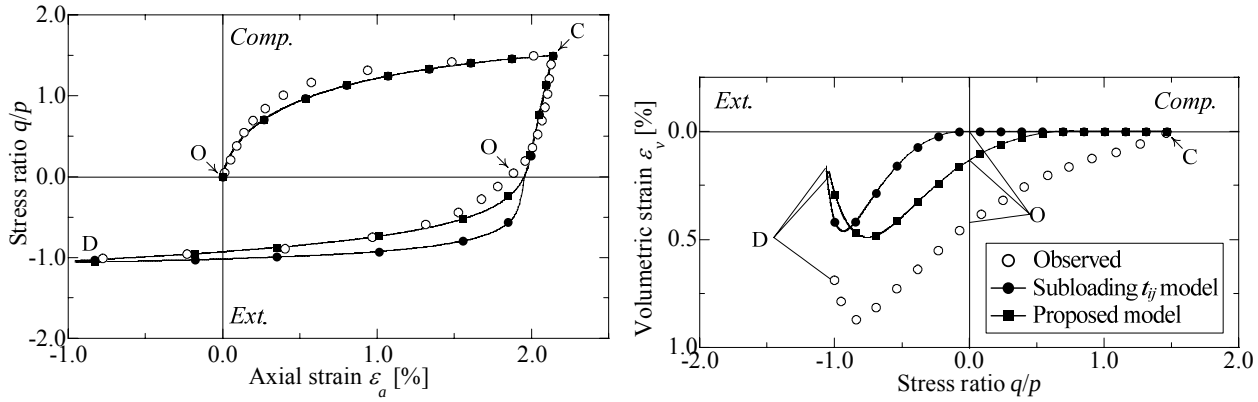


Figure 4.19 Comparison between experimental results of triaxial compression and subsequent extension test under constant mean stress on Toyoura sand with calculated results by subloading $t_{ij}$ model and subloading $t_{ij}^*$ model (left side: axial strain $\varepsilon_a$ and stress ratio $q/p$ relation, right side: stress ratio $q/p$ and volumetric strain $\varepsilon_v$ relation at BAF)

proposed model is completely same as result of subloading $t_{ij}$ model, and both agree well with the experimental result. It can be seen that, during subsequent triaxial extension path (C→O→D), the proposed model is capable of describing both the reduction of the stiffness and the negative dilatancy before isotropic stress state (C→O), while the original subloading $t_{ij}$ model exhibits only elastic deformation, i.e., non-volumetric change under constant mean stress. Also, it can be observed that the proposed model can describe a decaying of the influence of shear histories along with the plastic deformation, so that soils approach to unique residual strength.

Figures 4.20 and 4.21 show the corresponding calculated results of triaxial compression and

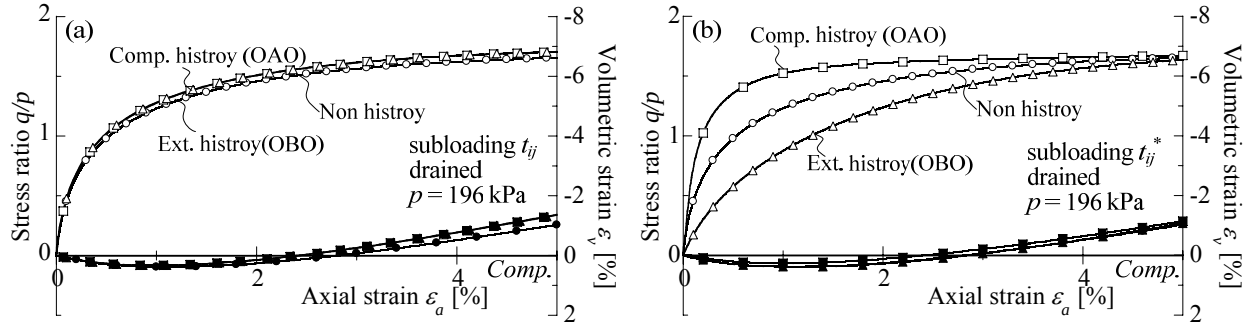


Figure 4.20 Calculated results of drained triaxial compression tests on samples (Toyoura sand) with comp. history, ext. history and non history by (a) subloading $t_{ij}$ model and (b) subloading $t_{ij}^*$ model – these simulations correspond to observed results shown in Figure 4.4.

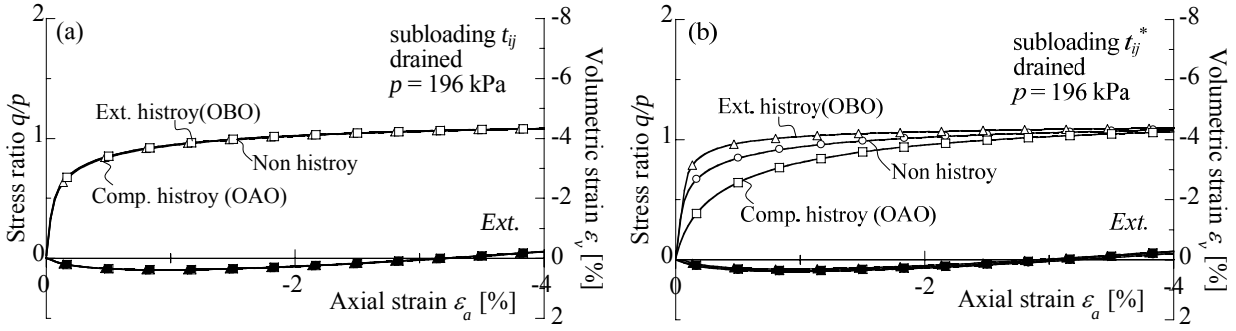


Figure 4.21 Calculated results of drained triaxial compression tests on samples (Toyoura sand) with comp. history, ext. history and non history by (a) subloading $t_{ij}$ model and (b) subloading $t_{ij}^*$ model – these simulations correspond to observed results shown in Figure 4.4.

extension tests to the experiment results shown in Figure 4.4 (b) and (c) in section 4.2, in which three kinds of samples preliminarily given stress paths: non shear history (circular plots); compression history - path OAO (square plots); extension history - path OBO (triangular plots). Comparing the experimental results with the calculated curves by the original subloading $t_{ij}$ model, it is found that the model almost cannot consider the influence of stress histories, i.e., those results are almost same regardless of stress histories. On the other hand, although the proposed model under-predict the tendency of positive dilatancy for the sample with compression history, its calculated results have good agreement with the observed results affected not only by the influence of the intermediate stress and density but also by the past stress history on the stiffness and dilatancy of soils. As mentioned above, these calculated curves finally approach to unique residual strength of soil regardless of stress histories.

Figure 4.22 shows the observed and calculated relationships of axial strain $\varepsilon_a$ and volumetric strain $\varepsilon_v$ during isotropic compression on samples with shear history (circular plots, path O'C'O' → isotropic consolidation $p$ = 588 kPa) and without shear history (square plots, path O' → isotropic consolidation $p$ = 588 kPa), respectively. Observed results are same as Figure 4.3 in section 4.2. From the experimental results, it can be seen that soil with compression history initially shows anisotropic behavior ($d\varepsilon_v > 3d\varepsilon_a$) even under

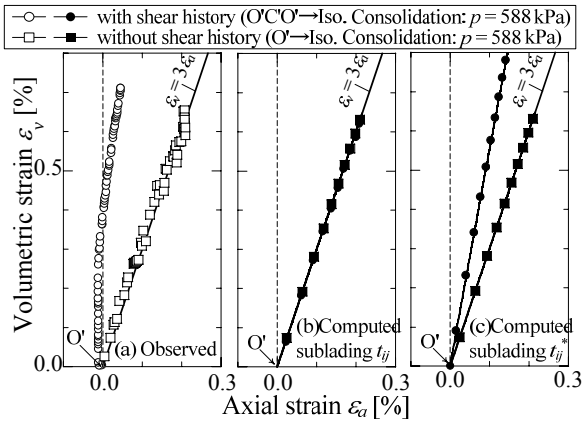


Figure 4.22 Comparison between experimental results of isotropic consolidation tests on samples with / without shear history with calculated results. (a) observed results (after Nagai, 2003), (b) subloading $t_{ij}^*$ model, (c) subloading $t_{ij}$ model

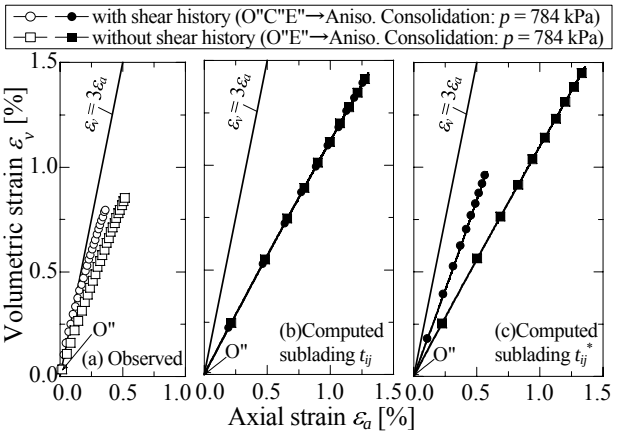


Figure 4.23 Comparison between experimental results of anisotropic consolidation tests ($\sigma_1/\sigma_3 = 2$) on samples with / without shear history with calculated results. (a) observed results (after Nagai, 2003), (b) subloading $t_{ij}^*$ model, (c) subloading $t_{ij}$ model

isotropic compression. It is also known that such anisotropy, however, decays with increasing of mean stress under isotropic compression ($d\varepsilon_v = 3d\varepsilon_a$). Calculated compression behaviors of both samples with and without shear history by subloading $t_{ij}$ model are almost same. On the other hand, although calculated results of the sample with shear history by the proposed model initially overestimate the axial strain $\varepsilon_a$, it can describe the anisotropic behavior even in isotropic consolidation and it also describes the dissolution of the influence of stress history due to the increase of mean stress as well as the observed results. Of course, calculated result of the sample without shear history by the proposed model corresponds with that by the original subloading $t_{ij}$ model.

Figure 4.23 indicates the observed results and the calculated results of anisotropic compression test under a constant principal stress ratio ($R$ ($\sigma_1/\sigma_3$) = 2). Two kinds of stress paths are considered: anisotropic compression with shear history (path O"C"E" → anisotropic consolidation $p$ = 784 kPa) and without shear history (path O"E" →anisotropic consolidation $p$ = 784 kPa). The Observed results were the same as Figure 4.8 in section 4.3. As mentioned in section 4.3, the sample with shear history ($R$ = 4) initially deforms isotropically ($d\varepsilon_v = 3d\varepsilon_a$) even under the anisotropic consolidation ($R$ = 2). Again, calculated results of both samples with and without shear history by subloading $t_{ij}$ model are almost same. On the other hand, although the proposed model overestimate the axial strain $\varepsilon_a$ ($d\varepsilon_v < 3d\varepsilon_a$) for sample with sheared history, its results qualitatively agree with the experimental results. In theory, the isotropic stress condition is represented in the modified stress $t_{ij}^*$-space, i.e., ($t_1^* : t_2^* : t_3^*$) = (1 : 1 : 1), and it is confirmed that the plastic strain increment determined employing flow rule in $t_{ij}^*$-space shows isotropic behavior. However, since the elastic strain increment obeying Hooke's law on ordinary stress $\sigma_{ij}$ exhibits remarkable anisotropic deformation, the axial strain $\varepsilon_a$ is overestimated in the proposed model. Moreover, it is shown from both calculated results in Figures 4.22 and 4.23 that the proposed model is able to describe the decay of the influence of stress histories due to the increase of stress under a constant stress ratio.

From comparison with a stress-strain behavior of such typical triaxial tests on Toyoura sand with / without shear history, it was indicated that the proposed model maintains the features of the original subloading $t_{ij}$ model, viz., considering the influences of the intermediate stress and density, and additionally consider the influence of the past stress histories.

*Parametric studies – True triaxial tests without / with the past shared history*

Figure 4.24 shows the three-dimensional behaviors of Hostun sand with shear history (anisotropic sample) and without shear history (isotropic sample) (after Lanier, 1987), which are organized as the contour lines of deviatoric strain along the different radial paths on octahedral plane. The left hand side in Figure 4.25 represents the result of an initially isotropic sample without shear history, and the right side represents the results of an initially anisotropic sample with shear history. It can be seen from left side figure that the curves of contour line are practically circular for small value of $\varepsilon_d$, and finally its shape is a rounded triangle. This implies that the deformation and strength characteristics of soils depend on the magnitude of $b$(= ($\sigma_2$-$\sigma_3$) / ($\sigma_1$-$\sigma_3$)), i.e., the influence of the relative magnitude of the intermediate principal stress $\sigma_2$. From right side figure, initial modulus decreases in a significant manner when the direction of the path changes away from the direction of the initial loading path (z-direction). In other words, contour lines are sparse in z-direction, and vice versa. The failure surface is, moreover, not affected by the initial anisotropy, which has been progressively erased by the subsequent deformation. Figure 4.25 shows the comparison with three-dimensional behaviors of sand with triaxial compression and extension histories. It is seen from these diagrams that each contour line keep the same shape but they are shifted in the direction of the first load application. A kinematic hardening due to the past stress history, i.e., the induced anisotropy, can be seen here.

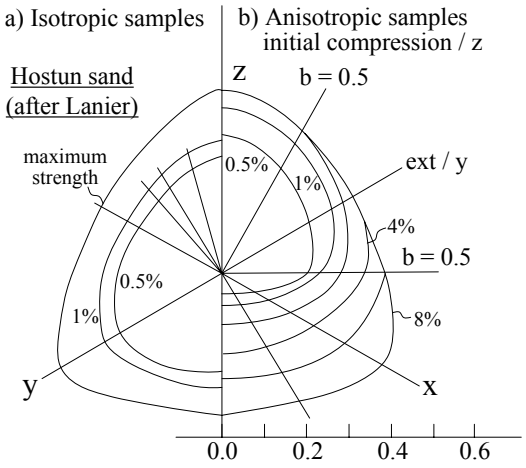


Figure 4.24 The evolution of the deviatoric strain along the different radial paths. Left side: a) isotropic sample, Right side: b) anisotropic samples – compression to z-direction (after Lanier, 1987)

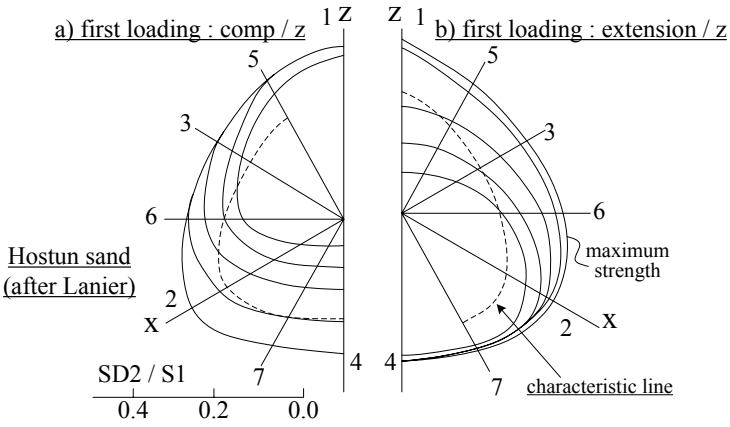


Figure 4.25 The evolution of the deviatoric strain along the different radial paths. Left side: a) anisotropic samples – z-direction triaxial compression history, Right side: b) anisotropic samples – z-direction triaxial extension history (after Lanier, 1987)

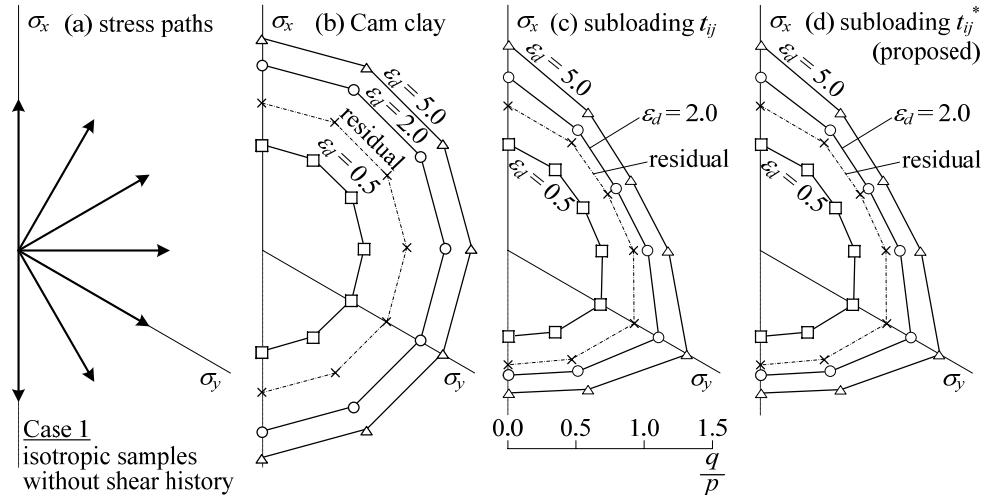


Figure 4.26 Contours of deviator strain in stress ratio plane obtained from the calculated results of drained monotonic true triaxial tests under constant mean stress and constant Lode angle: (a) stress paths, (b) subloading Cam clay model, (c) subloading $t_{ij}$ model, (d) proposed subloading $t_{ij}^*$ model

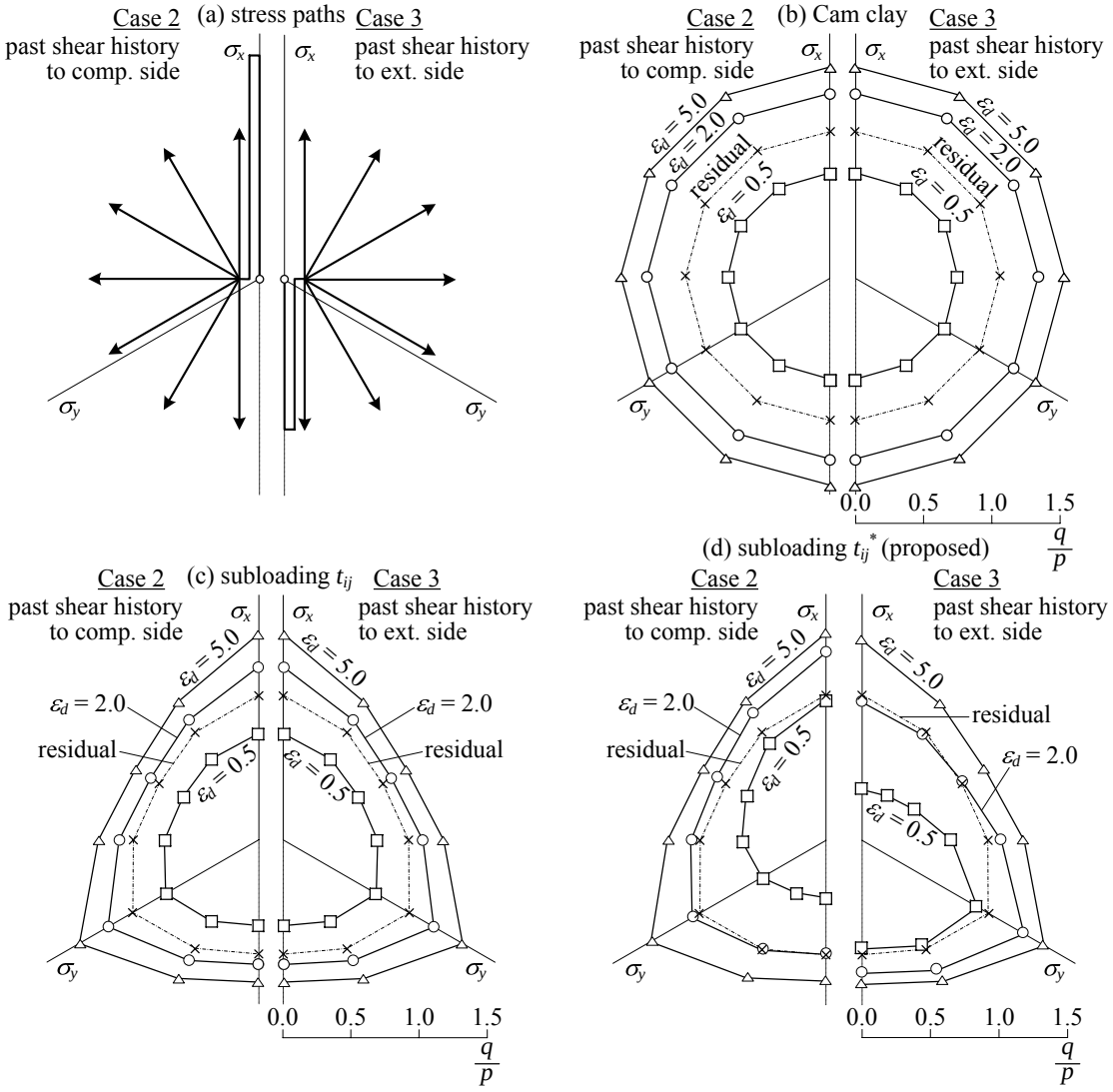


Figure 4.27 Contours of deviator strain in stress ratio plane obtained from drained true triaxial tests tests with the past shear history to compression/extension side under constant mean stress and constant Lode angle: (a) stress paths, (b) subloading Cam clay model, (c) subloading $t_{ij}$ model, (d) proposed subloading $t_{ij}^*$ model

Simulations of above three-dimensional behavior on three kinds of sample having no past sheared history (Case 1), with the past sheared history to triaxial compression side (Case 2) and extension side (Case 3) are conducted. Additionally, these samples assume medium dense Leighton Buzzard sand which is mainly used in the next investigations, so that its material parameters are shown in Table 4.4. In the simulations, all samples are sheared radially from initial isotropic condition on the octahedral plane under constant lode angle ($\theta$ = 0, 30, 60, 90, 120, 150 and 180 degrees), constant mean principal stress of $p$ = 34.5kPa in drained condition. Figure 4.26 shows the contour lines of deviator strain in octahedral plane for Case 1. The contour lines are drawn by plotting a stress state on octahedral plane at prescribed values of deviator strain ($\varepsilon_d$ = 0.5, 2.0, 5.0 [%] and residual condition). It is seen from this figure that Cam clay model draws the circular contour lines differently from the observed behaviors shown in the left side of Figure 4.24, while not only original subloading $t_{ij}$ model but also the proposed model suitably consider the influence of the intermediate principal stress, viz., rounded triangular contour lines, because the proposed model inherits the characteristic of modified stress $t_{ij}$. Figure 4.27 shows the calculated results of Case 2 and Case 3, which are conducted by using a sample having a past sheared history. It is seen from both results that the contour lines spread out in the direction to which the past shear history is given, while it contracts in the opposite direction. It means that soil becomes stiff in the direction having a sheared history, and it also becomes soft in the opposite direction. Failure strength is attained regardless of the past stress histories.

*True triaxial and directional shear cell tests under general stress state on Leighton Buzzard sand*

The applicability of the proposed model is verified by the comparison with the experimental results of the true triaxial and directional shear cell test, which can generate more general and practical stress path than such axisymmetric state as triaxial condition. True triaxial tests and directional shear cell test on dry Leighton Buzzard sand were performed to investigate experimentally the stress-strain behavior of sand under arbitrary deviatoric stress paths. Samples were prepared of medium dense Leighton Buzzard sand (specific gravity $G_s$ = 2.66, maximum void ratio $e_{max}$ = 0.815, and minimum void ratio $e_{min}$ = 0.516, relative density $D_r$ = 72 %) and had negligible initial stress anisotropy. The true triaxial tests were performed using an apparatus of the type originally developed by Ko and Scott (1967): three normal stresses are applied through fluid filled flexible cushions. Samples were firstly sheared, without rotation of the principal axes, to identical stress states, and then sets of probes on samples were applied under constant mean principal stress. The directional shear cell tests were performed using an apparatus of the type developed by Arthur et al. (1977). In this device, samples are tested in plane strain condition, with fixed rigid boundaries. The other two normal stresses as applied through flexible cushions in the same way as the true triaxial tests, but there cushions can also impose shear stresses on the face of the specimen. Sets of probes, with rotation of the principal axes, were applied to the samples from identical $\tau_{xy}$; ($\sigma_x$ - $\sigma_y$) / 2 stress states.

Table 4.4 shows the value of material parameters of Leighton Buzzard sand, which are determined by fitting the calculated results to the experimental results in the same way as Toyoura sand mentioned in previous section. From the isotropic consolidation test shown in Figure 4.28, the value of $\lambda$ : compression

Table 4.4 Material parameters of proposed model for Leighton Buzzard sand

| | | | |
|---|---|---|---|
| $\lambda$ | | 0.0320 | Same parameters as Cam clay model |
| $\kappa$ | | 0.0020 | |
| $e_{NC}$ at $p = 98$ kPa & $q = 0$ kPa | | 1.05 | |
| $R_{cs} = (\sigma_1/\sigma_3)_{cs(comp.)}$ | | 2.6 | |
| $\nu_e$ | | 0.2 | |
| $\beta$ | | 1.6 | Shape of yield surface (same as original Cam clay if $\beta = 1$) |
| $a$ | $a_{AF}$ | 15 | Influence of density and confining pressure |
| | $a_{IC}$ | 85 | |
| $\mu$ | | 40.0 | Influence of stress history |

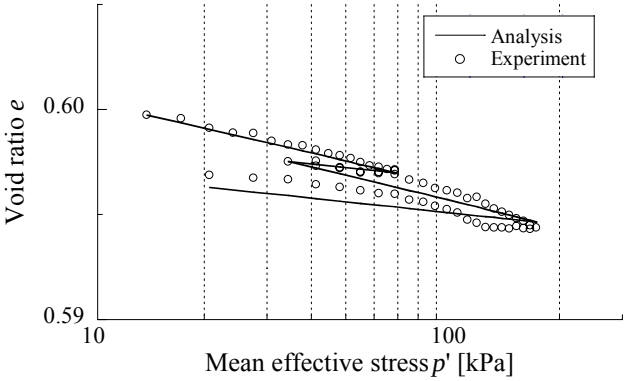


Figure 4.28 Experimental result of isotropic compression test on Leighton Buzzard sand and its simulation using subloading $t_{ij}^*$ model

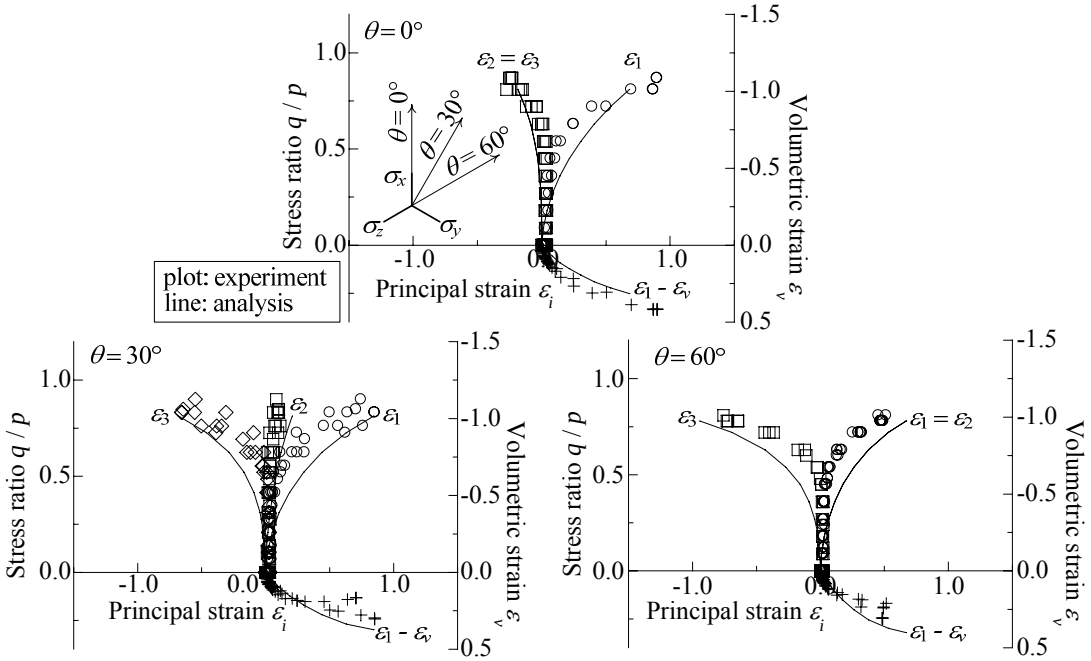


Figure 4.29 Comparison between experimental results of true triaxial tests under constant mean stress and constant Lode angle $\theta$ on Leighton Buzzard sand and calculated results by subloading $t_{ij}^*$ model: (a) $\theta = 0$ ° (triaxial comp.), (b) $\theta = 30°$, (c) $\theta = 60$ ° (triaxial ext.)

index, $\kappa$ : swelling index, $N$ : reference void ratio on *NCL* under $p = 98$ kPa, and $a_{IC}$ : the influence of density, are determined. The parameters $R_{CS}$ : residual strength at triaxial compression state, $\beta$ : shape of yield surface, and $a_{AF}$ : the influence of density, are determined from fitting the calculated curves to the observed results of true triaxial shear under constant lode angle ($\theta = 0°$, 30° and 60°) (see Figure 4.29). The material parameter $\mu$ representing the rate of dissolution of the influence of stress history is determined easily from one cycle loading test under constant lode angle $\theta$ such as ACI7 after shown in Figures 4.33 and 4.34.

True triaxial tests under constant mean stress $p$ = 34.5 kPa

97 true triaxial tests were performed under several constant mean principal stress ($p$ = 13.8, 34.5, 55.2 and 69.0 kPa). Concerning the test case under constant mean principal stress $p$ = 34.5, some of the comparison between experimental results and computed results under complex stress paths are shown and discussed here. The stress points at octahedral plane given in true triaxial tests are summarized in Figure 4.30. In the case of "ACI4", for instance, sample is firstly sheared radially on the octahedral plane from A (($\sigma_x$, $\sigma_y$, $\sigma_z$) = (34.5, 34.5, 34.5) kPa) to C ((52.2, 15.9, 32.4)kPa), which is a monotonic loading, and then unloaded to I ((41.4, 27.6, 34.5) kPa), subsequently. Then, the sample is sheared to the directions of 4 successively. Each stress states represent ($\sigma_x$, $\sigma_y$, $\sigma_z$ )= A:((34.5, 34.5, 34.5)kPa), B:((51.0, 17.9, 34.47)kPa), C:((53.8 15.7, 34.5)kPa), D:((53.8, 34.5, 15.7)kPa), E:((36.5, 49.6, 17.2) kPa), F:((20.0, 49.0, 34.5)kPa), G:((17.2, 33.4, 52.7)kPa), I:((45.5, 23.4, 34.5)kPa). Those test results are arranged in terms of the relations between stress ratio $q/p$ and the three principal strains ($\varepsilon_x$, $\varepsilon_y$ and $\varepsilon_z$), and the volumetric strain $\varepsilon_v$ and strain $\varepsilon_x$. Additionally, the vectors of deviatoric strain increment is shown in stress path, and the length of each vectors is obtained from the shear strain increment divided by the increment of shear stress ratio on octahedral plane.

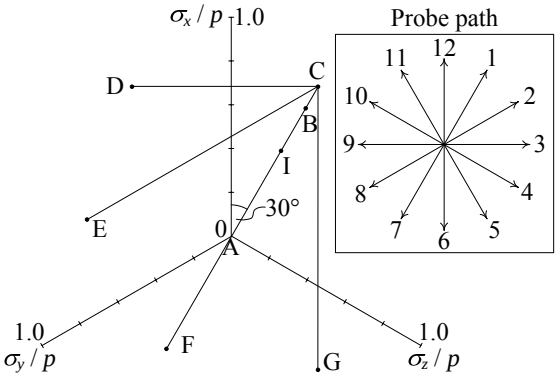


Figure 4.30 Each stress points (A - G) on octahedral plane and direction of probe path

[AB series – monotonic loading tests with monotonically increasing stress ratio]

Firstly, stress paths AB1, 4 and 7, in which the samples are radially shared on octahedral plane and stress ratio $q/p$ increases monotonically as shown in Figure 4.31, are discussed. Figure 4.31 shows those stress paths and the vectors of shear strain increment along each stress path (AB1, 4 and 7) on octahedral plane. Figure 4.32 shows the relationships between stress ratio ($q/p$), principal strains ($\varepsilon_x$, $\varepsilon_y$ and $\varepsilon_z$) and volumetric strain ($\varepsilon_v$), in which dots denote observed results, solid lines denote calculated results by the proposed model, and broken lines denote calculated results by the subloading $t_{ij}$ model. The influence of past stress histories doesn't appear in such stress path AB1 which is monotonic loading path under constant $\theta$ = 30°. The same calculated curves can be obtained from the proposed and subloading $t_{ij}$ models, since new modified stress $t_{ij}^*$ corresponds with the original modified stress $t_{ij}$ (and $a_{ij}^*$ = $a_{ij}$) in such stress path. Although the calculated results a little underestimate the initially stiffness of soil, both models can describe typical dilatancy and deformation characteristics of sand. Other cases AB4 and AB10 are non-monotonic path with changing stress path to directions of 4 and 10. Since difference between $t_{ij}^*$ and $t_{ij}$ ($a_{ij}^*$ and $a_{ij}$) arises due to change of $\alpha$ in Equation (4.15) in such non-monotonic loading path, the proposed model describes the influence of stress history (the indeuced anisotropy). It can be seen from the results of AB4 and AB10 in both figures that the calculated results of the proposed model differ from that of subloading $t_{ij}$ model and the proposed model can describe

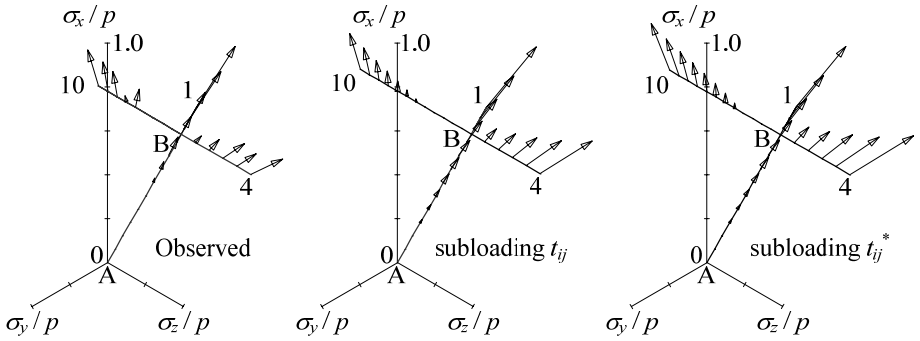


Figure 4.31 Stress paths and strain increment vectors in stress ratio plane obtained from the simulations of drained true triaxial tests under constant mean stress : series AB (a) experiments (b) subloading $t_{ij}$ model (c) subloading $t_{ij}^*$ model

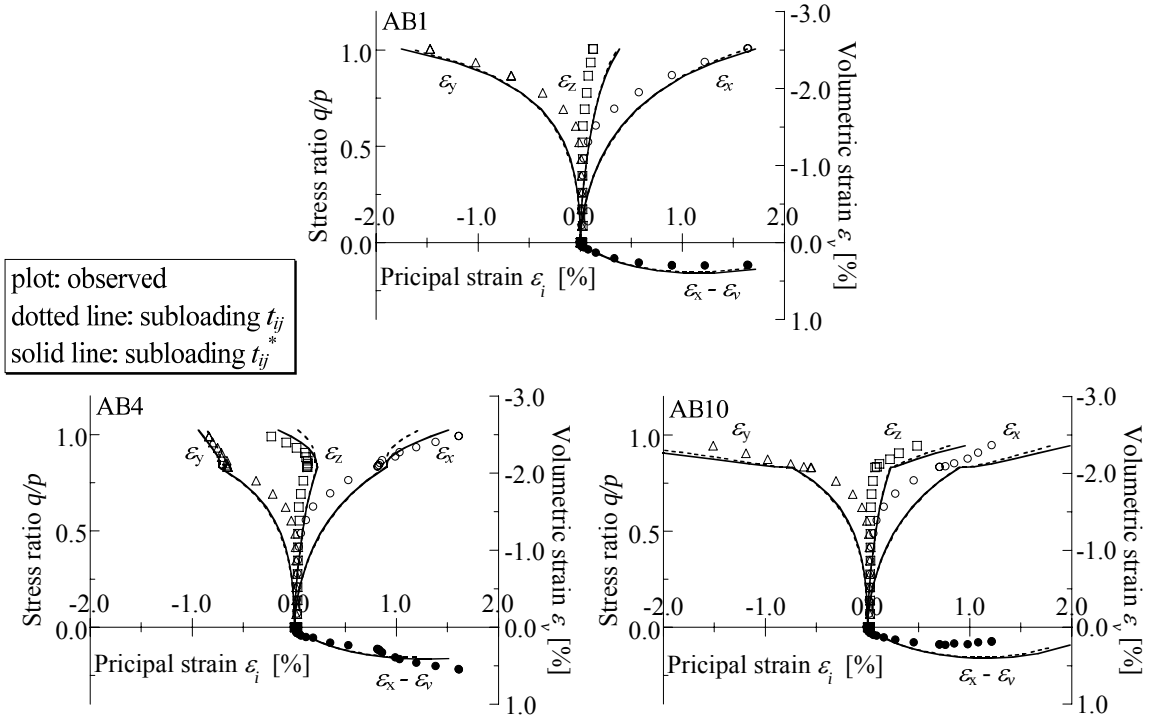


Figure 4.32 Stress strain relations obtained from the simulations of drained true triaxial tests under constant mean stress : series AB (a) path AB1 (b) path AB4 (c) path AB10

the observed behavior affected by stress histories more precisely than subloading $t_{ij}$ model. In the paths from B to 4 and 10 in Figure 4.31, especially, the proposed model can represent the vectors of stain increment inclining to loading direction due to a past stress histories. On the other hand, subloading $t_{ij}$ model does not completely coincide with the experimental results about the direction of shear stain after change of stress path. This is because the direction of plastic strain is only determined by the present stress condition regardless of the stress histories, i.e., associated flow rule, in an ordinary isotropic hardening model.

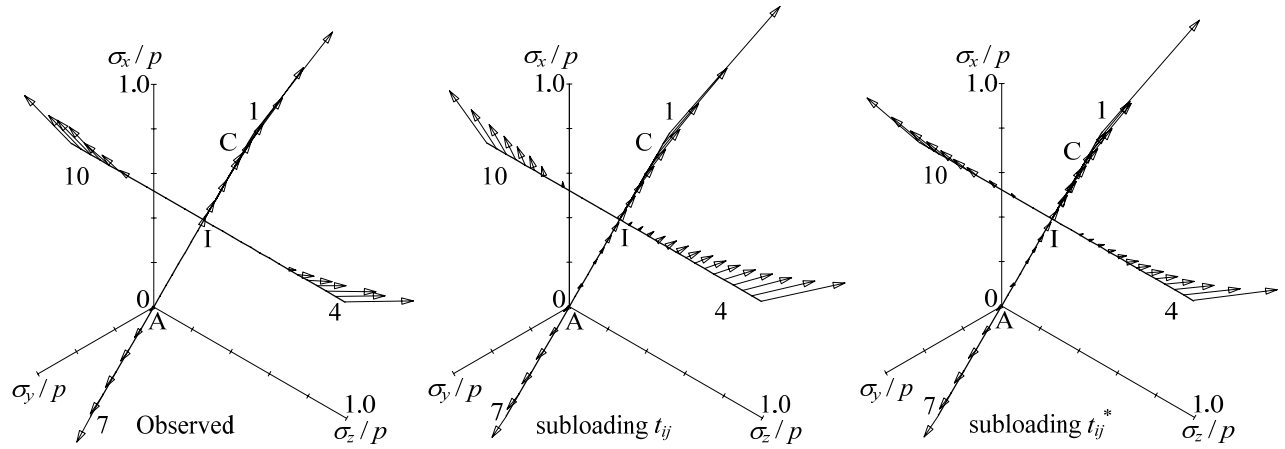


Figure 4.33 Stress paths and strain increment vectors in stress ratio plane obtained from the simulations of drained true triaxial tests tests under constant mean stress : series ACI (a) experiments (b) subloading $t_{ij}$ model (c) subloading $t_{ij}^*$ model

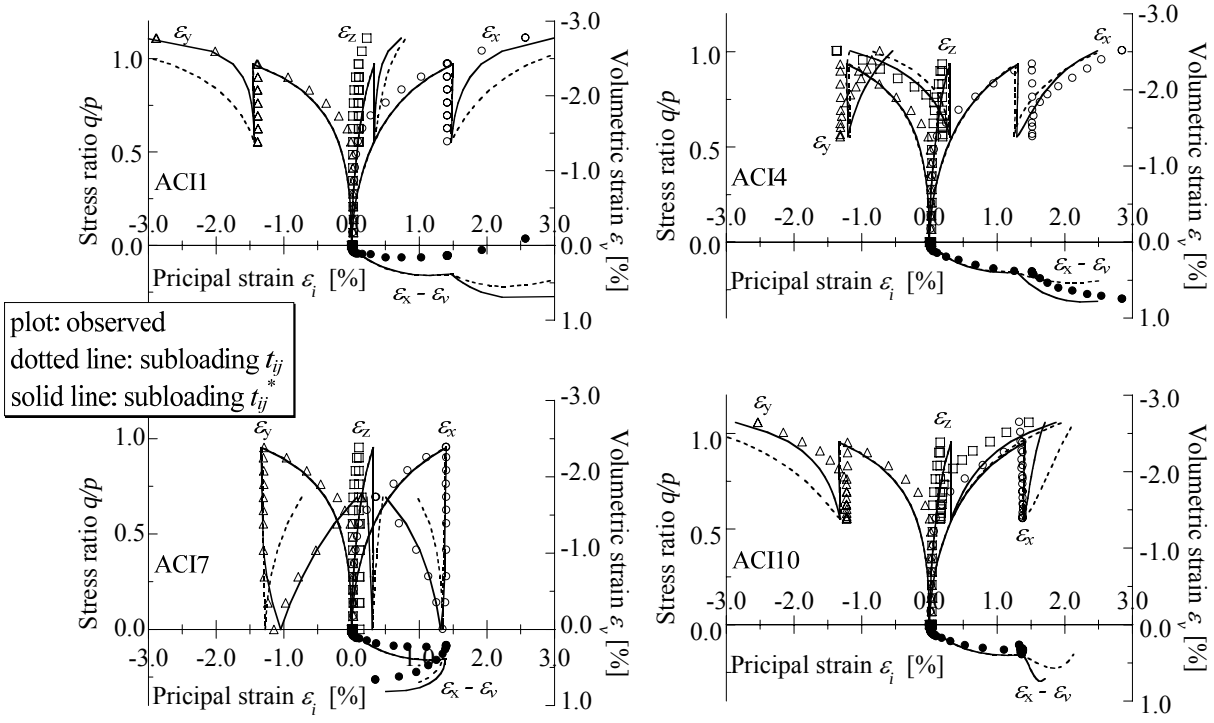


Figure 4.34 Stress strain relations obtained from the simulations of drained true triaxial tests under constant mean stress : series ACI (a) path ACI1 (b) path ACI4 (c) path ACI7 (d) path ACI10

[ACI series – non-monotonic loading tests with reversal unloading path]

Next, stress paths ACI1, 4, 7 and 10 which are the non-monotonic stress paths including the unloading reversal path from C to I before probe path to 1, 4, 7 and 10 are discussed. Figure 4.33 shows those stress paths and the vectors of shear strain increment along each stress path (AC1, 4, 7, 10) on octahedral plane. Figure 4.34 shows the relationships between stress ratio ($q/p$), principal strains ($\varepsilon_x$, $\varepsilon_y$ and $\varepsilon_z$) and volumetric strain ($\varepsilon_v$), in a similar manner as Figure 4.33. In loading path from A to C and subsequent unloading path to I,

the computed results of the proposed model completely coincides with that of subloading $t_{ij}$ model, and both calculated results agree well with the experimental results in the probes A to C. In the unloading path (probes C to I), both models properly describe the elastic behavior as observed in the tests, and then $a_{ij}^*$ remains at "$a_{ij}$ at the stress state A" during unloading (reversal loading) path. The calculated results by the proposed model, therefore, become different from that by subloading $t_{ij}$ model after the stress state I. During reloading stress path from I to 1 under constant lode angle $\theta = 30$, it is seen from the experimental results that the stress ratio $q/p$ initially increases rapidly, and the stiffness of soil gradually decrease with increasing of stress ratio due to the influence of the past stress histories. Subloading $t_{ij}$ model underestimate the increase of initial shear stiffness, since soils show elastoplastic behavior in the reloading path due to concept of subloading surface. On the other hand, the proposed model is able to describe the increasing of stiffness in the reloading path precisely, and finally reaches to unique soil strength. In stress path ACI7, the proposed model is capable of describing both the reduction of the stiffness and the early compression before isotropic stress state along path C-I-7, while subloading $t_{ij}$ model exhibits only elastic deformation in the same path. From the observed vectors of shear strain increment in Figure 4.33, the elastic region centering on point I, in which soils hardly deform, can be observed. Such observed kinematic hardening behavior due to stress histories is described by the proposed model based on the new modified stress $t_{ij}^*$, which can properly consider the influence of the stress histories in spite of isotropic hardening model.

[ACF series – complicated loading tests with cyclic stress path]

The observed and calculated results of cases ACF1, 3 and 11 are summarized in Figures 4.35 and 4.35. Samples are initially given reversal shearing path ACF, and then different probes to 1, 3 and 11 are applied. During the reversal loading from C to F, the proposed model can properly describe the reduction of the stiffness and the early compression before isotropic state as mentioned in ACI7. Overall, the calculated results of the proposed model show good agreement with the complicated experimental results even in subsequent probes to 1, 3 and 11 about both stress-strain behavior and increment strain vectors. The influence of stress histories represented as the difference between $a_{ij}^*$ and $a_{ij}$ diminishes due to the development of plastic deformation as expressed in Equations (4.13) and (4.16) during the reversal loading path from C to F (especially A to F), and the new modified stress $t_{ij}^*$ (and $a_{ij}^*$) nearly corresponds to the original modified stress $t_{ij}$ (and $a_{ij}$). Therefore, the difference between calculated behaviors by the proposed model and original subloading $t_{ij}$ model from point F are not much bigger than those from point C to F. It can be understood from such comparison with the calculated and observed results that the proposed model can represent not only the influence of the induced anisotropy (stress history) on deformation and strength of soil but also its development and degradation under complicated stress paths.

[ACG - complicated true triaxial tests]

Figures 4.37 and 4.38 show the experimental and corresponding calculated results of three kinds of complicated true triaxial tests: ACG2, ACG10 and ACG12. Even in such complicated 3-dimensional stress paths, the proposed model can suitably describe the variations in shear stiffness and dilatancy characteristic as

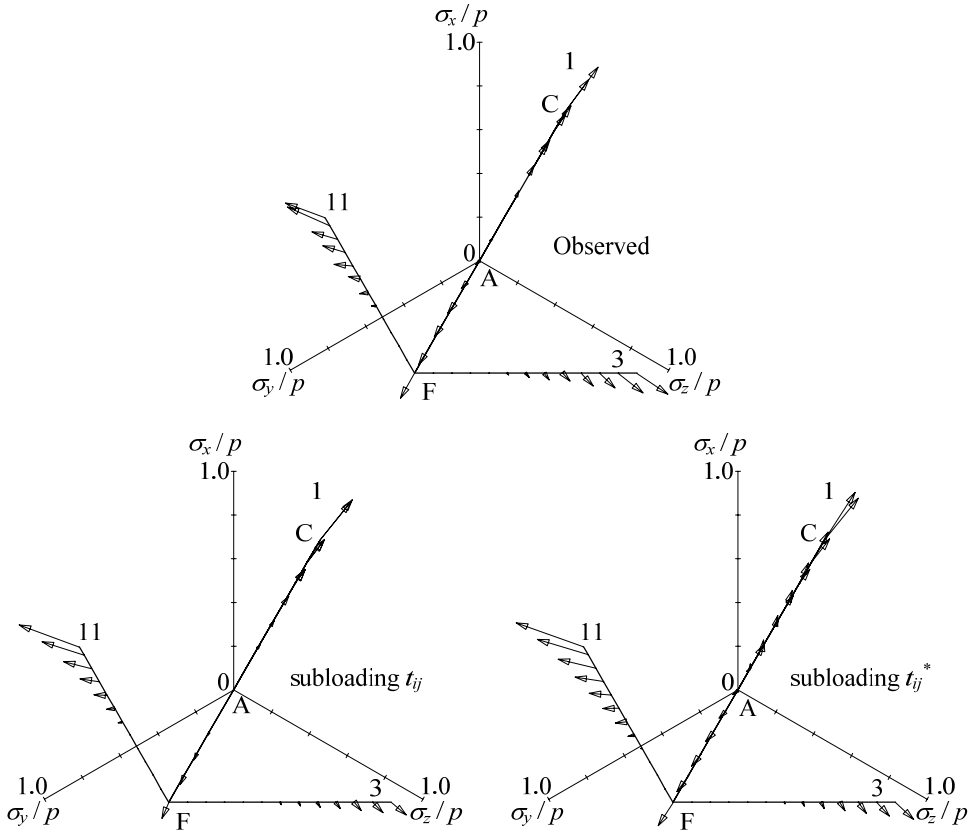


Figure 4.35 Stress paths and strain increment vectors in stress ratio plane obtained from the simulations of drained true triaxial tests under constant mean stress : series ACF (a) experiments (b) subloading $t_{ij}$ model (c) subloading $t_{ij}^*$ model

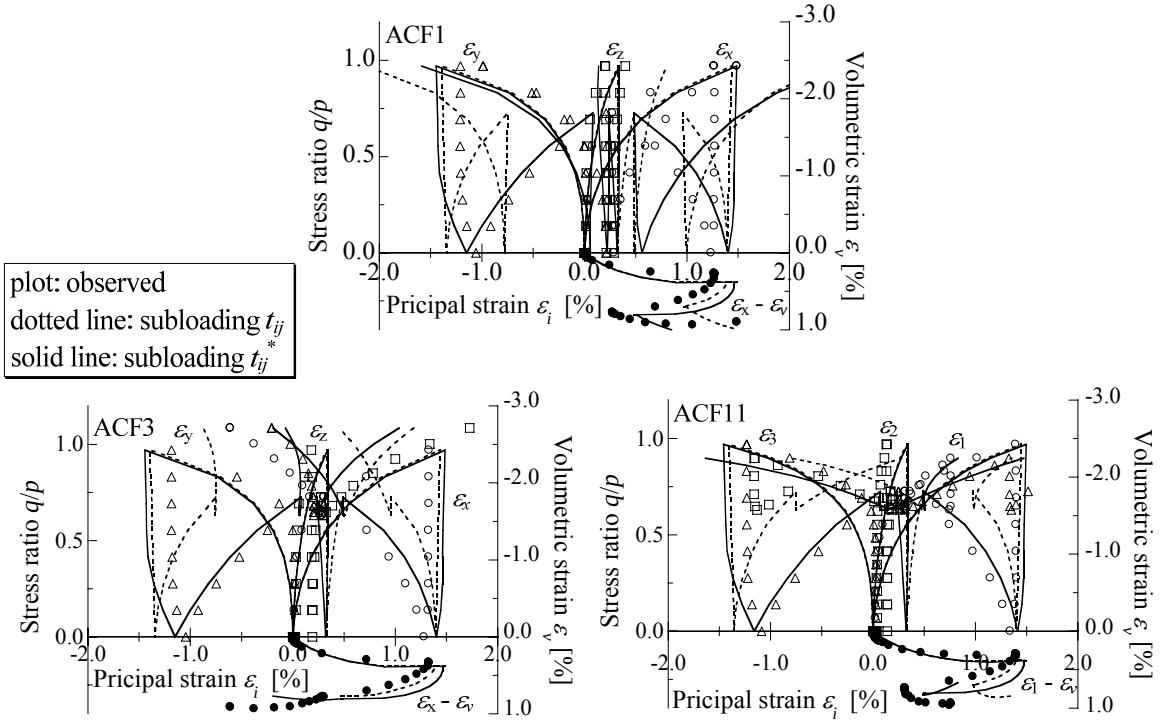


Figure 4.36 Stress strain relations obtained from the simulations of drained true triaxial tests under constant mean stress : series ACF (a) path ACF1 (b) path ACF3 (c) path ACF11

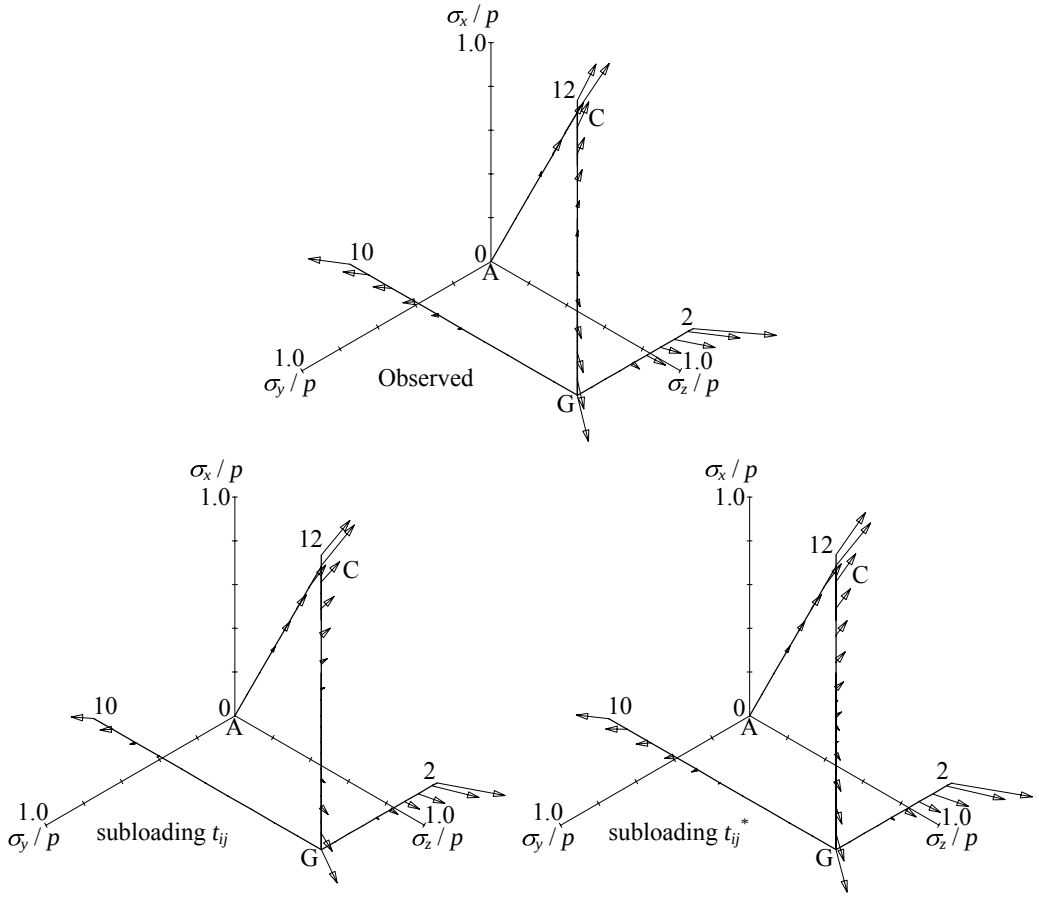


Figure 4.37 Stress paths and strain increment vector in stress ratio plane obtained from the simulations of drained true triaxial tests tests under constant mean stress : series ACG (a) experiments (b) subloading $t_{ij}$ model (c) subloading $t_{ij}^*$ model

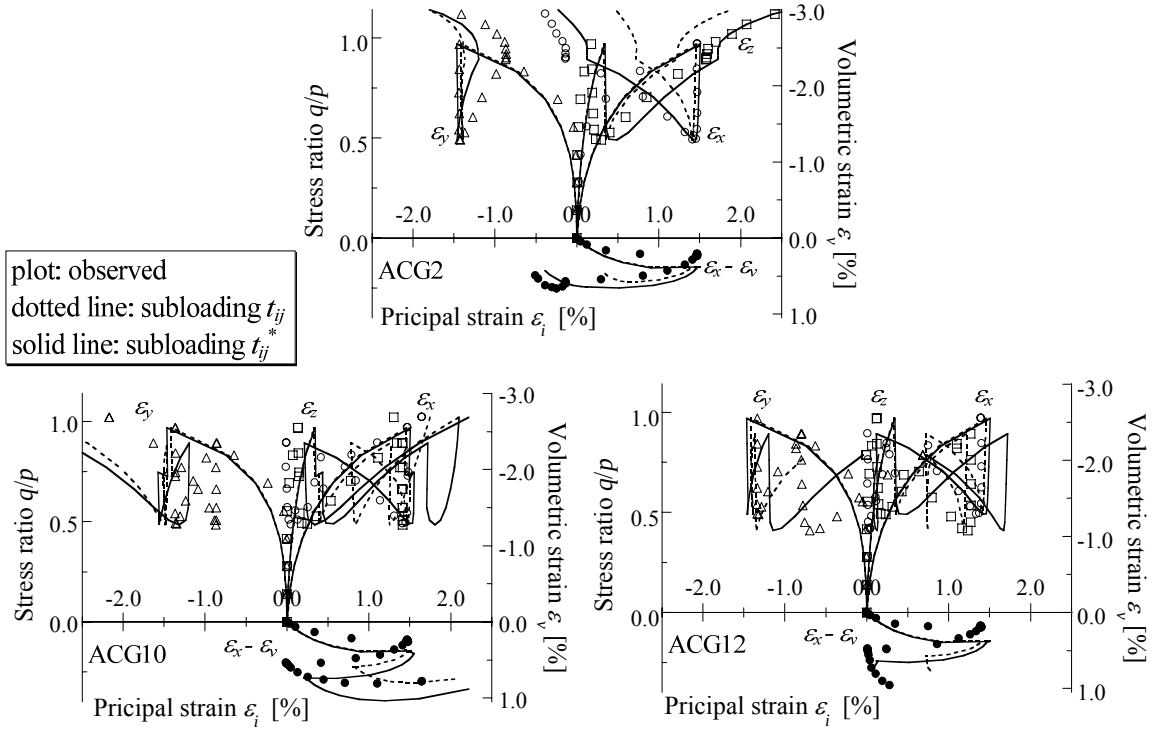


Figure 4.38 Stress strain relations obtained from the simulations of drained true triaxial tests under constant mean stress : series ACG (a) path ACG2 (b) path ACG10 (c) path ACG12

can be seen in the experimental results (Figure 4.38). As concerns strain increment vectors shown in Figure 4.37, furthermore, both direction and length of the calculated vectors by the proposed model show much better agreement with that of the observed results than the calculated one by the original subloading $t_{ij}$ model. So, the simple isotropic hardening model based on the modified stress $t_{ij}^*$ can exquisitely represent complex change of shear stiffness and strain increment due to the induced anisotropy which develops and decay under the difference of principal stress condition with no rotation of the principal axes.

Directional shear cell tests

32 directional shear cell tests were performed under plane strain conditions ($\varepsilon_z$ = 0). The mean stress in shearing plane has been held constant in all the tests. Stress probe tests with rotation of the principal axes and a test in which the principal axes are rotated at constant principal stresses are shown.

[AB series]

Figures 4.39 (a) and (b) show the stress paths of probe tests in the $\tau_{xy}$ : ($\sigma_x$ - $\sigma_y$) / 2 plane and the observed (solid line) and calculated (dot line: (a) subloading $t_{ij}$ model and (b) proposed subloading $t_{ij}^*$ model)) vectors of strain increments indicated in the $d\gamma_{xy}$ / 2 : ($d\varepsilon_x$ - $d\varepsilon_y$) / 2 plane which is conjugate to the $\tau_{xy}$ : ($\sigma_x$ - $\sigma_y$) / 2 plane. In these tests, the samples have been firstly compressed isotropically to A ($\sigma_x$ = $\sigma_y$ = $\sigma_z$ = 34.5 kPa) and sheared in plane strain to B (($\sigma_x$ - $\sigma_y$)/2= 18.6 kPa, $\tau_{xy}$ = 0 kPa), without rotation of the principal axes. Probes in different directions (($\sigma_x$ - $\sigma_y$)/2, $\tau_{xy}$) = B: (18.6, 0.0) kPa, C: (20.7, 5.2) kPa, D: (18. 1, 11.4) kPa, E: (-4.8, 23.4) kPa, F: (-16.5, 13.8) kPa) have then been applied. Although the calculated results by both proposed model and subloading $t_{ij}$ model can describe the behavior of the experimental results in stress path ABC, both length and direction of calculated vectors by those models are not necessarily agreement with those of the observed vectors in stress path ABD, E and F in which the rotation angle of the principal axes is larger. From the observed results in path ABD, E and F, moreover, the non-coaxiality between stress and strain increment, which means that the direction of strain increment deviate from the radial directions on the $\tau_{xy}$ : ($\sigma_x$ - $\sigma_y$) / 2 plane, with rotating of the principal axes of stress can be observed. It can be seen from strain increment on $\tau_{xy}$ axis in stress path ABE and ABF that proposed model can represent such non-coaxiality between stress and strain increments, while the original subloading $t_{ij}$ model in which plastic strain increment is uniquely

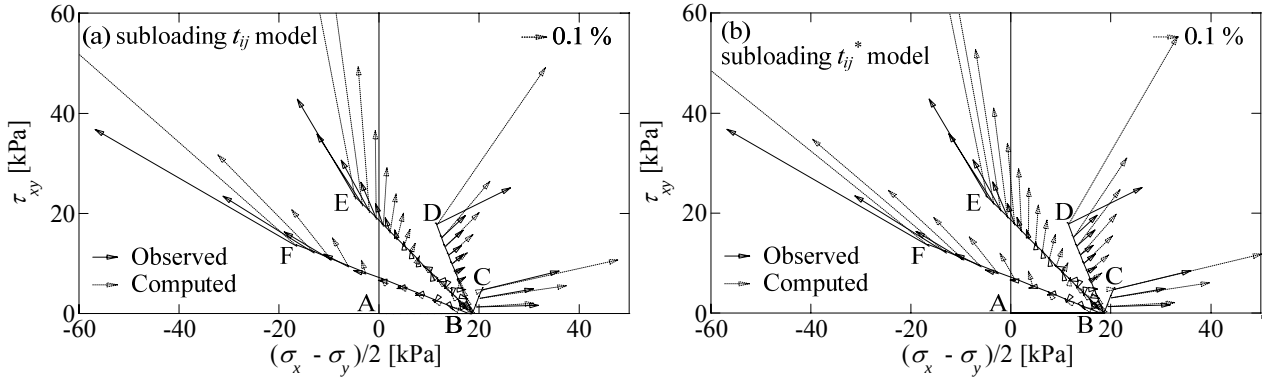


Figure 4.39 Stress paths and strain increment vector in the $\tau_{xy}$ : ($\sigma_x$ - $\sigma_y$) / 2 plane obtained from the simulations of drained directional shear tests under plane strain condition : series AB (a) subloading $t_{ij}$ model, (b) subloading $t_{ij}^*$ model

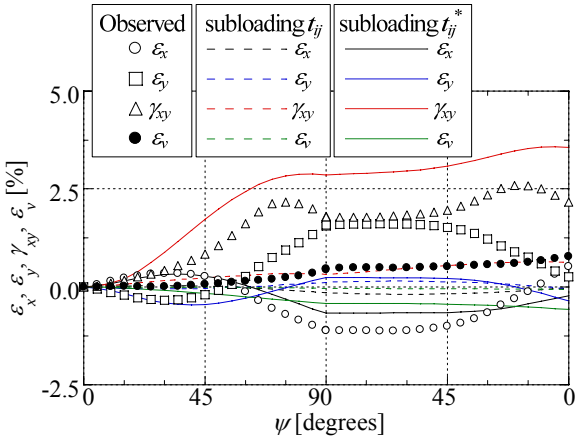


Figure 4.40 Comparison between experimental results of the directional shear test with rotating principal stress axes 90 degrees under plane strain condition ($\varepsilon_z = 0$) with calculated results by subloading $t_{ij}$ model and subloading $t_{ij}^*$ model

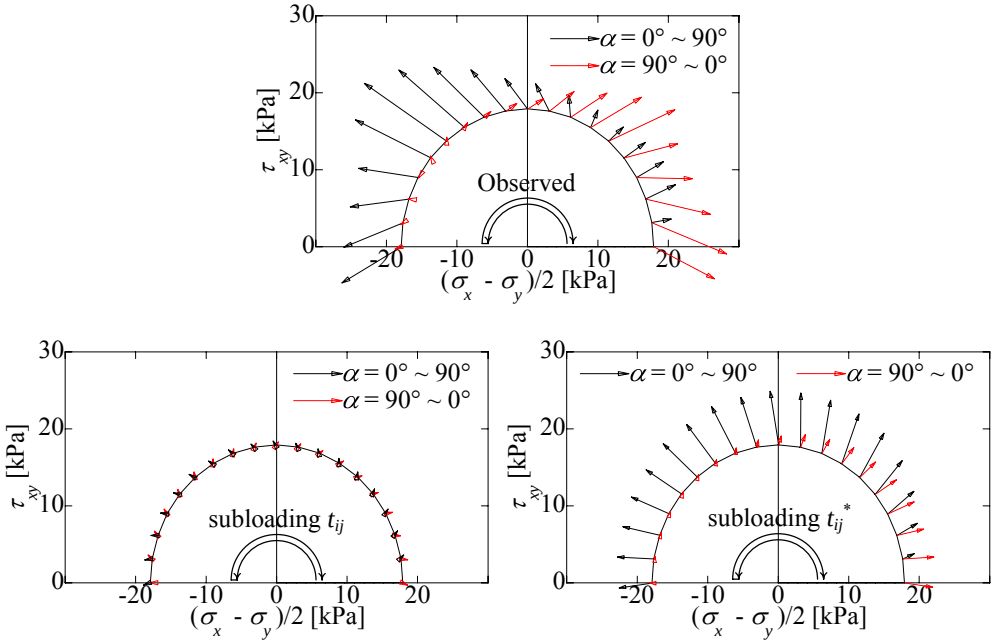


Figure 4.41 Stress paths and strain increment vector in the $\tau_{xy}$ : $(\sigma_x - \sigma_y) / 2$ plane obtained from the simulations of drained directional shear tests under plane strain condition : series CIR (a) experiment, (b) subloading $t_{ij}$ model, (c) subloading $t_{ij}^*$ model

determined from the current stress state, viz., associated flow rule, cannot represent such phenomenon. As explained in section 4.4, this is because that the non-coaxiality between new modified stress $t_{ij}^*$ (or transformation tensor $a_{ij}^*$) and ordinary stress $\sigma_{ij}$ is considered here.

[CIR series with rotation of principal stress axes]

Figure 4.40 and 4.41 show the observed and calculated results of rotation of principal stress axes. The principal stress axes rotate 90 degrees under plane strain condition ($\varepsilon_z = 0$) from a stress state ($(\sigma_x - \sigma_y) / 2 = 17.9$ kPa, $\tau_{xy} = 0$ kPa) and then back to the original state of stress. Figure 4.40 indicates the variation of each

strain component with the angle between $x$-axis and major principal stress axis. In Figure 4.41, the stress paths in the $(\sigma_x - \sigma_y) / 2 : \tau_{xy}$ plane are shown together with the directions of strain increments represented by the conjugate $d\gamma_{xy} / 2 : (d\varepsilon_x - d\varepsilon_y) / 2$ relation, in which dots denote observed results, solid lines denote calculated results by the proposed model and original subloading $t_{ij}$ model. From the experimental results, there seems that non-coaxiality between stresses and strain increments during the rotation of the principal axes occurs; the elastic region exists just after reversed rotation in a similar manner as reversed shear loading. The original subloading $t_{ij}$ model exhibits little strain during the rotation of the principal stress axes because stress invariants of ordinary isotropic hardening model ($t_N$ and $t_S$) remains constant under pure rotation of the principal stress axes. In contrast, there is rather good agreement between the observed results and the results calculated by the proposed model. So, the proposed model can represent the development of plastic strain due to the rotation of the principal stress axes and the non-coaxiality of stress and strain increments.

## 4.6 Summary

The elastoplastic constitutive models in which the void ratio is the main state variable to describe the various isotropic features of soil are shown in Chapters 2 and 3, while the modeling of anisotropic deformation and strength characteristics of soil due to the change of the interparticle contacts situation, which are not considered in those models, have been discussed and proposed in this chapter. By applying not kinematic / rotational hardening rule in ordinary stress space $\sigma_{ij}$ but the modified stress already considering the influence of anisotropy, the induced anisotropy, in which the influence of intermediate stress $\sigma_2$ and stress history are considered, was modeled in a simple isotropic hardening model. The validation of proposed model was verified by parametric study and comparison with experimental results. The main results of this chapter are summarized as follows:

(1) The soil anisotropy is discriminated between the inherent anisotropy and the induced anisotropy. In this study, the induced anisotropy is regarded as a dominant factor of investigation of soil anisotropy, because the inherent anisotropy can be treated as a certain type of the stiff induced anisotropy developing by the gravity force in sediment process. The induced anisotropy develops with changing of the situation of interparticle contacts (the variation in contact normals) under any anisotropic loading path. The fabric tensor $F_{ij}$ representing the orientation of contact normals is well known as the proper tensor quantity evaluating the soil fabric.

(2) In the kinematic / rotational hardening rule, the variables determining the position of yield surface and its evolution rule have no physical meaning and are determined by juts fitting to experimental results. On the other hand, the physical meaning of the modeling based on fabric tensor reflecting on the orientation of contact normals is very clear, and it can be applied to a simple isotropic hardening model. It is, however, difficult to quantitatively estimate the variation of the fabric change. Appropriate models formulated with the fabric tensor, therefore, which can be applied to the analysis of initial / boundary value problems have

not been developed yet.

(3) It was indicated from the experimental (Oda, Satake) and analytical (Maeda) results that the transformation tensor $a_{ij}$ based on $t_{ij}$ concept corresponds to observed fabric tensor $F_{ij}$, i.e., the influence of the intermediated stress $\sigma_2$ is regarded as a part of the induced anisotropy, under monotonic loading. The modified stress $t_{ij}$ (and the transformation tensor $a_{ij}$), therefore, were extended to the new modified stress $t_{ij}^*$ (and the transformation tensor $a_{ij}^*$) considering the influence of the intermediate stress $\sigma_2$ and stress histories simultaneously in this study.

(4) An evolution rule of the transformation tensor $a_{ij}^*$ used for obtaining the new modified stress tensor $t_{ij}^*$ is given to satisfy the following experimental facts; Ⓓ The deformation and strength characteristic of soil is independent of the past stress histories: $da_{ij}^* = da_{ij}$ & $a_{ij}^* = a_{ij}$ *during monotonic loading and at failure*, Ⓔsoil fabric is constant during unloading as the fabric of interparticle contact hardly changes under unloading condition: $da_{ij}^* = 0$ & $a_{ij}^* \perp a_{ij}$ *during reversal loading*, ⒻAfter the non-monotonic loading path (changing the direction of stress path on octahedral plane), soil is affected by the influence of the stress histories in subsequent stress path: $da_{ij}^* \perp da_{ij}$ & $a_{ij}^* \perp a_{ij}$ *during non-monotonic loading*, ⒼThe influence of the stress histories gradually decays with the development of plastic deformation: $da_{ij}^* \bowtie \|d\varepsilon_{ij}^p\|$( $a_{ij} \rightarrow a_{ij}^*$)

(5) Only by defining the yield function $f$ with the parameters of $t_{ij}^*$ ($t_N^*$, $t_S^*$) instead of that of $\sigma_{ij}$ ($p$, $q$) and assuming associated flow rule in $t_{ij}^*$-space, any isotropic hardening model can be extended to one considering the induced anisotropy with keeping the features of original model. Subloading $t_{ij}$ model as an example was extended in this study. The flow rule determining the direction of plastic strain increment is assumed in $t_{ij}^*$-space. $t_{ij}^*$-space is not necessarily coaxial to $\sigma_{ij}$-space, moreover, so that the proposed method can describe the non-coaxiality between ordinary stress $\sigma_{ij}$ and the plastic strain increment $d\varepsilon_{ij}^p$.

(6) The validation of the proposed model was verified through the parametric study and comparison with the observed results of various laboratory tests. It was indicated from the parametric study that the proposed model can represent the three-dimensional behavior of soil with past stress history as seen in the experimental results on Hostun sand by Lanier. From comparison of the results of triaxial tests on Toyoura sand with the corresponding calculated results, it was revealed that the proposed model adequately describes the increasing and decreasing of stiffness during reloading and reversal loading path, anisotropic deformation under isotropic condition and others due to the past sheared histories. From comparison with the results of true triaxial tests on Leighton Buzzard sand, it was shown that the proposed model, which obeys isotropic hardening rule and follows associated flow rule in $t_{ij}^*$ space, can follow the variation in stiffness and the direction of strain increment affected by the past stress histories under complicated three dimensional stress paths. It could be seen from comparison with the directional shear cell tests, moreover, that proposed model can represent the non-coaxiality between stress and strain

increment, and the development of plastic deformation with rotating of the principal stress axes under constant stress ration $q/p$.

# Appendix
# Extension to model considering stress path dependency on the direction of plastic flow

According to usual plasticity, the direction of plastic flow (direction of plastic strain increments) is independent of the direction of stress increment. It is, however, experimentally known that the direction of plastic flow is influenced by the direction of stress increments except at and after peak strength. In the previous models for clay and sand ($t_{ij}$-clay model (Nakai) and $t_{ij}$-sand model (Nakai)), such stress path dependency was considered by dividing the plastic strain increment into two components – the plastic strain increment $d\varepsilon_{ij}^{p(\mathrm{AF})}$ satisfying the associated flow rule in $t_{ij}$ space as mentioned above and the isotropic plastic strain increment $d\varepsilon_{ij}^{p(\mathrm{IC})}$ under increasing mean stress – in spite of using just one yield function and one strain hardening parameter. The same method is employed in the present modeling to consider the stress path dependency on the direction of plastic flow. Referring to Equation (4.28) and (4.32), we can express the plastic volumetric strain increment by

$$d\varepsilon_v^p = d\varepsilon_{mm}^p = \Lambda \frac{\partial f}{\partial t_{mm}^*} = \frac{\left( \dfrac{\partial f}{\partial \sigma_{ij}} + \dfrac{\partial f}{\partial a_{kl}^*} \dfrac{\partial a_{kl}^*}{\partial \sigma_{ij}} \right) d\sigma_{ij}}{\dfrac{1}{C_p} \dfrac{\partial f}{\partial t_{kk}^*} - \mu \dfrac{\partial f}{\partial a_{ij}^*} \left( a_{ij}^* - a_{ij} \right) \left\| \dfrac{\partial f}{\partial t_{kl}^*} \right\|} \cdot \frac{\partial f}{\partial t_{mm}^*} \tag{A1}$$

Under isotropic compression condition ($X^* = 0$), the following equation hold.

$$t_{N1}^* = t_N^* = p \tag{A2}$$

$$\frac{\partial f}{\partial t_{mm}^*} = \frac{1}{t_N^*} a_{mm}^{\#} \tag{A3}$$

and the plastic volumetric strain increment is expressed as

$$d\varepsilon_v^p = \frac{1}{\dfrac{1}{C_p}\left(1 + \dfrac{G(\rho)}{a_{mm}^{\#}}\right)} \cdot \frac{dt_N^*}{t_N^*} \tag{A4}$$

It is assumed that the plastic volumetric isotropic strain increment $d\varepsilon_v^{p(\mathrm{IC})}$ in general stress conditions, which occurs at $dt_N^* > 0$, is $t_N^* / t_{N1}^*$ of the plastic volumetric strain $d\varepsilon_v^p$ given by Equation (A4) in the same way as the $t_{ij}$-clay model (Nakai and Matsuoka, 1986)

$$d\varepsilon_v^{p(IC)} = \frac{1}{\dfrac{1}{C_p}\left(1 + \dfrac{G(\rho)}{a_{mm}^{\#}}\right)} \cdot \frac{\left\langle dt_N^* \right\rangle}{t_N^*} \cdot \frac{t_N^*}{t_{N1}^*} \tag{A5}$$

where, form Equation (4.21), the ration $t_N^* / t_{N1}^*$ is expressed by the following equation:

$$\frac{t_N^*}{t_{N1}^*} = \exp\left(-\varsigma\left(X^*\right)\right) = \exp\left( -\frac{1}{\beta}\left(\frac{X^*}{M^*}\right)^{\beta} \right) \tag{A6}$$

The expression for $dt_N^*$ is shown in Appendix IV, together with the derivatives of some functions based on the $t_{ij}^*$-concept. Therefore, the plastic strain increment is $d\varepsilon_{ij}^{p(\mathrm{IC})}$ give by

$$d\varepsilon_{ij}^{p(IC)} = d\varepsilon_v^{p(IC)}\frac{\delta_{ij}}{3} = \frac{\dfrac{1}{t_N^*}\left\langle dt_N^*\right\rangle}{\dfrac{1}{C_p}\left(1+\dfrac{G(\rho)}{a_{mm}^{\#}}\right)}\cdot\frac{\delta_{ij}}{3} = \frac{\dfrac{1}{t_N^*}\left\langle dt_N^*\right\rangle}{\dfrac{1}{C_p}\left(1+\dfrac{a_{IC}\rho^2}{a_{mm}^{\#}}\right)}\cdot\frac{\delta_{ij}}{3} \tag{A7}$$

Where the symbol < > denotes the Macaulay bracket as mentioned before.

When the Cam clay model was formulated, it was based on Henkel's (1960) experimental results on normally consolidated clays, which showed a unique surface in $p - q - e$ space independent of stress paths. Therefore, we assume that in the same ways as the $t_{ij}$-clay model the present model satisfies the unique relation between $\varepsilon_v^p$ and stresses at normally consolidated state ($\rho = 0$; $G(\rho) = 0$), even though the strain increment consists of the two components. From Equation (4.21), (4.22), (4.28) and (A7), normally consolidated soils satisfy the following condition.

$$\begin{aligned}
&\frac{\partial f}{\partial\sigma_{ij}}d\sigma_{ij}+\frac{\partial f}{\partial a_{ij}^*}da_{ij}^* = \frac{1}{C_p}d\varepsilon_v^p = \frac{1}{C_p}\left(d\varepsilon_v^{p(AF)}+d\varepsilon_v^{p(IC)}\right) = \frac{1}{C_p}\left(\Lambda^{(AF)}\frac{\partial f}{\partial t_{kk}^*}+C_p\frac{1}{t_{N1}^*}\left\langle dt_N^*\right\rangle\right)\\
&\left(\frac{\partial f}{\partial\sigma_{ij}}+\frac{\partial f}{\partial a_{kl}^*}\frac{\partial a_{kl}^*}{\partial\sigma_{ij}}\right)d\sigma_{ij} = \frac{1}{C_p}\left(\Lambda^{(AF)}\frac{\partial f}{\partial t_{kk}^*}+C_p\frac{1}{t_{N1}^*}\left\langle dt_N^*\right\rangle\right)-\mu\Lambda^{(AF)}\left\|\frac{\partial f}{\partial t_{kl}^*}\right\|\frac{\partial f}{\partial a_{ij}^*}\left(a_{ij}-a_{ij}^*\right)
\end{aligned} \tag{A8}$$

From this equation, we can obtain the proportionality constant of $d\varepsilon_{ij}^{p(\mathrm{AF})}$ at normally consolidated state ($\rho = 0$; $G(\rho) = 0$) by the following equation, which is the same as that in the $t_{ij}$-clay model (Nakai and Matsuoka, 1986).

$$\Lambda^{(AF)} = \frac{\left(\dfrac{\partial f}{\partial\sigma_{ij}}+\dfrac{\partial f}{\partial a_{kl}^*}\dfrac{\partial a_{kl}^*}{\partial\sigma_{ij}}\right)d\sigma_{kl}-\dfrac{1}{t_{N1}^*}\left\langle dt_N^*\right\rangle}{\dfrac{1}{C_p}\dfrac{\partial f}{\partial t_{kk}^*}-\mu\left\|\dfrac{\partial f}{\partial t_{kl}^*}\right\|\dfrac{\partial f}{\partial a_{ij}^*}\left(a_{ij}-a_{ij}^*\right)} = \frac{\partial f_\sigma-\dfrac{1}{t_{N1}^*}\left\langle dt_N^*\right\rangle}{h^p} \tag{A9}$$

We the define the stain increment $d\varepsilon_{ij}^{p(\mathrm{AF})}$ at over consolidated as well as normally consolidated state in the following form, referring to Equation (4.32) and (A9),

$$\begin{aligned}
d\varepsilon_{ij}^{p(AF)} &= \Lambda^{(AF)}\frac{\partial f}{\partial t_{ij}^*} = \frac{\left(\dfrac{\partial f}{\partial\sigma_{ij}}+\dfrac{\partial f}{\partial a_{kl}^*}\dfrac{\partial a_{kl}^*}{\partial\sigma_{ij}}\right)d\sigma_{kl}-\dfrac{1}{t_{N1}^*}\left\langle dt_N^*\right\rangle}{\dfrac{1}{C_p}\left(\dfrac{\partial f}{\partial t_{kk}^*}+\dfrac{G(\rho)}{t_N^*}\right)-\mu\left\|\dfrac{\partial f}{\partial t_{kl}^*}\right\|\dfrac{\partial f}{\partial a_{ij}^*}\left(a_{ij}-a_{ij}^*\right)}\cdot\frac{\partial f}{\partial t_{ij}^*}\\
&= \frac{\left(\dfrac{\partial f}{\partial\sigma_{ij}}+\dfrac{\partial f}{\partial a_{kl}^*}\dfrac{\partial a_{kl}^*}{\partial\sigma_{ij}}\right)d\sigma_{kl}-\dfrac{1}{t_{N1}^*}\left\langle dt_N^*\right\rangle}{\dfrac{1}{C_p}\left(\dfrac{\partial f}{\partial t_{kk}^*}+\dfrac{a_{AF}\rho^2}{t_N^*}\right)-\mu\left\|\dfrac{\partial f}{\partial t_{kl}^*}\right\|\dfrac{\partial f}{\partial a_{ij}^*}\left(a_{ij}-a_{ij}^*\right)}\cdot\frac{\partial f}{\partial t_{ij}^*} = \frac{\partial f_\sigma-\dfrac{1}{t_{N1}^*}\left\langle dt_N^*\right\rangle}{h^p}\cdot\frac{\partial f}{\partial t_{ij}^*}
\end{aligned} \tag{A10}$$

Hence, the strain increments, of which the stress path dependency on plastic flow is considered, are

summarized as follows:

(i) elastic region ($\Lambda = df_\sigma / h_p < 0$)

$$d\varepsilon_{ij} = d\varepsilon_{ij}^{e} = \frac{1+\nu_e}{E_e} d\sigma_{ij} - \frac{\nu_e}{E_e} d\sigma_{kk}\delta_{ij} \tag{A11}$$

(ii) elastoplastic region with strain hardening ($\Lambda = df_\sigma / h_p \vdash 0$ and $h_p \vdash 0$)

$$\begin{aligned} d\varepsilon_{ij} &= d\varepsilon_{ij}^{e} + d\varepsilon_{ij}^{p(AF)} + d\varepsilon_{ij}^{p(IC)} \\ &= \frac{1+\nu_e}{E_e} d\sigma_{ij} - \frac{\nu_e}{E_e} d\sigma_{kk}\delta_{ij} \\ &+ \frac{\left(\dfrac{\partial f}{\partial \sigma_{ij}} + \dfrac{\partial f}{\partial a_{kl}^*}\dfrac{\partial a_{kl}^*}{\partial \sigma_{ij}}\right) d\sigma_{kl} - \dfrac{1}{t_{N1}^*}\left\langle dt_N^* \right\rangle}{\dfrac{1}{C_p}\left(\dfrac{\partial f}{\partial t_{kk}^*} + \dfrac{a_{AF}\rho^2}{t_N^*}\right) - \mu\left\| \dfrac{\partial f}{\partial t_{kl}^*} \right\| \dfrac{\partial f}{\partial a_{ij}^*}\left(a_{ij} - a_{ij}^*\right)} \cdot \frac{\partial f}{\partial t_{ij}^*} + \frac{\dfrac{1}{t_N^*}\left\langle dt_N^* \right\rangle}{\dfrac{1}{C_p}\left(1 + \dfrac{a_{IC}\rho^2}{a_{mm}^{\#}}\right)} \cdot \frac{\delta_{ij}}{3} \end{aligned} \tag{A12}$$

(iii) elastoplastic region with strain softening ($\Lambda = df_\sigma / h_p \vdash 0$ and $h_p < 0$)

$$d\varepsilon_{ij} = d\varepsilon_{ij}^{e} + d\varepsilon_{ij}^{p} = \frac{1+\nu_e}{E_e} d\sigma_{ij} - \frac{\nu_e}{E_e} d\sigma_{kk}\delta_{ij} + \frac{\left(\dfrac{\partial f}{\partial \sigma_{ij}} + \dfrac{\partial f}{\partial a_{kl}^*}\dfrac{\partial a_{kl}^*}{\partial \sigma_{ij}}\right) d\sigma_{kl} - \dfrac{1}{t_{N1}^*}\left\langle dt_N^* \right\rangle}{\dfrac{1}{C_p}\left(\dfrac{\partial f}{\partial t_{kk}^*} + \dfrac{a_{AF}\rho^2}{t_N^*}\right) - \mu\left\| \dfrac{\partial f}{\partial t_{kl}^*} \right\| \dfrac{\partial f}{\partial a_{ij}^*}\left(a_{ij} - a_{ij}^*\right)} \cdot \frac{\partial f}{\partial t_{ij}^*} \tag{A13}$$

Figure A1 shows the yield surface $f$ and the present stress state P on the yield surface in $t_N^*$ - $t_S^*$ plane, in which the direction of plastic strain increment $d\varepsilon_{ij}^{p(\mathrm{AF})}$ is indicated by the arrow. Here, the directions of $d\varepsilon_{\mathrm{N}}^{*p}$ and $d\varepsilon_{\mathrm{S}}^{*p}$ coincide with those of $t_N^*$ and $t_S^*$, respectively. When $\Lambda$ is negative and the stress state moves to inside the yield surface (region I), only elastic strain occurs. In the elastoplastic region with strain hardening where the stress state moves to region II, the plastic strain increment is only $d\varepsilon_{ij}^{p(\mathrm{AF})}$. On the other hand, if the stress state moves to region III, the plastic strain increment can be divided into $d\varepsilon_{ij}^{p(\mathrm{AF})}$ and $d\varepsilon_{ij}^{p(\mathrm{IC})}$. The present formulation allows continuous development of strain increment between region II and region III, and the directions of plastic flow are influenced by the stress path at region III. Now, though the proportionality constant $\Lambda^{(\mathrm{AF})}$ of $d\varepsilon_{ij}^{p(\mathrm{AF})}$ is negative if $df_\sigma - dt_{\mathrm{N}}^* / t_{\mathrm{N1}}^*$ becomes negative under some specific path in region III, it is confirmed numerically that the 2nd orderplastic work increment is $dt_{ij}^* d\varepsilon_{ij}^{p}$ still positive even in such case, i.e., $dt_N^*( d\varepsilon_N^{*p(\mathrm{AF})} + d\varepsilon_N^{*p(\mathrm{IC})}) + dt_S^*( d\varepsilon_S^{*p(\mathrm{AF})} + d\varepsilon_S^{*p(\mathrm{IC})}) > 0$.

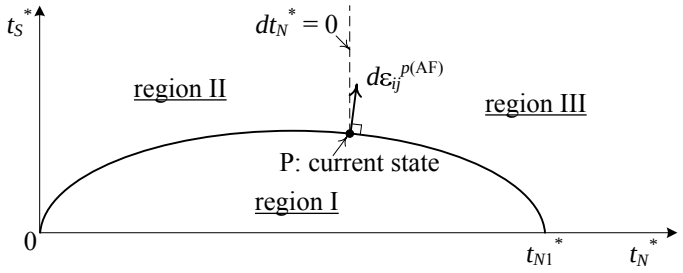


Figure A1 Region in which three kinds of strain increment occur

# Reference


Alawi, M.M., S. Sture and H. Y. Ko (1987): True triaxial and directional shear cell experiments on dry sand, *Interim technical report, University of Colorado*.

Alwaji, H., M. Alawi, H. Y. Ko, S. Sture, J. F. Peters and D. M. Wood (1990): Experimental observation of anisotropy in some stress-controlled tests on dry sand, *Yielding, damage and failure of anisotropic solids (ed. J. P. Boehler) Mechanical Engineering Publications*, London EGF5, 251-264.

Arthur, J. R. F. and Menzies, B. K. (1972): Inherent anisotropy in a sand, *Geotechnique*, Vol. 22, No. 1, 115-129.

Arthur, J. R. F., K. S. Chua and T. Dustan (1977): Induced anisotropy in a sand, *Geotechnique*, Vol. 27, No. 1, 13-30.

Cassagrande, A., and Carillo, N. (1944): Shear failure of anisotropic materials, *Proc. Boston Soc. Civ. Engrs.*, Vol. 31, 74-87.

Chang, C.C. and Hicher, P. Y. (2005): An elastic-plastic model for granular material with microstructural consideration, *International Journal of Solids and Structures*, Vol. 42, 4258-4277.

Dafalias, Y. F. (1986): An anisotropic critical state soil plasticity model:, Mechanics Research Communications, Vol. 13, No. 6, 341-347.

Dafalias, Y. F., Papadimitriou, A. G. and Li, X. S. (2004): Sand plasticity model accounting for inherent fabric anisotropy, *Journal of Engineering Mechanics*, Vol. 130, No. 11, 1319-1333.

Gardiner, B. S. and Tordesillas, A. (2005): Micromechanical constitutive modeling of granular media: evolution and loss of contact in particle clusters, *Journal of Engineering Mathematics*, Vol. 52, 93-106.

Hashiguchi, K. (1980): Constitutive equation of elastoplastic materials with elasto-plastic transition, *J. of Applied Mech.*, ASME, 102(2), 266-272.

Hashiguchi, K. (2001): Description of inherent / induced anisotropy of soils: rotational hardening ruled with objectivity, *Soils and Foundations*, Vol. 41, No.6, 139-145.

Iai, S. (1993): Concept of effective strain in constitutive modeling of granular materials, *Soils and Foundations*, Vol. 33, No. 2, 171-180.

Kanatani, K. (1981): A theory of contact force distribution in granular materials, *Powder Technology*, Vol. 28, No. 2, 167-172.

Kikumoto, M., Nakai, T., Zhang, F., Hinokio, M. and Kyokawa, H. (2007): Expression of induced anisotropy of soils using isotropic hardening rule in modified stress space, *Proc. of the International conference on Numerical Models in Geomechanics* (NUMOG X), Rhodes, Greece, 85-91.

Kikumoto, M., Nakai, T., Kyokawa, H., Zhang, F. and Shahin, H. M. (2008): A unified method to describe the influence of intermediate principal stress and stress history in constitutive modeling, *Proc. of the 2nd international workshop on Geotechnics of Soft Soils Focus on Ground Improvement*, Glasgow, United Kingdom, 151-157.

Kikumoto, M., Nakai, T. and Kyokawa, H. (2009): New description of stress-induced anisotropy using modified stress, *Proc. of the 17th International Conf. on Soil Mechanics and Geotechnical Engineering*, Alexandria, Egypt, 550-553.

Ko, H. Y. and R. F. Scott (1967): A new soil testing apparatus, *Geotechnique*, Vol. 17, No. 1, 40-57.

Kyokawa, H., Kikumoto, M. and Nakai, T. (2008): Extension of the modified stress tij to describe the induced anisotropy, *Proc. of the 4th international workshop in New Frontiers in Computational Geotechnics*, Pittsburgh, USA, 13-18.

Kyokawa, H., Kikumoto, M. and Nakai, T. (2010): Description of stress-induced anisotropy of soils by modified stress within an Isotropic hardening elastoplastic model, *Japanese Geotechnical Journal*, Vol. 5, No.4 (accepted). (in Japanese)

Lanier, J. (1987): Essais tridimensionnels sur le sable d'Hostun, *Rapport Scientifique Greco Geomateriaux*.

Li, X. S. and Dafalias, Y. F. (2002): Constitutive modeling of inherently anisotropic sand behaviour, *Journal of Geotech. Geoenviron. Engng. ASCE*, Vol. 128, No. 10, 868-880.

Li, X. S. and Dafalias, Y. F. (2002): A constitutive framework for anisotropic sand including non-proportional loading, *Geotechnique*, Vol. 54, No. 1, 41-55.

Maeda, K. and Hirabayashi, H. (2006): Influence of grain properties on macro mechanical behaviors of granular media by DEM, Applied Mechanics, Vol. 9, 623-630.

Majmudar, T. S. and Behriger, R. P. (2005): Contact forces and stress induced anisotropy, *Proc. of the 5th Int. Conf. on Micromechanics of Granular Media* (*Powders and Grains 2005*).

Miura, K., Miura, S. and Toki, S. (1986): Deformation behavior of anisotropic dense sand under principal stress axes rotation, *Soils and Foundations*, Vol. 26, No. 1, 36-52.

M. M. Mehrabadi and S. Nemat-Nasser (1983): Stress, dilatancy and fabric in granular materials, *Mechanics of Materials*, Vol. 2, 155-161.

Nagai, H. (2003): *Master's Thesis, Nagoya Institute of Technology*.

Nakai, T. and Hinokio, M. (2004): A simple elastoplastic model for normally and over consolidated soils with unified material parameters, *Soils and Foundations*, Vol. 44, No. 2, 53-70.

Nakai, T., Hoshikawa, T., Hinokio, M., Yoshida, H., Korenaga, Y. and Chowdhury, E. Q. (2001): Formulation of the influence of the density and the stress path dependency of plastic flow in sand, *Proc.of Powders and Grains*, 217-221.

Nakai, T. and Matsuoka, H. (1986): A generalized elastoplastic constitutive model for clay in three-dimensional stresses, *Soils and Foundations*, Vol. 26, No. 3, 81-98.

Nakai, T. and Mihara, Y. (1984): A new mechanical quantity for soils and its application to elastoplastic constitutive models, *Soils and Foundations*, vol. 24, No. 2, 82-94.

Nakata, Y., Hyodo, M., Murata, H. and Yasufuku, N. (1998): Flow deformation of sands subjected to principal stress rotation, *Soils and Foundations*, Vol. 38, No. 2, 115-128.

Oda, M. (1972): The mechanism of fabric changes during compressional deformation of sand, *Soils and Foundations*, Vol. 12, No. 2, 1-18.

Oda, M. (1993): Inherent and induced anisotropy in plasticity theory of granular soils, *Mechanics of Materials*, Vol. 16, Issues 1-2, 35-45.

Oda, M., Nakayama, H. (1988): Introduction of inherent anisotropy of soils in the yield function, Micromechanics of Granular Materials, 81-90.

Oda, M., S. Nemat-Nasser and M. M. Mehrabadi (1982): A statistical study of fabric in a random assembly of spherical granules, *Int, J, Num, Anal, Merhods Geomech*, Vol. 6, 77-94

Oda, M., Nemat-Nasser, S. and Konishi, J. (1985): Stress-induced anisotropy in granular masses, Soils and Foundations, Vol. 25, No. 3, 85-97.

Oda, M. and Sudoo, T. (1989): Fabric tensor showing anisotropy of granular soils and its application to soil plasticity, *Powders and Grains*, 155-161.

Stake, M. (1978): Constitution of mechanics of granular materials through the graph theory, *U.S.-Japapan Seminar on Continuum-Mechanics and Statistical Approaches in the Mechanics of Granular Materials*, 47-62.

Satake, M. (1982): Fabric tensor in granular materials, *Proc. of IUTAM-Conference on Deformation and Failure of Granular Materials*, pp. 63-68.

Satake, M. (1984): Consideration on induced anisotropy by use of the fabric tensor, *Proc. of conference of the Japanese soil mechanics society in Matsuyama*, No. 128, 301-302. (in Japanese)

Tanaka, Y., Nakase, H. and Kato, K. (2009): DD DEM simulation of hollow cylinder drained testing and fabric anisotropy of sand, *Report of research center for urban safety and security Kobe University*, Vol. 13, 21-27.

Tatsuoka, F., Sakamoto, T., Kawamura, T. and Fukushima, S. (1986): Strength and deformation characteristics of sand in plane strain compression at extremely low pressures, *Soils and Foundations*, Vol. 26, No. 1, 65-84.

Tobita, Y. (1988): Yield condition of anisotropic granular materials, *Soils and Foundations*, Vol. 28, No. 2, 113-126.

Tobita, Y. and Yanagisawa, E. (1988): Contact tensor in constitutive model for granular materials, *Micromechanics of Granular Materials*, 263-271.

Yang, Z. X., Li, X. S. and Yang, J. (2008): Quantifying and modeling fabric anisotropy of granular soils, *Geotechnique*, Vol. 58, No. 4, 237-248.

Yimsiri, S. and Soga, K. (2010): DEM analysis of soil fabric effects on behaviour of sand, Geotechnique, Vol. 60, No. 6, 483-495.

Yoshimine, M. (2006): Generalized Coulomb's criterion for 3-dimensional stress conditions, *Soils and Foundations*, Vol. 46, No.2, 259-266.

Yoshimine, M. and Ishihara, K. (1998): Flow potential of sand during liquefaction, *Soils and Foundations*, Vol. 38, No. 3, 187-196.

Yoshimine, M., Ishihara, K. and Bargas, W. (1998): Effects of principal stress direction and intermediate principal stress on drained shear behavior of sand, *Soils and Foundations*, Vol. 38, No. 3, 177-186.

# Chapter 5 Conclusion and Future work

## 5.1 Summary and Conclusion

Although the stress-strain behavior of soils as the granular materials is different depending on its ingredients (e.g., grain shape and size), it is also affected by its property (density, bonding, degree of saturation, temperature) and several loading condition (e.g., cyclic loading, stress history, strain rate and creep). In this study, various features of soil were described inclusively on the basis of the Cam clay model, which can describes the deformation and strength of soil due to “consolidation” and “shear” simultaneously. The explanation of modeling in this study is, then, divided to two parts as shown in Figure 5.1.

The first part is the modeling of scalar indices features affecting on the mechanical characteristics of soil (Chapter 2 & 3), viz., density, bonding, temperature, strain-rate and partial saturation shown in the upper part of Figure 5.1. Such scalar quantities as change of void ratio or reference state if current void ratio, i.e., the normally consolidated line (or critical state line), are focused on in the modeling. The second part is the modeling of the anisotropy (Chapter 4), viz., the influence of the intermediate principal stress, stress histories, non-coaxiality shown in the lower part of Figure 5.1. Tensor quantity such as a fabric tensor representing the distribution of contact normals is, then, needed for the modeling of such anisotropic effects. The essential findings in this thesis are summarized as follows:

*Modeling of the effect of several features affecting on the volumetric characteristics of soil - the influences of density, bonding, temperature, strain-rate, partial saturation* (*Chapter 2 &3*)

In Chapter 2, in order to formulate the elastoplastic constitutive model of soils considering the various isotropic features of soil behavior, the one-dimensional model (the relation between one-dimensional stress $\sigma$ and void ratio $e$) for normally consolidated soil was firstly presented. This model was then extended to one considering the influence of density, bonding and external factors (i.e., temperature, strain-rate, degree of saturation and others) with reference to the experimental evidences. Since all of such features can be incorporated to simple one-dimensional model, it is easy to understand the interpretation of such behavior and also elastoplastic modeling. And those one-dimensional models can be extended to the corresponding multi-dimensional models (the relation between stress tensor $\sigma_{ij}$ and strain tensor $\varepsilon_{ij}$) easily.

(1) The modeling of normally consolidated soil; The fundamental one-dimensional yield function (stress-strain relation), in which hardening parameter is given as the plastic change of void ratio $(-\Delta e)^p$, is derived from general isotropic consolidation test on normally consolidated soil.

(2) Over consolidated soil shows elastoplastic behavior even in elastic region and stiffer behavior with larger over consolidation ratio. A simple method to describe the behavior of over consolidated soil was developed by introducing one state variables “$\rho$”, which is a vertical distance between current void ratio and void ratio at *NCL* under same stress level, and its evolution rule.

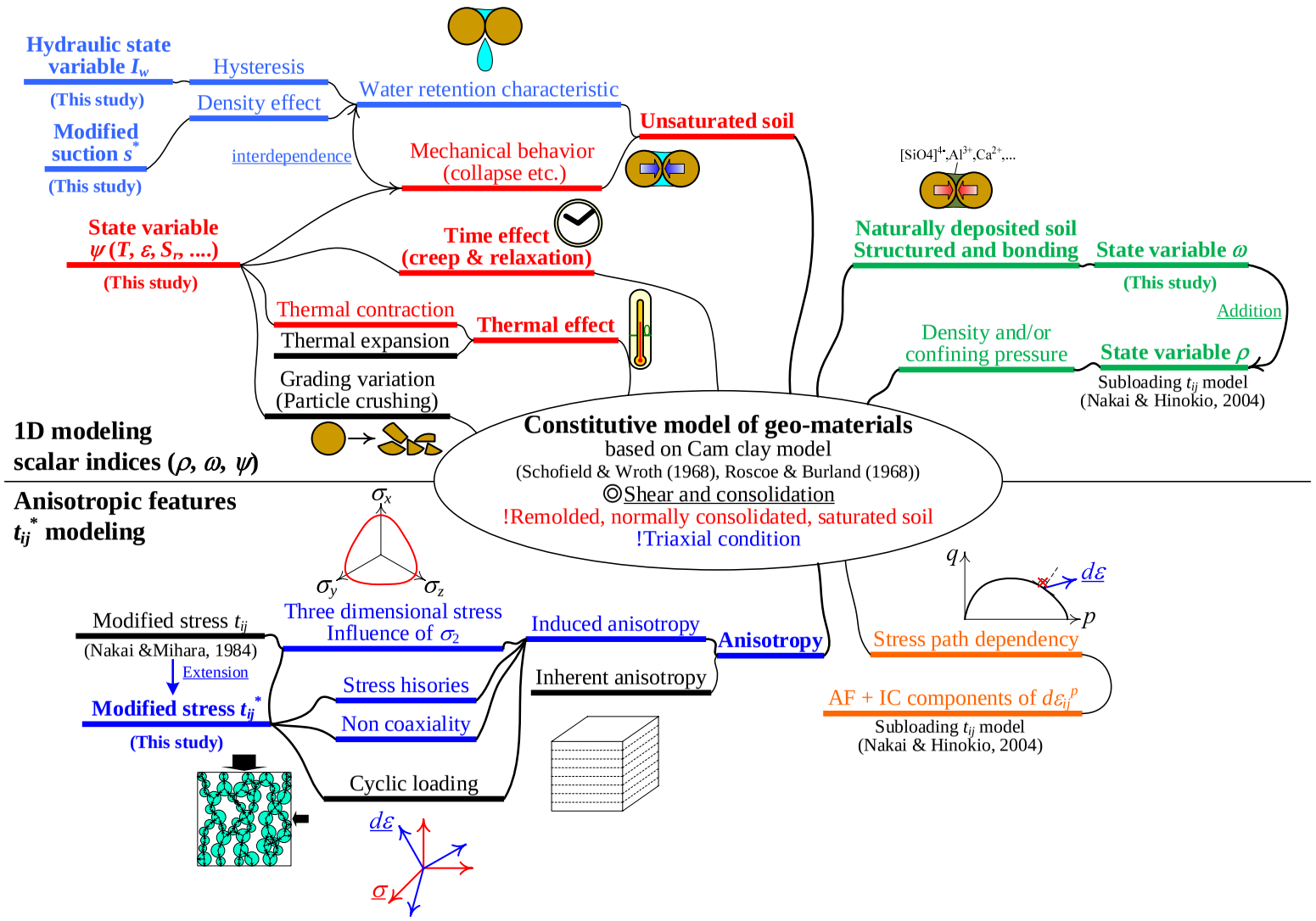


Figure 5.1 The relationships between unified constitutive model of geo-materials and its various features in this study.
The explanation of modeling in this study is divided to two parts. One is on the modeling of scalar indices features affecting on the mechanical characteristics of soils. Another one is on the modeling of the anisotropic features.

The structured soil is stiffer than non-structured over consolidated soil, even if the density state variable $\rho$ is the same. By adding the influence of bonding "$\omega$" to an evolution rule of state variable "$\rho$", therefore, the behavior of structured soil which shows the complex stiffness change with dissipation of bonding was described.

(3) It is experimentally known that temperature, strain rate and partial saturation (degree of saturation and suction) isotropically affect on the behavior of soils as well as the effects of density and bonding. And it was supposed from past experimental results about those effect that the position of normally consolidated line (*NCL*) shifts due to variation in each parameter, i.e., temperature $T$, strain rate $\dot{\varepsilon}$, and degree of saturation $S_r$. In order to model theses features, a state valuable $\psi$ given as a function of temperature, strain rate (rate of void ratio change), degree of saturation and others, was introduced. It was shown from parametric studies that the proposed model can represent the pre-consolidation pressure increase (and decreasing) according to cooling (and heating), increasing (and decreasing) strain rate, and decreasing (/ increasing) degree of saturation; soil compresses due to rising of temperature, creep characteristic and soaking collapse.

(4) In order to extend the one-dimensional model to the multi-dimensional model, the yield function for the multi-dimensional model is given only by replacing $\sigma_0$ and $\sigma$ in the yield function of any one-dimensional model with $p_0$ and $p_1$. And the associated flow rule is assumed in ordinary stress space to determine the direction of plastic strain increment. Moreover, by using the invariants of modified stress $t_{ij}$ concept: $t_{N0}$ and $t_{N1}$ instead of $p_0$ and $p_1$, and assuming the flow rule in $t_{ij}$ space, this model can take account of the influence of intermediate principal stress $\sigma_2$ on strength and deformation characteristics of soil automatically.

(5) It was shown from parametric studies of multi-dimensional model based on the modified stress $t_{ij}$ for over consolidated structured soil that: the present model can describe the stress-strain behavior of over consolidated soil including positive and negative dilatancy under different void ratio by using the material parameters common with the one-dimensional model; It can also describe the well-known drained and undrained shear behaviors of structured soils in three-dimensional stresses as well as consolidation (one-dimensional) behavior of structured soil only by considering the influence of bonding $\omega$ on the evolution rule of $\rho$.

(6) It was shown from past experimental results that soils with lower temperature, faster strain rate and lower degree of saturation show stiffer behavior and higher strength, even if having the same density and mean stress. Such influences of external factors in multi-dimensional problem can be considered only by changing the positions of normally consolidated line (*NCL*) and critical state line (*CSL*) in the same way as one-dimensional model.

In Chapter 3, the modeling of unsaturated soil which is indispensable for predicting the behavior of real ground was carried out. In addition to the modeling of stress-strain behavior of unsaturated soil, the hydraulic relation of unsaturated soil between suction and degree of saturation, viz., soil water characteristic curve, was modeled in this chapter. By investigating the features of unsaturated soil with reference to past experimental results, the mechanical and hydraulic model on the basis of simple assumptions was proposed in Chapter 3. The main findings are summarized as follows:

(1) Bishop's effective stress tensor is proper for arranging experimental results and formulating the constitutive model, since it was indicated that the critical state strength, the stress-dilatancy relation and the shape of yield surface of saturated soil can be applied to that of unsaturated soil by using this stress tensor.

(2) Soil water characteristic curve (SWCC), which is ordinary represented as the unique relation between degree of saturation $S_r$ and suction $s$, is affected by suction history (hydraulic hysteresis), density, temperature and others. In order to describe the hydraulic hysteresis, new state variable $I_w$ defined as the ratio of interior division of the current hydraulic state ($s$, $S_r$) between two reference states on the main drying and wetting curves was applied to classical SWCC model, van Genuchten model as an example. In order to consider the influence of density (and other external effect), moreover, the modified suction $s^*$ which is formulated by not only suction but also void ratio, temperature and other variables was proposed, and then the ordinary SWCC model is formulated by $s^*$ instead of ordinary $s$. It was shown from the calculated results by the present SWCC model that this model suitably represents that: the scanning curves (hydraulic hysteresis) during cyclic drying and wetting process; the air entry value and water entry value are affected by density; degree of saturation increase with decreasing of void ration (volumetric compression) even under constant suction.

(3) With reference to past experimental results, it was supposed that the influence of degree of saturation on compression and shear characteristics of unsaturated soil can be incorporated by shifting both normally consolidated line (*NCL*) and critical state line (*CSL*) of unsaturated soil downward (or upward) in $e$ – ln $p''$ due to the increase (or decrease) of degree of saturation. Introducing the state variable $\psi$ given as a function of degree of saturation for unsaturated soil, the position of *NCL* (also *CSL*) was shifted. In a similar manner as Chapter 2, one-dimensional model and three-dimensional for unsaturated soil based on Bishop's $\sigma''_{ij}$ were presented.

(4) It was indicated through the simulations that the proposed model suitably describes typical behaviors of unsaturated soils. The compression line drawn by the proposed model represents the various types of experimental compression lines inclusively. The proposed model, furthermore, properly considers the soaking collapse phenomena depending on confining pressure and density. Concerning the shear behavior, it could be seen that proposed model describes the strength, deformation and dilatancy characteristics

depending on degree of saturation $S_r$, and the development of deviatoric deformation during soaking under anisotropic stress condition as can be seen in observed results.

(5) The proposed model was applied to the compaction of soils. The proposed model described the well-known compaction curves of soils and also the transition of those curves with increasing of the applied stress. And, it was concluded that the water content of soils is critical for the mechanism of soil compaction, viz., lack of void water results inadequate compaction as dried soil is more resistant to compaction; on the other hand, too much moisture also leads to insufficient compaction as applied pressure is cancelled out by excess pore water pressure and hence effective stress hardly increases. Therefore, soil having intermediate water content is effectively compacted and the highest dry density is achieved.

*Modeling of the features anisotropically affecting on the mechanical characteristics of soil - the induced anisotropy (the influence of the intermediate principal stress, stress histories, non-coaxiality)* (*Chapter 4*)

It seems that the anisotropic influences of the relative magnitude of intermediate principal stress $\sigma_2$, stress histories and non-coaxiality on strength and deformation characteristics of soil occurs due to change of interparticle contacts situation, viz., fabric change of soil. By not applying the kinematic / rotational hardening rule for changing the shape of yield surface in ordinary stress space $\sigma_{ij}$ but the modified stress $t_{ij}^*$ reflecting the interparticle contact situation, the induced anisotropy was modeled inclusively in a simple isotropic hardening model in Chapter 4. The main results of this paper chapter summarized as follows:

(1) The induced anisotropy is caused by the developing of anisotropic situation of interparticle contacts (variation in contact normals) under any anisotropic loading path. The fabric tensor $F_{ij}$ representing such orientation of contact normals is well known as the proper tensor quantity evaluating the variation in soil fabric. From the experimental and analytical results, it could be indicated from both experimental and analytical investigations that the transformation tensor $a_{ij}$ based on $t_{ij}$ concept corresponds with observed fabric tensor $F_{ij}$. So, the influence of the intermediated stress $\sigma_2$ can be regarded as a part of the induced anisotropy under monotonic loading condition. In this paper, therefore, the modified stress tensor $t_{ij}$ (and the transformation tensor $a_{ij}$) were extended to new modified stress tensor $t_{ij}^*$ (and the transformation tensor $a_{ij}^*$) considering the influence of the intermediate stress $\sigma_2$ and stress histories, simultaneously.

(2) An evolution rule of the transformation tensor $a_{ij}^*$ used for obtaining the new modified stress tensor $t_{ij}^*$ was given to satisfy the following experimental facts; Ⓓ*The deformation and strength characteristic of soil is independent of the past stress histories:* $da_{ij}^* = da_{ij}$ & $a_{ij}^* = a_{ij}$ *during monotonic loading and at failure*, Ⓔsoil fabric is constant during unloading as the fabric of interparticle contact hardly changes under unloading condition: $da_{ij}^* = 0$ & $a_{ij}^* \perp a_{ij}$ *during reversal loading*, ⒻAfter the non-monotonic loading path (changing the direction of stress path on octahedral plane), soil is affected by the influence of the stress histories in subsequent stress path: $da_{ij}^* \perp da_{ij}$ & $a_{ij}^* \perp a_{ij}$ *during non-monotonic loading*, Ⓖ

The influence of the stress histories gradually decays with the development of plastic deformation: $da_{ij}^{*} \bowtie \|d\varepsilon_{ij}^{p}\|(a_{ij} \nrightarrow a_{ij}^{*})$

(3) In order to extend the ordinary isotropic hardening model by using the new modified stress $t_{ij}^{*}$, the yield function $f$ was defined with invariants of $t_{ij}^{*}$ : ($t_N$, $t_S$) instead of those of $\sigma_{ij}$ ($p$, $q$), and associated flow rule was assumed in $t_{ij}^{*}$-space. The features of original model, then, are kept in such modeling used $t_{ij}^{*}$. Subloading $t_{ij}$ model as an example was extended in this chapter. So, the proposed model can consider the influence of the induced anisotropy (stress history and the intermediate principal stress $\sigma_2$) and also density and/or confining pressure. Moreover, the flow rule determining the direction of plastic strain increment is assumed in $t_{ij}^{*}$-space which is not necessarily coaxial to $\sigma_{ij}$-space, so that the proposed method can describe the non-coaxiality between ordinary stress $\sigma_{ij}$ and the plastic strain increment $d\varepsilon_{ij}^{p}$.

(4) The validation of the proposed model was verified by the parametric studies and the comparison with observed results of triaxial tests on medium dense Toyoura sand, true triaxial tests and directional shear tests on medium dense Leighton Buzzard sand. It was indicated from the parametric studies of 12-directions monotonic shear tests with constant lode angle $\theta$ on octahedral plane that the proposed model can represent the three-dimensional behavior of soils with the past stress histories as experimental results on Hostun sand by Lanier: the rounded triangular contour lines of deviatoric strain and unique failure criterion; the contour lines spread out in the direction to which the past shear history was given. From comparing triaxial tests on Toyoura sand with the corresponding calculated results, it was revealed that the proposed model adequately describes that: the increasing and decreasing of stiffness during reloading and reversal loading path; the early occurrence of elastoplastic negative dilatancy before isotropic stress state during reversal loading (e.g., Comp. ∫∫ Ext.); anisotropic deformation during isotropic consolidation due to the past sheared histories. From comparison with the results of true triaxial tests on Leighton Buzzard sand, moreover, it was shown also that the proposed model can appropriately describe the variation in stiffness and the direction of strain increment affected by the past stress histories under various complicated three-dimensional stress paths. Also from comparison with the directional shear cell tests, it was indicated that proposed model, which obeys isotropic hardening rule and follows associated flow rule in $t_{ij}^{*}$ space, can represent the non-coaxiality between stress and strain increment, and the development of plastic deformation with rotating of principal stress axes under constant stress ratio $q/p$.

## 5.2 Future work

The topics of research, which need to be addressed in the future, are listed below.

(a) It is hard to investigate the influences of temperature, strain rate, unsaturated condition on mechanical characteristics of soil by ordinary element test apparatus in laboratory. Therefore, special apparatus which can control temperature, strain rate, suction, degree of saturation and others are needed and now triaxial

test apparatus and oedometer test apparatus for unsaturated soil and oedometer test apparatus with various strain rates are possessed with our research group. By using these apparatuses, the details of such features are investigated and the validation of present model is verified. Additionally, the present model is improved on demand.

Such features multiply affects on mechanical behavior of soil, e.g., creep and swelling with different temperatures, rising and falling temperature with different degree of saturation, and other combinations. Such coupled problems, therefore, will need to be investigated in future.

(b) Although the behavior of soil under complicated multi-dimensional stress path including the rotation of the principal axis was discussed and modeled properly by using new modified stress tensor $t_{ij}^*$, particularly the cyclic behavior of soil has not been investigated. The cyclic characteristic of soil, however, relates closely to liquefaction phenomena under undrained condition and tamping behavior under drained condition. It is well known that the induced anisotropy dominantly affects on such cyclic behavior of soil. Therefore, the applicability of new modified stress tensor $t_{ij}^*$ to cyclic characteristic of soils under both drained and undrained conditions will be verified. And then, if necessary, the evolution rule of transformation tensor $a_{ij}^*$ will be modified.

The cyclic stress condition acting on soil in real ground is not such simple axisymmetric stress condition as triaxial condition but complicated different three principal stress condition with the rotation of principal axis. So, by conducting the true triaxial test and hollow cylinder test, the details of cyclic characteristic of soil under such general stress conditions need to be investigated.

(c) The present model taking account of various features of soil will be applied to initial-boundary-value problem (e.g., finite element method) in basis of the governing equations suitably considering the interactions between such features, viz., temperature, time, air, water, simultaneously. Consequently, the deformation and failure prediction method of actual ground considering the various situations, e.g., seismic shaking, torrential rains, such temperature problem as nuclear fuel, long term consolidation settlement and those combinations, will be developed.